AFRRI REPORTS

October • November • December 1988

Defense Nuclear Agency
Armed Forces Radiobiology Research Institute
Bethesda, Maryland 20814-5415

UNCLASSIFIED
SECURITY CLASSIFICATION OF THIS PAGE

ADA206531

REPORT DOCUMENTATION PAGE

1a. REPORT SECURITY CLASSIFICATION UNCLASSIFIED	1b. RESTRICTIVE MARKINGS
2a. SECURITY CLASSIFICATION AUTHORITY	3 DISTRIBUTION/AVAILABILITY OF REPORT Approved for public release; distribution unlimited.
2b. DECLASSIFICATION/DOWNGRADING SCHEDULE	
4. PERFORMING ORGANIZATION REPORT NUMBER(S) SR88-30 - SR88-49	5. MONITORING ORGANIZATION REPORT NUMBER(S)
6a. NAME OF PERFORMING ORGANIZATION Armed Forces Radiobiology Research Institute 6b OFFICE SYMBOL (If applicable) AFRRI	7a. NAME OF MONITORING ORGANIZATION
6c. ADDRESS (City, State, and ZIP Code) Defense Nuclear Agency Bethesda, MD 20814-5145	7b. ADDRESS (City, State, and ZIP Code)
8a. NAME OF FUNDING/SPONSORING ORGANIZATION Defense Nuclear Agency 8b. OFFICE SYMBOL (If applicable) DNA	9. PROCUREMENT INSTRUMENT IDENTIFICATION NUMBER
8c. ADDRESS (City, State, and ZIP Code) Washington DC 20305	10. SOURCE OF FUNDING NUMBERS PROGRAM ELEMENT NO. NWED QAXM / PROJECT NO. / TASK NO. / WORK UNIT ACCESSION NO.
11 TITLE (Include Security Classification) AFRRI Reports, Oct-Dec 1988	
12. PERSONAL AUTHOR(S)	
13a. TYPE OF REPORT Reprints/Technical 13b. TIME COVERED FROM _____ TO _____	14. DATE OF REPORT (Year, Month, Day) 1988 October 15. PAGE COUNT 206
16. SUPPLEMENTARY NOTATION	
17 COSATI CODES FIELD / GROUP / SUB-GROUP	18. SUBJECT TERMS (Continue on reverse if necessary and identify by block number)

19 ABSTRACT (Continue on reverse if necessary and identify by block number)

This volume contains AFRRI Scientific Reports SR88-30 through SR88-49 for Oct-Dec 1988.

... to; glut... ...ine; adrenoceptors; prostaglandins; eicosanoids; mast cells; fluorescence imagery; macrophage; gall bladder; radiation effects; interleukin; (KT)

20. DISTRIBUTION/AVAILABILITY OF ABSTRACT ☐ UNCLASSIFIED/UNLIMITED ☒ SAME AS RPT. ☐ DTIC USERS	21. ABSTRACT SECURITY CLASSIFICATION UNCLASSIFIED
22a. NAME OF RESPONSIBLE INDIVIDUAL M. E. Greenville	22b. TELEPHONE (Include Area Code) (301)295-3536 22c. OFFICE SYMBOL ISDP

DD FORM 1473, 84 MAR — 83 APR edition may be used until exhausted. All other editions are obsolete.

SECURITY CLASSIFICATION OF THIS PAGE
UNCLASSIFIED

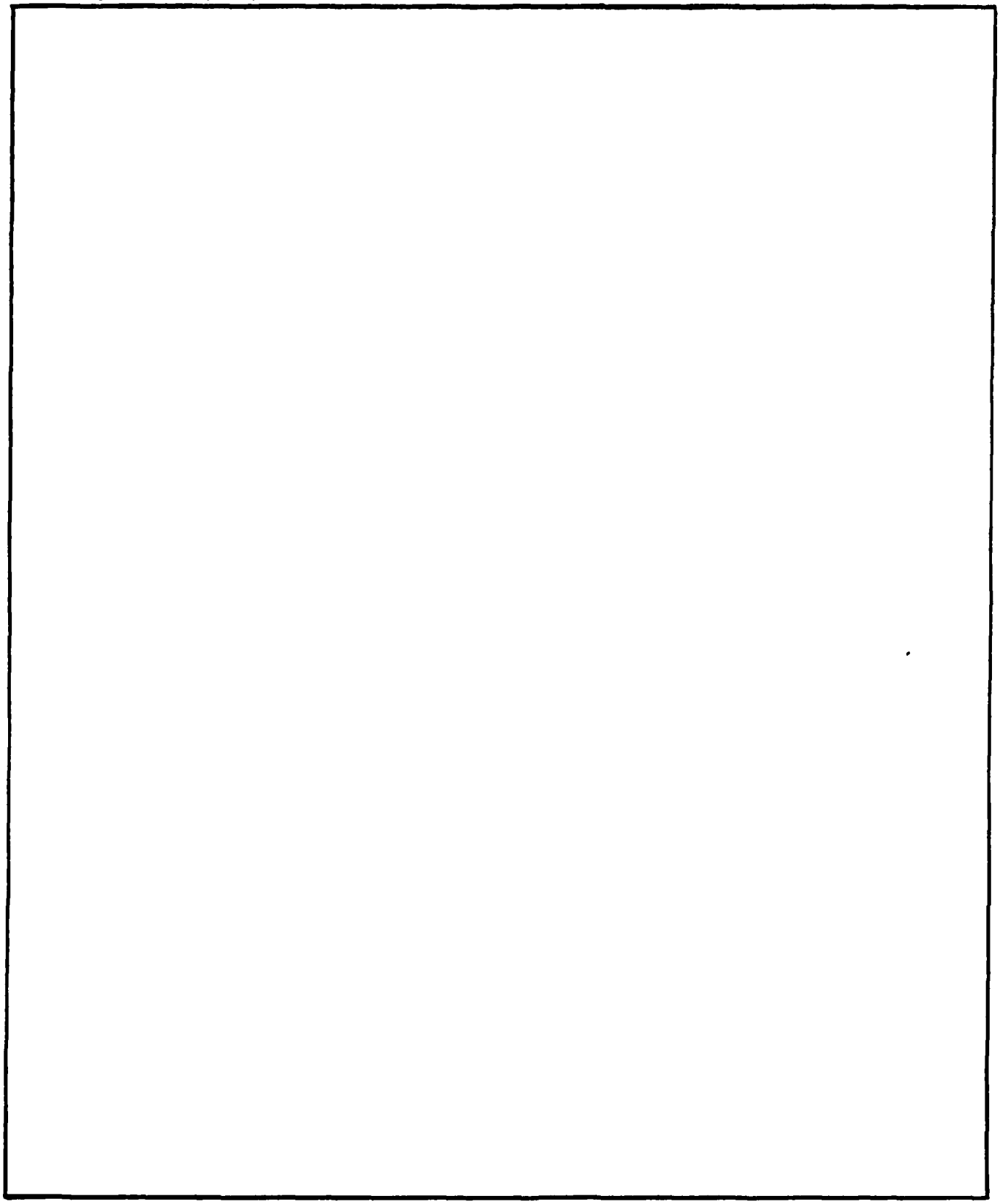

CONTENTS

Scientific Reports

SR88-44: Neta, R., Vogel, S. N., Sipe, J. D., Wong, G. G., and Nordan, R. P. Comparison of in vivo effects of human recombinant IL 1 and human recombinant IL 6 in mice.

SR88-45: Pellmar, T. C., Tolliver, J. M., and Neel, K. L. Radiation-induced impairment of neuronal excitability.

SR88-46: Schwartz, G. N., Neta, R., Vigneulle, R. M., Patchen, M. L., and MacVittie, T. J. Recovery of hematopoietic colony-forming cells in irradiated mice pretreated with interleukin-1 (IL-1).

SR88-47: Weiss, J. F., and Kumar, K. S. Antioxidant mechanisms in radiation injury and radioprotection.

SR88-48: Zabrenetzky, V., and Gallin, E. K. Inositol 1,4,5-trisphosphate concentrations increase after adherence in the macrophage-like cell line J774.1.

SR88-49: Zeman, G. H., Dooley, M., Eagleson, D. M., Goodman, L. J., Schwartz, R. B., Eisenhauer, C. M., and McDonald, J. C. Intercomparison of neutron dosimetry techniques at the AFRRI TRIGA reactor.

Cell-cycle Dependence of X-ray Oxygen Effect: Role of Endogenous Glutathione [1]

E. A. Blakely,[2,*] R. J. Roots,[2] P. Y. Chang,[2] L. Lommel,[2] L. M. Craise,[2] E. H. Goodwin,[2] E. Yee,[2,3] D. P. Dodgen,[4] and W. F. Blakely[4]

ABSTRACT—The oxygen effect was measured in human T-1 cell populations synchronized by mitotic selection and x-irradiated in vitro after they were allowed to progress to six different ages during the division cycle. Survival curves and dose-ratio calculations with 95% confidence intervals were obtained from computer fits of the data to the linear-quadratic model. The oxygen enhancement ratio (OER) values at the 1% survival level were 2.6 ± 0.08 in G_1/early S phase and increased to 3.0 ± 0.15 in late S/G_2 phase. The OER values at 10% survival increased linearly from 2.6 ± 0.2 for G_1-phase cells to 3.2 ± 0.2 for late S/G_2-phase cells. The increased OER in S-phase cells was the result of a greater hypoxic radioresistance compared with that measured with G_1-phase cells. In parallel experiments with synchronized cell populations, glutathione (GSH) and glutathione disulfide levels were measured by the Tietze assay and also were found to increase over the same period. The molecular mechanisms responsible for the radiation response involve a number of factors, one of which in this cell line may be GSH levels, especially under conditions of hypoxic exposure. Our data are consistent with the hypothesis that G_1- to late S-phase, age-dependent fluctuations in GSH content may be correlated with changes in OER during the human T-1 cell cycle. Changes in GSH content relative to its constitutive levels in the cell and alternative reductive factors (i.e., protein thiols), as well as their cellular location, may be important factors in the comparison of these findings to other cell lines.—NCI Monogr 6:217-223, 1988.

One of the early descriptions of the OER phenomenon in mammalian cells was made by Gray (*1*). Subsequently, the response to low linear energy transfer radiation during the cell division cycle was investigated for several cell lines under aerobic conditions (*2-6*). Few researchers (*7-13*) have compared the radiosensitivity of hypoxic to aerobic cells in different phases of the cell generation cycle. However, these investigations have in several cases suffered from poor experimental hypoxia, possible perturbations caused by drugs or agents used to induce synchrony or lack of a full cell-cycle analysis. In general, after sparsely ionizing (low linear energy transfer) irradiation under aerobic conditions, mammalian cells at the G_1 and the G_2/M positions in the generation cycle are more radiosensitive than are cells positioned in other phases, the most resistant phase being the late S phase. At reasonably low doses, i.e., a dose required to reduce survival to 0.37 or one required to reduce survival e^{-1} along the exponential portion of a survival curve for asynchronously growing cells, these differences are fairly small.

When the sensitivity of hypoxically irradiated cells has been compared with aerobically maintained cells for evaluation of the OER throughout the generation cycle (*7-13*), the conclusion commonly has been that the OER varied little if any during the cell generation cycle (*8-11*), although a lower OER in mitotic and early G_1-phase cells compared with the later S- and G_2-phase stages has been reported (*7,12,13*). In the latter cases, perturbations by methotrexate (*7*), a drug cytocidal to S-phase cells and therefore causing a partial synchrony, or a prolonged exposure to hypoxia (*12*) may have caused DNA perturbations and abnormal cell progression. Because we do not have available in the literature a complete study of the dependence or independence of the OER on cell age, we have measured OER values from an early G_1 stage into the following mitosis. In these experiments, OER magnitudes were measured throughout the generation cycle of human T-1 cells synchronized by mitotic selection. We observed statistically significant differences between the OER of G_1 cells and those measured for cells in late S/G_2 phase. These OER measurements vary in two ways, with survival level as has also been shown by others [e.g., *see* (*14,15*)], and secondly, with cell age, a phenomenon which hitherto has remained unresolved. In addition, preliminary measurements indicated that the intracellular total GSH levels may be related to the OER changes in the cell cycle.

MATERIALS AND METHODS

Cell line, culture conditions, and cell synchrony.—The human T-1 cell line and culturing conditions have been described in detail elsewhere (*16*). Mitotic T-1 cells were selected without drugs from an exponentially growing population with an automatic Talandic cell synchronizer as reported in (*17*). Cell volume distributions and autoradiography of [^{3}H]dThd-pulsed samples were completed for each experiment reported.

ABBREVIATIONS: OER = oxygen enhancement ratio(s); GSH = glutathione; NPSH = nonprotein sulfhydryl.

[1] Supported by Public Health Service grant CA-15184 from the National Cancer Institute, National Institutes of Health, Department of Health and Human Services; grant DE AC03-76SF00098 from the Department of Energy; and funding from the Defense Nuclear Agency Work Unit B5103.

[2] Biology and Medicine Division, Lawrence Berkeley Laboratory, University of California, Berkeley.

[3] Student Employment and Training Program, University of California, Riverside.

[4] Radiation Sciences Division, Armed Forces Radiobiological Research Institute, Bethesda, MD.

* *Reprint requests:* E. A. Blakely, Ph.D., Lawrence Berkeley Laboratory, 1 Cyclotron Rd., Bldg. 10, Rm. 209, Berkeley, CA 94720.

Irradiation methods.—Mitotically harvested cells were plated into custom-made 35-mm diameter glass dishes at about 2×10^4 cells/cm^2. At the appropriate cell age, the dishes were loaded into specially designed aluminum gassing chambers, and the cells were covered with 0.2 ml culture medium and then gassed for 20 minutes (*16*). Humidified nitrogen gas with 5% CO_2 and humidified air plus 5% CO_2 were used. A slight positive gas pressure was maintained during irradiation.

X-Irradiation of the cells was performed with a Philips RT250 x-ray unit operated at 225 kilovolt peak and 15 milliamperes at a dose rate of about 5.5 Gy/minute. The doses reported were not corrected for the dose back scattered from the glass. The exposures for the complete dose-response curves were planned so that the reported age of the cells at the time of irradiation represented the mean age of cultures exposed to generate the whole survival curve. After irradiation, the cells were covered with fresh culture medium and processed for clonogenic assays in a routine manner (*16*).

Three experiments were completed in which cellular survival was measured at 0.50- to 1.25-hour intervals covering the G_1 phase, through S phase, and into the first G_2/M border postmitotic harvest. All aerobically irradiated samples received an absorbed dose of 3.5 Gy, and hypoxically irradiated cells received an absorbed dose of 9.8 Gy, a 2.8-fold larger dose, which is approximately the OER value obtained at 10% survival for exponentially growing T-1 cells irradiated under these conditions (*16*). In another set of experiments, complete dose-response curves were generated for both air- and nitrogen-gassed samples at 3, 5, 8.1, 11, 14, and 17 hours after mitotic selection.

Autoradiography.— In each experiment, cell progression was monitored by incorporation of [^{3}H]dThd as described in (*17*). The autoradiography samples were held at room temperature for 20 minutes prior to labeling to coincide with the gas exchange period. The cooling of the cells to room temperature slowed the progression slightly, as compared with the kinetics of untreated cell populations we reported previously (*17*). From the data presented in figure 1, the duration of the phases of the cell cycle for the experiments reported here were calculated to be 6.5 hours (G_1 plus M), 9 hours (S phase), 4 hours (G_2 plus 1/2 M), and a total generation time of 19.5 hours. More than approximately 95% of the cells incorporated [^{3}H]dThd 11 hours after synchronization, an indication of reproducibly high-quality synchrony.

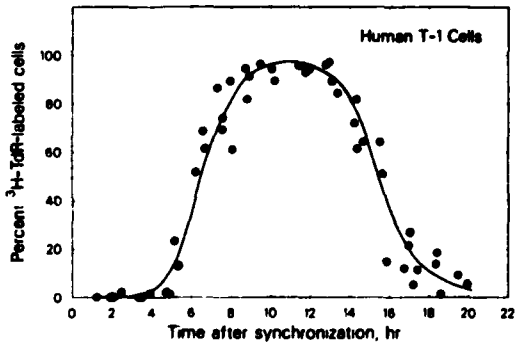

FIGURE 1. Reproducibility of DNA synthetic phase in synchronized controls. Composite of DNA labeling patterns from autoradiographs of unirradiated controls pooled from 4 experiments pulsed with [^{3}H]TdR (dThd) at various times after synchronization. These control cultures were held at room temperature for a 20-min period prior to labeling to correspond to the gas exchange time in the irradiated samples. Analysis of these data indicated that under the conditions of the experiments reported here, the duration of the cell-cycle phases were M = 0.7 hr, G_1 = 6.2 hr, S = 9 hr, and G_2 = 3.7 hr.

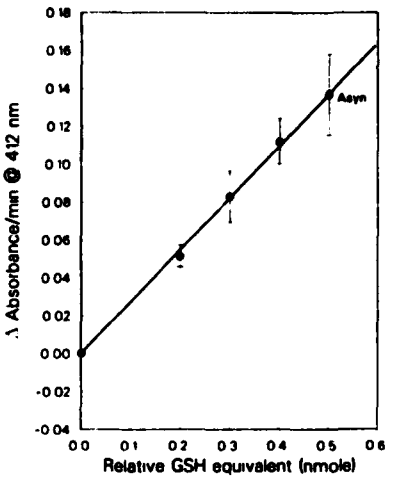

FIGURE 2. A GSH-equivalent standard curve. Levels of cellular GSH and glutathione disulfide were measured by the Tietze assay with the internal standard technique on acid-extracted and heat-denatured cell extract supernatants from each cell population. Example standard curve shown here is for asynchronous cell populations. Linear regression best fits of the change in absorbance at 412 nm/min vs. relative GSH-equivalents (in nanomoles) was 0.78 ± 0.02.

Glutathione measurements.—Both GSH and glutathione disulfide levels, expressed as GSH equivalents, were measured by the Tietze assay (*18*). Sample extracts were prepared by the addition of 0.5 ml of 0.6% 5-sulfosalicylic acid at 4° C to cell pellets which were then stored at −70° C until subsequent analysis. We found that γ-glutamyl transpeptidase, an enzyme capable of degrading GSH, was completely inhibited by a brief exposure to 0.6% of the acid (data not shown). At the time of GSH analysis, the 5-sulfosalicylic acid cell extract was rapidly thawed and incubated at 56° C for 20 minutes to facilitate protein denaturation and then was chilled to 4° C. Following centrifugation, the supernatant was removed and maintained at 4° C until measurements of GSH levels were completed, usually within 24 hours. An internal calibration standard (GSH) was used in the GSH measurements. Figure 2 presents the standard curve for the thiol measurements with asynchronous T-1 cells. A standard curve was generated for cells at each stage of the cell cycle studied. Ten to 20 aliquots were assayed for GSH from the samples at each time point.

Protein measurements.—Total cell protein was determined according to the Bio-Rad protein assay (Bio-Rad Laboratories, Richmond, CA) which is based on the binding of Coomassie brilliant blue to protein (*19*). Aliquots of cells were lysed by sonication, and bovine serum albumin was used as the protein standard. Three or four replicates were measured for each sample.

Data analysis.—The intracellular contents of GSH and glutathione disulfide are expressed as GSH equivalents per total cell protein (nanomoles GSH/milligram protein). An

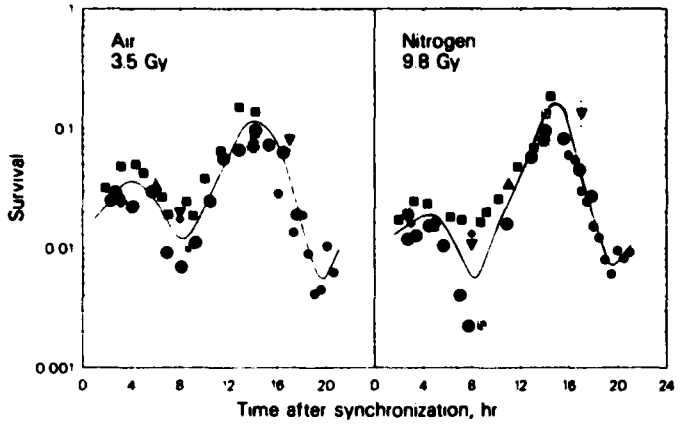

FIGURE 3. X-Ray age response for exposures in air and in nitrogen. Survival data are pooled from 8 experiments, 5 of which represent survival measurements from complete dose response curves at the 3.5- and 9.8-Gy dose levels for air- and nitrogen-saturated cells, respectively. Other three sets of data represent multiple survival measurements from cultures at various cell ages x-irradiated with 3.5 Gy in air or 9.8 Gy in nitrogen on glass petri dishes. Curves are best eye fits.

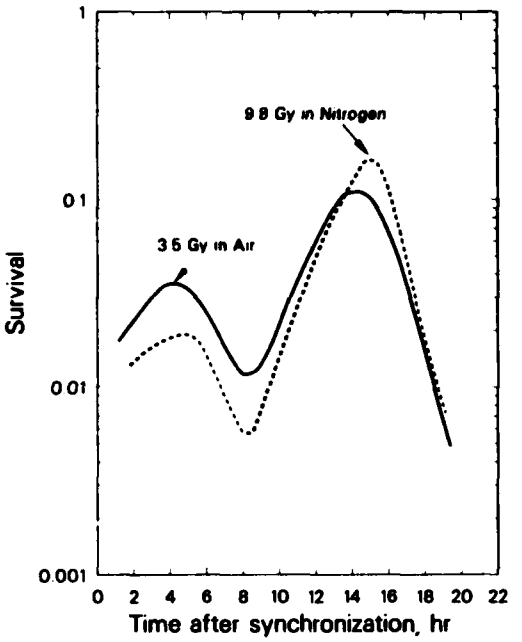

FIGURE 4. Superimposed plots of best air and nitrogen fits of the data from fig. 3. Perfect superimposition of the curves would indicate an OER at 10% survival of 2.8 at all ages. Comparison shows qualitatively that lower OER values are observed in the early part of the cell cycle and higher OER values later in S phase.

SE was estimated for each value based on the variances associated with GSH and cell protein measurements as described by Cleland (*20*).

Survival curves, dose-ratio calculations of OER, and associated 95% confidence intervals were obtained from computer fits of the data to the linear-quadratic model with programs developed by Albright (*21*).

RESULTS

Aerobic and Hypoxic Age Response Single Doses

Our initial experiments to examine the cell-cycle dependence of the oxygen effect were completed by synchronizing cells by mitotic selection, allowing them to progress to various ages, and then irradiating them with a fixed single dose under aerobic or hypoxic conditions. The survival data from 3 experiments of this type are plotted in figure 3. This figure also summarizes the survival measurements at the appropriate dose level taken from 5 experiments in which complete dose-response curves were generated. A curve has been drawn by eye through the compiled data for each gas condition of exposure with arithmetic means of the data.

There is some scatter in the data summarized from the 8 experiments, especially at the G_1/S phase interface (i.e., 5-8 hr after synchronization) under hypoxia; however, qualitatively, a trend in the data of figure 3 can be noted. Figure 4 permits an examination of the superimposed mean curves from figure 3. Perfect superimposition of the curves would indicate an OER of 2.8 at 10% survival at all ages for the x-ray dose studies. A comparison of the curves in figure 4 shows qualitatively that lower OER values are observed in the early part of the cell cycle and higher OER values later in S phase. It should be noted that the pooled data shown in figure 3 represent results from 8 experiments performed over a period of about 2 years.

To evaluate this observation in a more quantitative fashion, we constructed complete aerobic and hypoxic survival estimates from the data of figure 3. At the 3.4-Gy aerobic dose level, cellular radioresistance decreased as the cells aged from mid-G_1 to late S phase. This trend also occurred under hypoxic irradiation, but the radioresistance decreased more at the G_1/S interface and increased more in the middle to late S phase (data not shown).

Aerobic and Hypoxic Age Response Complete Dose Curves

Based on the data described above, a series of 5 experiments was completed under the conditions in which cells were mitotically selected, allowed to progress to various ages, and then irradiated with graded doses under aerobic

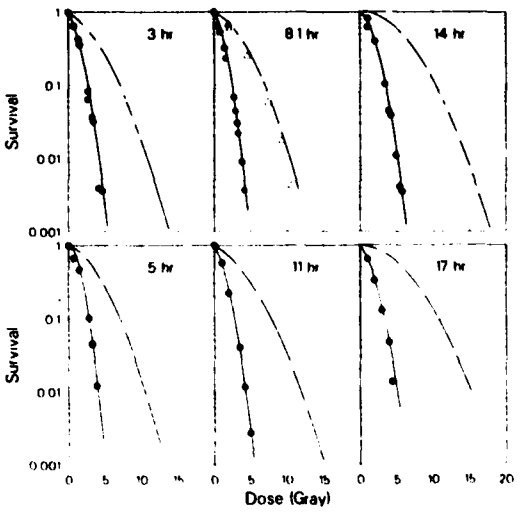

FIGURE 5. Complete x-ray dose response curves for cell populations irradiated postsynchronization in air (●) or in nitrogen (○) at 3, 8.1, or 14 hr (*upper panel*) or at 5, 11, or 17 hr (*lower panel*).

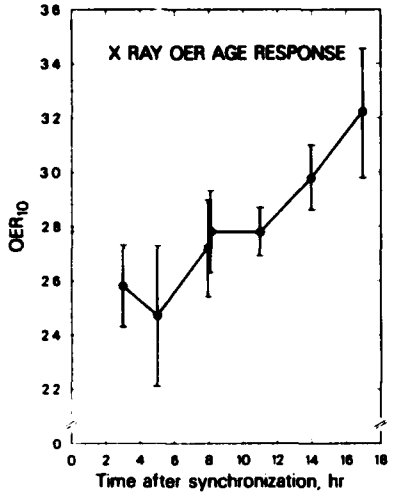

FIGURE 6.—Summary plot of computer-fitted OER values at 10% survival from complete aerobic and hypoxic dose-response curves measured with synchronized populations at six cell ages. Data are from 5 experiments.

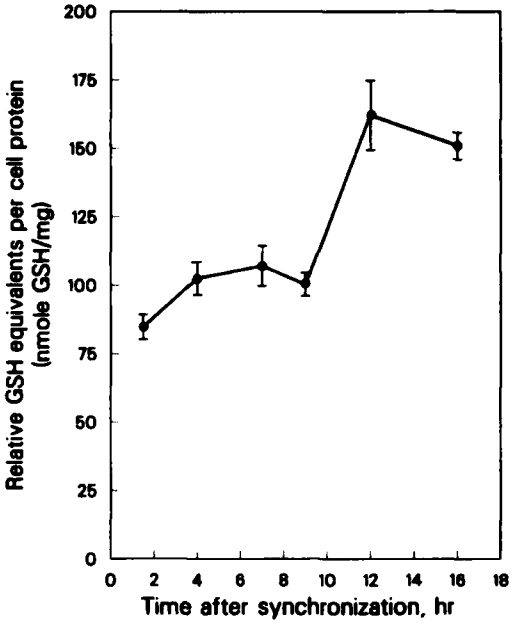

FIGURE 7.—Relative GSH equivalents (nanomoles) per milligram cell protein (±SE) measured in synchronized cell populations at various times during the cell cycle.

and hypoxic conditions. The data from cell populations positioned at six phases in the cell cycle between 3 and 17 hours after synchronization are summarized in figure 5. The curves drawn through the data points are computer-assisted, best-fit regressions. Replicate experiments were completed for cell populations at 3, 8.1, and 14 hours. Only single experiments were completed at 5, 11, and 17 hours.

Dose-ratio calculations of OER values were made for the pair of curves at each cell age and are presented in table 1. At high doses (e.g., 1% survival level), the OER values increase from approximately 2.6 ± 0.1 in G_1/early S phase to 3.0 ± 0.2 in late S/G_2 phase. At lower doses (e.g., 10% survival level), the same trend is observed with the OER values again increasing from approximately 2.6 ± 0.2 in G_1-phase cells to 3.2 ± 0.2 in late S/G_2-phase cells. These results are also plotted in figure 6. An approximately linear increase in the OER is noted as the cells progressed from G_1 to G_2 phase.

Age-dependent Variation in Glutathione Levels

In an attempt to find a possible mechanism for the observed cell-cycle-dependent increase in the OER, we made some preliminary measurements of GSH at various periods during the generation time. Although the constitutive GSH levels varied among experiments, all 3 experiments completed showed a similar qualitative pattern of increase in GSH levels, expressed as GSH equivalents per cell, as the T-1 cells progressed from G_1 phase into late S phase (data not shown). Protein measurements determined in parallel with 1 of these experiments permitted the normalization of GSH levels per milligram cell protein, known to vary in proportion with cell volume (fig. 7). A progressive change in GSH equivalents per milligram cell protein was observed as cells progressed from G_1 to late S phase, with an indication of a decrease late in the cycle. Additional experiments are planned that will permit further quantitative assessment of age-dependent fluctuations in GSH concentration with survival OER in human T-1 cells.

DISCUSSION

Survival Oxygen Enhancement Ratio and the Cell Cycle

We have reexamined the question of possible variations in aerobic and hypoxic radiosensitivity during the cell division cycle. We observed an increase in the OER value for x-irradiated human T-1 cell fibroblasts in vitro that was approximately linear as the cells progressed from early G_1 through G_2 phase. The increase in OER was significant based on 95% confidence limits at both the 10% and 1% survival level.

A few reports in the literature (*7–13*) describe experiments designed to measure the OER in synchronously dividing mammalian cells in vitro with x-rays. Researchers find these experiments difficult to complete because there

TABLE 1.—Oxygen enhancement ratios[a]

Survival level	Time after synchronization, hr					
	3	5	8.1	11	14	17
10%	2.58 ± 0.15	2.47 ± 0.27	2.75 ± 0.16	2.73 ± 0.09	2.98 ± 0.12	3.22 ± 0.24
1%	2.57 ± 0.08	2.56 ± 0.13	2.58 ± 0.08	2.76 ± 0.04	2.86 ± 0.06	2.99 ± 0.15

[a] Values include ± 95% confidence interval.

are many experimental variables that are hard to control. The published reports are divided between those investigators who report that OER values do change through the cell cycle (*7,12,13*) and those who report that they do not (*8-11*). Comparisons are confounded by experimental differences including the use of drugs in some cases to induce synchrony, the manner in which hypoxia was achieved, and the cell line that was studied. For example, Legrys and Hall (*9*) used Chinese hamster cells partially synchronized with hydroxyurea. Hypoxia was achieved by outgassing a Lucite jig holding the cells grown on plastic petri dishes. They (*9*) reported that the pattern of response to a single dose of 8 Gy in air or 20 Gy under hypoxia was very similar, which implied no significant change in the OER with stage in the generation cycle. Complete dose-response curves yielded OER values of 2.6 for populations synchronized in M or S phase (*9*). Other reports in the literature (*8,10,11*) with different biologic and physical systems confirm their observations.

On the other hand, the OER variations reported by us now are in agreement with those of other investigators (*7,12,13*), who found reduced OER values in the early to mid-G_1 phase of the cell cycle. In particular, we confirm the work of Pettersen et al. (*13*) who studied human NHIK 3025 carcinoma cells of the uterine cervix. The NHIK cells were synchronized by mitotic selection without drugs and were degassed and x-irradiated in glass vessels (*13*). The sensitizing effect of oxygen on cells in mid-G_1 phase was found also to increase with increasing dose (*13*). Sapozink (*12*) reported a significantly lower OER early in the cell cycle of HeLa cells synchronized with calcium-free medium and made hypoxic with culturing in a dense feeder cell population. Hence researchers in 3 laboratories who used hamster cells with a short (1.5 hr) G_1-phase duration reported negligible changes in x-ray OER survival as a function of cell age, whereas those in 3 others, using human cells with longer G_1 phases, demonstrated changes through the cell cycle.

Survival Oxygen Enhancement Ratios and Glutathione

Several recent reviews (*22-26*) have been published on the importance of thiols to radiosensitivity and chemosensitivity. Cellular GSH levels have been shown to have a major influence on the radiation response of asynchronous mammalian cells irradiated under hypoxic conditions (*27,28*). Several lines of experimental evidence support this conclusion. Cell lines derived from individuals with genetic defects in GSH metabolism (primarily altered levels of the enzyme GSH synthetase) have provided mutant cell lines with decreased intracellular GSH levels. These cell lines have been reported to exhibit a reduced OER, principally caused by a greater sensitization of the hypoxic compared with the aerobic response (*29-32*). It is acknowledged, however, that it cannot be ruled out that these cell lines (as well as other mutant GSH-deficient cell lines) may also have a deficiency in some other biochemical system responsible for the reduction in their OER values.

In a second type of approach, some have used thiol-modifying agents to evaluate the importance of GSH in the radiation response. Agents like *N*-ethylmaleimide, diethyl maleate, and L-buthionine sulfoximine have been used to decrease intracellular GSH levels with some commensurate increase in the sensitization of the hypoxic radiation response (*33-35*). The effect of thiol-depleting agents on the aerobic response is less clear. In those studies, when no aerobic sensitization occurs, the OER is reduced by the radiosensitizing agents (*33,35*), whereas other investigators report no appreciable alteration in the OER due to simultaneous aerobic and hypoxic sensitization (*36*) or only after conditions of long-term incubation in L-buthionine sulfoximine (*37*) or combined L-buthionine sulfoximine and diethyl maleate treatment (*38*). It might be expected that intracellular concentrations of these agents will be uncertain and that the biochemical reaction may not be fully known.

A third approach was used by Russo et al. (*39*) in an attempt to elevate intracellular thiol levels and measure the effect on the OER. Intracellular thiol levels in Chinese hamster V79 cells were increased 200% upon the addition of 2-oxothiazolidine-4-carboxylate, with a corresponding increase in the OER produced by protection of the hypoxic response with no effect on the aerobic response (*39*). Based on this report, a modification of intracellular thiol levels would predict a commensurate change in the hypoxic x-ray response and in certain instances the OER value.

Variations in Glutathione During the Cell Cycle

In the late 1960s and early 1970s, several reports were published that indicated a diversity of observations including: 1) no consistent change in NPSH content between late G_1- and late S-phase cells (*40-43*), 2) a trend of increasing NPSH levels with cell progression from early G_1-phase through late S-phase cells (*42,44*), or even 3) an increasing trend from G_1 to early S phase and then decreasing values with cell aging from early to late S phase (*45*). It is worth noting that the methods researchers used to measure GSH were either Ellman's technique (*44*) or [^{14}C]*N*-ethylmaleimide binding (*40-43,45*). Harris and Teng (*42*), using the latter binding technique, only found an age-dependent increase in NPSH if they studied G_1-phase cells released from plateau phase. They did not see an increased NPSH in synchronized populations mitotically selected with demecolcine and then allowed to progress.

Our preliminary measurements of GSH made with the Tietze assay on mitotically selected synchronized populations indicated an increase in GSH, normalized on a per total cell protein basis, as the cells progress from early G_1 to late G_2 phase. The increase in intracellular GSH levels appears to correlate with the approximately linear increase in OER in cells aging over the same period.

CONCLUSIONS AND IMPLICATIONS FOR FUNDAMENTAL MECHANISMS

Oxygen can be an effective modifier of radiation-induced damage. Most importantly, oxygen competes with endogenous reducing agents such as GSH in reactions with radiation-induced free radical sites in vital cellular molecules. For sparsely ionizing radiation, a certain number of the DNA radical sites of damage may be restored by reducing species such as GSH, unless oxygen has fixated them first.

In normally aerated Chinese hamster cells, subjected to a 20% oxygen atmosphere, a full OER characteristic to the system can be obtained when stringent hypoxia is administered for the irradiation. If, however, hypoxic cells are supplied with oxygen (1%-50%) in less than 5 mseconds

prior to irradiation, only a partial but constant OER of 1.7 is obtained (*46,47*). The explanation has been that there are two components to the oxygen effect. One target, possibly the membrane, to which oxygen diffuses readily would account for the 1.7 portion of the full OER, and another target, which is possibly nuclear DNA, would involve the rest of the full OER value, which is approximately 2.8 to 3.0 in many mammalian cells. If these theoretical targets varied during the cell cycle or if the concentration of a compound such as GSH varied during the cell progression cycle, this might reflect a variable OER during the generation cycle.

In addition to providing a potential modification of both the initial damage yields and spectrum, GSH levels or, more relevantly, GSH contribution to the redox state, may play an important role in the cells' capacity to repair radiation injury. Clearly, further work in this area is needed. It is also important, in our opinion, for one to realize that studies designed to explore the mechanisms of thiol-dependent responses and or chemoresponses of cells may be confounded by the use of asynchronous populations.

REFERENCES

(*1*) GRAY LH: Actions of radiations on living cells. Br J Radiol 25:235–244, 1952.

(*2*) TERASIMA T, TOLMACH LJ: Changes in X-ray sensitivity of HeLa cells during the division cycle. Nature 190:1210–1211, 1961.

(*3*) TERASIMA T, TOLMACH LJ: Variations in several responses of HeLa cells to X-irradiation during the division cycle. Biophys J 3:11–33, 1963.

(*4*) ELKIND MM, WHITMORE GF: The Radiobiology of Cultured Mammalian Cells. New York: Gordon & Breach, 1967, pp 85–103.

(*5*) SINCLAIR WK: Cyclic X-ray responses in mammalian cells in vitro. Radiat Res 33:620–643, 1968.

(*6*) SINCLAIR WK: Cell cycle dependence of the lethal radiation response in mammalian cells. Curr Top Radiat Res Q 7:264–285, 1972.

(*7*) BERRY RJ: A reduced oxygen enhancement ratio for X-ray survival of HeLa cells in vitro, after treatment with methotrexate. Nature 208:1108–1109, 1965.

(*8*) KRUUV J, SINCLAIR WK: X-ray sensitivity of synchronized Chinese hamster cells irradiated during hypoxia. Radiat Res 36:45–54, 1968.

(*9*) LEGRYS GA, HALL EJ: The oxygen effect and X-ray sensitivity in synchronously dividing cultures of Chinese hamster cells. Radiat Res 37:161–172, 1969.

(*10*) KIMLER BF, SINCLAIR WK, ELKIND MM: *N*-Ethylmaleimide sensitization of X-irradiated hypoxic Chinese hamster cells. Radiat Res 71:204–213, 1977.

(*11*) CHAPMAN JD, WEBB RG, BORSA J: Radiosensitization of mammalian cells by *p*-nitroacetophenone. I. Characterization in asynchronous and synchronous populations. Int J Radiat Biol 19:561–573, 1971.

(*12*) SAPOZINK MS: Oxygen enhancement ratios in synchronous HeLa cells exposed to low-LET radiation. Radiat Res 69:27–39, 1977.

(*13*) PETTERSEN EO, CHRISTENSEN T, BAKKE O, et al: A change in the oxygen effect throughout the cell cycle of human cells of the line NHIK-3025 cultivated in vitro. Int J Radiat Biol 31:171–184, 1977.

(*14*) PALCIC B, SKARSGARD LD: Reduced oxygen enhancement ratio at low doses of ionizing radiation. Radiat Res 100:328–339, 1984.

(*15*) PALCIC B, BROSING JW, SKARSGARD LD: Survival measurements at low doses: Oxygen enhancement ratios. Br J Cancer 46:980–984, 1984.

(*16*) BLAKELY EA, TOBIAS CA, YANG TCH, et al: Inactivation of human kidney cells by high energy monoenergetic heavy-ion beams. Radiat Res 80:122–160, 1979.

(*17*) BLAKELY EA, CHANG PY, LOMMEL L: Cell-cycle dependent recovery from heavy-ion damage in G_1-phase cells. Radiat Res 104:s-145–s-157, 1985.

(*18*) TIETZE F: Enzymatic method for quantitative determination of nanogram amounts of total and oxidized glutathione: Applications to mammalian blood and other tissues. Anal Biochem 27:502–522, 1969.

(*19*) BRADFORD MM: A rapid and sensitive method for the quantitation of microgram quantities of protein utilizing the principle of protein-dye binding. Anal Biochem 72:248–254, 1976.

(*20*) CLELAND WW: The statistical analysis of enzyme kinetic data. Adv Enzymol 29:1–32, 1967.

(*21*) ALBRIGHT NW: Computer programs for the analysis of cell survival date. Radiat Res 112:331–340, 1987.

(*22*) VOS O, VAN DER SCHANS GP, ROOS-VERHEY WSD: Reduction of intracellular glutathione content and radiosensitivity. Int J Radiat Biol 50:155–165, 1985.

(*23*) EDGREN MR, SOLEN G, REVESZ L: Specificity of endogenous glutathione in determining the oxygen enhancement of cellular radiosensitivity. Int J Radiat Oncol Biol Phys 12:1147–1150, 1986.

(*24*) CLARK EP: Thiol induced biochemical modification of chemo- and radioresponses. Int J Radiat Oncol Biol Phys 12:1121–1126, 1986.

(*25*) BIAGLOW JE, VARNES ME, CLARK EP, et al: The role of thiols in cellular response to radiation and drugs. Radiat Res 95:437–455, 1983.

(*26*) DURAND RE: Roles of thiols in cellular radiosensitivity. Int J Radiat Oncol Biol Phys 10:1235–1236, 1984.

(*27*) CULLEN BM, MICHALOWSKI A, WALKER H, et al: Studies on the radiobiological oxygen constant, K, for mammalian cells: Correlation between K and the non-protein sulfhydryl content of mammalian cells. Int J Radiat Biol 38:525–536, 1980.

(*28*) HODGKISS RJ, JONES NR, WATTS ME, et al: Glutathione depletion enhances the lifetime of oxygen-reactive radicals in mammalian cells. Int J Radiat Biol 46:673–674, 1984.

(*29*) MALAISE EP: Reduced oxygen enhancement of the radiosensitivity of glutathione-deficient fibroblasts. Radiat Res 95:486–494, 1983.

(*30*) REVESZ L: The role of endogenous thiols in intrinsic radioprotection. Int J Radiat Biol 47:361–368, 1986.

(*31*) DEBIEC D, DESCHAVANNE PJ, MIDANDER J, et al: Survival curves of glutathione synthetase deficient human fibroblasts: Correlation between radiosensitization in hypoxia and glutathione synthetase activity. Int J Radiat Biol 48:525–543, 1985.

(*32*) ASTOR MB: Oxygen concentration and the OER for acutely or chronically thiol deficient cells. Int J Radiat Oncol Biol Phys 12:1131–1134, 1986.

(*33*) BUMP EA, YU NY, BROWN JM: Radiosensitization of hypoxic tumor cells by depletion of intracellular glutathione. Science 217:544–545, 1982.

(*34*) KOCH CJ, STOBBE CC, BAER KA: Combined radiation-protective and radiation-sensitizing agents. III. Radiosensitization by misonidazole as a function of concentration of endogenous glutathione or exogenous thiols. Int J Radiat Oncol Biol Phys 12:1151–1155, 1986.

(*35*) CLARK EP, EPP ER, BIAGLOW JE, et al: Glutathione depletion, radiosensitization, and other misonidazole potentiation in hypoxic Chinese hamster ovary cells by buthionine sulfoximine. Radiat Res 98:370–380, 1984.

(*36*) MITCHELL JB, RUSSO A, BIAGLOW JE, et al: Cellular gluta-

thione depletion by diethyl maleate or buthionine sulfoximine: No effect of glutathione depletion on the oxygen enhancement ratio. Radiat Res 96:422–428, 1983.

(*37*) ASTOR MB, HALL EJ, BIAGLOW JE, et al: Effects of D,L-buthionine-*S,R* sulfoximine on cellular thiol levels and the oxygen effect in Chinese hamster V79 cells. Int J Radiat Oncol Biol Phys 10:1239–1242, 1984.

(*38*) BIAGLOW JE, CLARK EP, EPP ER, et al: Nonprotein thiols and the radiation response of A549 human lung carcinoma cells. Int J Radiat Biol 44:489–495, 1983.

(*39*) RUSSO A, MITCHELL JB, FINKELSTEIN E, et al: The effects of cellular glutathione elevation on the oxygen enhancement ratio. Radiat Res 103:232–239, 1985.

(*40*) KLEIN P, ROBBINS E: An ultrasensitive assay for soluble sulfhydryl and its application to the study of glutathione levels during the HeLa life cycle. J Cell Biol 46:165–168, 1970.

(*41*) HARRIS JW, PAINTER RB, HAHN GM: Endogenous nonprotein sulfhydryl and cellular radiosensitivity. Int J Radiat Biol 15:289–292, 1969.

(*42*) HARRIS JW, TENG SS: Sulfhydryl groups during the S-phase: Comparison of cells from G_1, plateau-phase G_1, G_0. J Cell Physiol 81:91–96, 1972.

(*43*) HARRIS JW: Non-protein sulfhydryl content of Ehrlich ascites tumor cells exposed to hyperbaric oxygen or X-irradiation. Exp Cell Res 50:293–305, 1968.

(*44*) OHARA H, TERASIMA T: Variations of cellular sulfhydryl content during cell cycle of HeLa cells and its correlation to cyclic change of X-ray sensitivity. Exp Cell Res 58:182–185, 1969.

(*45*) SINCLAIR WK: Modification of cell cycle response of synchronous mammalian cells to ionizing radiation by inhibition of repair. *In* Control of Proliferation in Animal Cells. Cold Spring Harbor Conferences on Cell Proliferation, vol 1. Cold Spring Harbor, NY: Cold Spring Harbor Laboratory, 1974, pp 985–994.

(*46*) SHENOY MA, ASQUITH JC, ADAMS GE, et al: Time-resolved oxygen effects in irradiated bacteria and mammalian cells: A rapid-mix study. Radiat Res 62:498–512, 1975.

(*47*) MICHAEL BD, HARROP HA: Time scale and mechanism of radiosensitization and radioprotection at the cellular level. *In* Proceedings of the Key Biscayne Conference on Combined Modalities in Cancer Treatment: Radiation Sensitizers and Protectors (Brady LW, ed). New York: Masson, 1980, pp 14–22.

Circulatory Shock 26:331-339 (1988)

Alterations in Rat Aortic Alpha$_1$-Adrenoceptors and Alpha$_1$-Adrenergic Stimulated Phosphoinositide Hydrolysis in Intraperitoneal Sepsis

J.A. Carcillo, R.Z. Litten, E.A. Suba, and B.L. Roth

Naval Medical Research Institute, (J.A.C., E.A.S., B.L.R.) and the Armed Forces Radiobiological Research Institute, Bethesda, Maryland (R.Z.L.), and Department of Anesthesiology, Critical Care Medicine, and Child Health and Development, George Washington University School of Medicine, Washington, District of Columbia (J.A.C.)

We investigated the alterations of rat aortic alpha$_1$-adrenoceptors and alpha$_1$-adrenergic stimulated phosphoinositide (PI) metabolism in intraperitoneal sepsis. An analysis of [^{125}I]-hydroxyethylaminotetralone (HEAT) binding to alpha$_1$-adrenoceptors on rat aortic membranes revealed decreased numbers of receptors without changes in affinity.The maximum number of binding sites decreased from 349 ± 35 fmol/mg to 146 ± 16 fmol/mg ($P < 0.05$ vs. control). PI metabolism was similarly attenuated in aortae from septic rats. The norepinephrine-stimulated hydrolysis of [^{32}P]-phosphatidylinositol-4,5-bisphosphate was significantly decreased in aortae from septic rats as was the alpha$_1$-adrenoceptor stimulated accumulation of [^{3}H]-inositol monophosphate. Finally, the basal labeling of [^{32}P]-phosphatidylinositol-4,5-bisphosphate but not of [^{32}P]-phosphatidylinositol or [^{32}P]-phosphatidic acid was significantly diminished. These results imply that signal transduction induced by alpha$_1$-adrenoceptor agonists in rat aorta is significantly altered in intraperitoneal sepsis. These findings may help define the mechanisms of depressed aortic contractility in models of sepsis and endotoxic shock.

Key words: septic shock, phosphoinositide metabolism, vascular contraction, vasoconstriction, signal transduction

INTRODUCTION

Sepsis and septic shock are major causes of death in the United States among critically ill patients. Despite sophisticated and aggressive surgical and medical

Submitted for publication December 4, 1987; revised May 26, 1988.

A preliminary account of these findings was presented at the first International Shock Conference and published in abstract form [36].

Address reprint requests to Bryan L. Roth, M.D., Ph.D., Room S-253, Stanford University Medical Center, Stanford, CA 94305.

interventions, the mortality rate in septic shock remains between 40 and 60% [1]. In dissecting the pathophysiology of sepsis and endotoxemia, numerous investigators have noted diminished peripheral vascular responsiveness to norepinephrine in both humans [2] and in animal models of sepsis and endotoxemia [3,4]. Furthermore, an attenuated response to exogenously applied norepinephrine (NE) has been noted in isolated aorta by several groups of investigators [5,6] using a variety of models of sepsis and endotoxemia. The mechanism of this phenomenon remains unknown [see refs. 3,4 for review], but could reside in part in the signal transduction apparatus.

We recently found that NE-induced contraction of rat aorta, which is mediated by alpha$_1$-adrenoceptors, appears to correlate with the breakdown of phosphoinositides (PI) [7]. Our original observations have now been replicated [8]. We also noted that the potent vasoconstrictor 5-hydroxytryptamine [9] and several vasoactive prostaglandins [10] also appear to induce rat aortic contraction, at least in part, via PI breakdown [for review see refs. 3,4]. According to this scheme, following binding of a ligand to the receptor a phosphoinositide-specific phospholipase C is activated which cleaves phosphatidylinositol-4,5-bisphosphate to release inositol-triphosphate (IP_3) as well as diacylglycerol (DAG). It is proposed that IP_3 mobilizes intracellular calcium [11–15] while DAG activates protein kinase C. Phorbol esters, which mimic the effects of endogenous DAG, are potent inducers of rat aortic contraction. Phorbol esters induce vasoconstriction in part by the mobilization of extracellular calcium in a nitrendipine-sensitive fashion [16].

We previously discovered that hepatic alpha$_1$-adrenoceptors [17], as well as vasopressin receptors [18], were decreased in intraperitoneal sepsis as well as in chronic endotoxin infusion models of sepsis [19]. Spitzer and colleagues [20] found that the alpha$_1$-adrenoceptors and vasopressin receptor-mediated mobilization of intracellular calcium and activation of phosphoinositide hydrolysis were altered in intraperitoneal sepsis and in endotoxemia. These findings suggested to us that vascular PI metabolism and adrenoceptors might be similarly altered in intraperitoneal sepsis.

In this paper we report significant alterations in aortic PI metabolism in rat intraperitoneal sepsis. We also discovered diminution of aortic alpha$_1$-adrenoceptors. These results suggest that experimental sepsis in the rat induces alterations in receptor-coupled signal transduction in the aorta.

MATERIALS AND METHODS

Animals and Their Treatment

Sprague-Dawley rats (Taconic Farms, Baltimore, MD) weighing 200–350 g were used in all experiments. Cecal ligation with two-hole puncture (CLP) was performed as previously detailed [17]. The sham procedure was identical except that the cecum was not devascularized, ligated or punctured. At 18–24 hr post-procedure, surviving animals (60–70% survival at this time point) were sacrificed by decapitation. Surviving animals displayed the signs of sepsis described by Wichterman et al. [21] including piloerection, a bloody discharge from the nose and mucous membranes, bloody diarrhea and lethargy.

Phosphoinositide Metabolism

PI turnover in the rat aorta measuring [^{3}H]-inositol monophosphate accumulation in the presence of 10 mM LiCl was determined by a modification of the

procedures of Berridge et al. [22] as previously described [7,9,23,24] using [^{3}H]-myo-inositol (16 Ci/mmole, New England Nuclear, Boston, MA). We previously showed that this procedure accurately separates inositol mono-, bis- and tris-phosphates.

For measurement of [^{32}P]-phosphoinositide metabolism, rat aortic rings (4 mm length) were prepared [10] and pre-incubated for 15 min in an oxygenated Hepes buffer of the following composition (in mM) at 37°C: 140 NaCl, 10 D-glucose, 5 Hepes, 1.0 $MgCl_2$, 1.5 $CaCl_2$ pH-7.40. The segments were then incubated in [^{32}P]-orthophosphate (carrier free, Amersham) containing Hepes buffer (30μ Ci/ml) for 30 min to label phosphoinositide pools. Preliminary experiments disclosed steady-state labeling of PI pools by this time period. Test agents were then added for various periods of time and the reaction terminated by the addition of 0.9 ml chloroform/methanol/HCl (100:200:0.1) solution followed by the addition of 0.3 ml water and 0.3 ml chloroform. Following lipid extraction, the lower phase was removed, washed twice with upper phase and concentrated in a Speed-Vac. The samples were then applied to oxalate pre-coated high performance thin layer chromatography plates (HPTLC) prepared and run according to Jolles et al. [25]. [^{32}P]-phosphoinositides were identified by autoradiography with Kodak X-OMAT film (XAR-2) and by authentic standards (Sigma Chemical Co., St. Louis, MO). The spots so identified were scraped into scintillation vials and quantified by liquid scintillation spectrometry.

Alpha$_1$-Adrenoceptor Measurements in Rat Aorta

Aortas from 12 rats (sham or CLP) were homogenized in 20 mM Tris-Cl buffer (pH–7.40, 25°C) with a polytron homogenizer and then rehomogenized with a tightly-fitting glass-glass homogenizer. This homogenate was centrifuged at 1,000 × g for 15 min (4°C) to sediment cellular debris and then a crude plasma membrane fraction was prepared by centrifugation at 35,000 × g for 45 min. The resulting pellet was resuspended in binding buffer [17] and incubated (0.5 ml t.v.) at 25°C for 60 min in the presence of increasing doses of the selective alpha$_1$-agonist [^{125}I]-hydroxyethylaminotetralone (HEAT) (2,200 Ci/mmole, New England Nuclear, Boston, MA) in the presence and absence of 1μM prazosin to determine specific binding. Membranes were harvested by filtration on GF/B filters (Whatman) and washed by three 5–ml washes of ice-cold binding buffer. Filters were placed into vials and counted in a gamma counter.

Binding data were analyzed and binding parameters (Kd, Bmax) determined using the nonlinear least-squares computerized curve fitting program (LIGAND) as previously detailed [26] using the NIH DEC/10 computer. This iterative procedure constructs models of binding according to the law of mass action for the interaction of multiple ligands with multiple binding sites. The results of three or more experiments were averaged to provide a weighted mean and SEM. Protein concentration was determined as described by Bradford [27].

Materials

Solvents were of reagent grade or better (Fisher Chemical Co., St. Louis, MO); all other materials, unless otherwise specified, were from Sigma Chemical Co. (St. Louis, MO).

RESULTS

Alterations in Rat Aortic PI Metabolism

Recent findings [20] have suggested that alterations might exist in hepatic PI metabolism in various sepsis and endotoxin models. We wished to determine whether similar changes might occur in aorta. Figure 1 shows that the NE-activated PI hydrolysis, as measured by the accumulation of [^{3}H]-inositol monophosphate, (PI) was significantly attenuated in the aortas from septic rats, when compared with sham-operated controls. Dose-response studies for a short time of incubation have disclosed an EC_{50} of 0.93 $\pm$ 0.6 μM for NE-induced [^{3}H]-IP accumulation [see ref. 21]; prazosin, a selective alpha$_1$-antagonist inhibits the response with an IC_{50} of 3nM, while yohimbine (an alpha$_2$-antagonist) has an IC_{50} of 100 nM [7]. Thus, the measurement of NE-induced [^{3}H]-IP accumulation in rat aorta accurately reflects the activity of alpha$_1$-adrenoceptors.

Since phosphatidylinositol–4,5–bisphosphate (PIP_2) is thought to be the primary substrate for PI hydrolysis in rat aorta [28], we sought to measure the accumulation of [^{3}H]-inositol triphosphate (IP_3) using our previously described technique. Because of the very small amounts of IP_3 released which are not degraded into IP we were unable to measure this metabolite (not shown). We were, however, able to measure the NE-stimulated breakdown of [^{32}P]-phosphatidylinositol–4,5–bisphosphate. After a 30 sec exposure to 10 μM NE, [^{32}P]-PIP_2 levels were decreased in aortas from sham-operated rats, but unchanged in aortas from septic rats (Table I). After a 1 min exposure to 10 μM NE [^{32}P]-PIP_2 levels returned to baseline (Table II). This effect is similar to that reported by Rapoport in rat aorta [29].

Because the basal levels of [^{32}P]-PIP_2 as well as basal [^{3}H]-IP accumulation were diminished, we sought to determine whether these alterations represented generalized changes in PI synthesis. Accordingly, we measured the labeling of various PI metabolites in aortas from septic and sham-operated rats (Table II) in the basal state

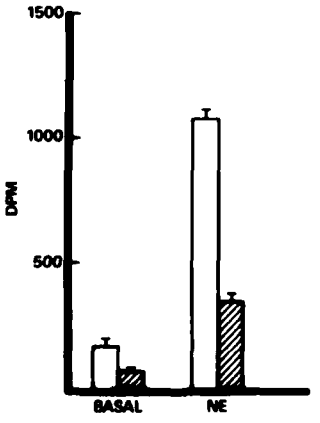

Fig. 1. The effect of intraperitoneal sepsis on norepinephrine-stimulated phosphoinositide hydrolysis in rat aorta. Aortic rings from control (open bars) and septic (hatched bars) were incubated in the presence and absence of 10 μM norepinephrine and [^{3}H]-inositol monophosphate accumulation determined. Data represent mean $\pm$ SEM for 16 individual determinations. The differences in basal and stimulated accumulation are significant ($P < 0.01$).

TABLE I. Altered NE Induced PIP_2 Hydrolysis in Sepsis

	Sham	Septic
Control aorta	700 ± 76 dpm	438 ± 89 dpm[a]
30 sec 10 M NE	567 ± 79 dpm	413 ± 39 dpm[b]

[a]($P < 0.05$) vs. control in sham operated rats.
[b]($P > 0.05$) or no significant change vs. control in septic rats.

TABLE II. Time Course [^{32}P] Incorporation Into Phosphoinositides in the Presence of 10 M NE (dpm/mg) in Rat Aorta

	Sham	
	0 min	1 min
PI	311 ± 510	326 ± 95
PIP	159 ± 56	187 ± 69
PIP_2	294 ± 130	362 ± 160
PA	202 ± 61	295 ± 93
	Septic	
Time	0 min	1 min
PI	311 ± 75	471 ± 182
PIP	110 ± 51	186 ± 40
PIP_2	152 ± 53[a]	157 ± 38[a]
PA	206 ± 27	523 ± 284

[a]$P < 0.05$ vs. sham. Data represent mean ± SEM of six individual determinations.

as well as after a 1 min exposure 10 μM NE. Decreased PIP_2 labeling continues at the 1 min time points as well as at the 30 sec time point in septic aorta.

As is seen (Fig. 2) there was apparently a selective decrease in [^{32}P]-PIP_2 labeling in aortas from septic rats, without changes in the basal levels of [P]-PIP, [^{32}P]-PI or [^{32}P]-PA. Since PIP_2 has recently been shown to be the preferential substrate for the guanine nucleotide activated phospholipase C in rat aorta [28], this decreased substrate availability could account, in part, for the observed decrease in [^{3}H]-IP accumulation. It does not account for the diminished [^{32}P]-PIP_2 breakdown. These results suggested to us that earlier events in the signal transduction pathway for aortic alpha$_1$-adrenoceptors might be perturbed in intraperitoneal sepsis.

Alpha$_1$-Adrenoceptor Alterations in Sepsis

Since we had previously found changes in hepatic alpha$_1$-adrenoceptors, it was reasonable to suggest that aortic receptors might be similarly altered. Figure 3 shows, using [^{125}I]-HEAT as a ligand, a 50% reduction in rat aortic alpha$_1$-adrenoceptors during sepsis. The maximum number of binding sites is decreased without a change in affinity (Table III), suggesting fewer ligand recognition sites. These results suggest that the decrease in number in alpha$_1$-adrenoceptors could *contribute* to the observed alterations in signal transduction.

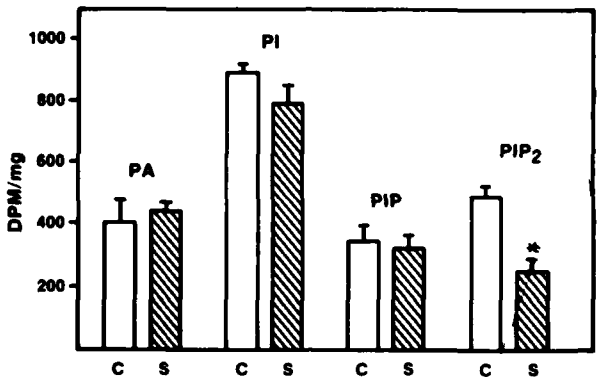

Fig. 2. The effect of intraperitoneal sepsis on basal polyphospoinositide labeling in rat aorta. Rat aortic rings were incubated with [^{32}P]-orthophosphate as described in Methods and phospholipids isolated and quantitated. Data represent mean ± SEM for six individual determinations. (*$P < 0.01$). C = control; S = septic.

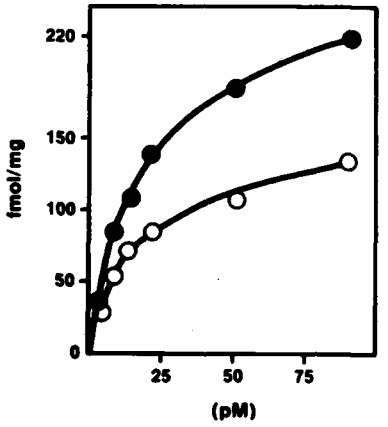

Fig. 3. The effect of intraperitoneal sepsis on rat aortic alpha$_1$-adrenergic receptors. Rat membranes were prepared and incubated with increasing doses of [^{125}I]-HEAT as described in Methods. Data represent mean of duplicate determinations of specific binding for a typical experiment which has been replicated three times. Computer-derived parameter estimates for sham (closed circles) and septic (open circles) rats are shown in Table III.

TABLE III. Alpha$_1$-Adrenoceptor Alteration in Sepsis

	Control		Septic	
Aorta	Kd(nM)	Bmax (Fmol/mg)	Kd(nM)	Bmax (Fmol/mg)
Alpha$_1$-adrenergic receptors	0.016 ± 0.003	349 ± 35	0.013 ± 0.013	146 ± 16[a]

[a]$P < 0.05$ vs. sham operated control rats. Data represent mean ± SEM of computer derived estimates for N = 3–4 separate experiments.

DISCUSSION

Our findings demonstrate that rat aortic alpha$_1$-adrenoceptor mediated PI hydrolysis, as well as alpha$_1$-adrenoceptors, are significantly altered in rat intraperitoneal sepsis. Studies employing rat aortic preparations in vitro have also demonstrated attenuated alpha$_1$-adrenoceptor responsiveness [5]; our findings suggest that at least a part of this change in responsiveness could be related to the signal transduction pathway involving alpha$_1$-adrenoceptors. Our findings further suggest that defects may reside in the synthesis of the substrate (i.e., PIP_2) for the nucleotide-activated phospholipase C. We have recently obtained evidence suggesting that these observed biochemical alterations have further consequences. For example, we discovered that NE-induced bidirectional calcium fluxes [37] as well as NE-induced phosphorylation of contractile proteins is similarly decreased in aortas from septic rats [30].

The mechanism of these observations is unknown and will require further investigation. The absence of changes in receptor affinity argues against the presence of a reversibly bound inhibitor. Such a substance would cause a decrease in affinity without changing the number of binding sites. Generalized receptor down-regulation as well seems unlikely since we have measured several other receptor types in this sepsis model (e.g., opiate, serotonergic, hepatic beta adrenergic) which were unchanged (not shown).

It is significant that we were able to verify the alterations in NE-induced PI breakdown by two independent techniques. The first was the measurement of [^{3}H]-IP accumulation in the presence of LiCl. The main advantage of this technique is its simplicity. This method has certain disadvantages which include the difficulty in measuring the predominant product (IP_3) in rat aorta. The inability to measure this metabolite in rat aorta has been seen by others [29]. We elected to use a second, independent method which entails the measurement of [^{32}P]-PIP_2 breakdown. Although this technique is more laborious, it gave quite similar results. These two techniques showed that the NE-induced PI hydrolysis was significantly decreased in sepsis.

It is conceivable that an endotoxin-derived molecule could elicit the biochemical changes we have discovered. Endotoxin derived molecules have been shown in vitro to activate protein kinase C [31]. It is also known that activation of protein kinase C by phorbol esters induces many of the same changes in PI metabolism in rat aorta as are found in this chronic sepsis model [32]. Thus we showed that phorbol-12,13-dibutyrate as well as phorbol-myristate diacetate attenuated the NE-stimulate PI breakdown in rat aorta [32]. It is also possible that other, unknown, factors contribute to the changes in receptor number and PI metabolism described in this paper.

It is important to note that hepatic alpha$_1$-adrenoceptors and vasopressin receptors are also decreased in experimental sepsis and endotoxemia models [17–20]. These findings have been demonstrated to correlate with the attenuation of alpha$_1$-adrenoceptor and vasopressin-receptor mediated PIP_2 breakdown, intracellular calcium release and phosphorylase a activation in hepatocytes from septic and endotoxin-treated rats [20,33]. Like aorta, the liver shows a marked insensitivity to alpha$_1$-adrenoceptor stimulation in intraperitoneal sepsis [33–36].

In conclusion, we found that rat aortic alpha$_1$-adrenoceptor mediated PI hydrolysis, PIP_2 breakdown and receptor numbers were all decreased in intraperitoneal sepsis. We speculate that such alterations could contribute to the previously observed changes in aortic responsivity to NE in sepsis and endotoxemia.

ACKNOWLEDGMENT

This study was supported by Naval Medical Research and Development Command, Work Unit No. MR04120.05-0001. The opinions and assertions contained herein are the private ones of the writers and are not to be construed as official at large. The excellent technical assistance of J. Disimone and editorial assistance of Deborah A. Hicks are gratefully acknowledged.

REFERENCES

1. Pollack MM, Fields AI, Ruttiman UE: Sequential cardiopulmonary variables of infants and children in septic shock. Crit Care Med 12:554–559, 1984.
2. Chernow B, Rainey TG, Lake CR: Endogenous and exogenous catecholamines in critical care medicine. Crit Care Med 10:409–416, 1982.
3. Chernow B, Roth BL: The pharmacologic support of the cardiovasculature in septic shock. In Sprung CL, Sibbald W (eds): "New Horizons Focus on Septic Shock." Fullerton: Society of Critical Care Medicine, 1986, Chapter 3.
4. Chernow B, Roth BL: Pharmacologic manipulation of the peripheral vasculature in shock: Clinical and experimental aspects. Circ Shock 18:141–155, 1986.
5. Wakabayashi I, Hatake K, Kakishita E, Nagai W: Diminution of contractile response of the aorta from endotoxin-injected rats. Eur J Pharmacol 141:117–122, 1987.
6. Pomerantz W, Casey L, Fletcher JR, Ramwell PB: Vascular reactivity in endotoxin. Adv Shock Res 7:191–198, 1982.
7. Legan E, Chernow B, Parillo J, Roth BL: Activation of phosphatidylinositol turnover in rat aorta by alpha$_1$-adrenergic receptor stimulation. Eur J Pharmacol 110:389–390, 1985.
8. Chiu AT, Pozarth JM, Timmermans PBMWM: Relationship between phosphatidylinositol turnover and Ca^{++} mobilization induced by alpha$_1$-adrenoceptor stimulation in rat aorta. J Pharmacol Exp Ther 240:123–127, 1987.
9. Roth BL, Nakaki T, Chuang D-M, Costa E: Aortic recognition sites for serotonin (5-HT) are coupled to phospholipase C in rat aorta and modulate phosphatidylinositol turnover. Neuropharmacology 23:1223–1235, 1984.
10. Suba E, Roth BL: Prostaglandins activate phosphoinositide metabolism in rat aorta. Eur J Pharmacol 136:325–332, 1987.
11. Majerus PW, Neufield EJ, Wilson DB: Production of phosphoinositide-derived messengers. Cell 37:701–703, 1984.
12. Berridge MJ: Inositol triphosphate and diacylglycerol as second messengers. Biochem J 220:345–360, 1984.
13. Nishizuka Y: The role of protein kinase C in cell surface signal transduction and tumor production. Nature 308:693–698, 1984.
14. Suematsu E, Hirata M, Hashimoto T, Kuriyami H: Inositol-1,4,5-triphosphate releases Ca^{++} from intracellular store sites in skinned single cells of procine coronary artery. Biochem Biophys Res Commun 120:481–485, 1984.
15. Michael RH: Inositol phospholipids and cell surface function. Biochem Biophys Acta 415:81–147, 1975.
16. Litten RZ, Suba EA, Roth BL: Effects of a phorbol ester on rat aortic contraction and calcium influx in the presence and absence of BAY k 8644. Eur J Pharmacol 144(2):185–193, 1987.
17. McMillan M, Chernow B, Roth BL: Alterations in hepatic alpha$_1$-adrenergic receptors in a rat model of chronic sepsis. Circ Shock 19:185–194, 1986.
18. Carcillo JA, Lai J, Venter JC, Roth BL: Alterations in hepatic phospholipase C linked receptors in rat intraperitoneal sepsis. J Surg Res, submitted for publication.
19. Roth BL, Spitzer JA: Altered hepatic vasopressin and alpha$_1$-adrenergic receptors after chronic endotoxin infusion. Am J Physiol 252:E699–E702, 1987.
20. Spitzer JA, Turco ER, Deaciuc IV, Roth BL: Perturbations of transmembrane signaling mechanisms in acute and chronic endotoxemia. In Schlag G and Heinz R (eds): "First Vienna Shock Forum." Prog Clin Biol Res 236A:401–418, 1986.

21. Wichterman K, Baue AI, Chaudry IH: Sepsis and septic shock: A review of laboratory models and a proposal. J Surg Res 29:189–201, 1980.
22. Prpic V, Green KC, Blackmore PF, Exton JR: Vasopressin angiotensin II and alpha$_1$-adrenergic induced inhibition of Ca^{++} transport by rat liver plasma membrane vesicles. J Biol Chem 259:1382–1383, 1984.
23. Roth BL, Nakaki T, Chuang D-M, Costa E: Characterization of $5HT_2$ receptors coupled to phospholipase C in rat aorta: Modulation of phosphoinositide metabolism by phorbol esters. J Pharmacol Exp Ther. 238:486–490, 1986.
24. Nakaki T, Roth BL, Chuang D-M, Costa E: Phasic and tonic components in $5HT_2$ receptor mediated rat aorta contraction: Participation of Ca^{++} channels and phospholipase C. J Pharmacol Exp Ther 234:442–446, 1985.
25. Jolles J, Zwiers H, Dekker A, Wirtz KWA, Gispen WH: Corticotropin-(1–24)-tetracosapeptide affects protein phosphorylation and polyphosphoinositide metabolism in rat brain. Biochem J 194:283–291, 1981.
26. Munson PB, Rodbard D: Ligand: A versatile computerized approach for characterization of ligand binding systems. Anal Biochem 107:220–239, 1980.
27. Bradford MM: A rapid and sensitive method for the quantitation of microgram quantities of protein utilizing the principle of protein-dye binding. Anal Biochem 72:248–254, 1976.
28. Roth BL: Modulation of phosphatidylinositol-4,5-bisphosphate hydrolysis in rat aorta by guanine nucleotides, calcium and magnesium. Life Sci 41:629–634, 1987.
29. Rapoport, RM: Effects of norepinephrine on contraction and hydrolysis of phosphatidylinositols in rat aorta. J Pharm Exp Ther 241:188–194, 1987.
30. Litten RZ, Carcillo JA, Roth BL. Vascular calcium metabolism and protein phosphorylation in rat intraperitoneal sepsis. Circ Shock 21:332, 1987.
31. Wightman PD, Raetz CRH: The activation of protein kinase C by biologically active lipid moieties of lipopolysaccharide. J Biol Chem 259:10048–10052, 1984.
32. McMillan M, Chernow B, Roth BL: Phorbol esters inhibit alpha$_1$-adrenergic receptor stimulated phosphoinositide hydrolysis and contraction in rat aorta: Evidence for a link between vascular contraction and phosphoinositide metabolism. Biochem Biophys Res Commun 134:970–974, 1986.
33. Deaciuc IV, Spitzer, JA: Rat liver free cytosolic Ca^{2+} glycogen phosphorylase in endotoxicosis and sepsis. Am J Physiol 251:R984–R995, 1986.
34. Clemens MG, Chaudry IH, McDermott PH: Regulation of glucose production from lactate in experimental sepsis. Am J Physiol 244:R794–R800, 1983.
35. Clemens MG, Chaudry IH, Daijneau N, Baue AE: Insulin resistance and depressed gluconeogenic capability during early hyperdynamic sepsis. J Trauma 24:701–708, 1984.
36. Carcillo JA, Lai J, Venter JC, Roth BL: Molecular properties of altered alpha$_1$-adrenergic receptors in rat intraperitoneal sepsis. Circ Shock 21:302, 1987.
37. Litten RZ, Carcillo JA, Roth BL: Alterations in bidirectional transmembrane calcium flux occur without changes in protein kinase Ç levels in rat aorta during sepsis. Circ Shock 25:125–130, 1988.

The experiments described in this paper were performed in adherence to the NIH guidelines for the use of experimental animals.

Vol. 156, No. 3, 1988 BIOCHEMICAL AND BIOPHYSICAL RESEARCH COMMUNICATIONS
November 15, 1988 Pages 1308-1315

Reprinted from Biochemical and Biophysical Research Communications 156, 1308-1315 (1988)

SYNTHESIS OF PROSTAGLANDINS AND EICOSANOIDS BY THE MAST CELL SECRETORY GRANULE

Stephen P. Chock* and Elsa A. Schmauder-Chock

Department of Experimental Hematology, Armed Forces Radiobiology Research Institute, Bethesda, MD 20814-5145

Received September 30, 1988

The identification of a non-bilayer phospholipid storage in the secretory granule and the linking of the eicosanoid production with the release of histamine have prompted us to examine whether the secretory granule may also serve as both the source as well as the site of prostaglandin synthesis during exocytosis. By exposing the contents of purified granules to exogenous arachidonic acid at neutral pH, we observed the rapid formation of many eicosanoids. The presence of prostaglandins E_2, D_2 and F_{2a} were identified. The kinetics of E_2 formation was also followed. The localization of the arachidonic acid cascade to the secretory granule explains why the production of eicosanoids is so intimately tied to the process of granule exocytosis.

Eicosanoid production and phospholipid turnover have been linked to mast cell granule exocytosis (1,2). The products of the arachidonic acid cascade, such as prostaglandins, leukotrienes, and thromboxanes, are main constituents of the so-called "slow reacting substance of anaphylaxis" (SRS-A) (1,3). Like many other cell types, the mast cell can incorporate exogenous arachidonic acid into its cellular phospholipid. The stimulation of mast cells which have been pre-loaded with radioactive arachidonic acid can result in the release of both labeled arachidonic acid and eicosanoids (4,5). However, the phospholipid pool which provides the arachidonic acid for the synthesis of eicosanoids has not been identified.

Recently, we found that the secretory granule of the quiescent mast cell contains a large amount of matrix-bound phospholipid which exists in non-bilayer form[a]. This pool of phospholipid is believed to be responsible for sustaining the process of de novo membrane assembly which takes place during secretory granule activation (6-9). On activation of the granule, some of this phospholipid rapidly assembles into bilayer vesicles which insert into

*Correspondence address: 203 Cedar Avenue, Gaithersburg. MD 20877, USA.

Abbreviations used: PGE_2, prostaglandin E_2; PGD_2, prostaglandin D_2; $PGF_{2\alpha}$, prostaglandin $F_{2\alpha}$; PGH_2, prostaglandin H_2; LTB_4, leukotriene B_4; HEPES, 4-(2-hydroxyethyl)-1-piperazineethanesulfonic acid; PMSF, phenylmethylsulfonyl fluoride; RIA, radioimmunoassay; TLC, thin layer chromatography.

[a]Manuscript submitted.

0006-291X/88 $1.50

the perigranular membrane. The insertion of these newly assembled vesicles enables the perigranular membrane of the activated granule to enlarge and approach contact with other membranes. The contact between the enlarging perigranular membrane and the plasma membrane results in their fusion and the formation of a pore through which the granule contents are extruded. Since this membrane-expanding event may not require the complete utilization of the matrix-stored phospholipid, a significant amount of it may be secreted with other granule components during exocytosis. This remnant phospholipid which also contains arachidonic acid, can serve as the substrate needed for the synthesis of eicosanoids (10). If the enzymes of the arachidonic acid cascade are also present in the granule matrix along with the phospholipid, a concomitant activation of these enzymes during granule activation would account for the parallel kinetics of prostaglandin production with the release of histamine during anaphylaxis.

In this communication, we present evidence which suggests the presence of the enzymes of the arachidonic acid cascade within the secretory granule of the mast cell. By simply exposing [1-^{14}C]-arachidonic acid to the contents of purified granules at neutral pH, we have detected the rapid formation of at least 10 different arachidonic acid metabolites. From these, the presence of PGE_2, PGD_2, and PGF_{2a} have been identified. Based on these results, we conclude that the secretory granule can serve as the source as well as the site of prostaglandin and eicosanoid synthesis during histamine release. This also implies that the process of granule activation is accompanied by the initiation of the arachidonic acid cascade leading to the production of the various lipid-derived mediators during exocytosis.

MATERIALS AND METHODS The procedure for granule preparation is similar to that which has been described for the determination of granule phospholipid contents[a]. Briefly, purified mast cells were obtained from Sprague-Dawley rats according to published procedure using a serum albumin gradient. Granules were obtained by graded sonication of the mast cells using a sonifier (Bramson W350) equipped with a microprobe. The combined supernatants which contained the granules were centrifuged at 72xg for 10 min to remove aggregates. The granules were pelleted at 960xg for 15 min. To avoid cytosolic contamination, granules were washed by resuspension in buffer and pelleted at 960xg. The purity of the granule can be seen in Fig. 1. Routine electron microscopy was carried out as described previously (6-7).

To assay for prostaglandins, the granule pellet was resuspended in an assay buffer containing 0.1% (w/v) digitonin (Fluka Bio Chemika), 0.5 mM $CaCl_2$, 0.05 mg/ml PMSF, 0.1 mg/ml leupeptin (Sigma Chemicals), 10 mM HEPES pH 6.8, and 37 uM of [1-^{14}C]-arachidonic acid (New England Nuclear, Du Pont). After a brief sonication (3x 3-sec burst), the reaction mixture was incubated in room temperature (21 ^{o}C) for a specified length of time. The reaction was quenched with cold acetone and prostaglandins were extracted according to the procedure of Salmon and Flower (11). The solvent systems for TLC were: (I) the organic phase of ethyl acetate:2,2,4-trimethylpentane:acetic acid:water (110:50:20:100, v/v/v/v) and (II) diethylether:methanol:acetic acid (90:1:2, v/v/v) (11,12). PGE_2 was also verified and quantitated using an RIA procedure (New England Nuclear, Du Pont). The HP-K high performance TLC plates were

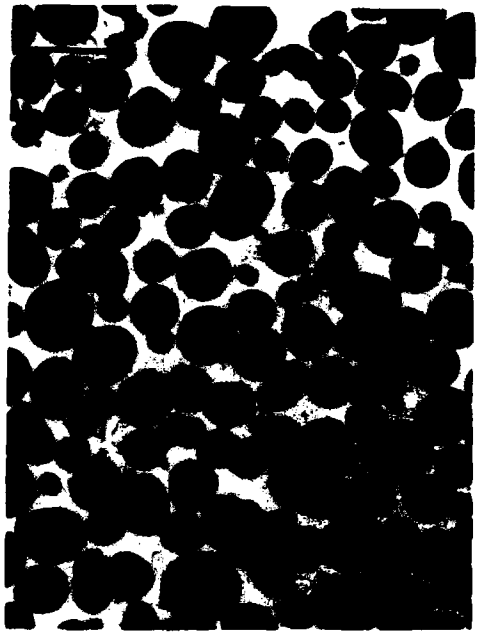

Fig. 1. Electron micrograph of the purified mast cell granules. The bar in the lower right corner represents 1 μm.

from Whatmann and were used without pre-activation. Eicosanoid standards were purchased from Cayman Chemical (Ann Arbor, MI). All other chemicals used were of reagent grade.

RESULTS By exposing a small amount of [1-^{14}C]-arachidonic acid to the contents of purified granules at 21 ^{o}C, pH 6.8, we can demonstrate a rapid conversion of this labeled substrate into various eicosanoids including PGE_2 and PGD_2. A typical result of such an experiment is shown in Fig. 2. In this figure, lane A is the control while lanes B, C, and D represent individual samples incubated for 0, 10, and 30 min respectively. The main reaction products are distributed in 7 major bands with the approximate Rf values of 0, 0.23, 0.37, 0.55, 0.64, 0.75, and 0.91 respectively. When compared with the Rf values of standard eicosanoids, Band 1, Band 2, Band 3, Band 4, Band 5, and Band 7 have similar mobility as phospholipid, PGF_{2a}, PGE_2, PGD_2, LTB_4, and arachidonic acid, which have corresponding Rf values of 0, 0.24, 0.38, 0.5, 0.61, and 0.95 respectively in the same TLC solvent system.

Fig. 3 shows that when a 5-minute reaction mixture is analyzed using a two-dimensional chromatography system, each of the major bands seen in Fig. 2 can be further resolved into more than one radioactive product. Band 1 has been identified as phospholipid. Band 2 is tentatively identified as PGF_{2a}. Band 3 is made up of at least 2 components and the major one is identified as PGE_2. There is also a spot between band 3 and band 4. Band 4 has relative

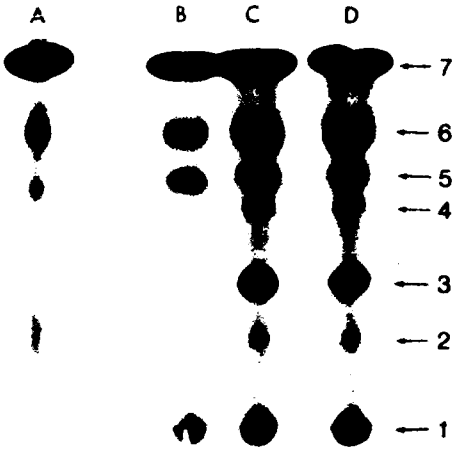

Fig. 2. Autoradiogram of eicosanoids produced by the incubation of [1-^{14}C]-arachidonic acid with dispersed mast cell secretory granules in vitro. Lanes A-D represent chromatograms of control (substrate in reaction mixture without protein), 0 min, 10 min, and 30 min samples incubated at 21°C respectively. The minor spots in the control sample (lane A) are inherent impurities of the substrate. The resulted eicosanoids are resolved into 7 major bands by TLC solvent system (I). The major components of each band are: phospholipids (Band 1), PGF_{2a} (Band 2), PGE_2 (Band 3), PGD_2 (Band 4), and arachidonic acid (Band 7). (Band 5) and (Band 6) contain several unidentified eicosanoids along with the contaminants of arachidonic acid. The Rf values for the various bands are: 0, 0.23, 0.37, 0.55, 0.64, 0.75, and 0.91 respectively.

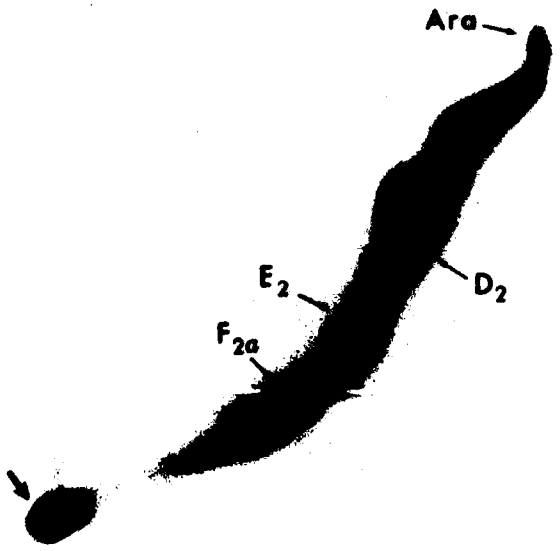

Fig. 3. Two-dimensional TLC resolution of labeled eicosanoids resulted from a 5-minute incubation of [1-^{14}C]-arachidonic acid with granule matrix contents. Sample was spotted at the lower left corner (arrow) and chromatographed in solvent system (I) to resolve the sample vertically into a similar 7-band pattern with Rf values corresponding to those shown in Fig. 2. The horizontal direction was chromatographed in solvent system (II) to further resolve each major band horizontally into several components. Spots for arachidonic acid, PGD_2, PGE_2, and PGF_{2a} have been assigned.

mobility similar to that of PGD_2 which is a known mast cell eicosanoid (1). Band 5 and Band 6 are each composed of at least two different components. One of the spots of Band 5 might be LTB_4 which has similar mobility in this TLC system. The bulk of band 7 is unreacted arachidonic acid. Without counting the components of band 1, there are at least 10 eicosanoids synthesized within 5 min at 21 ^{o}C by the mast cell granule enzymes when exogenous arachidonic acid is added.

When the time course of PGE_2 production is followed by using the RIA procedure, its rate of production appeared quite linear for the first five minutes (Fig. 4). The initial rate of PGE_2 production for this particular experiment is equal to approximately 30 pg/ul/min which corresponds to about 25 pg/min/ug granule protein. The protein concentration is estimated by assuming that an average granule contained about 0.38 pg protein[a] and the assay solution contained approximately $3x10^6$ granules/ul. This rate is expected to vary according to experimental conditions. Our results may not represent those that can be achieved under the optimal assay conditions.

DISCUSSION As much as 18% of the total phospholipid fatty acid of the mast cell is made up of arachidonic acid (13). Since the current dogma assumes that cellular phospholipid exists only in bilayer form, it follows that the phospholipid which provides the arachidonic acid for the eicosanoid synthesis

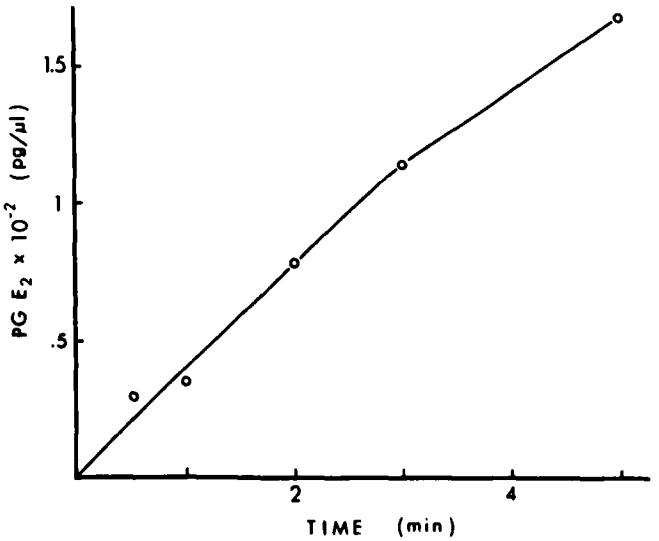

Fig. 4. The time course of prostaglandin E_2 production by granule enzymes as determined by the RIA procedure. The experiment was carried out as described in Materials and Methods. The protein concentration was about 1.2 mg/ml and the added arachidonic acid was 37 µM. The initial rate of about 30 pg/ul/min is equivalent to approximate 25 pg PGE_2/µg protein/min when the granule protein concentration is taken into account.

must also originate from the cellular membrane (14, 15). However, this assumption cannot explain how the arachidonic acid or the phospholipid can become so readily available to the eicosanoid synthesizing enzymes during the stimulation-secretion coupling process. For the mast cell, the antigen challenge of the IgE receptor-mediated exocytosis also results in triggering the arachidonic acid cascade leading to the rapid formation of eicosanoids (1, 16). The initial time course for the eicosanoid production also closely parallels the time course for the histamine release during an anaphylactic reaction (4,16). The time course of histamine release can be very rapid (17). Since receptor activation is a membrane-mediated event, to explain the rapid and intimate coupling of these two processes, it is tempting to assume that the eicosanoid synthesizing enzymes might be localized on the plasma membrane near the IgE receptors. However, such an assumption would also require the availability of a high calcium pool needed for the enzyme activity. To date, the presence of a high calcium pool in association with the plasma membrane has not been demonstrated. The use of immunocytochemical technique has also failed to demonstrate cyclo-oxygenase activity at the plasma membrane (18). Furthermore, the major enzymes for the conversion of PGH_2 to PGD_2 in the eicosanoid biosynthetic pathway are found in the cytosol instead of the microsomal fraction (19). All these contradictions suggest the existence of a different explanation for the intimate linking between the arachidonic acid cascade and the release of histamine.

Our recent identification of a non-bilayer phospholipid storage in the secretory granules of the mast cell raises a strong possibility that this phospholipid pool may be responsible for providing the bulk of the arachidonic acid needed in the synthesis of the eicosanoids during histamine release (10). The presence of a high calcium pool in the granule can easily satisfy the calcium requirement for the various enzyme activities (20). The present finding which localizes the eicosanoid synthesizing enzymes to the secretory granule not only makes the linking of the histamine-release process to the production of eicosanoids a physical possibility, it also explains why the initial time courses for both the histamine release and the production of eicosanoids are so closely parallel. The simultaneous activation of the granule and the initiation of the arachidonic acid cascade provide the basis for the coupling of exocytosis to the formation of lipid-derived mediators.

In this communication, we have demonstrated that exposure of arachidonic acid to the granule matrix contents at neutral pH is sufficient to initiate the arachidonic acid cascade. This finding underscores the important role of pH in granule activation. Many enzymes are inhibited by an acidic pH. In fact the pH of the quiescent granule has been suggested to be about 5 (21). This acidic pH is necessary to suppress the granule protease activity which can cause the elevation of intragranular pH and osmotic pressure. If we are

correct in postulating that an influx of cellular water into the granule is the early event in the activation of the granule, then this water influx may also contribute to local pH changes. If the influx of cellular water were tied to an influx of alkaline ions, this would provide an effective way to raise the intragranular pH and to activate the granule enzymes which include those involved in the arachidonic acid cascade. The possibility for the existence of a K^+/H^+ or Na^+/H^+ exchange mechanism on the perigranular membrane should be investigated.

Following the fusion of the activated granule with the plasma membrane, the granule contents are exteriorized and become exposed to the extracellular pH. This alkalization assures the activation of the various granule enzymes and the continued synthesis of eicosanoids. This continued synthesis may account for the accumulation of PGD_2 detected beyond the time point when the release of histamine has already leveled off or decreased. The exposure of an eicosanoid synthesizing machinery to the extracellular environment may also have profound effects on the production and the breakdown of the mediators. The nonenzymatic conversion of PGH_2 to PGD_2 in the presence of serum albumin is an example of how the local environment can alter the outcome of the arachidonic acid cascade (22).

Although we have not identified any product of the lipoxygenase pathways in this study, yet we have implied that these enzymes, if present, can also be found in the granule along with the cyclo-oxygenase. This implication is based on the fact that many products of the lipoxygenase pathways, such as the leukotrienes, the hydroperoxy- and hydroxy-eicosatetraenoic acids, have already been detected together with prostaglandins and other products of the cyclo-oxygenase pathways during the anaphylactic reaction (1). Although our present experimental conditions may not be conducive for the activity of the lipoxygenases, we suspect that LTB_4 might be present in Band 5 (Fig. 2) since Band 5 contains component of similar Rf value as the LTB_4 standard. Some of the hydroperoxyeicosatetraenoic acids and the hydroxyeicosatetraenoic acids may also be present in Band 6 and Band 7 in Fig. 2. Until proven otherwise, it might be superfluous at this point to postulate a different cellular compartment for the lipoxygenases.

To extrapolate our present findings to the mechanism of anaphylaxis, it is important to realize that the triggering of the arachidonic acid cascade during granule activation also depends on the availability of the substrate, arachidonic acid. This means that the release of the arachidonic acid from the hydrolysis of matrix-bound phospholipid by phospholipases is crucial to the initiation of the arachidonic acid cascade *in vivo*. In agreement with this, our preliminary data has also suggested the presence of a phospholipase A_2 activity in the mast cell granule, and its presence has enabled us to elucidate the synthesis of PGE_2 from endogenous arachidonic acid. Since the

granules can also rapidly synthesize phospholipids from exogenous arachidonic acid (Band 1 in Fig. 2) it suggests that the granules must also possess the machinery for phospholipid turnover. All these suggest that the secretory granule may hold the key to the many rapid biochemical events associated with exocytosis, which includes de novo membrane assembly, rapid phospholipid turnover, and the production of the lipid-derived mediators.

ACKNOWLEDGMENTS We wish to thank Dr. Thomas L. Walden for help in the RIA assays, Mr. Joe L. Parker and Miss Christine S. Cho for technical assistance, and Dr. Sue Goo Rhee for scientific hospitality.

REFERENCES

1. Metcalfe, D.D., Kaliner, M., and Donlon, M.A. (1981) CRC Crit. Rev. Immunol. 3, 23-74.
2. Cockcroft, S. (1982) Cell Calcium 3, 337-349.
3. Yecies, L.D., Wedmer, H.J., Johnson, S.M., Jakschik, B.A., and Parker, C.W. (1979) J. Immunol. 122, 2083-2089.
4. Kawabe, H., Hayashi, H., and Hayaishi, O. (1987) Biochem. Biophys. Res. Commun. 143, 467-474.
5. Garcia-Gil, M. and Siraganian, R.P. (1986) J. Immunol. 136, 3825-3828.
6. Chock, S.P. and Schmauder-Chock, E.A (1985) Biochem. Biophys. Res. Commun. 132, 134-139.
7. Schmauder-Chock, E.A. and Chock, S.P. (1987) Histochemical J. 19, 413-418.
8. Chock, S.P. and Chock, E.S. (1985) Fed. Proc. 44, 1324 (5341 abs.).
9. Schmauder-Chock, E.A. and Chock, S.P. (1987) In: Proceedings of the 45th Annual Meeting of the Electron Microscopy Society of America. (Bailey, G.W. ed.) pp.782-783. San Francisco Press.
10. Chock, S.P. and Schmauder-Chock, E. (1987). In: Prostaglandins and Lipid Metabolism in Radiation Injury. (Walden, T.L. and Hughes, H.N., eds.) pp 127-132. Plenum Press, N.Y.
11. Salmon, J.A. and Flower, R.J. (1982) In Methods in Enzymology (Lands, W.E.M. and Smith, W.L. eds.) Vol. 86 pp.477-493. Academic Press N.Y.
12. Bailey, J.M., Bryant, R.W., Feinmark, S.J., and Makheja, A.N. (1977) Prostaglandins 13, 479-492.
13. Strandberg, K. and Westerberg, S. (1976) Mol. Cell. Bioch. 11, 103-107
14. Samuelsson B. (1982) Biosci. Rep. 3, 791-813.
15. Alberts, B., Bray, D., Lewis, J., Raff, M., Roberts, K., and Watson, J.D. (1983) Molecular biology of the cell. p350. Garland Publishing Inc., N.Y. and London.
16. Ishizaka, T. and Ishizaka, K. (1984) Prog. Allergy 34, 188-235.
17. Douglas, W.W. (1974) Biochem. Soc. Symp. 39, 1-28.
18. Rollins, T.E., and Smith, W.L. (1980) J. Biol. Chem. 255, 4872-4875.
19. Shimizu, T., Yamamoto, S., and Hayaishi, O. (1979) J. Biol. Chem. 254, 5222-5228.
20. Chock, E.S., Donlon, M.A., Fiori, C.E., and Catravas, G.N. (1982) J. Cell Biol. 95, 409a.
21. Lagunoff, D. and Rickard, A. (1983) Exptl. Cell Res. 144, 353-360.
22. Hamberg, M. and Fredholm, B.B. (1976) Biochim. Biophys. Acta 431, 189-193.

INT. J. RADIAT. BIOL., 1988, VOL. 54, NO. 2, 195–204

Effect of DNA conformation on the hydroxyl radical-induced formation of 8,5′-cyclopurine 2′-deoxyribonucleoside residues in DNA

MARIE-LUISE DIRKSEN†, WILLIAM F. BLAKELY‡, ERIC HOLWITT‡, and MIRAL DIZDAROGLU§

† Dermatology Branch, National Cancer Institute, National Institutes of Health, Bethesda, MD 20892
‡ Radiation Science Department, Armed Forces Radiobiology Research Institute, Bethesda, MD 20814, and
§ Center for Chemical Physics, National Bureau of Standards, Gaithersburg, MD 20899, U.S.A.

(Recieved 11 September 1987; revision 17 February 1988; accepted 18 February 1988)

Reactions of hydroxyl radicals with DNA form a variety of base and sugar products and 8,5′-cyclopurine 2′-deoxyribonucleoside residues in DNA. Here we report the effect of DNA conformation on the yields of 8,5′-cyclopurine 2′-deoxynucleosides and the ratios of their (5′R)- and (5′S)-diastereomers. Calf thymus DNA in native (double-stranded DNA) or heat-denatured form (single-stranded DNA) was exposed to hydroxyl radicals generated by ionizing radiation in nitrous oxide-saturated phosphate buffer. Doses ranging from 10 to 40 Gy were used to ensure low levels of damage to DNA and thus to preserve its secondary structure in experiments with double-stranded DNA (ds-DNA). After irradiation, DNA was hydrolysed enzymatically to 2′-deoxyribonucleosides. The hydrolysates were dried, trimethylsilyated, and analyzed by capillary gas chromatography–mass spectrometry with selected-ion monitoring. An internal standard was used for quantitative measurements and added to DNA samples prior to enzymatic hydrolysis. The yields of 8,5′-cyclo-2′-deoxyadenosine and 8,5′-cyclo-2′-deoxyguanosine in single-stranded DNA (ss-DNA) were higher than those in ds-DNA. The (5′R)-diastereomers of both compounds were found to predominate over their (5′S)-diastereomers in ss-DNA. In contrast, the yields of the (5′S)-diastereomers in ds-DNA were slightly higher than those of the (5′R)-diastereomers. The *G* values of 8,5′-cyclo-2′-deoxyadenosine in ss-DNA and ds-DNA were 0·042 and 0·025, respectively. Those of 8,5′-cyclo-2′-deoxyguanosine in ss-DNA and ds-DNA were 0·038 and 0·017, respectively.

1. Introduction

Free radicals generated *in vivo* by cellular metabolism appear to play an important role in a number of human diseases (for a review see Halliwell and Gutteridge 1985). The interaction of external agents, such as ionizing radiations, with cellular water can also form free radicals in living systems. Since DNA is considered a critical cellular target for attack by free radicals, e.g. hydroxyl radicals, the free radical chemistry of DNA has been the subject of extensive study (for a review see von Sonntag 1987). A large number of products from both the sugar moiety and the heterocyclic bases in DNA have been isolated and identified (von Sonntag 1987).

In the case of purine nucleosides and nucleotides, one unique reaction induced by hydroxyl radicals is the intramolecular cyclization between the carbon-5′ (C–5′) of the sugar and the C-8 of the purine in the absence of oxygen. This reaction has been observed in adenosine-5′-monophosphate (5′-AMP) (Keck 1968, Raleigh *et al.* 1976, Raleigh and Fuciarelli 1985), in 2′-deoxyadenosine (dAdo) (Mariaggi *et al.* 1976), in polyadenlyic acid (polyA) (Fuciarelli *et al.* 1986), and in 2′-deoxyguanosine (dGuo) (Dizdaroglu 1986 a) and the resulting products have been isolated and identified. Recently, the (5′R)- and (5′S)-diastereomers of 8,5′-cyclo-dGuo have been identified in DNA γ-irradiated in aqueous solution and in DNA isolated from γ-irradiated human cells (Dizdaroglu 1986 a, Dizdaroglu *et al.* 1987). An immunochemical assay of 8,5′-cyclo-dAdo (as the sum of the (5′R)- and (5′S)-diasteromers) in DNA γ-irradiated in aqueous solution has also been reported (Fuciarelli *et al.* 1985). The stereoselectivity of the cyclization process appears to depend much on the nature of the substrate, as variations have been reported for the ratios of the (5′R)- and (5′S)-diastereomers of 8,5′-cyclo-Ado formed from adenosine and from 5′-AMP and in polyA (Fuciarelli *et al.* 1986). Moreover, the ratio of the (5′R)- and (5′S)-diastereomers of 8,5′-cyclo-dGuo in DNA γ-irradiated in unbuffered aqueous solution has been found to be different from that in DNA isolated from γ-irradiated human cells (Dizdaroglu 1986 a, Dizdaroglu *et al.* 1987). These findings, and the findings by Fuciarelli *et al.* (1986), prompted us to investigate the effect of DNA conformation on the yield and ratios of the diastereomers of 8,5′-cyclopurine 2′-deoxyribonucleoside residues produced in DNA in aqueous solution by ionizing radiation-generated hydroxyl radicals. This paper also describes for the first time the identification of both the (5′R)- and (5′S)-diastereomers of 8,5′-cyclo-dAdo in DNA γ-irradiated in N_2O-saturated aqueous solution.

2. Experimental†

2.1. *Materials*

Calf thymus DNA, 2′-deoxyadenosine (dAdo), deoxyribonuclease I, snake venom exonuclease, and spleen exonuclease were obtained from Sigma Chemical Co. Alkaline phosphatase was from Boehringer Mannheim. Acetonitrile and bis(trimethylsilyl)trifluoroacetamide (BSTFA) were purchased from Pierce Chemical Co. Samples of (5′S)-8,5′-cyclo-adenosine [(5′S)-8,5′-cyclo-Ado], and (5′R)- and (5′S)-diastereomers of 8,5′-cyclo-dAdo were kindly provided by Dr J. A. Raleigh (Cross Cancer Institute, Edmonton, Alberta, Canada), and Dr K. T. Wheeler (Bowman Gray School of Medicine, Winston-Salem, NC), respectively.

2.2. *Preparation of DNA solutions and irradiations*

Double-stranded DNA (ds-DNA) solutions were prepared by dissolving calf thymus DNA (0·5 mg/ml) in 30 mmol dm^{-3} phosphate buffer (pH 7·2). The melting temperature of the DNA in this solution was 78·2°C. Single-stranded DNA (ss-DNA) was prepared as described by Alberts and Herrick (1971). Briefly,

† Certain commercial equipment or materials are identified in this paper in order to specify adequately the experimental procedure. Such identification does not imply recommendation or endorsement by the National Bureau of Standards, nor does it imply that the materials or equipment identified are necessarily the best available for the purpose.

an aliquot of the ds-DNA solution was heated to 95°C for 5 min followed by rapid cooling on ice. Solutions of ds-DNA and ss-DNA were saturated with oxygen-free nitrous oxide and then irradiated in a ^{60}Co-γ-source at doses ranging from 10 to 40 Gy at a dose rate of 5 Gy/min. The dose rate of the source was determined by ionization chambers. Aliquots of unirradiated and irradiated DNA solutions were exhaustively dialyzed against water and then lyophilized. A solution of dAdo (1 mmol dm^{-3}) was saturated with nitrous oxide, γ-irradiated at a dose of 200 Gy, and then lyophilized.

2.3. *Enzymatic hydrolysis and derivatization*

One milligram DNA samples were dissolved in 0·5 ml of 10 mmol dm^{-3} Tris·HCl buffer (pH 8·5) containing 2 mmol dm^{-3} $MgCl_2$, and then an aliquot of the internal standard, i.e. (5'S)-8,5'-cyclo-Ado, was added. The samples were incubated with deoxyribonuclease I (100 units), spleen exonuclease (0·01 unit), snake venom exonuclease (0·5 unit), and alkaline phosphatase (10 units) for 24 h at 37°C. Subsequently, samples were lyophilized and trimethylsilylated in polytetrafluoroethylene-capped hypovials (Pierce) with 0·2 ml of a mixture of BSTFA and acetonitrile (1:1) by heating for 30 min at 130°C. Unirradiated samples were treated in the same manner. Samples of dAdo were derivatized as above.

2.4. *Gas chromatography–mass spectrometry (GC–MS)*

A Hewlett-Packard Model 5970A Mass Selective Detector controlled by a Hewlett-Packard Model 59970A Computer Work Station and interfaced to a Hewlett-Packard Model 5890A Gas Chromatograph was used. The injection port, the ion source and the GC–MS interface were maintained at 250°C. Separations were carried out using a fused silica capillary column (25 m × 0·32 mm internal diameter) coated with crosslinked 5 percent phenyl methylsilicone gum phase (film thickness, 0·17 μm). Helium was used as carrier gas at an inlet pressure of 20 kPa. Mass spectra were obtained at 70 eV. The split mode was used for injections.

3. Results

3.1. *Identification of (5'R)- and (5'S)-8,5'-cyclo-dAdo in DNA*

Samples of dAdo γ-irradiated in N_2O-saturated aqueous solution were trimethylsilylated and analyzed by GC–MS to determine whether both the (5'R)- and (5'S)-diastereomers of 8,5'-cyclo-dAdo were present, and to obtain information about their gas chromatographic and mass spectral properties. The GC–MS technique has been shown previously to be a useful tool for characterization of free radical-induced sugar and base damage in DNA (for a review see Dizdaroglu 1986 b).

Figure 1 shows a total-ion chromatogram obtained from a trimethylsilylated sample of γ-irradiated dAdo. Peaks 1 and 6 correspond to the trimethylsilyl (Me_3Si) derivatives of adenine and dAdo, respectively. Peak 2 also represents dAdo with one Me_3Si group missing from the molecule. Peak 5 corresponds to the Me_3Si derivative of 8-hydroxy-dAdo. The expected molecular ion (m/z 465) of the Me_3Si derivative of 8,5'-cyclo-dAdo [8,5'-cyclo-dAdo$(Me_3Si)_3$] was monitored simultaneously (not shown here) and found to be present in the mass spectra of the products represented by peaks 3 and 4. The mass spectra taken from these peaks are illustrated in figures 2A and 2B, respectively. As can be seen, these mass spectra are essentially identical to each other with only slight differences in the intensities of the

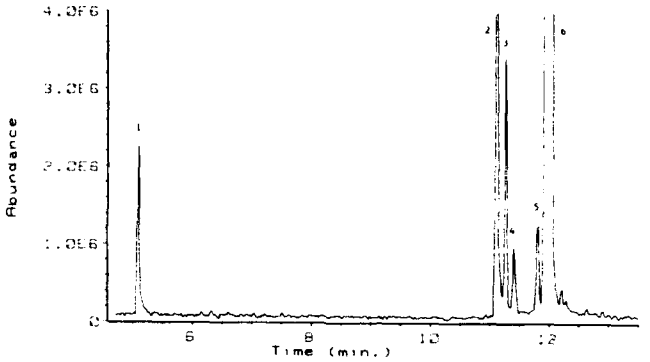

Figure 1. Total-ion chromatogram obtained from a trimethylsilylated sample of dAdo γ-irradiated in N_2O-saturated aqueous solution (dose 200 Gy). Column details were as in the Experimental section. Temperature program was from 150 to 250°C at 10°C/min. *Peaks*: **1:** adenine $(Me_3Si)_2$; **2:** dAdo$(Me_3Si)_2$; **3:** (5'R)-8,5'-cyclo-dAdo$(Me_3Si)_3$; **4:** (5'S)-8,5'-cyclo-dAdo$(Me_3Si)_3$; **5:** 8-hydroxy-dAdo$(Me_3Si)_4$; **6:** dAdo$(Me_3Si)_3$.

characteristic ions. This clearly indicates the presence of two isomeric compounds. The mass spectra in figures 2A and 2B could be interpreted here as the two possible (5'R)- and (5'S)-diastereomers of 8,5'-cyclo-dAdo$(Me_3Si)_3$ (peaks 3 and 4, respectively) on the basis of the gas chromatographic and mass spectral behaviour of the Me_3Si *derivatives* of other 8,5'-cyclo-purine nucleosides, which have been documented recently (Dizdaroglu 1986a). A GC–MS analysis of authentic compounds, which were available, confirmed these interpretations. A fragmentation mechanism of 8,5'-cyclo-dAdo$(Me_3Si)_3$ depicting the formation of the characteristic ions is shown below:

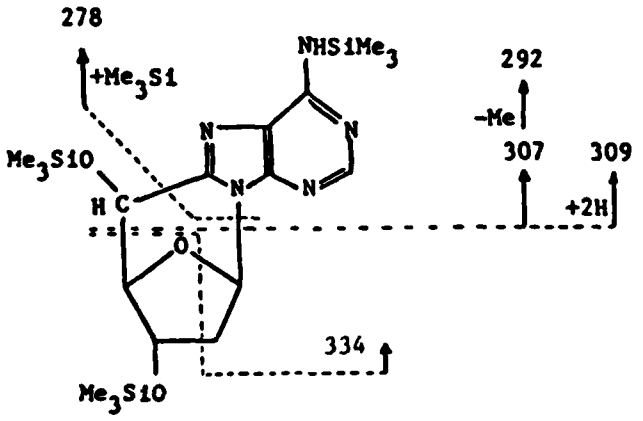

Ions at m/z 465, 450 and 360 in figures 2A and 2B (not shown in the scheme above) correspond to the molecular ion $(M^+\cdot)$, $(M-CH_3)^+$ and $(M-CH_3-Me_3SiOH)^+$, respectively.

Using the information obtained above, the GC–MS technique with selected-ion monitoring (GC–MS/SIM) was used to search for the (5'R)- and (5'S)-

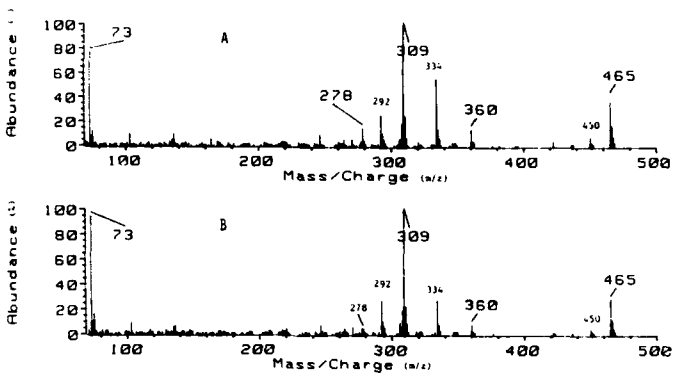

Figure 2. **A:** Mass spectrum taken from peak 3 in figure 1; **B:** mass spectrum taken from peak 4 in figure 1.

diastereomers of 8,5'-cyclo-dAdo in the enzymatic hydrolysates of DNA γ-irradiated in N_2O-saturated aqueous solution at doses ranging from 10 to 40 Gy. For this purpose a number of characterisitic ions, i.e. m/z 465, 450, 360, 334, 309, 292 and 278, from the mass spectrum of 8,5'-cyclo-dAdo$(Me_3Si)_3$ (see figure 2) were monitored simultaneously. Figures 3A and 3B illustrate the ion-current profiles at m/z 465 obtained from samples of ds-DNA and ss-DNA, respectively, γ-irradiated at 40 Gy. Figures 3A and 3B also contain the ion-current profiles of m/z 553, which is the $M^+\cdot$ of 8,5'-cyclo-dGuo$(Me_3Si)_4$. This compound has recently been identified in γ-irradiated DNA (Dizdaroglu 1986a). Peaks 3 and 5 correspond to the (5'R)- and (5'S)-diastereomers of 8,5'-cyclo-dGuo$(Me_3Si)_4$. The

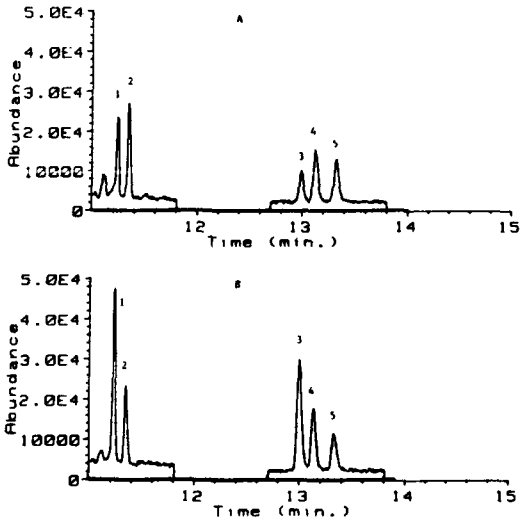

Figure 3. Ion current profiles at m/z 465 and 553 obtained during GC–MS/SIM analysis of trimethylsilylated enzymatic hydrolysates of DNA samples γ-irradiated in N_2O-saturated aqueous solution at 40 Gy. **A:** ds-DNA; **B:** ss-DNA. Column details were as in Figure 1. *Peaks*: **1** and **2:** (5'R)- and (5'S)-diastereomers of 8,5'-cyclo-dAdo$(Me_3Si)_3$, respectively; **3** and **5:** (5'R)- and (5'S)-diastereomers of 8,5'-cyclo-dGuo$(Me_3Si)_4$, respectively; **4:** (5'S)-8,5'-cyclo-Ado$(Me_3Si)_4$ (internal standard).

m/z 553 ion is also the $M^+ \cdot$ of the Me_3Si derivative of 8,5′-cyclo-Ado (peak 4 in figure 3), which was added as an internal standard to the DNA samples prior to enzymatic hydrolysis. In Figures 3A and 3B, discernible peaks of m/z 465, i.e. peaks 1 and 2, are seen at the expected retention times of (5′R)- and (5′S)-diastereomers of 8,5′-cyclo-dAdo$(Me_3Si)_3$. For identification, partial mass spectra were obtained subsequently on the basis of the recorded characteristic ions of 8,5′-cyclo-dAdo$(Me_3Si)_3$ and their relative abundances. As an example, a partial spectrum obtained from the signals at the elution time of (5′S)-8,5′-cyclo-dAdo$(Me_3Si)_3$ (peak 2 in figure 3) is illustrated in figure 4. This partial spectrum is directly correlatable to that of (5′S)-8,5′-cyclo-dAdo$(Me_3Si)_3$ in figure 2B. Similarly, the partial spectrum obtained from the signals at the GC-retention time of (5′R)-8,5′-cyclo-dAdo$(Me_3Si)_3$ (peak 1 in figure 3) was also correlated to the mass spectrum of (5′R)-8,5′-cyclo-dAdo$(Me_3Si)_3$ illustrated in figure 2A (results not shown here). This indicates that both the (5′R)- and (5′S)-diastereomers of 8,5′-cyclo-dAdo were identified in γ-irradiated DNA.

3.2. *Yields of 8,5′-cyclopurine 2′-deoxynucleoside residues in DNA*

The quantitative measurement of 8,5′-cyclopurine 2′-deoxynucleoside residues in DNA γ-irradiated in N_2O-saturated aqueous solution at doses ranging from 10 to 40 Gy was carried out using the GC–MS/SIM technique. For this purpose, (5′S)-8,5′-cyclo-Ado was used as an internal standard. DNA samples containing a known amount of the internal standard were hydrolyzed enzymatically. This was followed by trimethylsilylation and GC–MS/SIM analysis. The Me_3Si derivative of (5′S)-8,5′-cyclo-Ado has the same fragmentation patterns as 8,5′-cyclo-dGuo$(Me_3Si)_4$ (Dizdaroglu 1986a) and 8,5′-cyclo-dAdo$(Me_3Si)_3$ (see above). Moreover, the mass spectra of these compounds show molecular ions with nearly equal relative intensities. For this reason, the m/z 465 ion for 8,5′-cyclo-dAdo$(Me_3Si)_3$ and the m/z 553 ion for both 8,5′-cyclo-dGuo$(Me_3Si)_4$ and 8,5′-cyclo-Ado$(Me_3Si)_4$ were recorded simultaneously for quantitative analysis and the relative molar response factors of molecular ions for these three compounds were assumed to be equal. Figures 3A and 3B illustrate representative ion-current profiles at m/z 465 and 553 obtained during the GC-MS/SIM analysis of samples of ds-DNA and ss-DNA, respectively. These profiles clearly show the differences between the ratios of the diastereomers of each 8,5′-cyclopurine 2′-deoxynucleoside and between their yields in ds-DNA and ss-DNA. A plot of the total yields of 8,5′-cyclopurine 2′-deoxynucleosides in ds-DNA and ss-DNA versus radiation dose shows a linear dose-yield relationship (figures 5 and 6). The yield of each of the 8,5′-cyclopurine 2′-deoxynucleosides in ss-DNA was higher than in ds-DNA. A comparison of figures 5 and 6 shows that the yields of both 8,5′-cyclopurine

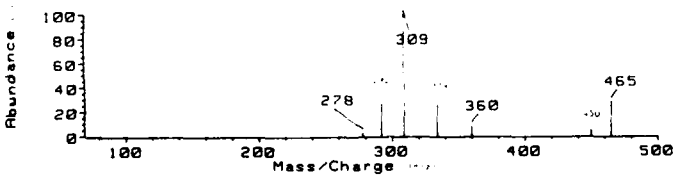

Figure 4. Partial mass spectrum generated on the basis of the monitored ions and their area counts at the elution position of (5′S)-8,5′-cyclo-dAdo$(Me_3Si)_3$ (peak 2 in figure 3).

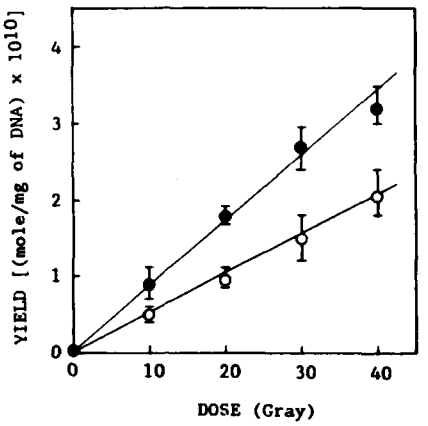

Figure 5. Dose–yield plots of 8,5'-cyclo-dAd in DNA; ●: ss-DNA; ○: in ds-DNA. Each point represents the mean (±standard deviation) of three independent experiments.

2'-deoxynucleosides were similar in ss-DNA, whereas the yield of 8,5'-cycl -dAdo was higher than that of 8,5'-cyclo-dGuo in ds-DNA. The *G* values (number of molecules formed per 100 eV of radiation energy) of these products calculated from the dose–yield plots and the ratios of their diastereomers [(5'R)/(5'S)] are listed in table 1. As can be seen from table 1, the yields of (5'R)-diastereomers of both 8,5'-cyclopurine 2'-deoxynucleosides in ss-DNA were greater than those of (5'S)-diastereomers. In contrast, in ds-DNA, the yields of the (5'S)-diastereomers were greater than those of the (5'R)-diastereomers.

4. Discussion

Our interpretation of the data presented is that the nature of the DNA, whether single- or double-stranded, affects the involvement of its purine 2'-deoxynucleoside residues in the hydroxyl radical-induced formation of 8,5'-cyclopurine 2'-deoxynucleosides. The salient features in this argument are that the yields of 8,5'-cyclopurine 2'-deoxynucleosides are higher in ss-DNA than in ds-DNA, suggesting 'protection' by the secondary structure of the DNA. Furthermore, in ss-DNA,

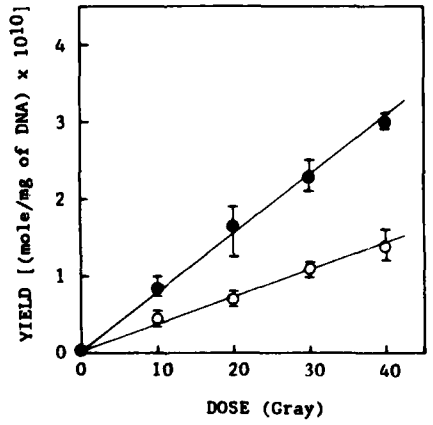

Figure 6. Dose–yield plots of 8,5'-cyclo-dGuo in DNA; ●: ss-DNA; ○: in ds-DNA. Each point represents the mean (±standard deviation) of three independent experiments.

Table 1. *G* values of 8,5′-cyclopurine 2′-deoxyribonucleosides and the ratios of their diastereomers in DNA.

	G value		(5′R)/(5′S)	
Substrate	8,5′-cyclo-dAdo	8,5′-cyclo-dGuo	8,5′-cyclo-dAdo	8,5′-cyclo-dGuo
ss-DNA	0·042	0·038	1·8	2·7
ds-DNA	0·025	0·017	0·8	0·8

the yield of 8,5′-cyclo-dAdo is very similar to that of 8,5′-cyclo-dGuo. In contrast, in ds-DNA, the yield of 8,5′-cyclo-dAdo is approximately 50 percent higher than that of 8,5′-cyclo-dGuo (table 1). This observation is in agreement with the general idea of protection by double-strandedness of DNA, if we assume that the higher yield of 8,5′-cyclo-dAdo in ds-DNA was derived from adenine-thymine (A–T) rich segments of DNA. Such segments would undergo opening ⇆ closing or strand separation reactions, i.e. 'structural breathing', to a greater extent and at a higher rate than random or guanine-cytosine (G–C) rich segments of DNA (von Hippel and Felsenfeld 1964). These A–T-rich, more open segments would produce a 'local' environment favourable to the formation of 8,5′-cyclo-dAdo. Supporting this concept are the findings of Rafi *et al.* (1968), who determined the yield of radiation-induced base damage in DNAs of varying base composition. They demonstrated that the *G* value for base damage increases with increasing A–T content of DNA much like the transition temperature of DNA decreases with an increase in A–T/G–C ratio (Marmur and Doty 1959).

Extensive work on the effect of DNA conformation on free radical-induced base destruction led to the 'shielded base hypothesis' (Ward and Kuo 1978). In general, the *G* values for base destruction are lower in native than in random coil or in monomeric substrates. In this hypothesis there is assumed to be a shift in the probability of the initial radical attack toward the sugar phosphate backbone in native DNA because of its peripheral position relative to the central axis in the double helix. In other words, the ratio of sugar radicals to base radicals would increase significantly when the polynucleotide chain is in native conformation. The formation of cyclo-purine nucleosides is generally considered to be the result of initial hydrogen atom abstraction by hydroxyl radicals from the C-5′ of the sugar moiety followed by intramolecular cyclization (Keck 1968). If this mechanism were applicable, and if the effect of DNA conformation on resulting products were due to physical hiding or exposure of parts of the polymeric substrate, it would be expected that the cyclization of purine nucleosides would indeed be favoured in native DNA. However, our results do not bear out this prediction. It is not possible from the information at hand to decide whether the mechanism suggested by Keck (1968) for the formation of 8,5′-cyclopurine 2′-ribonucleosides does not apply, or whether an adjustment in the concept of shielding of target moieties or of the initial radical attack in DNA is in order. Another possible mechanism might involve an initial attack at a purine base resulting in formation of an N-centered hydroxyl adduct radical, as has been suggested for formation of a different type of product from dGuo (Langfinger and von Sonntag 1985). The base adduct radical might then attack the sugar moiety by abstracting a hydrogen atom from the C-5′ to form a C-5′-centered radical, which would undergo intramolecular cyclization. Restitution of the purine base is required in this process, if the base radical is a part of the

same nucleotide subunit (Langfinger and von Sonntag 1985). However, in DNA the hydrogen atom abstraction from the sugar moiety might also occur through a neighbouring or a distant base radical. Evidence for such a mechanism has been obtained with polyuridylic acid (Lemaire *et al.* 1984, Schulte-Frohlinde and Bothe 1984), and thymine oligo- and polynucleotides (Karam *et al.* 1988).

Our results contradict the findings by Fuciarelli *et al.* (1985) on the yields of 8,5′-cyclo-dAdo in ss-DNA vs. ds-DNA, which were measured by a competitive enzyme-linked immunosorbent assay (ELISA). The lowest radiation dose used was 200 Gy, which is five times higher than the highest dose (40 Gy) used here. The data by Fuciarelli *et al.* (1985) show that the effect of the DNA conformation on the yield of 8,5′-cyclo-dAdo was negligible at 200 Gy under both gasing conditions used. At doses above 200 Gy the yield of 8,5′-cyclo-dAdo was higher in ds-DNA than in ss-DNA, which is in contrast to our results obtained at much lower doses. Furthermore, the data by Fuciarelli *et al.* (1985) show that only results obtained from ss-DNA irradiated in N_2-saturated solution can be readily fitted to a linear dose–response. Under all other conditions a nonlinear dose–yield response was obtained, suggesting a possible saturation of damage in DNA. A study by Ward and Kuo (1978) demonstrated that high amounts of damage due to high radiation doses will cause native DNA to denature because of increased amounts of strand breaks and base damage. Low doses ranging from 10 to 40 Gy were used in the present work to ensure the low amounts of damage to DNA in order to preserve its native state.

The pronounced effect of DNA conformation on the yield of the (5′R)- and (5′S)-diastereomers of 8,5′-cyclo-dAdo and 8,5′-cyclo-dGuo is another aspect of the cyclization of purine 2′-deoxyribonucleosides. In ss-DNA, the yield of the (5′R)-diastereomers is higher than that of the (5′S)-diastereomers (table 1). This observation parallels data obtained with γ-irradiated polyA (Fuciarelli *et al.* 1986). In ds-DNA, however, the yield of the (5′S)-diastereomers was found to be greater than that of the (5′R)-diastereomers. This is in agreement with the recent finding that (5′S)-8,5′-cyclo-dGuo was formed predominantly over (5′R)-8,5′-cyclo-dGuo in DNA of γ-irradiated human cells (Dizdaroglu *et al.* 1987). However, our results contradict the suggestion of Fuciarelli *et al.* (1986) that the (5′R)-diastereomers of 8,5′-cyclopurine 2′-deoxyribonucleosides would predominate in ds-DNA.

In conclusion, the results presented here show a pronounced effect of DNA conformation on the yields of hydroxyl radical-induced 8,5′-cyclopurine 2′-deoxyribonucleoside residues in DNA, and on the ratios of their diastereomers.

Acknowledgement

This work was supported in part by the Armed Forces Radiobiology Research Institute, Defense Nuclear Agency, Bethesda, Maryland, under Research Work Unit B5103 (the views expressed in this article are those of the authors and do not reflect the official views or position of the Department of Defense or the U.S. Government). We wish to acknowledge the expert technical assistance of Daniel P. Dodgen. We thank Dr J. H. Robbins (National Institutes of Health), and Dr A. F. Fuciarelli (National Bureau of Standards) for valuable discussions. We also thank Dr J. A. Raleigh (Cross Cancer Institute, Edmonton, Alberta, Canada) for the gift

of (5'S)-8,5'-cyclo-Ado, and Dr K. T. Wheeler (Bowman Gray School of Medicine, Winston-Salem, NC) for the gift of (5'R)- and (5'S)-diastereomers of 8,5'-cyclo-dAdo.

References

ALBERTS, B., and HERRICK, G., 1971, DNA cellulose chromatography. *Methods in Enzymology*, **21**, 198–217.

DIZDAROGLU, M., 1986 a, Free radical-induced formation of an 8,5'-cyclo-2'-deoxyguanosine moiety in deoxyribonucleic acid. *Biochemical Journal*, **238**, 247–254.

DIZDAROGLU, M., 1986 b, Chemical characterization of ionizing radiation-induced damage to DNA. *BioTechniques*, **4**, 536–546.

DIZDAROGLU, M., DIRKSEN, M.-L., JIANG, H., and ROBBINS, J. H., 1987, Ionizing radiation-induced damage in the DNA of cultured human cells. Identification of 8,5'-cyclo-2'-deoxyguanosine. *Biochemical Journal*, **241**, 929–932.

FUCIARELLI, A. F., MILLER, G. G., and RALEIGH, J. A., 1985, An immunochemical probe for 8,5'-cycloadenosine-5'-monophosphate and its deoxy analog in irradiated nucleic acids. *Radiation Research*, **104**, 272–283.

FUCIARELLI, A. F., SHUM, F. Y., and RALEIGH, J. A., 1986, Stereoselective intramolecular cyclization in irradiated nucleic acids: R- and S-8,5'-cycloadenosine in polyadenylic acid. *Biochemical and Biophysical Research Communications*, **134**, 883–887.

HALLIWELL, B., and GUTTERIDGE, J. M. C., 1985, The importance of free radicals and catalytic metal ions in human diseases. *Molecular Aspects in Medicine*, **8**, 89–193.

KARAM, L. R., DIZDAROGLU, M., and SIMIC, M. G., 1988, Intramolecular H atom abstraction from the sugar moiety by thymine radicals in oligo- and polydeoxynucleotides. *Radiation Research* (in press).

KECK, K., 1968, Bildung von Cyclonucleotiden bei Bestrahlung wässriger Lösungen von Purinnucleotiden. *Zeitschrift für Naturforschung*, **23 b**, 1034–1043.

LANGFINGER, D., and VON SONNTAG, C., 1985, Gamma-radiolysis of 2'-deoxyguanosine. The structure of the malondialdehyde-like product. *Zeitschrift für Naturforschung*, **40 c**, 446–448.

LEMAIRE, D. G. E., BOTHE, E., and SCHULTE-FROHLINDE, D., 1984, Yields of radiation-induced main chain scission of poly U in aqueous solution: strand break formation via base radicals. *International Journal of Radiation Biology*, **45**, 351–358.

MARIAGGI, N., CADET, J., and TEOULE, R., 1976, Cyclisation radicalaire de la desoxy-2'-adenosine en solution aqueuse, sous l'effet du rayonnement gamma. *Tetrahedron*, **32**, 2385–2387.

MARMUR, J., and DOTY, P., 1959, Heterogeneity in deoxyribonucleic acids I. Dependence on composition of the configurational stability of deoxyribonucleic acids. *Nature*, **183**, 1427–1429.

RAFI, A., WEISS, J. J., and WHEELER, C. M., 1968, Effect of gamma-radiation on aqueous solutions of DNA's of different base composition. *Biochimica et Biophysica Acta*, **169**, 230–240.

RALEIGH, J. A., and FUCIARELLI, A. F., 1985, Distribution of damage in irradiated 5'-AMP: 8,5'-cyclo-AMP, 8-hydroxy-AMP, and adenine release. *Radiation Research*, **102**, 165–175.

RALEIGH, J. A. KREMERS, W., and WHITEHOUSE, R., 1976, Radiation chemistry of nucleotides: 8,5'-cyclonucleotide formation and phosphate release initiated by hydroxyl radical attack on adenosine monophosphates. *Radiation Research*, **65**, 414–422.

SCHULTE-FROHLINDE, D., and BOTHE, E., 1984, Identification of a major pathway of strand break formation in poly U induced by OH radicals in presence of oxygen. *Zeitschrift für Naturforschung*, **39c**, 315–319.

VON HIPPEL, P. H., and FELSENFELD, G., 1964, Mirocal nuclease as a probe of DNA conformation. *Biochemistry*, **3**, 27–39.

VON SONNTAG, C., 1987, *The Chemical Basis of Radiation Biology*. (London: Taylor & Francis Ltd).

WARD, J. F., and KUO, I., 1978, Radiation damage to DNA in aqueous solution: a comparison of the response of the single-stranded form with that of the double-stranded form. *Radiation Research*, **75**, 278–285.

Simultaneous Nomarski and fluorescence imaging during video microscopy of cells

J. KEVIN FOSKETT
Physiology Department, Armed Forces Radiobiology Research Institute, Bethesda, Maryland 20814-5145

FOSKETT, J. KEVIN. *Simultaneous Nomarski and fluorescence imaging during video microscopy of cells.* Am. J. Physiol. 255 (Cell Physiol. 24): C566–C571, 1988.—A video microscope designed to allow low light level fluorescence imaging of cells during simultaneous high-resolution differential interference contrast (DIC) imaging, without the fluorescence light losses of 60–90% normally associated with this contrast-enhancement technique, is described. Transmitted light for DIC imaging, filtered at >620 nm, passes through standard DIC optical components, (¼ λ-plate, polarizer, and Wollaston prism) before illuminating the cells. Transmitted light and fluorescence emission pass through a second Wollaston prism but not through the analyzer, which is repositioned more distally in the optical path. Prisms designed to reflect light out a side port of the microscope to a video camera have been replaced with a dichroic mirror. This mirror reflects fluorescence emission out the side port to a low light-sensitive video camera. The spectrally distinct transmitted light continues through the dichroic mirror to an overhead camera through a polarizer (analyzer), which completes the DIC optical path. The fluorescence and DIC images can be viewed simultaneously on side-by-side video monitors, examined sequentially by an image-processing computer, or examined simultaneously using a video splitter/inserter. The ability to image cells with high resolution simultaneously with low light level fluorescence imaging should find wide applicability whenever it is necessary or desirable to correlate fluorescence intensity or distribution with specific cell structure or function.

differential interference contrast; low light level; fura-2

VIDEO IMAGING of fluorescence has recently become a very powerful tool in cell biology. The coupling of the video microscope to video image-processing systems has provided in the light microscope an instrument capable of quantitative fluorescence measurements within single cells. However, incorporation and illumination of fluorescent probes in living cells, especially at the single cell level, may not be without adverse physiological effects. For example, excited fluorescent probes (intrinsic and extrinsic) may generate toxic oxygen free radical species (6) and buffer intracellular ion levels and may have diverse metabolic or toxic effects (7). Two general strategies are employed to minimize these effects. First, attempts are made to minimize the amount of dye loaded into the cell. Second, the total excitation light flux is reduced, by exposing the cell to intermittent excitation and/or by attenuating the excitation intensity. Because fluorescence intensity is proportional to the amount of probe as well as the level of excitation illumination, these strategies require enhanced light-detection systems as well as the elimination of optical elements, including phase rings and polarizers, which attenuate fluorescence excitation and emission intensities. For example, an ideal polarizer transmits 50% of the incoming light, although in practice it generally transmits only 30–40%. In a microscope equipped for Nomarski differential interference contrast (DIC), the fluorescence emission will pass through a Wollaston prism and a polarizer. If the excitation light also passes through the same elements, then the resultant fluorescence intensity will be <10% compared with that of the same microscope without these elements. Thus low light level fluorescence imaging is generally associated with elimination of optical elements that provide high contrast in transmitted-light imaging. The loss of image resolution and contrast resulting from the elimination of these optical elements is further compounded by another necessity of video imaging. Because the video detector is operated in a low light level mode for the fluorescence imaging, the transmitted light intensity used for bright-field imaging must be greatly attenuated. This results in an image with poor signal characteristics that is degraded by noise in the camera. Even with digital image-processing systems where it is possible to integrate a number of sequential images, the resultant image is still degraded compared with that obtained under high light level conditions and with the expense of lost temporal resolution. As a result of the combined effects of eliminating contrast-enhancing optical elements and imaging under photon-poor conditions, low light level fluorescence is associated with poor transmitted light imaging, making correlation of fluorescence with simultaneous cell structure and function difficult.

I have developed a video microscope system to make quantitative fluorescence measurements in single living cells while they are simultaneously imaged with high contrast and resolution in Nomarski DIC optics, without the light losses normally associated with this contrast-

enhancement technique. This development allows good correlation between fluorescence and cell structure in real time.

METHODS

Microscope. The ability to image cells in DIC and fluorescence simultaneously without fluorescence light loss due to DIC optical components requires two video detectors, the means to separate spectrally the two images to the respective cameras, and a judicious placement of the polarizers in the optical path. The microscope (a Zeiss IM-35 inverted microscope equipped for epifluorescence) shown in Fig. 1 incorporates these elements. A standard 60-W halogen lamp is employed for transmitted light imaging, and a 75-W xenon arc is generally employed for fluorescence excitation. Most of my work employs a Zeiss Neofluor ×63, numerical aperture (NA) = 1.25 lens, since it combines high light-gathering capability with a fairly long (0.5 mm) working distance, which is helpful for examining thick specimens and in electrophysiology experiments. With an open-bath chamber a Zeiss water immersion ×40, NA = 0.75 lens is used as the condenser lens; for long-working distance applications, a Leitz ×32, NA = 0.40 lens is used instead. The transmitted light optical path incorporates the elements required for DIC imaging. The light from the halogen lamp is polarized by a calcite prism (Zeta International, Prospect, IL) and passes through a Wollaston prism before illuminating the preparation. Fluorescence excitation from the xenon arc is directed to the preparation by a standard Zeiss dichroic mirror encased in a Zeiss filter cube. Fluorescence emission as well as transmitted light that passes through the specimen pass through the objective lens and a second Wollaston prism associated with it. In the standard Zeiss configuration, the light would next pass through a second polarizer (analyzer). However, because this polarizer would be in the fluorescence emission light path, it was repositioned more distally in the optical path, as described later. In the standard microscope configuration, the light proceeds through the microscope to a set of prisms designed to either allow the light to continue to the oculars or to direct it at right angles through a side port to a video camera. With the use of a Zeiss Photochanger (or other trinocular), it is possible to mount, in addition to the one at the side port, a second camera above the oculars. The prisms can direct the light to either or both cameras. However, they cannot direct fluorescence emission to one camera and transmitted light to the other. To this end, I have replaced the prisms with a simple dichroic mirror mounted at 45° to the incident light path. The dichroic mirror can separate light based on spectral properties; thus it becomes possible to image the transmitted light and fluorescence separately if they are spectrally distinct. Because most biologically relevant probes have fluorescence emission <550 nm, the halogen light is initially filtered to allow only >620 nm light for transmitted light imaging. The dichroic mirror that reflects the fluorescence excitation to the preparation passes this red light without interference. The dichroic mirror that replaces the prisms to direct the light to the appropriate cameras is chosen to be able to pass >620 nm to the overhead camera for transmitted light imaging and reflect the fluorescence emission out the side port through an interference filter for fluorescence imaging. The analyzer (calcite prism) is positioned between this dichroic mirror and the transmitted light camera, completing the DIC light path. Thus the overhead camera views the preparation in high light, contrast, and resolution DIC optics, whereas the side-port camera views the low light level fluorescence. The only DIC optical element in the fluorescence light path is a Wollaston prism. My measurements indicate that each pass through this prism attenuates the light by 1–2% at wavelengths >~400 nm. At 340 nm, attenuation is ~5%. Thus the combination of DIC with fluorescence imaging results in a fluorescence diminution of ~2–4% for most wavelengths.

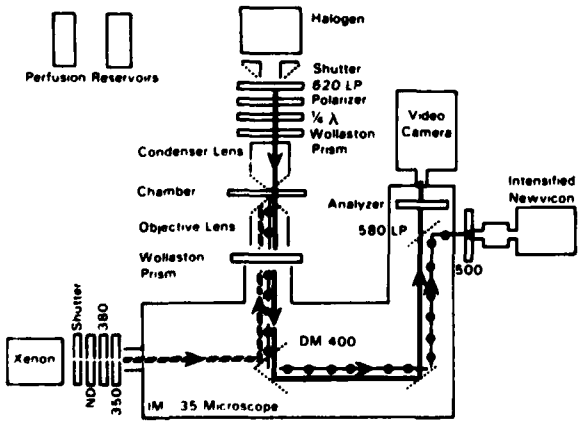

FIG. 1. Differential interference contrast fluorescence microscope. LP, long pass filter; DM, dichroic mirror; 350, 380, 500, band-pass interference filters; ND, neutral density filter. ■■■, Fluorescence excitation; ●–●–●, fluorescence emission; ———, transmitted light. See text for details.

Video image-processing system. The overhead camera that views the transmitted light image is coupled to the microscope by a Zeiss Photochanger (to direct light to the oculars or to the camera), a ×10 ocular, and a Hitachi zoom lens to adjust the magnification to that of the fluorescence camera. The ocular/zoom lens unit is adjusted to make the overhead, transmitted light camera parfocal with the side-port camera. The overhead camera currently used for transmitted light imaging is a silicon intensified target model (model 65 Dage-MTI, Michigan City, IN) simply because it was available. However, it is preferable to use a high-resolution, low-noise camera such as a Newvicon with gain and black-level controls.

The side-port camera that views the fluorescence emission is coupled to the microscope using the standard Zeiss coupling lenses incorporated into a tube that holds the 45° dichroic mirror in proper position. Although the local Zeiss representatives (Baltimore Instrument, Baltimore, MD) constructed this holder, a standard machine shop could easily make it. The camera should be sensitive to low light levels. I employ a two-stage, inverted-type image intensifier (model XX1380-FL, Amperex Electronic, Slatersville, RI) coupled by rely lenses (50-mm, f1.2, Nikon, Garden City, NY) to a Newvicon camera (model 65, Dage MTI) as described by Spring and Smith

(8). All automatic features (gain, black level) of this camera are disabled, and a provision for driving the sync signal from an external source is incorporated into it to allow images from the overhead (transmitted light) camera to be inserted into the video field of the intensified camera by the use of a video mixer (described below).

The video signal from the transmitted light camera is encoded for time and date (For-A, VTG-33, Los Angeles, CA), analog enhanced (For-A Contour Synthesizer, IV-530), and directed to a video tape recorder as well as a video switching device (Videotek, PVS-6, Pottstown, PA) (Fig. 2). The switching device feeds the signal to a video disk recorder (Precision Echo, EFS-1B, Santa Clara, CA) for recording and/or displaying on a video monitor. This image can be time-base corrected (Edutron, ccd 2h-1) and directed to the input of video image-processing boards (IP-512 series, Imaging Technology, Woburn, MA) housed in a Heurikon HK-68 computer (Madison, WI). The video signal from the fluorescence camera proceeds to a monitor and then to the image processor. Under software control, the image processor can select either camera as input and digitize images to 512 × 480 or 256 × 240 pixel resolution. The digitized images can be output to the video disk recorder. In a modified arrangement, the transmitted light image can be time/date coded and analog enhanced (as above) and inserted into the video signal of the fluorescence camera using a video splitter/inserter (RCA, TC1470A, Lancaster, PA). The advantage of this arrangement is that because the image processor can digitize signals from only one camera at a time, a signal containing both images results in no temporal dispersion between the time the image processor digitizes the images from the two cameras.

The fluorescence and DIC images can be viewed simultaneously in real time on side-by-side monitors or on one monitor if the splitter/inserter is used. However, the fluorescence image is inverted as a result of being reflected at right angles out of the microscope to the camera. Although this sometimes makes real time correlation of fluorescence with the DIC image somewhat difficult, it is advantageous for viewing both images on one monitor using the splitter/inserter, as shown in RESULTS. However, there are two ways to flip the image over in real time to facilitate viewing and comparing with the DIC image on side-by-side monitors. The first method is an optical approach. Placement of a dove prism in the optical path in front of the fluorescence camera will invert the image. I have not employed this prism in my microscope because of some difficulty in properly aligning it. The second method is an electronic approach. As an option on some video cameras, the raster scan can be initiated from the bottom of the field instead of the top.

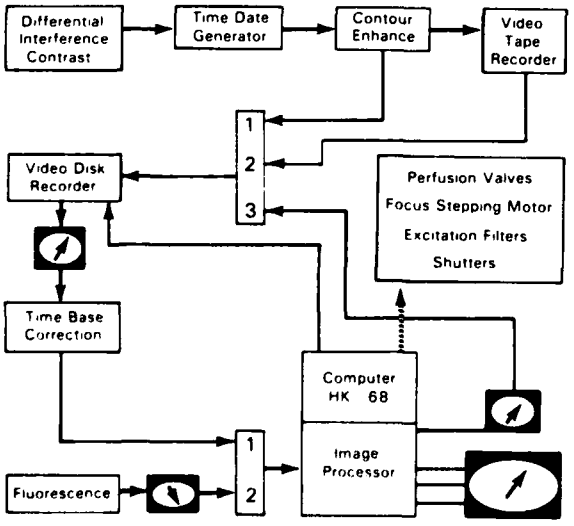

FIG. 2. Image-processing system. Video signals are from cameras viewing Nomarski image (*top*) and fluorescence image (*bottom*). Boxes with arrows, television monitors; larger box with arrow, a color monitor; arrows within boxes, indicate that fluorescence image is inverted from top to bottom compared with corresponding Nomarski image, until image processor creates an upright image to facilitate comparison between images. Boxes containing numbers, video switching devices. See text for further details.

Images digitized by this image-processing computer can be processed and/or stored in four video frame buffers (in real time), on video disk recorder (200 images in half real time), or laser disk recorder (24×10^3 images in real time), in 4-Mbyte random access memory (requiring a couple of seconds; it can be as fast as real time in some other image-processing systems), on 45-Mbyte Winchester disk, or on 65-MByte steaming tape (both requiring several seconds). The computer controls a stepping motor for microscope focus as well as shutters between the halogen and xenon lamps and the microscope and pinch valves to permit rapid changes of perfusion media. For examination of cells labeled with more than one dye, or for examination of dyes requiring more than one excitation wavelength, a custom-designed bank of solenoid-activated interference filter (1 in.; Ditric Optics, Hudson, MA) holders is positioned between the xenon arc and the microscope on a mechanically independent platform to prevent vibration transmission to the microscope. These filters can be called into and out of the light path under computer control. Switching between two wavelengths requires ~40 ms.

RESULTS

The advantages of DIC imaging have been reviewed (4). DIC images have a three-dimensional look, provide a shallow depth of field (out of focus information does not interfere), and provide high resolution and contrast. However, for low light level fluorescence imaging in a microscope with a single camera, DIC optical components are removed from the microscope, and the preparation is imaged in bright-field optics under low light level conditions. Figure 3 demonstrates the advantages of the two-camera system for imaging cells under low light level conditions. Figure 3*A* is a digitized fluorescence image of a field of living human monocytes recently plated onto a glass cover slip. The fluorescence is cell autofluorescence demonstrating the low light conditions in which the system is able to work and emphasizing the extreme sensitivity of the intensified Newvicon. Figure 3*B* shows the same field of cells imaged by the same camera at the same gain setting in low light level bright-field optics. In Figure 3*C*, the same field of cells is imaged in DIC optics with the second camera while simultane-

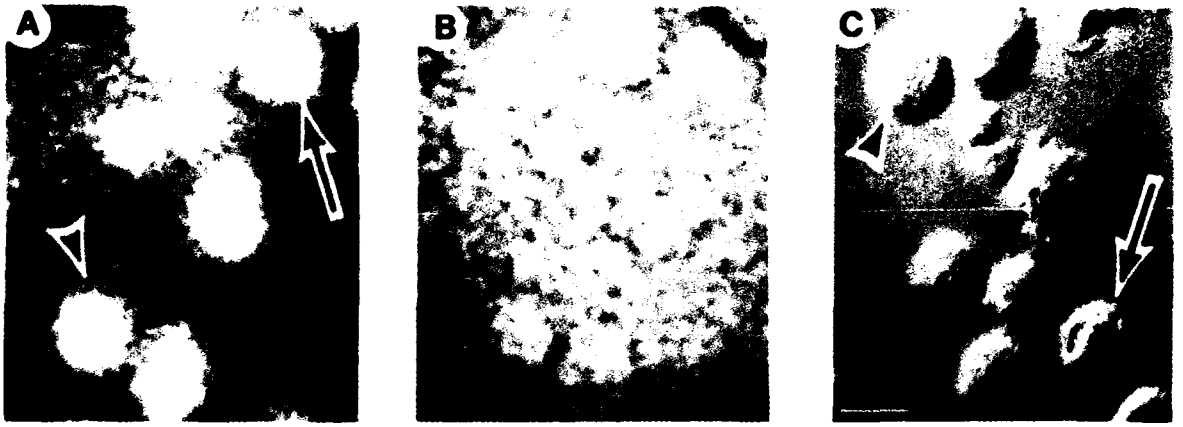

FIG. 3. Advantages of 2-camera system for imaging cells under low light level conditions. Human monocytes in fluorescence (*A*), low-light light level brightfield optics (*B*), and high light level differential interference contrast (DIC) optics (*C*). Fluorescence is cell autofluorescence (excitation 380 nm, emission 500 ± 20 nm). DIC image is inverted, from top to bottom, compared with other images, since it was obtained from a camera mounted at 90° to fluoresence/bright-field camera. Fluorescence image was obtained on 1 camera while simultaneously imaging in DIC optics on another. Arrows and arrowheads identify same cells, for orientation. See text for details. Bar, 15 μm.

ously imaging the fluorescence with the first camera. Figure 3*C* demonstrates the remarkable gain in transmitted light resolution and contrast obtained in this system compared with the single camera system under low light level conditions.

In the simplest configuration, the video-microscope system consists of two cameras with outputs that are directed to two monitors. In Fig. 4*A*, side-by-side monitors display live images of human monocytes grown in culture on glass cover slips. The field on the right is imaged in DIC optics, whereas on the left the same field

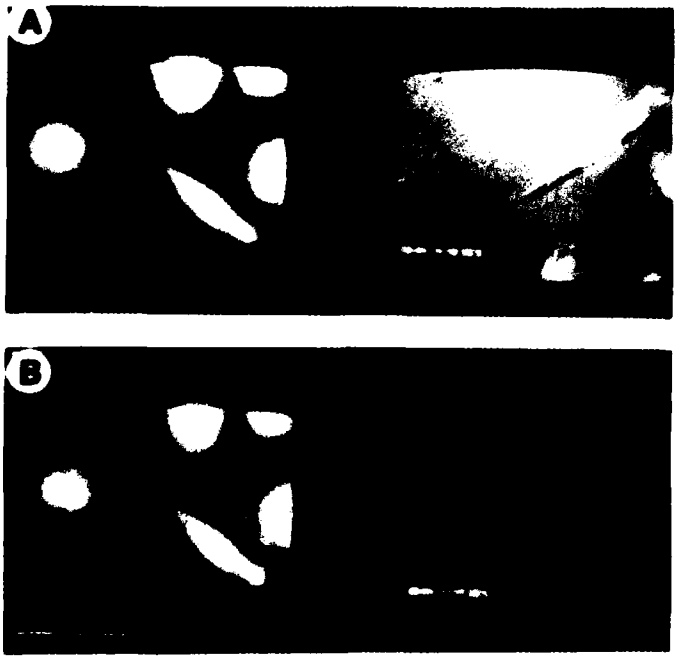

FIG. 4. Simultaneous differential interference contrast (DIC) and fluorescence imaging. Human monocytes, grown in culture, perfused on stage of microscope and loaded with Ca^{2+}-sensitive dye, fura-2. *Left monitor*: fluorescence emission. *Right monitor*: simultaneous DIC image. *Bottom*: transmitted light shuttered off. See text for details. Bar, 50 μm.

of cells is imaged simultaneously in fluorescence. The cells have been loaded with the Ca^{2+}-sensitive dye fura-2 and are being excited at 380 nm and observed at 500 ± 20 nm. The cells are imaged with high resolution and contrast in DIC while the fluorescence is likewise imaged in good detail. Figure 4*A* demonstrates the parfocality of the two images as well as the inverted (from *top to bottom*) nature of the fluorescence image compared with the DIC image as a result of being deflected at right angles out through the side port of the microscope.

It is possible to make quantitative measurements of fluorescence despite the high light throughout the DIC optical path. This is evident in Fig. 4*B*, which demonstrates that the fluorescence intensity is unaffected by the presence of the transmitted light, indicating that there is no "spectral contamination" of the two light paths. However, this may not always be the case, depending on conditions including the degree of spectral separation of the two light paths, the quality of the dichroic filter than separates the light to the two cameras, the gain and sensitivity of the fluorescence camera, and the intensities of the fluorescence and transmitted lights.

Although the cameras permit simultaneous imaging of DIC and fluorescence, the image-processing computer that I use can digitize input from only one camera at a time. However, under software control the computer can rapidly switch between the two. Figure 5 represents digitized images of living human monocytes loaded with fura-2 and excited at 380 nm, as previously described. Figure 5*A* represents a digitized (512 × 480, 128-frame integrated average) DIC image of these cells. Figure 5*B* is a digitized 128-frame average fluorescence image of the same cells obtained beginning 33 ms after the DIC image was grabbed. The image processor has constructed the inverted image to make comparison with the DIC image easier. The acceptable amount of time separating the two images will depend on the physiology of interest, the signal-to-noise of the images, and the degree of cell

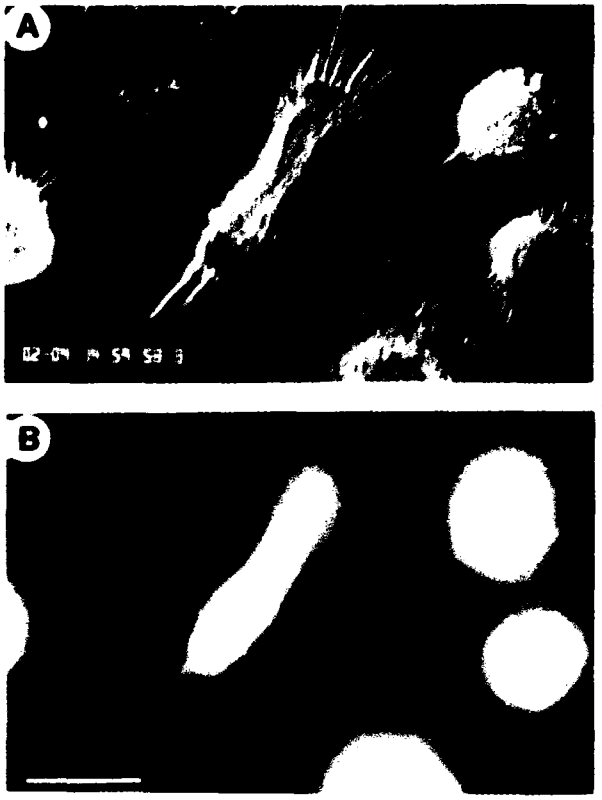

FIG. 5. Sequential differential interference contrast (DIC) (*A*) and fluorescence (*B*) imaging. Human monocytes perfused on stage of microscope and loaded with fura-2. Images are digitized 512 × 480, 128-frame integrated averages. See text for details. Bar, 25 μm.

movement. It may also depend on the amount of immediately available image-storage buffers. For example, to integrate two images, each to 16-bit resolution, requires three 8-bit frame buffers. If only two are available, the first image must be transferred out of one of the frame buffers into computer memory or an image-recording device such as a video disk or tape recorder. The amount of time required for such a transfer will also determine the minimum amount of time to separate acquisitions from each camera.

One solution to these problems is to mix the video signals from the two cameras with the use of a video splitter/inserter. A video splitter/inserter allows display of user-selected portions of video from two cameras on one video signal such that both can be simultaneously viewed, recorded, or digitized. In Fig. 6, fura-2-loaded monocytes are observed in DIC and fluorescence optics simultaneously digitized as a single video input from the video splitter/inserter.

DISCUSSION

The application of video techniques to fluorescence microscopy has led to an increased use of fluorescent dyes to probe living cells. Photographic techniques for examining fluorescence distribution in living cells is severely limited by the sensitivity of emulsion to low light levels. The resultant long exposures result in poor temporal resolution, probe bleaching, possible photodynamic damage to the cell, and cell movement artifacts. The

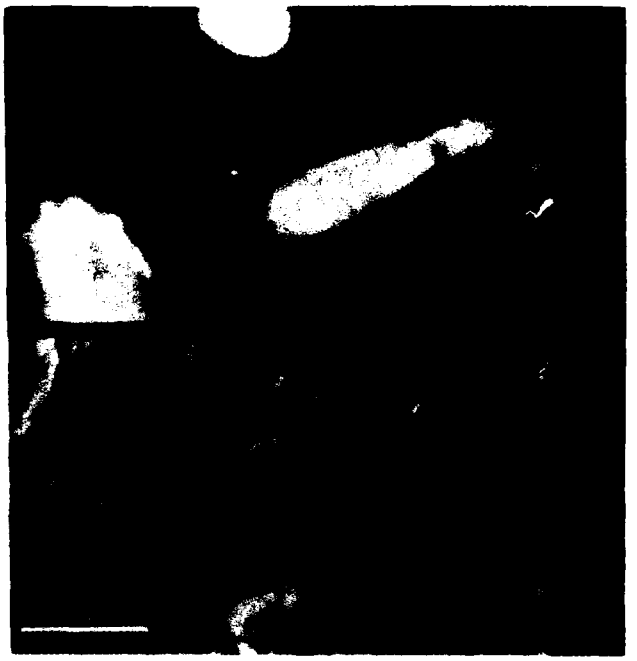

FIG. 6. Video splitter/inserted combined differential interference contrast (DIC) and fluorescence images. Cultured human monocytes loaded with fura-2. *Top*: DIC image. *Bottom*: simultaneous fluorescence image. See text for details. Bar, 15 μm.

speed and sensitivity of video overcomes these problems. Rapid changes in fluorescence intensity and distribution can be followed and recorded in real time. The use of ultra low light level-sensitive video detectors has made it possible to image fluorescence in living cells for relatively long periods of time with minimal photodynamic injury and dye bleaching. Furthermore, these cameras allow the cells to be loaded with less dye, thereby minimizing toxic or perturbing effects of the fluorescence probe. Thus video fluorescence microscopy affords the possibility to probe diverse intracellular environments simultaneously over time and under different physiological conditions. Because these capabilities largely accrue from the ability to work at very low light levels, the optical paths within the microscope should transmit excitation and emission wavelengths with as little light loss as possible. Therefore, a high numeral aperture objective is used, the number of reflecting surfaces within the microscope is minimized, the excitation lamp is focused and centered, and so forth. A generally employed technique has been to remove optical elements used to enhance contrast in transmitted light imaging. However, full advantage of the high spatial and temporal resolution provided by low light level video imaging of fluorescence is realized only when the cell structure can also be imaged with high contrast and resolution and with equivalent temporal resolution. In that way, a high correlation between cell structure and fluorescence can be achieved.

DIC imaging permits resolution of structural detail that surpasses other light microscopic methods. The use of video for DIC imaging has greatly extended the useful resolution and contrast provided by the light microscope (1, 4). Thus the combination of low light level fluorescence with DIC imaging provides the best means to

correlate fluorescence distribution with cell structure in living cells. However, at least one polarizer, and in some microscopes two polarizers, are present in the fluorescence light path, diminishing fluorescence intensity by 70–90%. The microscope described in the present paper allows simultaneous application of DIC imaging and low light level fluorescence without these light losses. This has been achieved by removing the DIC analyzer from the fluorescence optical path and by a modification of a standard Zeiss microscope to separate the transmitted light and fluorescence emission spectrally to two separate video cameras. This arrangement allows correlation of cell structure with fluorescence in real time. Because the two imaging modalities are not viewed with the same camera, different magnifications and geometrical distortions in the two cameras and optical paths do not permit a precise overlay of the fluorescence and DIC images (although sophisticated image-processing techniques could in fact precisely superimpose the two images). However, for most applications this will not be a serious limitation, since it will usually be possible to correlate fluorescence with the fine structure of the cell even when it is not possible to strictly superimpose the two images (see Figs. 5 and 6). For example, subtle retractions of the periphery of venous endothelial cells on stimulation with histamine have been observed during simultaneous spatial imaging of Ca^{2+} inside the same cells using the fluorescent dye fura-2 (3). In many instances, a correlation between fluorescence and cell fine structure is not important, although correlation with more macroscopic features of the cells may be important. For example, changes in cell volume and vacuole formation inside single cells and single acini isolated from rat parotid glands have been observed during simultaneous imaging of intracellular Ca^{2+} with fura-2 (2). At a somewhat more macroscopic level, this technique provides the ability to accurately identify different cell types in a morphologically heterogeneous population for correlation with single cell fluorescence. It should be pointed out that the fluorescence-imaging camera could be replaced with a photomultiplier tube. With an appropriate mask in an intermediate image plane, nonspatially resolved fluorescence can be correlated with cell structure and function. Finally, it seems worthwhile to consider the utility of this approach within the context of the recently described confocal microscope. In principle (see Fig. 1 of Ref. 9), the laser-scanning confocal microscope, appropriately modified, is an ideal method for imaging cells in Nomarski optics while simultaneously imaging them in fluorescence. The tremendously improved spatial resolution of fluorescence in the depth (z) and, to a lesser extent x–y-dimensions afforded by the confocal microscope allows fluorescence and Nomarksi optical sections to be perfectly resolved and registered. However, to this advancement must be weighed certain features of the present commercially available confocal microscope, of which the author is aware, that are less than ideal. First, the speed at which images are generated in the confocal microscope may be limiting in certain circumstances. Second, because the transmitted light wavelength is that used for epifluorescence illumination, continuous transmitted light imaging of the preparation will cause dye bleaching and possible direct and indirect phototoxic effects. Also, polarization of the fluorescence excitation beam may result in photoselection of fluorophores. Appropriate modifications to be used for the Nomarski imaging, such as including a second detector and allowing a second light beam filtered to longer wavelengths and polarized, will solve these problems. In either type of microscopy, the ability to image living cells in high resolution simultaneously with low light level fluorescence imaging should find wide applicability whenever it is necessary or desirable to correlate fluorescence intensity or distribution with specific cell structure and function.

This work was supported by the Armed Forces Radiobiology Research Institute, Defense Nuclear Agency, under Research Work Unit B00156.

The views presented in this paper are those of the authors. No endorsement by the Defense Nuclear Agency has been given or should be inferred.

Research was conducted according to the principles enunciated in the NIH "Guide for the Care and Use of Laboratory Animals" [DHEW Publication No. (NIH) 80-23, Revised 1978, Office of Science and Health Reports, DRR/NIH, Bethesda, MD 20205].

Received 9 February 1988; accepted in final form 3 May 1988.

REFERENCES

1. ALLEN, R. D., N. S. ALLEN, AND J. L. TRAVIS. Video enhanced contrast, differential interference contrast (AVEC-DIC) microscopy: a new method capable of analyzing microtubule-related motility in the reticulopodial network of *Allogromia laticollaris*. *Cell Motil.* 1: 291–302, 1981.
2. FOSKETT, J. K., J. E. MELVIN, AND R. J. TURNER. Simultaneous determinations of intracellular calcium (Ca_i^{2+}) and cell volume during stimulus-secretion coupling in individual parotid acini (Abstract). *J. Gen. Physiol.* 90: 18a, 1987.
3. FOSKETT, J. K., AND D. ROTROSEN. Digital imaging of intracellular calcium (Ca_i^{2+}) transients in single human endothelial cells (EC) (Abstract). *Federation Proc.* 46: 398, 1987.
4. INOUE, S. Video image processing greatly enhances contrast, quality and speed in polarization-based microscopy. *J. Cell Biol.* 89: 346–356, 1981.
5. INOUE, S. *Video Microscopy*. New York: Plenum, 1986, p. 1–584.
6. MARTIN, J. P., AND N. LOGSDON. Oxygen radicals are generated by dye-mediated intracellular photooxidations: a role for superoxide in photodynamic effects. *Arch. Biochem. Biophys.* 256: 39–49, 1987.
7. RINK, T. J., AND T. POZZAN. Using quin2 in cell suspensions. *Cell Calcium* 6: 133–144, 1985.
8. SPRING, K. R., AND P. D. SMITH. Illumination and detection systems for quantitative fluorescence microscopy. *J. Microsc. Oxf.* 147: 265–278, 1988.
9. WIJNAENDTS VAN RESANDT, R. W., H. J. B. MARSMAN, R. KAPLAN, J. DAVOUST, E. H. K. STELZER, AND R. STRICKER. Optical fluorescence microscopy in three dimensions: microtomoscopy. *J. Microsc. Oxf.* 138: 29–34, 1987.

J. Membrane Biol. 103, 55–66 (1988)

The Journal of
Membrane Biology

Patch-Clamp Studies in Human Macrophages: Single-Channel and Whole-Cell Characterization of Two K^+ Conductances

Elaine K. Gallin and Leslie C. McKinney
Physiology Department, Armed Forces Radiobiology Research Institute, Bethesda, Maryland 20814-5145

Summary. Human peripheral blood monocytes cultured for varying periods of time were studied using whole-cell and single-channel patch-clamp recording techniques. Whole-cell recordings revealed both an outward K current activating at potentials >20 mV and an inwardly rectifying K current present at potentials negative to −60 mV. Tail currents elicited by voltage steps that activated outward current reversed near E_K, indicating that the outward current was due to a K conductance. The *I-V* curve for the macroscopic outward current was similar to the mean single-channel *I-V* curve for the large conductance (240 pS in symmetrical K) calcium-activated K channel present in these cells. TEA and charybdotoxin blocked the whole-cell outward current and the single-channel current. Excised and cell-attached single-channel data showed that calcium-activated K channels were absent in freshly isolated monocytes but were present in >85% of patches from macrophages cultured for >7 days. Only 35% of the human macrophages cultured for >7 days exhibited whole-cell inward currents. The inward current was blocked by external barium and increased when $[K]_o$ increased. Inward-rectifying single-channel currents with a conductance of 28 pS were present in cells exhibiting inward whole-cell currents. These single-channel currents are similar to those described in detail in J774.1 cells (L.C. McKinney & E.K. Gallin, *J. Membrane Biol.* **103**:41–53, 1988).

Key Words potassium · patch clamp · K conductance · macrophage · ion channel

Introduction

Several voltage-dependent K conductances have been described in macrophages (Gallin & McKinney, in press). These include 1) an inwardly rectifying K conductance described in long-term cultures (5 to 30 days) of mouse peritoneal and spleen macrophages (Gallin, 1981; Gallin & Livengood, 1981), and adherent J774.1 cells (a mouse-derived macrophage-like cell line) (Gallin & Sheehy, 1985), 2) an outwardly rectifying K conductance in J774 cells 1 to 4 hr following adherence (Gallin & Sheehy, 1985) and in mouse peritoneal cells cultured for 1 to 5 days (Ypey & Clapham, 1984), and 3) a calcium-activated K conductance described at the single-channel level in long-term cultured human macrophages (Gallin, 1984; McCann, Keller & Guyre, 1987). These data imply that the K conductances expressed by the macrophage are different depending on the source of the macrophage, the culture conditions and the age of the cells. These differences are not surprising in view of the large variations in function that have been described in macrophages from different sources (Van Furth, 1984).

This study characterizes, on both the single-channel and the whole-cell levels, two voltage-dependent K conductances present in human monocytes that have been grown in tissue culture for varying periods of time. An outward current is described which has a similar voltage dependence and pharmacology to the calcium-activated K single-channel currents previously described (Gallin, 1984). Single-channel experiments indicate that this conductance is not present in freshly isolated peripheral blood monocytes but is expressed after several days of culture. In addition, we demonstrate for the first time that about one-third of human macrophages cultured for >7 days exhibit an inwardly rectifying K conductance similar to that described in mouse macrophages (Gallin, 1981; Gallin & Sheehy, 1985).

Materials and Methods

Cells

Human peripheral blood monocytes were isolated by density centrifugation on Ficoll-Hypaque® and Percoll® gradients (Metcalf et al., 1986). Cells were cultured either directly on glass cover slips or in Teflon® jars for several days and then plated. All cells were grown in RPMI 1640 supplemented with 5% glutamine, 5% fetal bovine serum, and 100 U/ml of penicillin-streptomycin. After varying times in culture the glass cover slip con-

taining macrophages was placed in a recording chamber containing 1 ml of recording solution (*see below*). Recordings were done at room temperature (21 to 25°C).

Patch-Clamp Techniques

Patch electrodes were prepared as previously described (McKinney & Gallin, 1988). Seal resistances ranged from 10 to 50 GΩ. Either an EP7 (List Instruments, West Germany) or an Axopatch (Axon Inst., Calif.) patch-clamp amplifier was used in these studies. Voltage pulses were generated by a computer and ramp stimuli by a Kron-Hite (Avon, Mass.) model 5200A waveform generator. During ramp stimuli voltages were changed from a pipette potential of 0 to 100 mV, then to −100 mV and back to 0 mV. Single-channel data were filtered at 500 Hz (−3 dB) with a 4-pole bessel filter and recorded on an FM tape recorder (bandwidth 0 to 5 kHz). Data were digitized off line at 1000 Hz using an Indec systems unit (Sunnyvale, Calif.) and a PDP 11/23 computer. Amplitude histograms showing open and closed current levels were constructed from single-channel current records 33 or 66 sec in duration. Analytical methods are described in the preceding paper (McKinney & Gallin, 1988).

For whole-cell recordings data were digitized on line at 500 Hz. In most recordings, capacitance and series resistance were compensated electronically, although a small residual capacitative transient sometimes remained. In the studies where capacitance and series resistance were not compensated currents were <1.5 nA. Since series resistance (measured directly from the amplifier after capacitance compensation) ranged from 3 to 8 MΩ the maximum possible error for the studies in which no compensation was used was 12 mV. In some cases, residual capacitative and leak currents were eliminated from current tracings by subtracting appropriately scaled current responses of the opposite polarity. When the current peaked rapidly peak current amplitude was measured after the settling of the capacitative transient.

The zero-current potential measured immediately (~30 sec) after obtaining the whole-cell configuration was taken to be a reasonable estimate of the resting membrane potential (resting V_m). Resting V_m for monocytes cultured for 11 to 15 days was -51 ± 3 mV ($n = 27$). Cells were held within several mV of the zero-current potential and stepped to varying potentials every 4 to 8 sec unless otherwise noted. Membrane resistance measured from steps to −40 or −60 mV was 1.8 ± 0.2 GΩ ($n = 25$). No consistent shift in the voltage at which the inward or outward current activated was noted during the first 10 min of recording. In some cases an increase in the magnitude of the outward currents was evident during the first 5 min of recording, presumably due to the high (3×10^{-6} M) $[Ca]_i$ in the pipette solution. Recordings were usually stable for 10 to 25 min.

Membrane capacitance was calculated by integrating the capacitative transients recorded in the absence of filtering. Human monocytes increase in size in culture so that by 11 to 14 days in culture cells were ~22 μ in diameter, compared to 10 to 14 μ in diameter when first isolated. Capacitance measurements ranged from 40 to 100 pF and averaged 79 pF. The value for the specific membrane capacitance of the macrophage membrane calculated from the surface area of a 22 μ sphere and the cell capacitance was 5.2 μF/cm², 5 times greater than the expected 1 μF/cm² value for the capacitance of most biological membranes. Thus the value of membrane surface area is probably an underestimate. This may be due to the prominent membrane infoldings evident in scanning electron micrographs of macrophages.

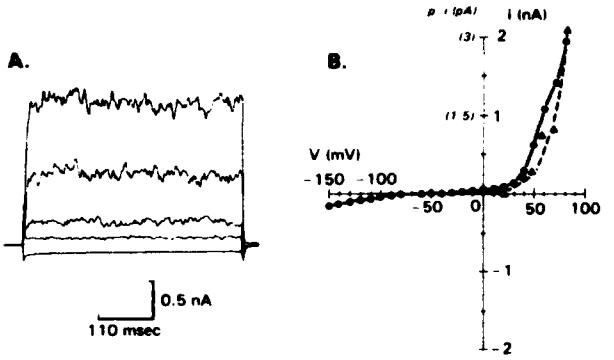

Fig. 1. (*A*) Whole-cell currents from a cell grown in tissue culture for 10 days. Patch electrode contained 3×10^{-6} M $[Ca]_i$ in KCl Hanks'. Input resistance of cell measured for step to −40 mV was 1.6×10^{-9} Ohms. Capacitance = 83 pF. $V_h = -33$ mV. Voltage steps to 20, 40, 60, 80, and −140 mV. (*B*) Peak *I-V* relation from cell in 1(*A*). Dashed line represents mean single-channel current [steady state open probability (from Fig. 3*B*) × single-channel current) obtained from fourteen excised inside-out patches with NaCl Hanks' in electrode and KCl Hanks' (3×10^{-6} M Ca) in bath

Solutions

NaCl Hanks' contained (in mM) 150 NaCl, 4.5 KCl, 1.6 $CaCl_2$, 1.13 $MgCl_2$, and 10 HEPES, pH 7.3. KCl Hanks' contained 150 KCl, 10 NaCl, 1.13 $MgCl_2$, 10 HEPES, 1.1 EGTA and varying concentrations of calcium, pH 7.2. For final ionized calcium levels of 3×10^{-6} M, 10^{-6} M, 10^{-7} M, and 10^{-8} M, the calcium concentrations were 1.07, 1.0, 0.55 and 0.1 mM, respectively. In studies where higher $[Ca]_i$ levels were required both EGTA and calcium were omitted, yielding $[Ca]_i$ levels (assessed with a calcium-sensitive electrode (WPI, Conn.)) of $\sim 10^{-5}$ M. In a few studies, equimolar Kisethionate was substituted for KCl.

Tetraethylammonium chloride (TEA) was obtained from Aldrich Chemical Co. (Milwaukee, Wis.). Partially purified charybdotoxin, obtained from Dr. C. Miller, was diluted in the appropriate Hanks' solution to a concentration of approximately 50 nM.

Results

Calcium-Activated Potassium Conductance

Whole-Cell Outward Currents

Stable (10 to 20 min) whole-cell currents could not be obtained routinely from freshly isolated or 1- to 2-day cultured human monocytes. The incidence of successful whole-cell recordings increased with time in culture. Therefore the whole-cell currents described in this paper were done on monocytes grown in culture for at least 5 days. Figure 1(*A*) shows the whole-cell currents of a human macro-

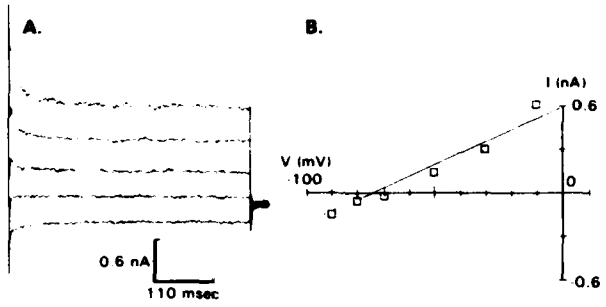

Fig. 2. (*A*) Tail currents. V_h = −75 mV. Cell was stepped to 50 mV for 200 msec and then to −10, −30, −50, −70 and −90 mV. (*B*) *I-V* relationship of tail currents was measured as difference in current 10 msec after initiation and 10 msec before the end of second step

phage cultured for 10 days. Voltage steps of >20 mV elicited outward currents characterized by a noisy baseline and no time-dependent inactivation. Hyperpolarizing voltage steps (−80 to −150 mV) produced small inward currents that were only slightly greater than the leak currents measured at −50 mV. The *I-V* relationship of this cell (solid line in Fig. 1*B*) shows prominent outward rectification.

In order to determine the reversal potential of the outward current, tail currents were measured in three different cells exhibiting large (~5 nA) outward currents. Cells were first stepped to potentials that activated the outward current (either 50 or 70 mV) and then stepped to a series of potentials ranging from −10 to −90 mV (Fig. 2*A*). Figure 2(*B*) plots tail current amplitude versus potential of the second step; the resulting *I-V* curve reverses at a potential of −75 mV. Similar data were obtained from two other cells. Under these recording conditions, calcium and sodium have positive reversal potentials, and the chloride reversal potential is 0 mV. The only ion with a negative reversal potential is potassium (E_K = −85 mV), providing strong evidence that the outward current must be carried predominantly by K.

Single-Channel Outward Currents

Previous studies in this laboratory have demonstrated that human macrophages grown in tissue culture express large conductance K channels that are activated by both intracellular calcium and voltage (Gallin, 1984). In 150 mM symmetrical KCl the *I-V* relationship and channel conductance is 240 pS. Under conditions of asymmetric K (150 mM $[K]_i$ and 150 $[Na]_o$) the *I-V* curve is nonlinear, single-channel conductance is reduced and the reversal potential shifts towards E_K (Gallin, 1984). This usually is the most prevalent channel present at depolarized potentials in patches of membrane from cultured (5 to 30 days) macrophages.

In order to compare the voltage dependence of this channel with that of the macroscopic outward current shown in Fig. 1(*A*), the steady-state channel open probability was determined in excised inside-out patches under ionic conditions which were similar to the whole-cell recordings (the patch electrode and bath contained NaCl Hanks' and KCl Hanks' [3 × 10^{-6} M calcium], respectively). Amplitude histograms were obtained from current records of 14 different patches (4 patches contained 1 channel, 7 patches contained 2 channels, 2 patches contained 3 channels and 1 patch contained 5 channels). Two representative histograms from a single patch are shown in Fig. 3(*A*). It was assumed that the channels behaved independently. Therefore, the open-state probability (p) was calculated from the equation:

$$p = \sum_{n=0}^{N} n \cdot Pn/N \qquad (1)$$

where Pn (the area under peak n) is the probability that n channels are open simultaneously, and N is the number of channels in the patch. The open-state probability plot is shown in Fig. 3(*B*). Before using these data to calculate the mean single-channel amplitude ($p \cdot i$), p was estimated by fitting the data to a sigmoidal equation:

$$p(V) = A + B/(1 + \exp(-(V - C)/D)) \qquad (2)$$

where A is the minimum open-state probability, $A + B$ is the maximum open-state probability, C is the midpoint of the curve, and D is the slope. These values were 0.001, 1.0, 98 and 12, respectively.

There was considerable variability between patches. For example, open-state probability at 60 mV ranged from 0.03 to 0.24. There was no correlation between the open-state probability at a given potential and the age of the macrophage in the 14 patches studied. Despite the variability, it is apparent that depolarization beyond 30 mV was needed to significantly activate the channels even though $[Ca]_i$ (3 × 10^{-6} M) was considerably higher than the $[Ca]_i$ values reported in resting phagocytes (Stickle, Daniele & Holian, 1984; Young, Ko & Cohn, 1984). In several studies in which $[Ca]_i$ was elevated to ~10^{-5} M, large increases in open-state probability were noted. At potentials of 20 and 40 mV, p increased to 0.21 and 0.75, respectively.

The voltage dependence of the single-channel current is compared with whole-cell data in Fig.

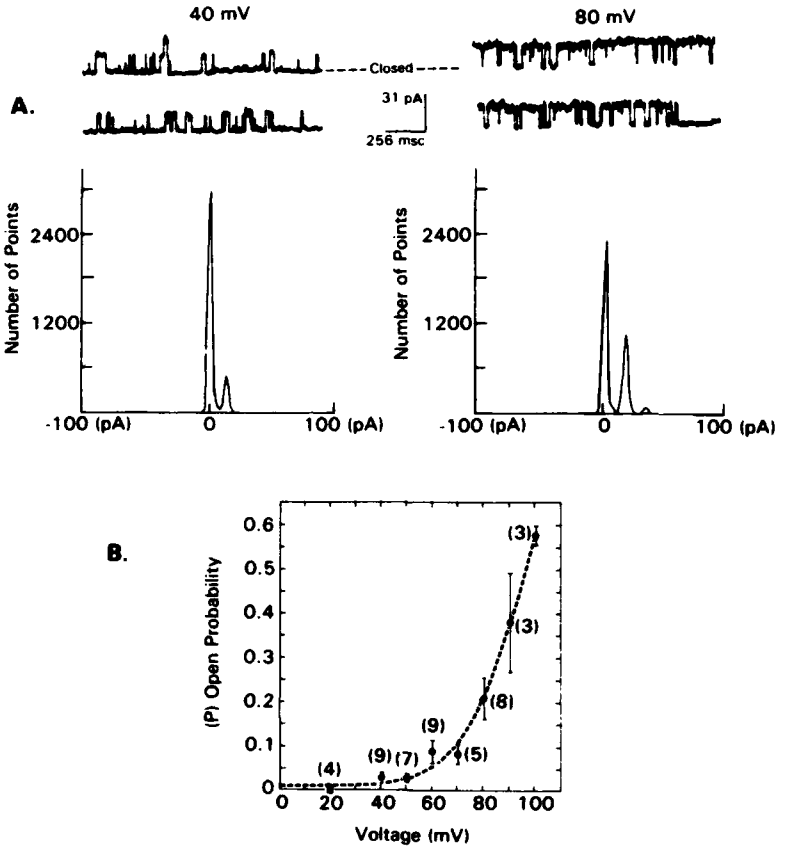

Fig. 3. (*A*) Single-channel activity from an excised inside-out patch from a cell cultured for 12 days. Electrode and bath contained NaCl Hanks' and KCl Hanks' 3×10^{-6} M $[Ca]_i$, respectively. Amplitude histograms determined for 60 sec of data at each potential are depicted under representative current tracings. Single-channel current records were leak subtracted. (*B*) Steady-state open probability versus voltage recorded under same conditions as in (*A*). Data points are mean ± SEM. Number of patches used to determine each point shown in parentheses. Curve fit to a sigmoidal relationship had a multiple R square of 0.99

1(*B*). The dashed line is a plot of the mean single-channel current amplitude ($p \cdot i$) calculated from the open-state probability (Fig. 3*B*) and the single-channel current amplitude. It is evident that the single-channel and the whole-cell currents have similar voltage dependencies. The number of channels in the cell depicted in Fig. 1 can be estimated from the relationship $I(V) = N \cdot p(V) \cdot i(V)$ where I is the whole-cell current amplitude at potential V, and N is the number of channels. The cell had approximately 660 channels.

Effect of TEA

The effect of TEA, which is a well-known blocker of large conductance calcium-activated K channels in other tissues (Iwatsuki & Petersen, 1985; Guggino, et al., 1987), was studied on the single channel and the macroscopic outward currents. Whole-cell outward currents were measured before and after bath addition of TEACl (15 to 20 mM) in 11 different cells. Data from one of these cells are shown in Fig. 4(*A*). The outward current for a step to 80 mV in the presence of TEACl was reduced by >90% whereas leak or inward currents were only slightly affected. Similar results were obtained in the other 10 cells studied.

Figure 4(*B*) depicts data from an experiment in which currents from calcium-activated K channels were recorded from a cell-attached patch before and after the electrode was perfused with TEACl (10 mM). Channel activity was abolished after exposure to TEACl. Because perfusion of the electrode often led to disruption of the patch, related studies were done in which channel activity was assessed in cell-attached patches with and without TEACl in the electrode. Eight patches obtained without TEACl in the electrode contained calcium-activated K channel activity (with 2 to 4 channels per patch). No large outward current fluctuations were present in the five patches obtained with electrodes containing 5 mM TEACl. Exposure of the inner surface of the membrane of excised inside-out patches to TEACl (5 mM) did not block channel activity, although there was a slight (10 to 20%) decrease in the channel conductance, similar to that reported in other preparations (Iwatsuki & Pererson, 1985).

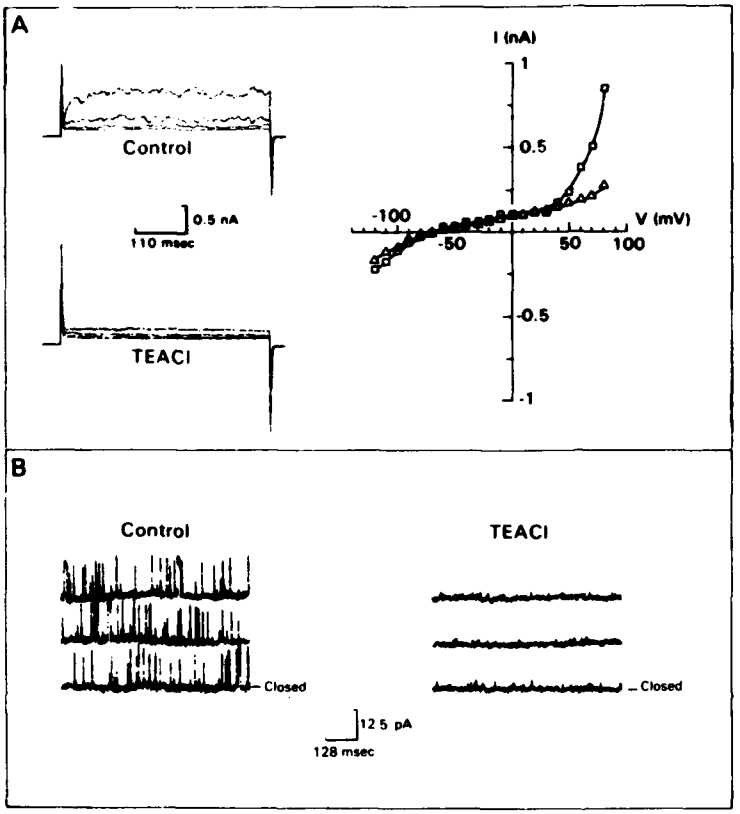

Fig. 4. (*A*) Effect of TEA on whole-cell currents. Macrophage was cultured for 7 days. V_h = −60 mV. Voltage steps were to 20, 40, 60, and 80 mV before and after TEACl (15 mM). *I-V* relationship before (□) and after (△) addition of TEACl. (*B*) Effect of TEACl on calcium-activated K channels. Cell-attached patch from a human macrophage cultured for 21 days before and after electrode was perfused with 10 mM TEACl. Bath and electrode contained KCl Hanks' solution. V_h = 80 mV

Effect of Charybdotoxin

Charybdotoxin, isolated from scorpion venom, is a high-affinity (K_d ~ 10 nM) blocker of the large conductance calcium-activated K channel (Miller et al., 1985, Guggino et al., 1987). The effects of charybdotoxin on whole-cell currents from a macrophage are shown in Fig. 5(*A*). Outward current was present for voltage steps to 70 and 90 mV. After the addition of charybdotoxin to the bath (~25 nM), the outward current was almost completely eliminated. This cell also exhibited inward currents for hyperpolarizing step to −100 mV or more negative. As shown in the *I-V* curves in Fig. 5(*A*), the inward current was not significantly affected by the addition of charybdotoxin. Similar results were obtained in two other experiments.

In other studies we tested the effect of charybdotoxin on single-channel currents. Excised inside-out patches were bathed in symmetrical KCl with the inside of the membrane exposed to 3×10^{-6} M $[Ca]_i$. Patches were obtained from human macrophages grown in tissue culture for at least one week. Three to four channels were present in each of seven patches in which the electrode contained only KCl Hanks' (Fig. 5*B*). In five other patches, done under the same ionic conditions, charybdotoxin (~25 nM) was present in the electrode. In three of these patches channel activity was absent at all potentials, while in two patches, channel openings were evident only at potentials >90 mV (Fig. 5*B*). The maximum channel amplitude at the holding potential of 100 mV corresponded to the channel size expected for the calcium-activated K channel under these conditions. However, no measurement of conductance was made in the presence of charybdotoxin since channels often did not open fully and were present only at extremely depolarized potentials. Exposure of the inside surface of the patch membrane to charybdotoxin did not affect channel activity.

Expression of the Calcium-Activated K Channel

Human peripheral blood monocytes grown in tissue culture differentiate into macrophages during the first week in culture (Bainton & Golde, 1978). In order to determine whether calcium-activated K channel expression changes during differentiation

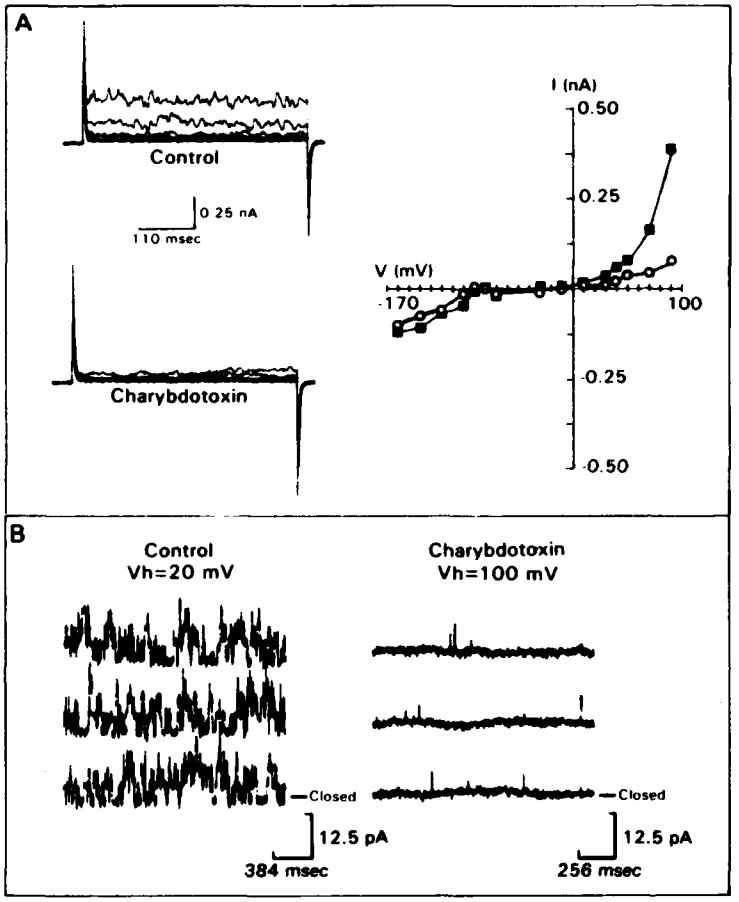

Fig. 5. (*A*) Effect of charybdotoxin on whole-cell currents. Outward current from a macrophage cultured for 4 weeks before and after addition of ~25 nM charybdotoxin. V_h = −40 mV. Voltage steps to 30, 40, 50, 70, and 90 mV. *I-V* relationship before (■) and after (○) addition of charybdotoxin. (*B*) Effect of charybdotoxin on calcium-activated K channels. Data from two excised inside-out patches in symmetrical KCl Hanks'. Inside surface of membranes was exposed to solution containing 3×10^{-6} M [Ca]. Charybdotoxin (25 nM) was present in electrode for tracings on the right

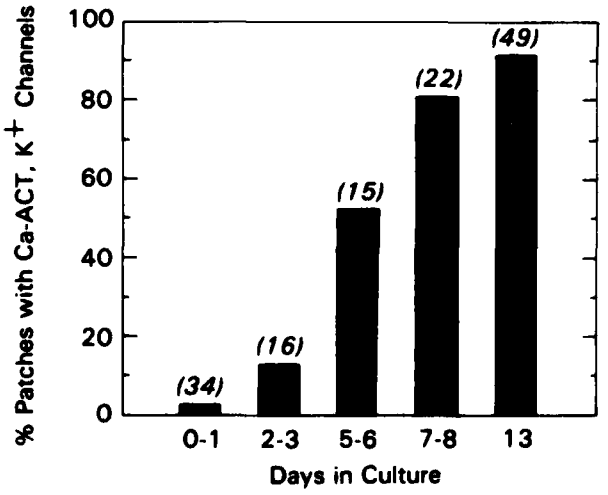

Fig. 6. Relationship between time in culture and presence of Ca-activated K channels. Data are from excised inside-out patches in symmetrical KCl with 3×10^{-6} M [Ca] in bath. Number of patches in each group are indicated in parentheses

cell-attached and excised inside-out patches were obtained from human monocytes cultured for differing periods of time. Only 1 out of 32 cell-attached patches from macrophages cultured for 24 hr or less contained calcium-activated K channels in response to depolarizing voltage steps. In contrast, 92% of cell-attached patches from monocytes cultured for >13 days exhibited these channels. In cell-attached patch experiments, the resting potential and $[Ca]_i$ (two parameters that influence channel activity) were uncontrolled, and may vary in cells cultured for different times. Therefore, experiments also were done on excised inside-out patches in symmetrical KCl with 3×10^{-6} M $[Ca]_i$. Under these recording conditions only one in 34 patches from cells cultured for <24 hr contained a calcium-activated K channel while 89% of the patches from cells cultured for >13 days had calcium-activated K channels. The data summarized in Fig. 6 indicate that the percentage of patches with calcium-activated K

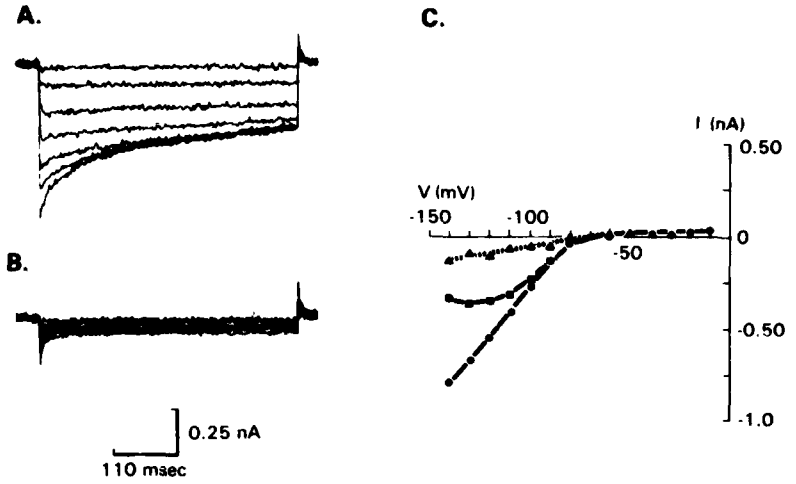

Fig. 7. (*A*) Currents recorded from a human macrophage cultured for 18 days. $V_h = -70$ mV. Input resistance for voltage step to −30 mV was 4×10^{-9} Ohms. Steps to −100, −110, −120, −130, and −140 mV before (*A*) and after (*B*) addition of 2 mM BaCl. (*C*) (●) Peak and (■) steady-state *I-V* curves. Dashed line shows peak current after BaCl

channel activity increased over the first week in culture.

To determine if the expression of calcium-activated K channels in human macrophages is affected by adherent versus suspended growth conditions monocytes were grown either in Teflon® dishes (nonadherent conditions) or in adherent conditions for 2 weeks. Teflon-grown cells were added to the recording chamber, and patch clamped within minutes of adherence and the recordings were compared to those obtained from adherent cells. Calcium-activated K channels were present in both groups of cells, indicating that adherent growth conditions were not required for channel expression.

Inwardly Rectifying Current

Whole-Cell Inward Currents

Approximately one-third of the cells studied under whole-cell recording conditions exhibited prominent ($G > 0.6$ nS at −110 mV) inward currents in responses to hyperpolarizing voltage steps. The current tracings and *I-V* curves from one of these cells are shown in Fig. 7. No outward currents were evident for voltage steps to 30 mV. Hyperpolarizing voltage steps produced inward currents. Time-dependent inactivation, typical of inward-rectifying K currents (Gallin & Sheehy, 1985; Leech & Stanfield, 1981), was evident for voltage steps to −100 mv or more negative. The ratio of the inward current measured at the peak of the current and the end of the voltage step declined from 0.81 to 0.37 between −100 and −140 mV, respectively (Fig. 7).

Previously we stated that the inward-rectifying conductance is important in setting the resting V_m of the macrophage (Gallin & Livengood, 1981; Gallin & Sheehy, 1985). The V_m of cells exhibiting prominent ($G > 0.6$ nS) inward rectification was compared to cells recorded on the same day that showed little or no inward rectification. Seventeen cells exhibiting inward-rectifying conductances (ranging from 0.7 to 3.8 nS) had an average resting V_m of -56 ± 4 mV while 19 cells in which this conductance was absent or quite small had an average resting V_m of -42 ± 2.5 mV.

Effect of Barium

The inward-rectifying K current in mouse peritoneal macrophages (Gallin & Livengood, 1981), the macrophage-like cell line J774 (Gallin & Sheehy, 1985) and other cells (Standen & Stanfield, 1978) is blocked by external barium. Figure 7 shows the *I-V* relationships for inward current in a human macrophage before and after addition of barium to the bath. The inward current was completely blocked whereas leak current was unaffected.

Effect of $[K]_o$

A characteristic of the inward-rectifying conductance is that the inward current increases with the square root of $[K]_o$. Figure 8 depicts inward currents from a cell in which $[K]_o$ was reduced from 148 to 31 mM. In 148 mM K/10 mM Na, currents were large and inactivation was largely absent, even for steps to −180 mV (Fig. 8*A*). In contrast, in 31 mM K/134 mM Na the inward currents were smaller, and inactivation was prominent for steps more negative than −120 mV. The peak *I-V* curve obtained

in each solution is plotted in Fig. 8(*C*). The whole-cell conductance was 17 nS in 31 mM $[K]_o$ and 26 nS in 148 mM $[K]_o$. The data agree with previous findings in the macrophage-like cell line, J774.1, that the inward-rectifying K conductance is proportional to the square root of $[K]_o$ (Gallin & Sheehy, 1985).

Single-Channel Inward Currents

Inward single-channel current fluctuations were observed in 37% of the cell-attached patches from human macrophages cultured for 7 to 20 days (Fig. 9).

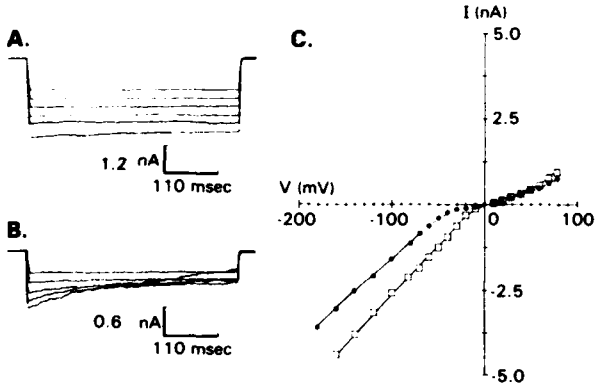

Fig. 8. Effect of $[K]_o$ on inward currents. Macrophage cultured for 8 days. V_h = 0 mV. Currents are leak subtracted. Steps to −80, −100, −120, −140, −160, and −180. (*A*) Currents were recorded in medium containing 148 mM KCl/10 mM NaCl. (*B*) Currents were recorded in media containing 31 mM KCl/134 mM NaCl. (*C*) Peak *I-V* curves for cell shown in (*A*) (□) 148 mM K, and in (*B*) (●) 31 mM K

Currents were observed at zero or negative pipette potentials and did not reverse. The single-channel *I-V* curve for the patch is shown in Fig. 9(*A*). The zero-current potential of this cell was not determined so the voltages represent the electrode holding potential only. Assuming the cell has a resting membrane potential of −51 mV (the average V_m) the channel reversal potential (E_{rev}) is 0 mV. Under these recording conditions, the equilibrium potential for $[K]_o$ will be close to zero, assuming $[K]_i$ is 158 mM. [The value of $[K]_i$ has not been measured in cultured human macrophages, therefore we used the value for $[K]_i$ in J774.1 cells (Sung et al., 1985).] The average channel conductance was 28 ± 1 pS (n = 12), similar to that reported for inwardly rectifying K channels in J774.1 cells (McKinney & Gallin, 1988).

Measuring the reversal potential of small channels, or channels that rectify can be difficult (*see* preceding paper by McKinney and Gallin). In addition to estimating the reversal potential by extrapolation of the *I-V* curve we also used voltage ramps (0.5 mV/sec) to determine the reversal potential. One of these studies is shown in Fig. 9(*B*). The resting potential of this cell was determined by breaking through the patch after the voltage ramp was completed. Therefore the voltage axis in Fig. 9(*B*) represents the true membrane potential across the patch. For clarity, the closed-current level was superimposed on the voltage axis and the open-current level was depicted by the dashed line. Inward currents that did not reverse polarity as the patch membrane was depolarized are evident in the ramp. The channel reversal potential determined from the intersec-

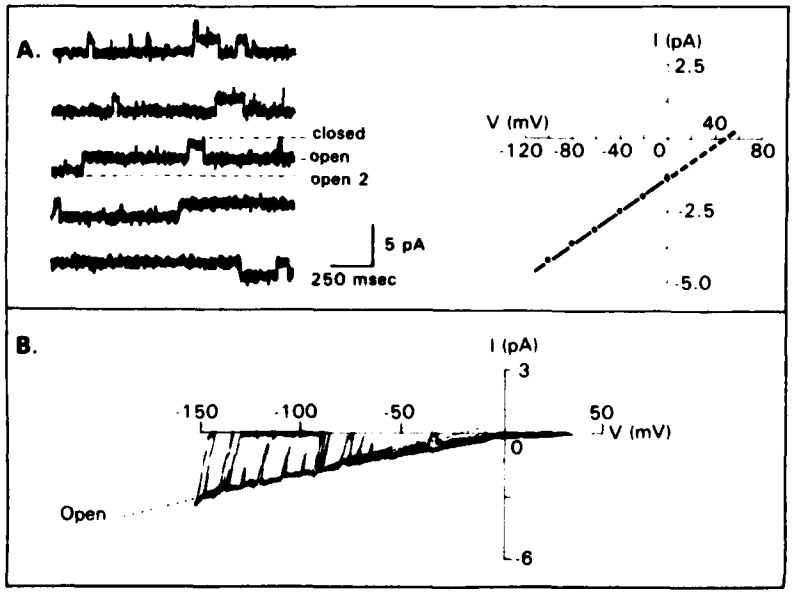

Fig. 9. Inward currents in cell-attached patches from human macrophages cultured for 20 and 22 days. Bath contained NaCl Hanks'; electrode contained KCl Hanks'. (*A*) Single-channel currents at holding potential, −70 mV. *I-V* relationship of single-channel currents shown on right. G = 28 pS. Potential represents electrode potential and does not include resting V_m. (*C*) *I-V* relationship from a different patch obtained with voltage ramp (0.36 mV/sec). Potential represents total potential across patch membrane and includes resting V_m which was −45 mV. Current trace was shifted so that the closed-current level was superimposed on the voltage axis. Dotted line was drawn through the open-current level between −150 to −100 mV. G determined from dotted line = 26 pS

tion of the closed- and open-current levels is close to 0 mV. In contrast, the dashed line superimposed on the open-current level in the region of −150 to −100 mV intersects the voltage axis at −20 mV rather than 0 mV. This is because there is a slight rectification of the *I-V* curve near the reversal potential.

To test for chloride permeability of the channel, several experiments were done with Kisethionate Hanks' in the patch electrode. Inward channels were present that had conductances of 28 pS and extrapolated reversal potentials of −10 and −8 mV. Assuming that isethionate is an impermeant anion, the results rule out chloride as a current carrier, since E_{Cl} under these recording conditions would be 30 mV [assuming $[Cl]_i \simeq 40$ mM (Melmed, Karaman & Berlin, 1981)].

Two representative current tracings at −80 and −100 mV, together with amplitude histograms, are shown in Fig. 10 for a cell-attached patch containing two channels. The actual potential across the patch membrane was determined from the electrode holding potential and the zero-current holding potential of the cell obtained after the channel recordings were completed. Channels are closed more at −100 mV than at −80 mV. These data along with additional data from the same patch at different holding potentials were used to determine the steady-state open probability (using Eq. 1) plotted in Fig. 10(*B*). As the potential was made more negative the open-state probability decreased, so that at −160 mV, it was only 10%.

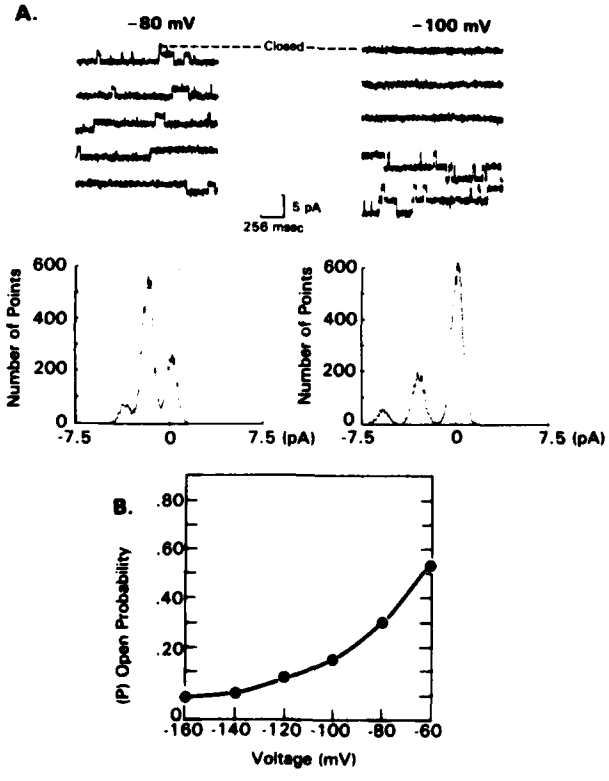

Fig. 10. (*A*) Inward currents in a cell-attached patch from a macrophage (20 days in culture) at membrane potentials of −80 and −100 mV. Ionic conditions were the same as in Fig. 9. Amplitude histograms (drawn as a line connecting individual points) for each potential obtained from 60 sec of channel data are shown under current tracings. (*B*) Steady-state open probability versus voltage for channels shown in (*A*)

Other Conductances

Two different amplitude single-channel outward currents ($G > 30$ and > 15 pS) sometimes were noted at depolarized potentials with KCl in the patch electrode. In several instances, patches were obtained that contained both of these small conductance channels as well as the calcium-activated K channel. If other outward currents exist in macrophage we would expect to see these under whole-cell recording conditions. However, only 2 out of >60 whole cell recordings revealed additional outward currents. In those two cases, inactivating outward currents that activated at voltages positive to −50 mV were seen. These currents were similar to those previously described in mouse peritoneal macrophages (Ypey & Clapham, 1984) and J774 cells (Sheehy & Gallin, 1985).

At negative or zero electrode potentials with KCl in the patch electrode and NaCl Hanks' in the bath, a second type of inward rectifying channel was recorded. The channel had a slightly larger single-channel conductance (ranging from 32 to 44 pS), than the 28 pS channel, did not reverse polarity and exhibited bursting activity. It was distinct from the inward 28 pS channel, occurring both in patches with and without the 28 pS channel. Preliminary experiments indicate that these channels can be activated by bath addition of the calcium ionophore, ionomycin (Gallin, 1988).

Discussion

Outward Calcium-Activated K Current

Previous patch-clamp studies of human macrophages have demonstrated the presence of large conductance calcium-activated K channels in human macrophages (Gallin, 1984). In this paper, we extend those observations to demonstrate whole-cell outward currents in macrophages that correspond to the activation of these channels. This view is supported by several findings. First, the reversal

potential of the tail currents indicated that the outward current was a K current. Second, as shown in Fig. 1(*B*), with similar $[Ca]_i$, the whole-cell *I-V* and the mean single-channel current ($p \cdot i$) *I-V* relationships have a similar voltage dependence, activating at voltages > 30 mV. In a few whole-cell studies, the $[Ca]_i$ was varied in an attempt to demonstrate the calcium sensitivity of the outward currents. Unfortunately there was so much variability in the amplitude of the outward currents from cell to cell that it was not possible to draw a correlation with $[Ca]_i$.

The $[Ca]_i$ sensitivity of calcium-activated K channels varies considerably in different cell types. For example, in rat skeletal muscle, the open-state probability at 20 mV for 3×10^{-6} M $[Ca]_i$ is 0.2 (Barrett, Magleby & Pallotta, 1982), while in pancreatic acinar cells, p is ~1.0 at 20 mV (Maruyama et al., 1983). In macrophages, although there was variability from patch to patch, this channel was quite insensitive to $[Ca]_i$, having an open-state probability of 0.004 at 20 mV in 3×10^{-6} M $[Ca]_i$. Increasing $[Ca]_i$ to ~10^{-5} M increased p to 0.21 at 20 mV. Assuming that the channel in situ has the same $[Ca]_i$ and voltage sensitivity as it does in excised patches, it is likely to play a minor role in ionic regulation, functioning primarily when $[Ca]_i$ changes from 10^{-6} to 10^{-5} M. Alternatively, it is possible that the calcium sensitivity in situ can be modulated, or that these channels are important in intracellular compartments where calcium levels may be quite high (Klempner, 1985). However, the observation that calcium-activated K channels are not present in 0- to 1-day-old peripheral blood monocytes indicates that these channels are not required (on the cell surface) for the monocyte to carry out phagocytosis, chemotaxis, and secretory processes which occur in these cells.

Outward current was reduced by bath addition of either TEA or charybdotoxin at concentrations that blocked single-channel activity also supporting the view that calcium-activated K channels underly the outward current. In cells treated with charybdotoxin, a small residual outward current usually remained at very depolarized potentials. Single calcium-activated K channel activity also was present at very positive voltages in the presence of charybdotoxin (Fig. 5). These two observations are consistent with studies in bilayers indicating that at high $[K]_i$ there is a voltage-dependent knockoff of charybdotoxin from calcium-activated K channels (MacKinnon & Miller, 1987). It is less clear why a small residual outward current sometimes remained following the addition of TEA (10 mM) since similar concentrations of TEA completely blocked the single channels. One possibility is that there is a small TEA-insensitive outward current in these cells.

Inward-Rectifying K Current

The inwardly rectifying whole-cell currents present in human macrophages are similar to those described in the macrophage-like cell line, J774 (Gallin & Sheehy, 1985; McKinney & Gallin, 1988) and mouse spleen and peritoneal macrophages (Gallin & Livengood, 1981). It is likely that the 28 pS channel described in this paper is responsible for the macroscopic inward current for several reasons. First, in cases where single-channel and whole-cell recordings were done on the same cell, the presence of 28 pS inwardly rectifying channels was always associated with inwardly rectifying whole-cell current. Second, the 28 pS single-channel currents described here are identical in conductance, and in the voltage dependence of activation and inactivation to the inwardly rectifying channels we characterized in detail in the preceding paper in J774 cells (McKinney & Gallin, 1988).

Human macrophages that express this conductance generally have a more negative resting V_m (−56 versus −42 mV), although not as negative as J774 cells (Gallin & Sheehy, 1985; McKinney & Gallin, 1988). This agrees with previous findings that the inward-rectifying K conductance was important in setting the resting V_m of mouse macrophages and the macrophage cell-line, J774 (Gallin & Livengood, 1981; Gallin & Sheehy, 1985). The rectifying *I-V* relationship of these cells enables them to have a resting V_m near E_K but remain sensitive to small depolarizing currents. Our value of −52 mV for the average resting V_m of cultured human peripheral blood monocytes agrees with that of Nelson et al. (1985) who reported an average resting V_m of −55 mV in human alveolar macrophages cultured for 1 day or longer, and −14 mV in freshly isolated cells.

Channel Expression

Human monocytes grown in tissue culture differentiate into macrophages over a period of 1 week. During this time changes occur in morphology (Zuckerman, Ackerman & Douglas, 1979) and function, although they are essentially a nondividing population (J. Sechler, *personal communication*). Functional changes include a decrease in peroxidase activity (Nichols, Bainton & Farqhuar, 1971), changes in surface antigens (Zwadlo et al., 1985), an increase in phagocytic ability (Wuest et al., 1981) and an initial increase followed by a decrease in H_2O_2 secreting ability (Nakagawara, Nathan & Cohn, 1981). It is thought that this differentiation process parallels the differentiation that normally

occurs when monocytes emigrate from the bloodstream into tissues. The data presented here provide evidence that an ionic conductance on the monocyte/macrophage surface also changes during this maturation period. That is, freshly isolated monocytes do not exhibit large conductance calcium-activated K channels whereas monocytes cultured for 5 days or longer do. The inward-rectifying channel was noted in only one-third of the patches from long-term cultured macrophages. Patches from cells cultured for 1–3 days frequently contained inwardly rectifying channels, but preliminary evidence indicates these are primarily the 32 to 44 pS channel; therefore, the expression of the 28 pS channel was not systematically investigated.

Other Currents

Under our whole-cell recording conditions the two K conductances described in this paper were the major voltage-dependent conductances present in human macrophages cultured for 5 to 25 days. Inactivating outward currents similar to those described in mouse peritoneal macrophages (Ypey & Clapham, 1984) and J774 cells (Gallin & Sheehy, 1985) were noted in only two cells. The single-channel small conductance outward currents present in some patches may be related to the inactivating outward currents seen in two of the cells. In a preliminary report, Nelson et al. (1986) reported a 4-aminopyridine-sensitive outward current activating at potentials above −30 mV in human macrophages cultured 1 to 10 days. However, the percentage of cells exhibiting this current was not discussed.

Our cell-attached patch single-channel recordings also revealed a second inwardly rectifying channel (when KCl is in the electrode and NaCl in the bath). We have not fully characterized this channel but it has a similar conductance (~36 pS) to a K channel described in human macrophages by McCann et al. (1987). However, in contrast to that study where channel reversal was noted, this channel did not reverse polarity in our studies. Preliminary studies indicate that this channel is activated by addition of ionomycin to the bath (Gallin, 1988). Whether this channel contributes to the whole-cell inward rectification described in this paper remains to be determined in future studies.

In conclusion, this paper characterizes two voltage-dependent K conductances at both the whole-cell and single-channel level in cultured human macrophages. It also demonstrates that the expression of at least one of these conductances, the 240 pS calcium-activated K conductance, changes during the time that the peripheral blood monocyte is maturing into the macrophage.

The authors thank Mr. Spencer Green for excellent technical assistance in isolating and maintaining monocyte cultures, and Ms. Marianne Owens for preparation of the manuscript. This work was supported by the Armed Forces Radiobiology Research Institute, Defense Nuclear Agency, under work unit 00020. Views presented in this paper are those of the authors; no endorsement by the Defense Nuclear Agency has been given or should be inferred.

References

Bainton, D., Golde, D. 1978. Differentiation of macrophages from normal human bone marrow in liquid culture. *J. Clin. Invest.* **62**:1555–1569

Barrett, J.N., Magleby, K.L., Pallotta, B.S. 1982. Properties of single calcium-activated potassium channels in cultured rat muscles. *J. Physiol. (London)* **331**:211–230

Gallin, E.K. 1981. Voltage-clamp studies in macrophages from mouse spleen cultures. *Science* **214**:458–460

Gallin, E.K. 1984. Calcium- and voltage-activated potassium channels in human macrophages. *Biophys. J.* **46**:821–825

Gallin, E.K. 1988. Inwardly rectifying K channels induced by ionomycin in human macrophages. *Biophys. J. (abstract)* **53**:548a

Gallin, E.K., Livengood, D.R. 1981. Inward rectification in mouse macrophages: Evidence for a negative slope resistance region. *Am. J. Physiol.* **241**:C9–C17

Gallin, E.K., McKinney, L.C. 1988. Ion transport in phagocytes. *In:* Neutrophil Physiology. M. Hallett, editor. *CRC Press*, Boca Raton, Florida *(in press)*

Gallin, E.K., Sheehy, P.A. 1985. Differential expression of inward and outward potassium currents in the macrophage-like cell line J774.1. *J. Physiol. (London)* **369**:475–499

Guggino, S., Guggino, W., Green, N., Sacktor, B. 1987. Blocking agents of calcium-activated K^+ channels in cultured medullary thick ascending limb cells. *Am. J. Physiol.* **21**:C128–C137

Iwatsuki, N., Peterson, O.H. 1985. Action of tetraethylammonium on calcium-activated potassium channels in pig pancreatic acinar cells studied by patch-clamp single-channel and whole-cell current recording. *J. Membrane Biol.* **86**:139–144

Klempner, M. 1985. An adenosine triphosphate-dependent calcium uptake pump in human neutrophils lysosomes. *J. Clin. Invest.* **76**:303–310

Leech, C.A., Stanfeld, P.R. 1981. Inward rectification in frog skeletal muscle fibres and its dependence on membrane potential and external K. *J. Physiol. (London)* **310**:295–309

McCann, F.V., Keller, T.M., Guyre, P.M. 1987. Ion channels in human macrophages compared with the U-937 cell line. *J. Membrane Biol.* **96**:57–64

McKinney, L.C., Gallin, E.K. 1988. Inwardly rectifying whole-cell and single-channel K currents in the murine macrophage cell line J774.1. *J. Membrane Biol.* **103**:41–53

MacKinnon, R., Miller, C. 1988. Mechanism of charybdotoxin block of the high conductance, Ca^{2+}-activated K^+ channel. *J. Gen. Physiol.* **91**:335–350

Maruyama, Y., Peterson, O., Flanagan, P., Pearson, G. 1983. Quantification of calcium-activated K^+ channels under hormonal control in pig pancreas acinar cells. *Nature (London)* **305**:228–232

Melmed, R., Karaman, P., Berlin, R. 1981. Control of cell volume in the J774 macrophage by microtubule disassembly and cyclic AMP. *J. Cell Biol.* **90**:761–768

Metcalf, J.A., Gallin, J.I., Nauseef, W.M., Root, R.K. 1986. Laboratory Manual of Neutrophil Function. pp. 2–6. Raven, New York

Miller, C., Moczydlowski, E., Latorre, R., Phillips, M. 1985. Charybdotoxin, a protein inhibitor of single Ca-activated K^+ channels from mammalian skeletal muscle. *Nature (London)* **313**:316–318

Nakagawara, A., Nathan, C., Cohn, Z. 1981. Hydrogen peroxide metabolism in human monocytes during differentiation *in vitro*. *J. Clin. Invest.* **68**:1243–1252

Nelson, D.J., Jacobs, E.R., Tang, J.M., Zeller, J.M., Bone, R.C. 1985. Immunoglobulin G-induced single ionic channels in human alveolar macrophage membranes. *J. Clin. Invest.* **76**:500–507

Nelson, D.J., Rufer, L., Nakayam, T., Zeller, J.M. 1986. Phorbol-ester block of voltage dependent K^+ current in monocyte-derived macrophages. *Biophys. J.* **49**:164a

Nichols, B., Bainton, D.F., Farquhar, M.G. 1971. Differentiation of monocytes. Origin, nature and fate of their azurophilic granules. *J. Cell Biol.* **50**:498

Standen, N.B., Stanfield, P.R. 1978. A potential and time-dependent blockade of inward rectification in frog skeletal muscle fibers by barium and strontium ions. *J. Physiol. (London)* **280**:169–191

Stickle, D.F., Daniele, R.P., Holian, A. 1984. Cytosolic calcium, calcium fluxes and regulation of alveolar macrophages superoxide anion production. *J. Cell. Physiol.* **121**:458–466

Sung, S.S., Young, J.D., Origlio, A.M., Heiple, J.M., Kaback, H.R., Silverstien, S.C. 1985. Extracellular ATP perturbs transmembrane ion fluxes, elevates cytosolic $[Ca^{2+}]$, and inhibits phagocytosis in mouse macrophages. *J. Biol. Chem.* **260**:13442–13449

Van Furth, R. 1984. Mononuclear Phagocytes. Martinus Nijhoff, Amsterdam

Wuest, D., Crane, R., Rinehart, J. 1981. Enhancement of Fc receptor function during human monocyte differentiation *in vitro*. *J. Reticuloendothelial Soc.* **30**:147–155

Young, D.J., Ko, S., Cohn, Z. 1984. The increases in intracellular free calcium associated with IgG γ2b/γFc receptor-ligand interactions: Role in phagocytosis. *Proc. Natl. Acad. Sci. USA* **81**:5430–5434

Ypey, D., Clapham, D.E. 1984. Development of a delayed outward-rectifying K^+ conductance in cultured mouse peritoneal macrophages. *Proc. Natl. Acad. Sci. USA* **81**:3083–3087

Zuckerman, S.H., Ackerman, S.K., Douglas, D. 1979. Long-term human peripheral blood monocytes: Establishment, metabolism and morphology of primary monocyte- macrophage cell cultures. *Immunology* **38**:401–411

Zwaldo, G., Brocker, E., Bassewitz, D. von, Feige, U., Sorg, C. 1985. Monoclonal antibody to a differentiation antigen present on mature human macrophages and absent from monocytes. *J. Immunol.* **134**:1487–1492

Received 22 July 1987; revised 24 November 1987

In: Cell Physiology of Blood. Gunn, R., and Parker, J., eds. The Rockefeller University Press, New York, 1988.

Chapter 26

Potassium Conductances in Macrophages

Elaine K. Gallin and Leslie C. McKinney

Department of Physiology, Armed Forces Radiobiology Research Institute, Bethesda, Maryland

Introduction

Macrophages are long-lived leukocytes, originating from bone marrow progenitor cells that migrate into the bloodstream as monocytes and then into tissues where they mature into macrophages (Van Furth, 1985). The macrophage, a phagocytic, motile, and secretory cell, plays a pivotal role in the defense against infective agents and neoplastic cells as well as in the removal of antigen–antibody complexes and damaged cells. They respond to numerous signaling agents that can modify or induce functional responses, including lymphokines, complement components, neuropeptides, and bacterial products (Van Furth, 1985). In general, the mechanisms involved in signal transduction in the macrophage are poorly defined. In many other secretory and motile cells, signal transduction is initiated by the opening of ionic channels in the plasma membrane (Eckert and Brehm, 1979; Peterson and Maruyama, 1984). There is evidence that, at least for one stimulus, this may be the case for macrophages as well (Young et al., 1983). With the recent development of the patch-clamp technique, the ionic conductances in leukocytes have begun to be characterized and their relationship to function has begun to be examined (for a review see Gallin and McKinney, in press).

Patch-clamp studies on macrophages from several sources have shown that different ionic conductances are present in cells, depending on the origin of the cell as well as the in vitro growth conditions (Ypey and Clapham, 1984; Gallin and Sheehy, 1985; Randriamampita and Trautmann, 1987; Gallin and McKinney, 1988). They include four different K conductances, a large conductance Cl channel (Schwarze and Kolb, 1984), and two cation channels, one of which is gated by the binding and cross-linking of the Fc receptor (Young et al., 1983), and one that may be gated by calcium (Lipton, 1986). No voltage-dependent calcium or sodium channels have been described in macrophages. This paper focuses on the four types of K conductances present in the macrophage. We will first briefly review early intracellular microelectrode studies and then describe more recent patch-clamp studies.

Intracellular Microelectrode Studies

Early studies using intracellular microelectrodes to record from macrophages demonstrated two types of K conductances: (*a*) one that could be activated by mechanical stimulation, or exposure to the calcium ionophore A23187 or chemotactic factors (Gallin et al., 1975; Gallin and Gallin, 1977), and (*b*) an inwardly rectifying K conductance (Gallin, 1981; Gallin and Livengood, 1981). Both these conductances play a role in regulating membrane potential, although it is not yet clear whether changes in potential are necessary for signal transduction in the macrophage (Pfefferkorn, 1984; Gallin and McKinney, in press).

Spontaneous membrane hyperpolarizations have been observed in cultured mouse and guinea pig peritoneal macrophages and in cultured human peripheral blood monocytes (Gallin et al., 1975; Dos Reis and Oliviero-Castro, 1977; Gallin and Gallin, 1977). In all instances, the membrane hyperpolarizations were associated with an increase in membrane conductance that was ascribed to the activation of a Ca-activated K conductance since (*a*) the reversal potential (E_{rev}) of the hyperpolarizations was close to the K equilibrium potential (E_K) (Gallin et al., 1975), (*b*) hyperpolarization could be blocked by addition of EGTA (Gallin et al., 1975), and (*c*) the intracellular injection of calcium induced a similar hyperpolarization (Persechini

et al., 1981). Data from a mouse spleen macrophage exhibiting spontaneous membrane hyperpolarizations are shown in Fig. 1. Initially the cell was current clamped. Microelectrode penetration (indicated by the first arrow) produced an initial hyperpolarization to −62 mV, after which the potential slowly changed to −43 mV. Transient hyperpolarizations (indicated by ●) were superimposed on the resting membrane potential (V_m). When the recording mode was switched to voltage clamp (holding potential (V_h) = −40 mV), outward currents of 5 nA or less were present. As is evident in the bottom current tracing, the transient outward currents decreased in amplitude as V_h was changed from −16 mV to −54 mV.

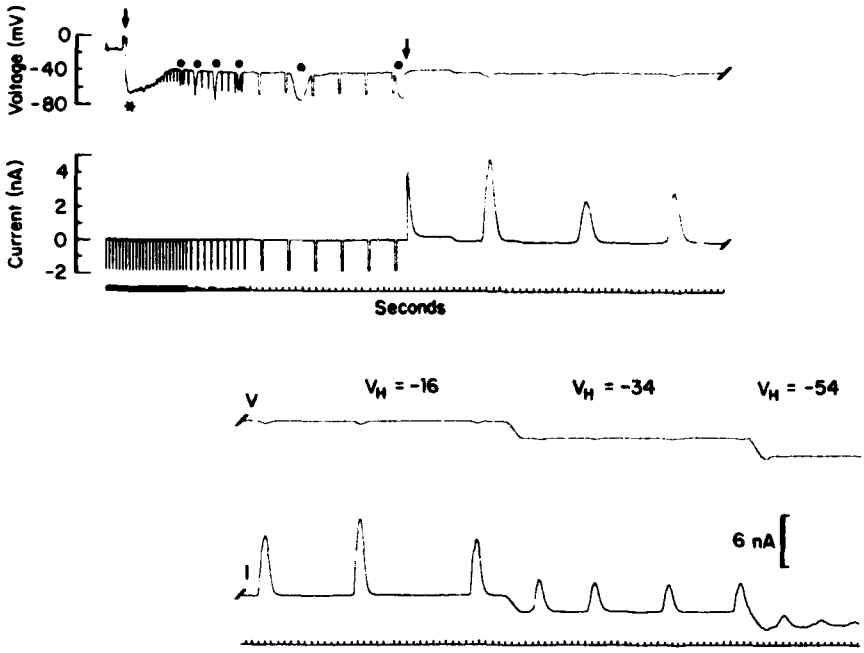

Figure 1. Chart recorder tracing of an intracellular microelectrode recording obtained using a single electrode voltage clamp from a mouse spleen macrophage cultured for 13 d. First arrow indicates impalement of the cell. Asterisk depicts initial hyperpolarization after electrode penetration. Initial segment of the recording was obtained under current clamp conditions; brief hyperpolarizing voltage steps were injected to monitor input resistance. Spontaneous hyperpolarizations are indicated (●). At the second arrow the recording mode was switched to voltage clamp and outward currents (upward deflections) are seen.

It is not clear whether spontaneous membrane hyperpolarizations occur physiologically in macrophages or whether they are due to the mechanical stimulation of microelectrode penetration and subsequent elevation of intracellular calcium ($[Ca]_i$). Ince et al. (1984) examined the rapid hyperpolarization induced immediately after electrode penetration, and concluded that it was an artifact of microelectrode damage. However, we have noted spontaneous current fluctuations that may correspond to membrane hyperpolarization in cell-attached patch recordings from cultured human macrophages where electrode-induced leak current was negligible (Gallin, 1988). In addition, Kruskal and Maxfeld (1988) have recently demonstrated oscillations in $[Ca]_i$

in macrophages immediately after adherence. These occur with a frequency similar to that of the spontaneous membrane hyperpolarizations. Taken together, these observations support the view that oscillations in membrane potential induced by the activation of a Ca-activated K conductance are not restricted to a microelectrode-induced damage and may occur under physiologically relevant conditions.

In addition to demonstrating a Ca-activated K conductance, intracellular studies in macrophages also revealed a prominent inward-rectifying K conductance in cultured mouse macrophages isolated form the peritoneal cavity or the spleen (Gallin, 1981; Gallin and Livengood, 1981). Cells exhibiting this conductance had current-voltage (I-V) relationships that showed inward rectification and often had a region of negative slope resistance between −60 and −30 mV. These cells usually had more negative resting membrane potentials (ranging from −65 to −95 mV) than did macrophages in which inward rectification was absent (−28 mV). The addition of either barium or rubidium to the bath inhibited inward rectification and depolarized cells by 20–30 mV (Gallin and Livengood, 1981). In some cells that showed prominent inward rectification and a region of negative slope resistance, two stable resting membrane potentials were present (Gallin, 1981). This behavior has been reported in cardiac ventricular cells and rat basophilic leukemia cells, which exhibit a similar K conductance (Gadsby and Cranefield, 1977; Lindau and Fernandez, 1986).

Patch-Clamp Studies

Calcium- and Voltage-activated K Conductance

Whole-cell current. Whole-cell, patch-clamp recordings of cultured human macrophages reveal an outward current that activates for voltage steps greater than +20 mV (Gallin and McKinney, 1988). Fig. 2 *A* shows current tracings from a whole-cell recording in which the patch electrode contained KCl Hanks' solution with 10^{-6} M $[Ca]_i$. Large outward currents characterized by a noisy baseline were present in response to voltage steps of +40 mV or greater, while hyperpolarizing steps produced small inward currents. The peak I-V relationship (Fig. 2 *B*) showed prominent outward rectification. The ionic selectivity of the outward current was determined from the instantaneous I-V relationship (data not shown). Cells were stepped to +50 mV for 200 ms to activate the outward current and then stepped down to various potentials. The resulting tail currents reversed at −75 mV, which was near E_K for these cells. Since no other ion present in the solution had a similar reversal potential, we concluded that the outward current was due predominantly to an increase in permeability to K.

Single-channel current. Cell-attached and excised patch recordings from human macrophages have demonstrated outward single-channel currents activating at depolarized potentials (Gallin, 1984). Fig. 3 *A* shows records from an inside-out excised patch illustrating the voltage and calcium sensitivity of these currents. At constant $[Ca]_i$, channel activity decreased as the voltage across the patch was made less positive; at constant V_m, channel activity decreased as $[Ca]_i$ was lowered from 3×10^{-6} M to 5×10^{-7} M. The calcium sensitivity of this channel is relatively low compared with similar channels in other secretory cells (Peterson and Maruyama, 1984). The open probability (p) of the channel at +80 mV in symmetrical KCl with 3×10^{-6} M $[Ca]_i$ was only 0.22 (mean of eight inside-out excised patches; Gallin and McKinney, 1988). Similarly, in cell-attached patches where resting $[Ca]_i$ is likely to be 10^{-7} M or lower,

channel activity was present only at very depolarized pipette potentials of +80 mV or above (this represents a true membrane potential greater than or equal to +30 mV, assuming a resting V_m of −50 mV). Assuming that the calcium sensitivity of the channel in situ is similar to that of the excised patch, for channels to be open at negative membrane potentials $[Ca]_i$ must be $>3 \times 10^{-6}$ M. Thus, it is unlikely that these channels are open very often under normal physiological conditions.

In an excised patch with symmetrical KCl, the I-V relationship of the channel was linear (Fig. 3 *B*); channel conductance determined from the slope of the line was 250 pS. This value is similar to those reported for the large conductance Ca-activated K channel in other cells (Barrett et al., 1982; Guggino et al., 1987). The ionic selectivity

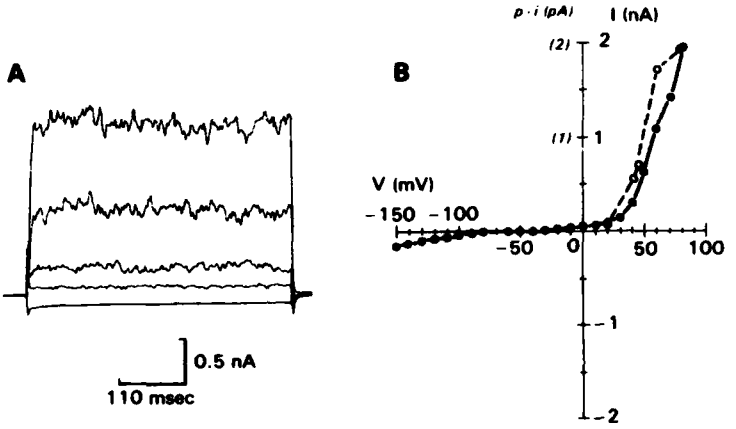

Figure 2. (*A*) Digitized whole-cell currents from a human macrophage grown in tissue culture for 10 d. Patch electrode contained 3×10^{-6} M Ca in KCl Hanks' solution. Cell capacitance was 83 pF. Holding potential (V_h) = the resting membrane potential (V_m) = −33 mV, defined as the zero current potential (ZCP). Voltage steps were to −140, 20, 40, 60, and 80 mV. (*B*) Peak I-V relation from cell shown in *A*. Dashed line represents mean single-channel current (p * I) obtained from excised inside-out patches with NaCl Hanks' solution in electrode and KCl Hanks' (3×10^{-6} M Ca) in bath. NaCl Hanks' solution consisted of 145 mM NaCl, 4.6 mM KCl, 1.1 mM $MgCl_2$, 1.6 mM $CaCl_2$, 10 mM HEPES, pH 7.3. KCl Hanks' solution contained 145 mM KCl, 10 mM NaCl, 1.1 mM $MgCl_2$, 1.1 mM EGTA, 1.07 mM $CaCl_2$, 10 mM HEPES, pH 7.3. (Gallin and McKinney, 1988).

of the channel was determined by changing the ionic constituents of the bath and/or electrode, and indicated that the channel was permeable to K and relatively impermeable to Cl or Na (Gallin, 1984).

To compare the voltage dependence of the single-channel current with that of the whole-cell outward current, the mean single-channel I-V relationship (refer back to Fig. 2 *B*, dashed line) of excised inside-out patches was measured under ionic conditions chosen to be similar to those of the whole-cell recording configuration, that is, $[K]_{pipette}$ = 4.6 mM and $[K]_{bath}$ = 148 mM. Mean single-channel current ($p * i$) was determined by measuring the single-channel open probability (p) and the single-channel current amplitude (i) at various voltages. If the number of channels (n) is constant, the mean single-channel current amplitude will be proportional to the

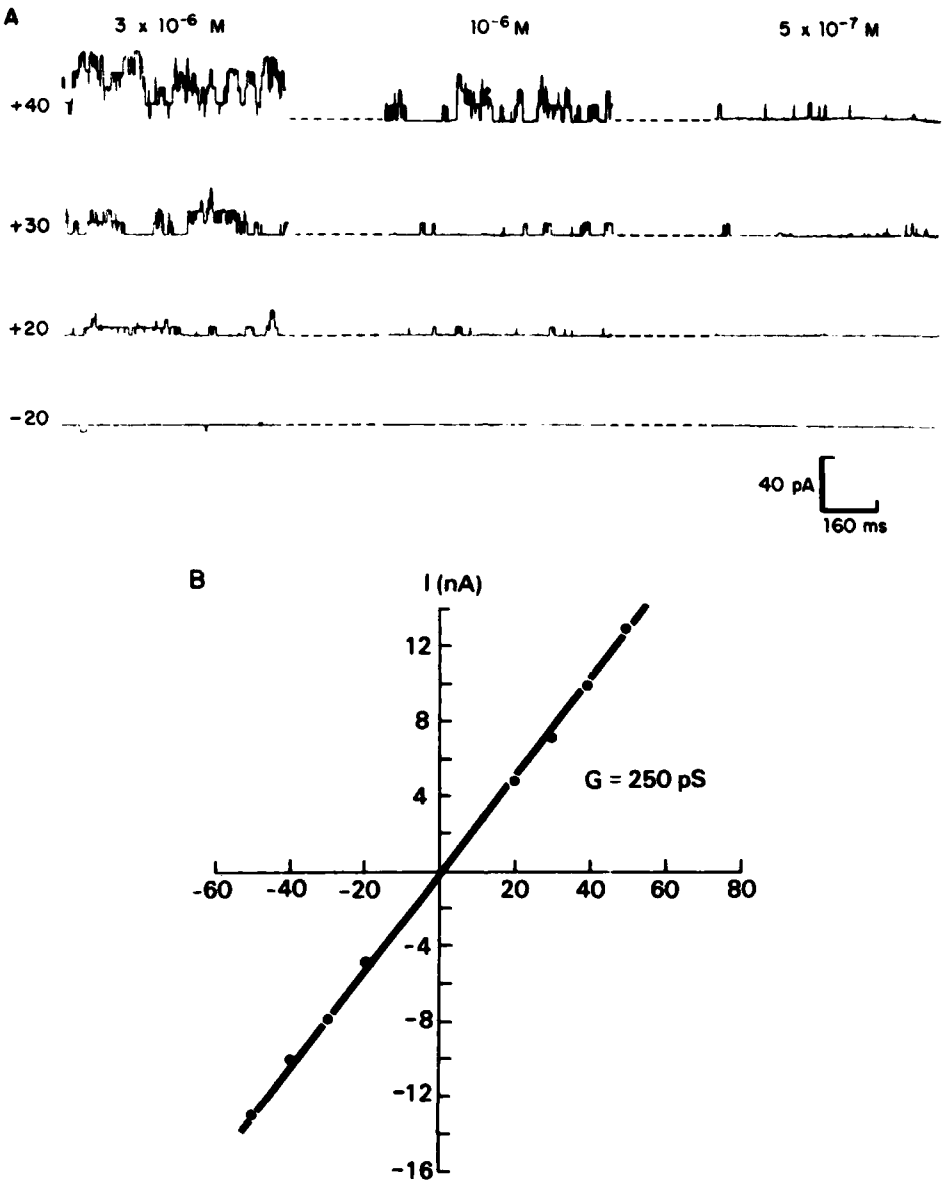

Figure 3. (*A*) Chart records of single-channel activity at four holding potentials from an excised inside-out patch from a human macrophage cultured for 14 d. Patch was exposed to symmetrical KCl Hanks' solution. Bath contained varying concentrations of $[Ca]_i$, as indicated. Patch contained a least six channels. In this and subsequent figures, upward deflections represent outward current. Dashed line represents closed current level. (*B*) I-V relationship of channels shown in *A*. (Gallin and McKinney, 1988).

whole-cell current amplitude (I) since $I = n * p * i$. It is evident from the two curves in Fig. 2 *B* that the single-channel and whole-cell currents have similar voltage dependencies, supporting the view that the single-channel Ca-activated K current fluctuations underlie the whole-cell outward current. From the relationship of the whole-cell current to the mean single-channel current we estimate the number of channels in the cell depicted in Fig. 1 to be 660.

Pharmacology. To show additional correspondence between single-channel and whole-cell Ca-activated K currents, we tested the action of two pharmacological agents, tetraethylammonium (TEA) and charybdotoxin, on the outward currents. Each is known to block Ca-activated K currents in other cells (Miller et al., 1985; Guggino et al., 1987). In the macrophage, addition of charybdotoxin (~25 nM) to the outside of the membrane blocked both whole-cell and single-channel currents (Gallin and McKinney, 1988). Addition of charybdotoxin to the inner surface of the membrane had no effect. Externally applied TEACl (10–15 mM) also blocked both the whole-cell and single-channel Ca-activated K current.

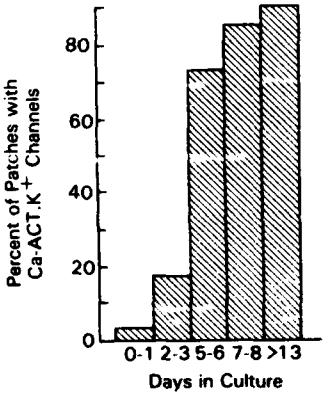

Figure 4. Relationship between time in culture and presence of large conductance Ca-activated K channels in human macrophages. Data are from excised inside-out patches in symmetrical KCl with 3×10^{-6} M Ca in bath. Number of patches in each group was 34, 16, 15, 22, and 49 (left to right). (Gallin and McKinney, 1988.)

Channel expression and functional relevance. Human peripheral blood monocytes differentiate into macrophages during the first week in tissue culture. This differentiation involves an increase in size, as well as changes in surface antigens (Zwadlo et al., 1985), enzyme content (Nichols et al., 1971), the extent of the oxidative burst, and phagocytosis (Nakagawara et al., 1981). So far, the data we have presented on the Ca-activated K conductance in the macrophage have been from cells that were cultured for 7 d or longer. To determine whether the expression of the Ca-activated K conductance changes during differentiation of the monocyte into a macrophage, monocytes were cultured for varying periods of time and the percent of patches containing Ca-activated K channels was measured. Fig. 4 shows a plot of the percentage of patches containing Ca-activated K channels versus time in culture. Only 1 of 34 patches from cells cultured for ≤24 h contained Ca-activated K channels, while 87% of the patches from cells cultured for >13 d did. Thus, the density of this channel in the membrane of monocytes changes in vitro as the cells are maturing.

Since the expression of other K conductances in the macrophage can be influenced by whether cells are grown under suspended or adherent conditions (Gallin and Sheehy, 1985), we also did experiments to determine whether the expression of the

Ca-activated K channel is affected by adherence. Cells grown in teflon jars (nonadherent conditions) for 2 wk and then plated for as little as several minutes had Ca-activated K channels, indicating that adherent growth conditions are not required for channel expression (Gallin and McKinney, 1988).

The functional role of the Ca-activated K channel is unknown. Freshly isolated monocytes have no Ca-activated K channels, yet are capable of both phagocytosis and chemotaxis. It is possible that activation of this conductance underlies the spontaneous membrane hyperpolarizations previously described. However, several observations make this seem unlikely. First, the voltage and calcium sensitivities of this channel (assuming that they are similar in situ and in the excised patch) are such that it will be closed at negative potentials unless $[Ca]_i$ is $> 3 \times 10^{-6}$ M. While large increases in $[Ca]_i$ may occur during penetration with intracellular microelectrodes, we have no evidence that such large increases occur in response to physiological stimuli. Second, we have noted oscillations in holding current in cell-attached patches where microelectrode damage is not present. Bursts of single-channel current were superimposed on these oscillations that were not due to the activity of the large conductance Ca-activated K channel, but instead were due to the activity of a distinctly different species of K channel (see the section on the bursting inward-rectifying K channel). Finally, exposure of cells to the calcium ionophore ionomycin during cell-attached patch recordings did not significantly increase the activity of the large conductance K channel ($V_m = -50$ mV), but it did increase the activity of a smaller conductance inward-rectifying K channel (see next section). Therefore, although the large conductance Ca-activated K channel will hyperpolarize the macrophage when $[Ca]_i$ is extremely high, it is not necessarily the primary channel involved in repetitive hyperpolarization.

Inwardly Rectifying K Conductances

Whole-cell current. An inwardly rectifying potassium current that activates at voltages negative to -60 mV was first described in mouse spleen and thioglycolate-induced macrophages cultured for several weeks (Gallin, 1981; Gallin and Livengood, 1981). This current is also present in cultured human peripheral blood monocytes (Gallin and McKinney, 1988), and in the mouse-derived macrophage-like cell line J774.1, where it has been characterized in some detail (Gallin and Sheehy, 1985; McKinney and Gallin, 1988). Fig. 5 shows whole-cell records obtained under three different conditions that illustrate the major properties of the inward current. Fig. 5 *A* shows currents recorded from a J774 cell bathed in normal Hanks' solution. Inward currents activated at potentials more negative than -70 mV and exhibited time-dependent inactivation for steps more negative than -120 mV. Fig. 5 B shows currents recorded from cells bathed in a Hanks' solution where all Na was replaced by K. Currents increased in size and showed less time-dependent inactivation. As is true for the inward-rectifying conductances of other tissues (Hagiwara and Takahashi, 1974; Leech and Stanfield, 1981), whole-cell conductance was proportional to the square root of external potassium concentration (in 4.5 and 145 mM $[K]_o$ the average conductance was 3.4 nS vs. 24 nS, respectively). Gating was also dependent on $[K]_o$. Activation of the current shifts to more positive potentials as $[K]_o$ increases (Gallin and Sheehy, 1985). Note that while time-dependent inactivation was reduced in Na-free media, it was not completely eliminated. The same amount of inactivation was observed when Na in the bath was replaced by *N*-methylglucamine (NMG) instead of K (Fig. 5 *C*), which

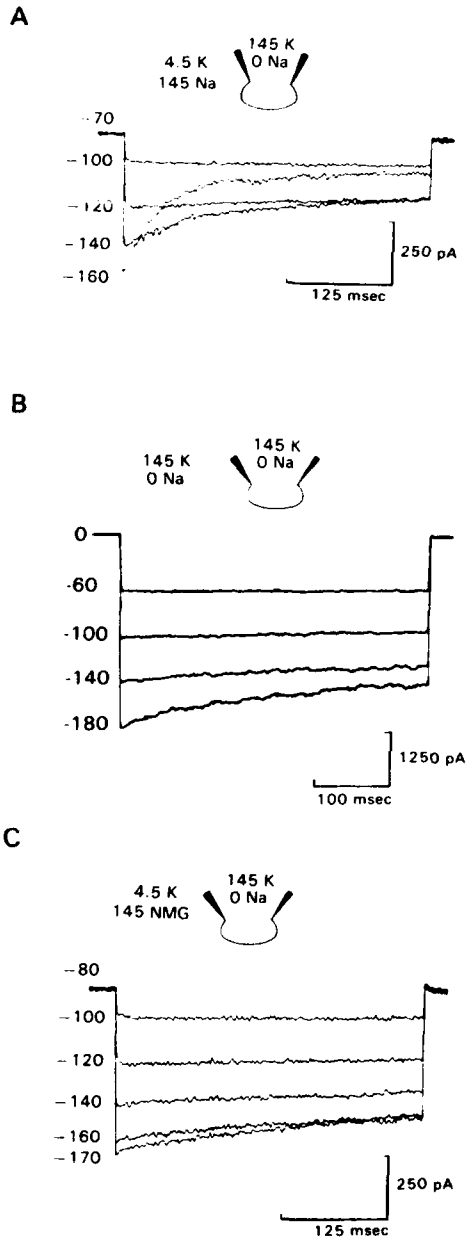

Figure 5. (*A*) Digitized whole-cell records from a J774 cell bathed in NaCl Hanks' solution. Inward currents were recorded in response to hyperpolarizing voltage steps to the potentials shown in the figure. $V_h = -70$ mV. (*B*) Whole-cell records from a cell bathed in Hanks' solution with all Na replaced by K. Average resting V_m of cells bathed in this solution was near 0 mV, so $V_h = 0$ mV. (*C*) Whole-cell records from a cell bathed in Hanks' solution with all Na replaced by NMG. Average resting V_m of cells in NMG Hanks' solution was -76 mV. $V_h = -80$ mV. Records in *A* and *B* have been corrected for leak and capacity current. Records in *C* were not corrected; leak conductance was ~10% of total.

indicates that inactivation was not current dependent. Barium, a classic blocker of inward-rectifying K currents (Hagiwara et al., 1978; Standen and Stanfield, 1978) produced both concentration- and voltage-dependent inhibition of inward current when applied to the bath (data not shown).

Single-channel current. Inward-rectifying single-channel current fluctuations have been recorded in both human macrophages (Gallin and McKinney, 1988) and J774 cells (McKinney and Gallin, 1988). Fig. 6 shows single-channel currents

recorded in the cell-attached patch mode from a J774 cell. Single-channel current was activated over the same voltage range as the macroscopic inward-rectifying current. Inward single-channel currents increased in amplitude as the patch was hyperpolarized, and did not reverse above E_K. Single-channel conductance in cell-attached patches with 145 mM K in the patch electrode was 30 pS and was proportional to the square root of $[K]_o$ (see Fig. 7, *A*, *B*, and *C*). E_{rev} was proportional to the log of $[K]_o$ with a slope of 63 mV per 10-fold change in $[K]_o$ (Fig. 7 *D*). Absolute values of the extrapolated E_{rev} are somewhat below the corresponding values of E_K across the patch membrane, probably due to the fact that the channel rectifies near E_K. More accurate E_{rev} values obtained using ramp stimuli were very close to E_K. Inward single-channel currents were blocked by the addition of barium to the external surface of the membrane (McKinney and Gallin, 1988). Neither macroscopic nor single-channel currents were affected by the replacement of external chloride by isethionate.

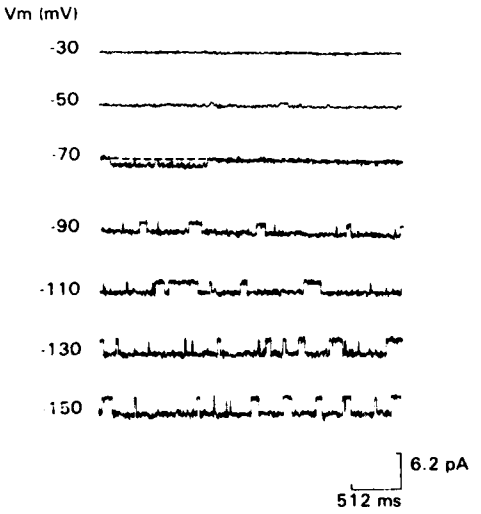

Figure 6. Cell-attached patch recording of single-channel currents at various holding potentials from a J774 cell bathed in Na Hanks' solution. V_m across the patch is given as pipette potential (V_p) + resting V_m (approximately −70 mV). Dashed line represents closed current level. Records were filtered at 50 Hz (upper two traces) or 200 Hz and digitized at >2× the filtering frequency. Pipette contained K Hanks' solution consisting of (in mM) 145 KCl, 10 NaCl, 1 $MgCl_2$, 1.1 EGTA, 0.1 $CaCl_2$, and 10 HEPES, pH 7.3. Free Ca^{++} in this solution was $<10^{-8}$ M.

In Fig. 5, we show that inward-rectifying whole-cell currents inactivate at very negative potentials, even in the absence of Na. Fig. 8 shows that inactivation is a property of single-channel currents as well. In the cell-attached patch configuration, we repetitively applied hyperpolarizing pulses to the membrane, and observed single-channel activity that declined with time during the pulse. These traces were summed and averaged, and produced a current record that showed clear evidence of inactivation.

Consistent with the above finding is the observation that the open state probability of inward-rectifying channels is voltage dependent. Single-channel open probability was measured in eight patches containing only one channel and from two patches containing two channels. As the potential across the patch became more negative, channel closures were longer (up to tens of seconds). Open probability declined from an average of 0.87 at −40 mV to 0.43 at −120 mV.

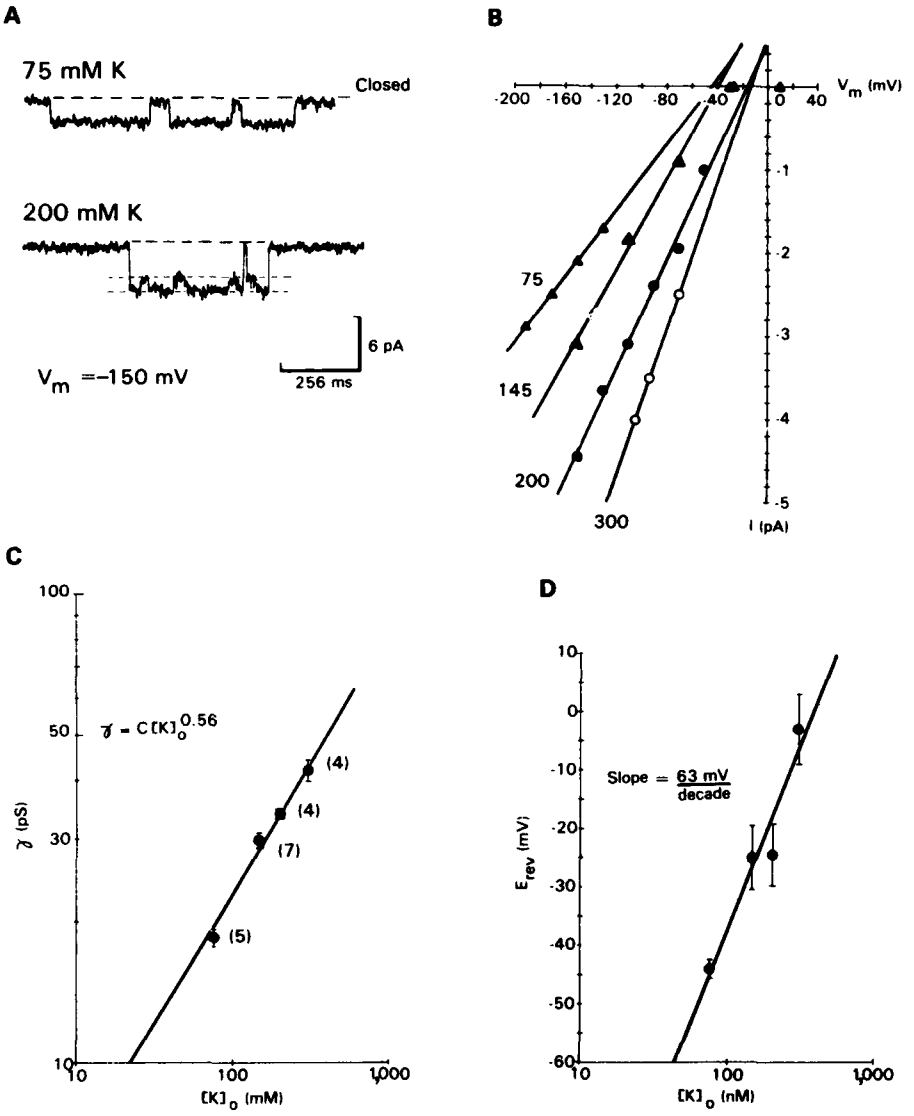

Figure 7. (*A*) Single-channel records from two cell-attached patches with different [K] in the pipette. Note subconductance level in the lower record. (*B*) Single-channel I-V relationships from four cells, each bathed in Na Hanks' solution, but with different [K] in the pipette; 75 (△), 145 (▲), 200 (●), or 300 (○) mM. [NA] in the pipette was 75, 10, 10, and 10 mM, respectively. (*C*) Log-log plot of single-channel conductance vs. $[K]_o$. Number of experiments at each [K] is given adjacent to each point. Data were fit to the equation γ (single-channel conductance) = $C[K]_o^x$, where x was 0.56. Limiting conductance in 4.5 $[K]_o$ was 4.1 pS. (*D*) Extrapolated E_{rev} vs. log $[K]_o$, fitted by a straight line with a slope of 63 mV per 10-fold change in $[K]_o$ (McKinney and Gallin, 1988).

Thus far, we have shown that inward-rectifying whole-cell and single-channel currents correspond in the following ways: (*a*) voltage dependence of activation is the same, (*b*) each is K selective, (*c*) whole-cell and single-channel conductances are proportional to the square root of $[K]_o$, (*d*) each is blocked by similar concentrations of barium, (*e*) each shows voltage-dependent inactivation in the absence of sodium. We would like to conclude that the current through the 30-pS inward-rectifying channel can fully account for the behavior of the macroscopic inward-rectifying current, and in J774 cells, this may be the case. However, some recent observations made on human macrophages make this conclusion less firm. Another inward-rectifying K current, of

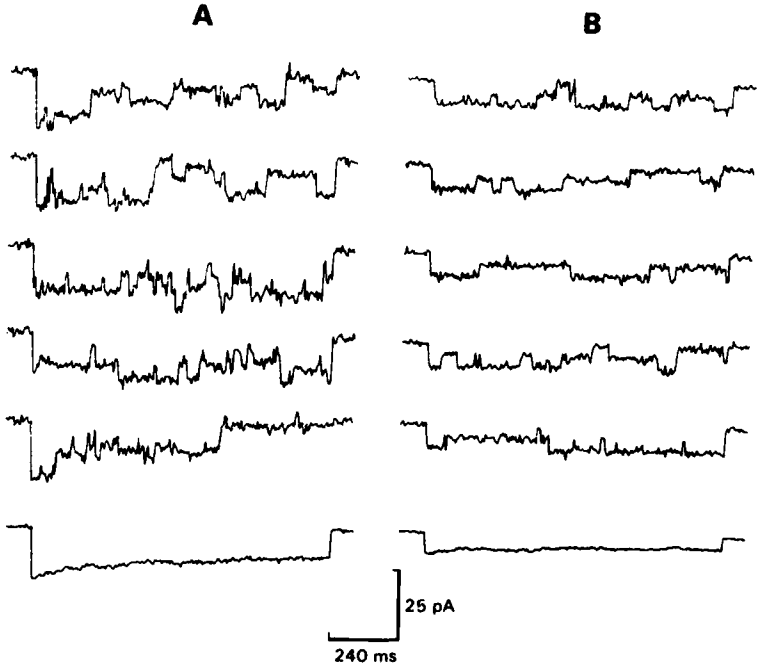

Figure 8. Single-channel records from a cell-attached patch elicited in response to repetitively applied hyperpolarizing steps. Patches were held at −30 mV and stepped to −190 (*A*) or −150 mV (*B*). At the bottom of each group of sweeps is the averaged current record for that voltage, comprising 40 or 48 sweeps applied at 5-s intervals. Leak and capacitative currents recorded in response to eight equal and opposite sized steps were averaged and subtracted from each record. J774 cell was bathed in Na Hanks' solution. Pipette contained Na-free K Hanks' solution to eliminate interference from Na (McKinney and Gallin, 1988).

slightly larger conductance, and possibly Ca activated, is present in human cells (see next section on bursting inward-rectifying K channel) and may account for some of the macroscopic inward current in these cells.

Expression and Functional Relevance. The only known function of the voltage-dependent inward-rectifying K conductance in macrophages is to help set the resting membrane potential of the cell near E_K. The resting membrane potential of adherent J774 cells in normal Hanks' solution is approximately −75 mV, a value in the same range as that obtained from measurements using the cationic lipophilic probe triphenylmethylphosphonium (−85 mV) (Sung et al., 1985). The dependence of

channel gating on $[K]_o$ may be significant since the macrophage is present in sites of dead and dying tissue, and may well be exposed to elevated $[K]_o$. A rise in $[K]_o$ will increase the conductance, yet preserve a steep I-V relationship so that the cells remain sensitive to small current fluctuations.

The expression of inward-rectifying channels cells appears to be regulated; it is present in only one-third of human macrophages, which consequently have a slightly more negative resting membrane potential than cells that do not exhibit this conductance (−56 vs. −42 mV; Gallin and McKinney, 1988). In J774 cells, inward currents increase in size with time after adherence (Gallin and Sheehy, 1985), which may account for part of the difference between the resting potential in the suspended state vs. adherent state (−14 mV vs. −85 mV; Sung et al., 1985). However, the appearance of this conductance has not been correlated with the appearance of any specific function in J774.1 cells. Its presence is not necessary for J774 cells to be able to carry out chemotaxis or phagocytosis or to generate an oxidative burst; these functions still occur in the presence of 2 mM barium (our unpublished results). The involvement of the inward-rectifying channel in other macrophage functions, such as secretion or target cell lysis, has not been tested. The inward-rectifying conductance is absent in mouse peritoneal macrophages cultured for 4 d (Ypey and Clapham, 1984) but is present in peritoneal macrophages cultured for longer periods (Gallin and Livengood, 1981; Randriamampita and Trautmann, 1987).

Bursting Inward K Channel

Single-channel current. Exposure of human macrophages to the calcium ionophore ionomycin activates a second type of inwardly rectifying K channel (Gallin, 1988). Fig. 9 A shows current tracings from a cell-attached patch obtained from a human macrophage before and after exposing the cell to 10^{-6} M ionomycin, which was locally applied by pressure injection from a patch pipette. In the absence of ionomycin, only one type of channel was evident, the ~30-pS inwardly rectifying channel described in the preceding section. After exposure to ionomycin, a second type of inward current appeared that was slightly larger in amplitude and showed bursting behavior. The current showed inward rectification; outward currents of similar amplitude were not observed when the patch was depolarized. At very positive potentials (+130 mV), small outward current fluctuations (~0.5 nAmp) were present which may have been due to outward current through this channel. Ionomycin induced this channel in 9 of 10 cells tested.

Fig. 9 *B* shows the I-V curves of both the larger bursting and the smaller inward-rectifying channels obtained in the presence of ionomycin. Conductances were 28 pS and 36 pS, respectively. The reversal potentials of the two channels were similar ($V_{pipette}$ = 49 and 54 mV). Assuming that the resting V_m was 50 mV, the potential across the patch was actually near zero, since $V_m = V_{pipette}$ + resting V_m. Since E_K was also near 0 mV, these data indicate that this channel is primarily K selective. Removal of Cl from that patch pipette had no effect on conductance or E_{rev}. We conclude that the 36-pS inward-rectifying K channel is distinct from the 30-pS inward-rectifying channel, since it has a different conductance, shows bursting kinetics and is found in patches with or without the 30-pS channel.

A similar conductance channel recently has been described in human macrophages (McCann et al., 1987) and mouse peritoneal macrophages (Somogyi et al., in

press) in the absence of ionomycin. The channel in mouse peritoneal cells showed inward rectification. However, McCann et al. (1987) report that the 36-pS channel in human macrophages did not rectify. We occasionally saw activity of the 36-pS channel in patches from cells not exposed to ionomycin but in our studies the channel always rectified. In these instances, channel activity was present immediately after obtaining a tight seal, and then frequently subsided. Unlike the large conductance Ca-activated K channel, this channel appears to be present in human monocytes that have been cultured for as little as 1 d. We are currently characterizing its calcium and voltage sensitivities and its pharmacology. We speculate that this channel, and not the large conductance Ca-activated K channel, is responsible for the repetitive membrane hyperpolarizations previously described, since (*a*) the bursting pattern of this channel is similar to the pattern of the spontaneous hyperpolarizations, and (*b*) ionomycin induces both channel activity and membrane hyperpolarizations (Gallin et al., 1975). A similar Ca-activated inward-rectifying K channel of slightly larger conductance (50 pS in 200 mM $[K]_o$) has recently been described in HeLa cells (Sauve et al., 1986). In

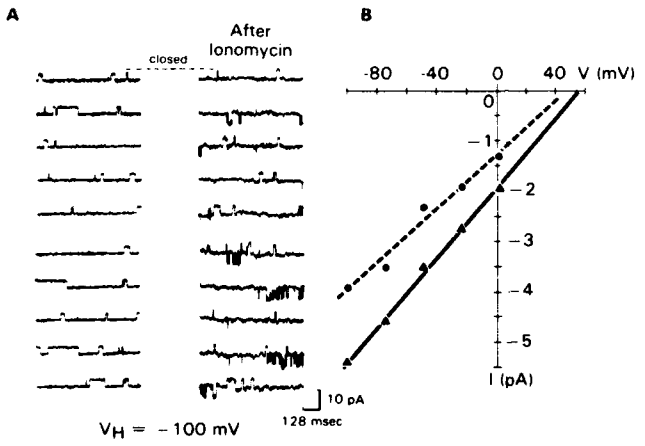

Figure 9. (*A*) Single-channel currents recorded from a cell-attached patch from a human macrophage before and after applying 10^{-6} M ionomycin from a second electrode. V_h = −100 mV. Data were filtered at 500 Hz and digitized at 1 kHz. Patch electrode contained KCl Hanks' solution; bath contained NaCl Hanks' solution. (*B*) I-V relationship of each of the channels present in the patch following exposure to ionomycin.

these cells the addition of histamine, which increases $[Ca]_i$, initiates oscillatory single-channel activity and membrane hyperpolarization (Sauve et al., 1987).

Outwardly Rectifying K Conductance

An outwardly rectifying K conductance has been described at the whole-cell current level in resident mouse peritoneal macrophages (Ypey and Claphan, 1984), cultured human monocytes (Nelson et al., 1986), and two macrophage cell lines, J774.1 (Gallin and Sheehy, 1985) and P388D1 (Sheridan and Bayer, 1986). This conductance activates at potentials positive to −50 mV, inactivates over a time course of seconds, and is blocked by 4-aminopyridine (Ypey and Clapham, 1984; Gallin and Sheehy, 1985). As is the case with the smaller inwardly rectifying K conductance, it appears to be variably expressed with time in culture. Ypey and Clapham (1984), using resident mouse peritoneal macrophages, reported that this conductance was absent during the first day after isolation but was present in 96% of the cells cultured for 1–4 d. It was not found in long-term (2–6 wk) cultured mouse peritoneal (Gallin and Livengood, 1981)

and spleen macrophages (Gallin, 1981). These findings have recently been confirmed by Randriamampita and Trautmann (1987) who report that in mouse peritoneal macrophages this conductance decreases with time in culture. In J774 cells, outward current is present 1–8 h after adherence, and is not present in long-term adherent cultures where the inward-rectifying K current is predominant (Gallin and Sheehy, 1985). The current appears to be continuously present in the mouse-derived cell line P388D1 (Sheridan and Bayer, 1986). An example of outward currents recorded from J774 cells is shown in Fig. 10.

The functional relevance of the outwardly rectifying K channel in the macrophage has not yet been determined. Similar currents have been described in detail in T lymphocytes (Cahalan et al., 1985). In T lymphocytes and natural killer cells, agents that block this current inhibit mitogenesis and cytotoxicity, respectively, which implies that it plays at least a permissive role in these processes (Chandy et al., 1984; Deutsch et al., 1986). Nelson et al. (1986) have reported that this conductance is inhibited by phorbol myristate acetate (PMA) in cultured human monocytes.

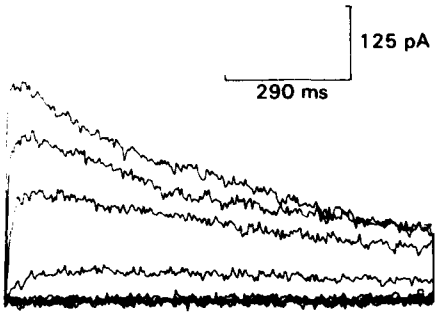

Figure 10. Digitized whole-cell records from a J774 cell plated for ~6 h and bathed in Na Hanks' solution. V_h = resting V_m = −66 mV. Depolarizing steps were applied in 10-mV increments from −60 to 0 mV.

Conclusion

To date, four different K conductances have been described in macrophages. They include a Ca-activated K conductance described at both the whole-cell and single-channel level in human macrophages that is not present in freshly isolated monocytes but is expressed during the first week in tissue culture. The absence of this conductance in monocytes implies that it is not required for phagocytosis, chemotaxis, or other functions of the immature macrophage. A second K conductance, described at both the whole-cell and single-channel level, is a voltage-dependent inward-rectifying K conductance that is present in a variety of macrophages, including cultured human peripheral blood monocytes, cultured mouse spleen and peritoneal macrophages, and J774 cells. It is important in setting the resting membrane potential of the cell, and in J774 cells is not necessary for chemotaxis or phagocytosis to occur. In addition to these two well-characterized K conductances, there are two other K conductances that have only been partially characterized. These are a second inward-rectifying K channel that may be activated by internal calcium, and an inactivating outward K current similar to that described in the T cell.

Acknowledgments

This work was supported by the Armed Forces Radiobiology Research Institute, Defense Nuclear Agency, under work unit 00020. Views presented in this paper are

those of the authors; no endorsement by the Defense Nuclear Agency has been given or should be inferred.

References

Barrett, J. N., K. L. Magleby, and B. S. Pallotta. 1982. Properties of single calcium-activated potassium channels in cultured rat muscle. *Journal of Physiology*. 331:211–230.

Cahalan, M. D., K. G. Chandy, T. E. DeCoursey, and S. A. Gupta. 1985. A voltage-gated potassium channel in human T-lymphocytes. *Journal of Physiology*. 357:197–238.

Chandy, K. G., T. E. DeCoursey, and M. D. Cahalan. 1984. Voltage-gated K channels are required for human T lymphocyte activation. *Journal of Experimental Medicine*. 160:369–385.

Deutsch, C., D. Krause, and S. C. Lee. 1986. Voltage-gated potassium conductance in human T lymphocytes stimulated with phorbol ester. *Journal of Physiology*. 372:405–423.

Dos Reis, G. A., and G. M. Oliveiro-Castro. 1977. Potassium dependent slow membrane hyperpolarizations in mice macrophages. *Biochimica et Biophysica Acta*. 469:257–263.

Eckert, R., and P. Brehm. 1979. Ionic mechanisms of excitation in Paramecium. *Annual Review of Biophysics and Bioengineering*. 8:353–383.

Gadsby, D. C., and P. F. Cranefield. 1977. Two levels of resting potential in cardiac Purkinje fibers. *Journal of General Physiology*. 70:725–746.

Gallin, E. K. 1981. Voltage clamp studies in macrophages from mouse spleen cultures. *Science*. 214:458–460.

Gallin, E. K. 1984. Calcium and voltage-activated potassium channels in human macrophages. *Biophysical Journal*. 46:821–825.

Gallin, E. K. 1988. Inwardly rectifying K^+ channels induced by Ionomycin in cultured human macrophages. *Biophysical Journal*. 53:548a. (Abstr.)

Gallin, E. K., and J. I. Gallin. 1977. Interaction of chemotactic factors with human macrophages: Electrophysiology of the response. *Journal of Cell Biology*. 75:277–289.

Gallin, E. K., and D. R. Livengood. 1981. Inward rectification in mouse macrophages: evidence for a negative slope resistance region. *American Journal of Physiology*. 241:C9–C17.

Gallin, E. K., and L. C. McKinney. 1988. Patch clamp studies in human macrophages: Single-channel and whole-cell characterization of two K conductances. *Journal of Membrane Biology*. 103:55–66.

Gallin, E. K., and L. C. McKinney. 1989. Ionic conductances and transport mechanisms in phagocytic leukocytes. *In The Cellular Biochemistry and Physiology of the Neutrophil*. M. Hallet, editor. CRC Press, Inc., Boca Raton, FL. In press.

Gallin, E. K., and P. A. Sheehy. 1985. Differential expression of inward and outward potassium currents in the macrophage-like cell line J774.1. *Journal of Physiology*. 369:475–499.

Gallin, E. K., M. Wiederhold, P. Lipsky, and A. Rosenthal. 1975. Spontaneous and induced membrane hyperpolarizations in macrophages. *Journal of Cellular Physiology*. 86:653–662.

Guggino, S. E., W. B. Guggino, N. Green, and B. Sacktor. 1987. Blocking agents of Ca-activated K channels in cultured medullary thick ascending limb cells. *American Journal of Physiology*. 252:C128–C137.

Hagiwara, S., S. Miyaszki, W. Moody, and J. Patlak. 1978. Blocking effects of barium and hydrogen ions on the potassium current during anomalous rectification in the starfish egg. *Journal of Physiology*. 279:167–185.

Hagiwara, S., and K. Takahashi. 1974. The anomalous rectification and cation selectivity of the membrane of a starfish egg cell. *Journal of Membrane Biology*. 18:61–80.

Ince, C., P. C. Leijh, M. Meijer, E. VanBavel, and D. Ypey. 1984. Oscillatory hyperpolarizations and resting membrane potentials of mouse fibroblast and macrophage cell lines. *Journal of Physiology*. 352:625–635.

Kruskal, B. J., and F. R. Maxfeld. 1987. Cytosolic free calcium increases before and oscillates during frustrated phagocytosis in macrophages. *Journal of Cell Biology*. 105:2685–2693.

Leech, C. A., and P. R. Stanfield. 1981. Inward rectification in frog skeletal muscle and its dependence on membrane potential and external potassium. *Journal of Physiology*. 319:295–309.

Lindau, M., and J. Fernandez. 1986. A patch clamp study of histamine secreting cells. *Journal of Physiology*. 88:349–368.

Lipton, S. A. 1986. Antibody activates cationic channels via second messenger Ca^{2+}. *Biochimica et Biophysica Acta* 856:59–67.

McCann, F., T. Keller, and P. Guyre. 1987. Ion channels in human macrophages compared with the U-937 cell line. *Journal of Membrane Biology*. 96:57–64.

McKinney, L. C., and E. K. Gallin. 1988. Inwardly rectifying whole-cell and single channel K currents in the murine macrophage cell line J774. *Journal of Membrane Biology*. 103:41–53.

Miller, C., E. Moczydlowski, R. Latorre, and M. Phillips. 1985. Charybdotoxin, a protein inhibitor of single channel Ca-activated K channels from mammalian skeletal muscle. *Nature*. 313:316-318.

Nakagawara, A., C. Nathan, and Z. Cohn. 1981. Hydrogen peroxide metabolism in human monocytes during differentiation in vitro. *Journal of Clinical Investigation*. 68:1243–1252.

Nelson, D. J., L. Rufer, T. Nakayama, and J. M. Zeller. 1986. Phorbol ester block of voltage-dependent K current in monocyte-derived macrophages. *Biophysical Journal*. 49:164*a*. (Abstr.)

Nichols, B., D. F. Bainton, and M. G. Farqhuar. 1971. Differentiation of monocytes. Origin nature and fate of azurophilic granules. *Journal of Cell Biology*. 50:498–510.

Persechini, P. M., E. G. Araujo, and G. M. Oliveiro-Castro. 1981. Electrophysiology of phagocytic membranes: induction of slow membrane hyperpolarizations in macrophages and macrophage polykaryons by intracellular calcium injections. *Journal of Membrane Biology*. 61:81–90.

Peterson, O. H., and Y. Maruyama. 1984. Calcium-activated potassium channels and their role in secretion. *Nature*. 307:693–696.

Pfefferkorn, L. 1984. Transmembrane signaling: an ion flux-independent model for signal transduction by complexed Fc receptor. *Journal of Cell Biology*. 99:2231–2240.

Randriamampita, C., and A. Trautmann. 1987. Ionic channels in murine macrophages. *Journal of Cell Biology*. 105:761–769.

Sauve, R., C. Simoneu, R. Monette, and G. Roy. 1986. Single-channel analysis of the potassium permeability in HeLa cancer cells: evidence for a calcium-activated potassium channel of small unitary conductance. *Journal of Membrane Biology*. 92:269–282.

Sauve, R., C. Simoneau, L. Parent, R. Monette and G. Roy. 1987. Oscillatory activation of calcium-dependent potassium channels in HeLa cells induced by histamine H1 receptor stimulation. A single channel study. *Journal of Membrane Biology*. 96:199–208.

Schwarze, W., and H. A. Kolb. 1984. Voltage-dependent kinetics of an ionic channel of large unit conductance in macrophages and myotube membranes. *Pflügers Archiv European Journal of Physiology*. 402:281–291.

Sheridan, R. E. and B. M. Bayer. 1986. Ionic membrane currents induced in macrophages during cytolysis. *Federation Proceedings*. 45:1009*a*. (Abstr.)

Somogyi, R., J. Ubl, and H. A. Kolb. 1987. Zymosan and potassium induced activation of single voltage-dependent ion channels in membranes of peritoneal macrophages. *Advances in the Biosciences*. 66:275–284.

Standen, N. B., and P. R. Stanfield. 1978. A potential and time-dependent blockade of inward rectification in frog skeletal muscle fibres by barium and strontium ions. *Journal of Physiology*. 820:169–191.

Sung, S. S., J. D. Young, A. M. Origlio, J. M. Heiple, H. R. Kaback, and S. C. Silverstein. 1985. Extracellular ATP perturbs transmembrane ion fluxes, elevates cytosolic [Ca] and inhibits phagocytosis in mouse macrophages. *Journal of Biological Chemistry*. 260:13442–13449.

Van Furth, R. 1985. Mononuclear Phagocytes. Characteristics, Physiology and Function. Martinus Nihoff, Boston-Dordrecht-Lancaster.

Young, D. J., J. Unkeless, T. Young, A. Mauro, and Z. Cohn. 1983. Role of mouse macrophage IgG Fc receptor as ligand-dependent ion channel. *Nature*. 306:186–189.

Ypey, D. L., and D. E. Clapham. 1984. Development of a delayed outward rectifying K conductance in cultured mouse peritoneal macrophages. *Proceedings of the National Academy of Sciences*. 81:3083–3087.

Zwadlo, G., E. Brocker, D. von Bassewitz, U. Feige, and C. Sorg. 1985. Monoclonal antibody to a differentiation antigen present in mature human macrophages and absent from monocytes. *Journal of Immunology*. 134:1487–1492.

Apical membrane potassium conductance in guinea pig gallbladder epithelial cells

PAMELA J. GUNTER-SMITH
Physiology Department, Armed Forces Radiobiology Research Institute, Bethesda, Maryland 20814-5145

GUNTER-SMITH, PAMELA J. *Apical membrane potassium conductance in guinea pig gallbladder epithelial cells.* Am. J. Physiol. 255 (Cell Physiol. 24): C808–C815, 1988.—The fractional resistance of the apical membrane (f_{Ra}) of guinea pig gallbladder epithelial cells was observed to vary with changes in apical membrane potential (V_a). Depolarizing V_a from a base-line potential of −60 to −30 mV decreased f_{Ra} from 0.79±0.03 to 0.59±0.05. A comparable hyperpolarization had no effect on f_{Ra}. The potassium channel blocker tetraethylammonium (TEA) inhibited the changes in f_{Ra} induced by voltage when added to the mucosal but not when added to the serosal solution. Mucosal addition of Ba^{2+} and decreased pH also inhibited changes in f_{Ra}, whereas quinidine and 4-amino-pyridine did not. These results indicate that an increase in the K^+ conductance of the apical membrane is responsible for changes in f_{Ra} with membrane depolarization. The current-voltage relation of this TEA-sensitive pathway was determined from differences in transepithelial current in the presence and absence of maximally effective concentrations of TEA and analyzed with respect to the Goldman constant-field equation. Computer-generated, best-fit analysis to the data indicated that they cannot be easily reconciled with K^+ movement through a voltage-independent pathway or channel. Taken together, the results suggest that activation of a voltage-dependent K^+ conductance in the apical membrane is responsible for changes in f_{Ra} with V_a. This conductance also appears to be Ca^{2+}-sensitive as ionomycin caused a shift in the relation between V_a and f_{Ra}.

voltage; fractional resistance; apical membrane potential

WITH THE APPLICATION of electrophysiological and patch-clamp techniques to the study of ion transport by epithelial cells, evidence generated by numerous laboratories indicates that conductive ion movements across the individual cell membranes of these cells occur through ion channels similar to those extensively studied in excitable cell membranes (for recent reviews see Refs. 31 and 32). Although a major role for intracellular mediators such as Ca^{2+}, pH, and cyclic nucleotides has been given in the regulation of these channels in epithelia, more recently, the importance of membrane voltage in the regulation of ion channels in these nonexcitable tissues has become recognized. For example, voltage-dependent anion conductances have been reported in toad skin (18), rabbit proximal tubule (10), dogfish rectal gland (12), and MDCK cells (19); and K^+ conductances have been reported in choroid plexus (3), medullary thick ascending limb cells (13), cortical collecting tubule (5, 9, 17, 25), toad urinary bladder (24), MDCK cells (1), *Necturus* (7) and *Triturus* gallbladders (23), and cultured renal cells (20). These voltage-dependent K^+ channels are also regulated by intracellular mediators such as Ca^{2+}. Furthermore, several distinct subsets of channels with respect to single channel conductance, pharmacology, and mode of regulation often reside in the same membrane (8, 12, 13) making individual contributions to the overall permeability of the membrane for a given ion. Although in most cases the exact physiological functions of these various channels are not known, channels in epithelia are thought to be important in maintaining the normal membrane potential of the cell, the vectorial transport of ions across the epithelial cell layer, and the regulation of cell volume.

In this study, I report on the apical membrane K^+ conductance and its regulation in guinea pig gallbladder epithelial cells. Evidence will be presented indicating that this conductance is regulated by both voltage and Ca^{2+}. Additionally, I will present evidence that the population of channels comprising the apical membrane K^+ conductance are distinct from those comprising that of the basolateral membrane. [Sections of these results have appeared previously in abstract form (14).]

METHODS

Animals and solutions. Male Hartley guinea pigs (300–800 g) used in these experiments were screened for evidence of disease before use. They were housed in groups in stainless steel cages, maintained in rooms at 21°C, 50% rh, 12-h light-dark cycle (no twilight), and allowed access to commercial chow and tap water ad libitum. Gallbladders were removed after death of the animals by halothane inhalation followed by cervical dislocation. The bladders were stripped of their underlying musculature by blunt dissection and mounted in a chamber having a diameter of 0.13 cm^2. Both mucosal and serosal surfaces were continuously superfused by Ringer solution from reserviors by gravity feed. Standard Ringer solution contained (in mM) 130 Na^+, 108 Cl^-, 5 K^+, 1.0 Ca^{2+}, 1.0 Mg^{2+}, 35 *N*-2-hydroxyethylpiperazine-*N'*-2-ethanesulfonic acid (HEPES), and 10 glucose (pH 7.4) and gassed with 100% O_2. Bath pH was decreased by replacement of HEPES with Na_2HPO_4-NaH_2PO_4. Bath K^+ was increased by equimolar replacement of *N*-methyl-D-glucamine (NMDG). In these experiments, 50 mM NaCl was initially replaced by an equivalent amount of NMDGCl.

Tetraethylammonium chloride (TEA) and $BaCl_2$ were added by equimolar substitution of NaCl. All other drugs were added directly to normal Ringer except ionomycin, which was initially dissolved in dimethyl sulfoxide (DMSO). Unless indicated differently, changes from and

additions to the standard Ringer were made to the mucosal bath alone. Experiments were performed at 37°C.

Electrical measurements. The transepithelial potential with respect to the mucosal bath (V_t) was monitored by means of calomel cells in contact with the bathing solution via Ringer-agar bridges. Transepithelial current (I_t) was passed by means of an automatic voltage-clamp device (Physiologic Instruments, Houston, TX) and Ag-AgCl electrodes. Tissues were normally maintained under short-circuit conditions except for brief periods (300 ms) during which they were clamped to ±10 mV to measure transepithelial resistance (R_t). The intracellular potential across the apical membrane (V_a) was measured by 0.5 M KCl-filled microelectrodes having a resistance of 80–100 MΩ. The intracellular potential across the basolateral membrane V_b was calculated from $V_t = V_a + V_b$. Values of V_a and V_b are reported with respect to their respective bathing solutions. The fractional resistance of the apical membrane (f_{Ra}) was calculated from the ratio of the deflections produced in V_a and V_t by the bipolar voltage pulses.

Changes in V_a with V_t were determined from two protocols. In the first (*protocol 1*), V_t was stepped in 10-mV increments to increasingly more positive or negative potentials with a duration of 2 s until $V_t = \pm 100$ mV; ~40 s were required to complete the sequence. f_{Ra} was calculated from $\Delta V_a/\Delta V_t$ produced by 200 ms bipolar deflections of 10 mV superimposed on the clamping step. In the second protocol (*protocol 2*), V_t was stepped from 0 to a positive potential for 100 ms, back to 0 for 200 ms, then to a negative potential for 100 ms. The value of the clamp potential in either direction was increased by 10 mV until $V_t = \pm 100$ mV. f_{Ra} was calculated from $\Delta V_a/\Delta V_t$. All clamping sequences were under computer control (INDEC Systems, Sunnyvale, CA) as were data collection and analysis. Deflections in V_a and V_t during the clamping sequences were measured 25–50 ms after initiation of the pulse and averaged over a 20-ms interval. As will be shown later, any existing voltage transients were over by this time. For calculation of transmembrane current (I), outward current is considered positive.

Statistics. Significant differences between means were determined by the Student's t test for paired or unpaired observations. Unless indicated otherwise, n refers to the number of tissues studied.

RESULTS

Effect of high K^+. The effect of increasing mucosal bath K^+ (5–50 mM) on V_a and f_{Ra} is shown in Fig 1. In three such experiments (10 cells), V_a and f_{Ra} averaged 60.8 ± 2.3 mV and 0.82 ± 0.03, respectively. V_a depolarized ($\Delta V_a = 11.9 \pm 1.9$) when mucosal K^+ was increased as predicted for a K^+-selective membrane. In most cells, f_{Ra} also decreased ($\Delta f_{Ra} = 0.05 \pm 0.01$, $n = 7$), whereas in others ($n = 3$), there was no change.[1] TEA (15 mM), which has previously been shown to block K^+ channels in a variety of tissues (22, 31, 32), inhibited the high K^+ depolarization and concomitant change in f_{Ra} but had little effect on initial V_a or f_{Ra}.

Effect of voltage. Also shown in Fig. 1 is the effect of clamping the V_t from zero to more serosa-positive potentials on V_a. Not only does V_a depolarize but f_{Ra} decreases as well. Although TEA did not block the depolarization induced by clamping V_t, it did block the accompanying change in f_{Ra}. TEA was ineffective when added to the serosal solution and, further, had no effect on high-K^+ depolarizations of the basolateral membrane induced by elevating serosal bath K^+ (data not shown).

The effect of transepithelial voltage on membrane potential of one of these cells is shown in more detail in Fig. 2 in which *protocol 1* was used. Increasing V_t depolarized V_a linearly until V_a reached aprroximately −30 mV. Basolateral membrane potential (V_b) hyperpolarized in a similar fashion. The magnitude of the change in V_a is clearly larger than that in V_b. This is expected because f_{Ra} is ~0.8 in these cells, indicating that the apical membrane resistance accounts for 80% of the total cellular resistance with the basolateral membrane comprising only 20%. At V_a more depolarized than −30 mV, the relation between V_a, V_b, and V_t becomes distinctly curvilinear and a greater percent change in V_b is observed than in V_a. In the presence of TEA, however, the relation between V_a, V_b, and V_t remains linear throughout the range of voltages used in the study.

Figure 3 shows the relation between V_a (varied by clamping V_t) and f_{Ra} determined for the same cell in Fig. 2. As was observed for the relation between V_a and V_t, depolarizing V_a below −30 mV drastically changes the relation such that depolarization beyond this voltage causes a progressive decrease in f_{Ra}. The potential (−30 mV) at which changes in f_{Ra} were observed was surprisingly constant from tissue to tissue. In a few cases, however, changes in f_{Ra} occurred at higher (−50 mV) or lower (−20 mV) potentials. In contrast to depolarizing pulses, hyperpolarization of V_a generally had little effect on f_{Ra}. In experiments in which hyperpolarization was effective (3 of 14), f_{Ra} increased rather than decreased.

Despite the magnitude of the changes in V_a and f_{Ra} discussed above, clamping V_t had little effect on R_t (Fig. 4). Clamping V_t to ±100 mV changed R_t by 7.1 ± 1.9% ($n = 14$). Further, the addition of TEA altered R_t by only 6.0 ± 2.6% ($n = 6$).

The time course of changes in V_a on clamping V_t is shown in greater detail with the oscilloscope traces in Fig. 5 of a cell in which clamping *protocol 2* was used. Hyperpolarizing pulses resulted in equal increments in V_a. As shown above, depolarizing V_a beyond −30 mV, however, resulted in an obvious departure from linearity and an increase in the time required to reach a steady state (~25 ms). In the presence of TEA, hyperpolarizing and depolarizing pulses are symmetrical. The relations between V_a and f_{Ra}, and V_a and V_t obtained using this clamping protocol (data not shown) are similar to that obtained using *protocol 1* (Figs. 2 and 3) in that changes in f_{Ra} were observed at V_a more depolarized than −30 mV. However, the absolute value of f_{Ra} obtained for a particular value of V_a differed from that obtained from

[1] Because changes in f_{Ra} were small, it is reasonable to suspect that sometimes changes were within the noise of the measuring system, perhaps accounting for the observation that in some cells no change was observed. It is not clear why the magnitude of changes in f_{Ra} with K_m elevation is so small. However, considering the magnitude of depolarization (~11 mV), it may reflect a small partial conductance of the membrane to K^+ under basal conditions. A similar conclusion was reached by Cremaschi et al. (4) who in addition demonstrated Na^+ and Cl^- conductances in the apical membrane of this tissue.

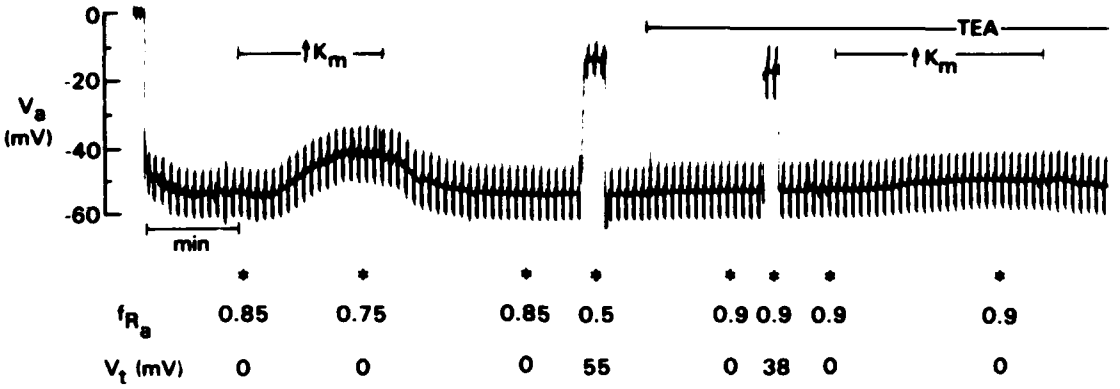

FIG. 1. Effect of increasing mucosal K^+ (K_m) and V_t on V_a and f_{Ra} in presence and absence of TEA (15 mM). K_m was increased from 5 to 50 mM. See text for definitions.

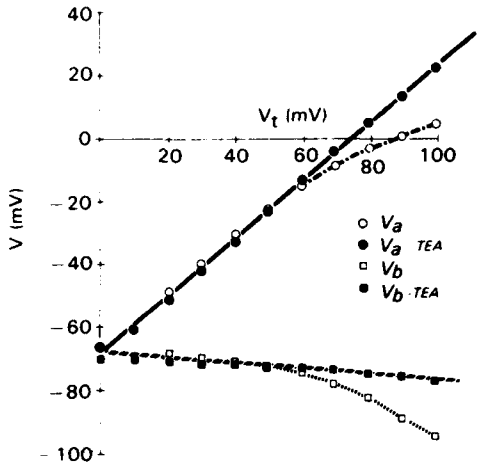

FIG. 2. Effect of clamping V_t on V_a and V_b in the absence and presence of TEA. Representative data obtained from a single impalement using *protocol 1*. See text for definitions.

protocol 1. This is expected because *protocol 2* calculates f_{Ra} from large changes in V_a (±100 mV) over regions in which the relation is not linear. Thus f_{Ra} calculated using *protocol 1* (i.e., 10 mV deflections superimposed on the

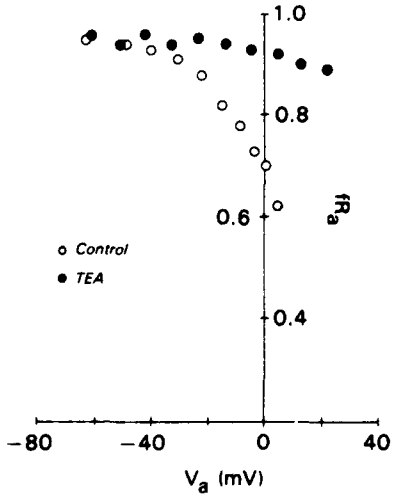

FIG. 3. Relation between V_a and f_{Ra} in absence and presence of TEA. Data from same impalement used in Fig. 2. See text for definitions.

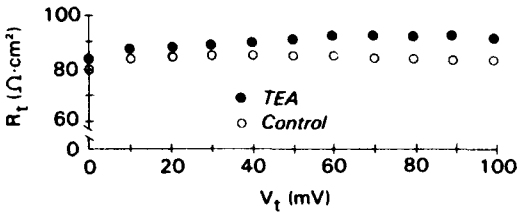

FIG. 4. Effect of clamping V_t on R_t in absence and presence of TEA. R_t was calculated as described in METHODS. Data are from same experiment as in Figs. 2 and 3. See text for definitions.

clamping step) more accurately reflects changes in relative membrane resistances with changes in membrane voltage.

Effect of K^+ channel blockers. Because changes in f_{Ra} with V_a were inhibited by the K^+ channel blocker, TEA, the ability of several other K^+ channel blockers to inhibit these changes was assessed to gain more information concerning the type of pathway responsible for the decline in f_{Ra} with voltage. Those tested included Ba^{2+}, reduced pH, 4-amino-pyridine (4-AP), and quinidine. Of these, Ba^{2+} (5 mM) and reduced pH (<5) affected the relation between V_a and f_{Ra} (Fig. 6). In both cases, the relation was shifted such that substantially greater depolarization was required to induce changes in f_{Ra}, consistent with voltage dependence of the inhibition. Unlike TEA, Ba^{2+} and pH also decreased basal V_a and increased f_{Ra} indicative of a decrease in basal K^+ conductance of the membrane (data not shown).

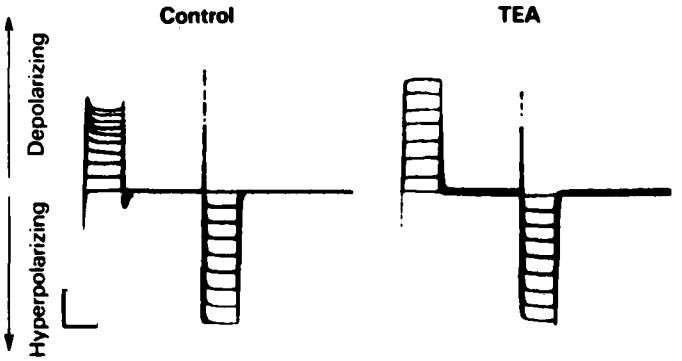

FIG. 5. Oscilloscope tracings of changes in V_a with V_t using clamping *protocol 2* before (*left*) and after (*right*) TEA. Results for both depolarizing and hyperpolarizing pulses are shown for a single impalement. Scale indicates 20 mV and 100 ms. See text for definitions.

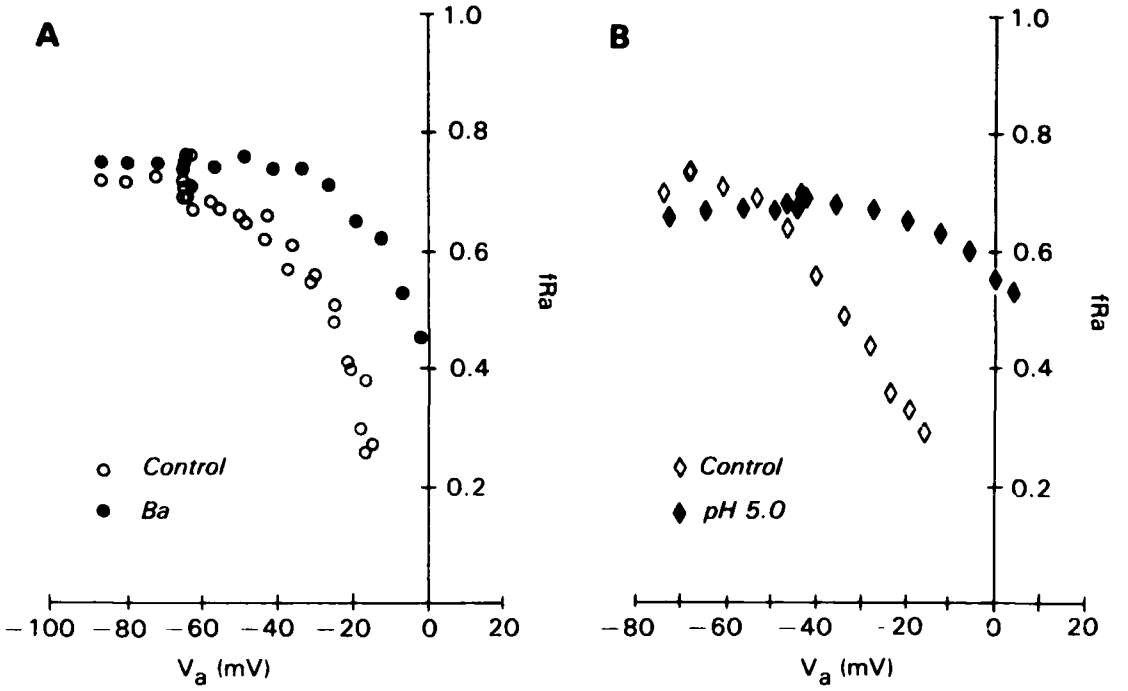

FIG. 6. Effect of Ba^{2+} (*A*) and pH (*B*) on V_a and f_{Ra} relation. *A* and *B*: representative experiments from different tissues (n = 4 and 3, for Ba^{2+} and pH, respectively). Control and inhibitor data, however, are from a single cell. See text for definitions.

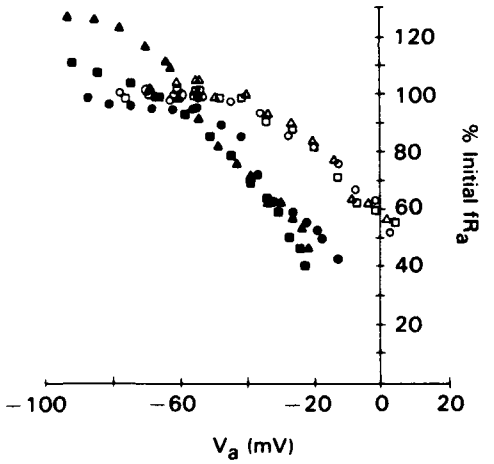

FIG. 7. Effect of ionomycin on the relation between V_a and f_{Ra}. Data are from a single tissue for three cells impaled before and 3 cells impaled after the addition of ionomycin. See text for definitions.

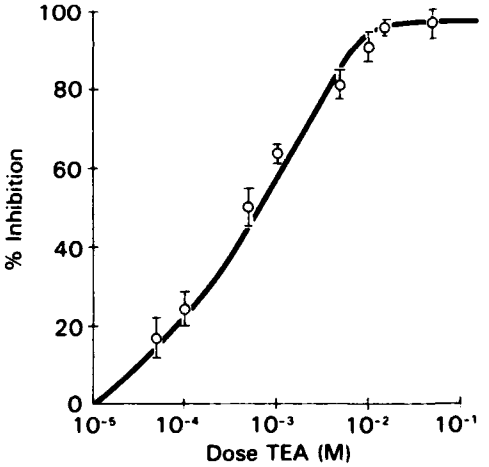

FIG. 8. Dose-response relation for TEA inhibition of changes in f_{Ra} with voltage. %Inhibition of f_{Ra} change for each dose was determined for V_a = −20 mV. Each point represents mean for at least 4 tissues. See text for definitions.

Effect of Ca^{2+} ionophore. The presence of 10^{-6} M ionomycin in the mucosal bath significantly altered the relation between V_a and f_{Ra}. As shown for the experiment in Fig. 7, changes in f_{Ra} occurred at more hyperpolarized potentials in the presence of the ionophore. In three experiments, depolarizing V_a to −30 mV decreased f_{Ra} to 83 ± 5%, whereas in the presence of ionophore depolarization to the same potential decreased f_{Ra} to 69 ± 2% of its initial value. Changes in f_{Ra} with V_a in the presence of ionomycin were also inhibited by mucosal TEA (data not shown).

Current-voltage relation of TEA-sensitive pathway. Of the K^+-channel blockers evaluated in this study, the most effective blocker of voltage induced changes in f_{Ra} was TEA. Assuming that TEA completely blocks the conductive pathway responsible for the changes in f_{Ra} without affecting other pathways, maximally effective concentrations of TEA can be used to evaluate the current-voltage (*I-V*) relation of this pathway as done previously by Thompson et al. (30) for the amiloride-sensitive pathway in rabbit colon provided that current through this pathway is not negligible with respect to paracellular current flow. The dose-response relation shown in Fig. 8 demonstrates that at concentrations exceeding 10 mM, TEA is virtually 100% effective in preventing changes in f_{Ra} over the range of voltages studied. Furthermore, as shown in Fig. 9 (V_a vs. I_t), I_t was substantially different in the presence and absence of 15 mM TEA. Thus subtraction of the two curves in Fig. 9 gives the current

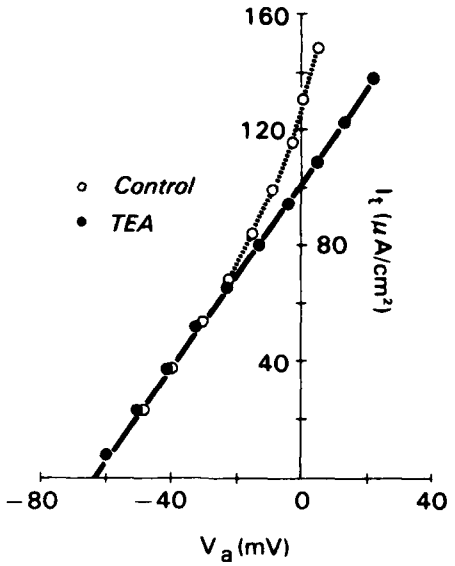

FIG. 9. V_a vs. current required to clamp V_a (I_t) before and after TEA. Data are from same impalement as that in Figs. 2–4 (*protocol 1*). Identical results were obtained from *protocol 2*. See text for definitions.

through the TEA-sensitive pathway. The resulting *I-V* relation is shown in Fig. 10 where I_{TEA} is the current through this pathway at a given V_a. This relation closely approximates that of the TEA-sensitive current across the apical membrane assuming that driving forces for TEA-insensitive pathways at this membrane are not affected by the inhibitor.

Because this current is blocked by Ba^{2+} and low-mucosal pH in addition to TEA, the most likely ionic species carrying this current is K^+. Therefore, the data shown in Fig. 10 were fit to the Goldman constant-field equation for voltage-independent K^+ movement across the apical membrane

$$I_K = V_a P_K F^2/RT \frac{[K_m - K_c \exp(V_a F/RT)]}{1 - \exp(V_a F/RT)}$$

where I_K is the K^+ current across the membrane, P_K is the K^+ permeability, K_c and K_m are the intracellular and mucosal bath K^+ activities, respectively, and RT and F have their usual meanings. Initial values of K_c were selected from measurements made in this tissue by Cremaschi et al. (4). Because P_K has not been measured, initial values of P_K were based on that determined by Reuss et al. (28) for *Necturus* gallbladder.[2] Clearly the computer-generated, best-fit curve shown in Fig. 10 does not adequately describe the relation between I_{TEA} and V_a. Similar results were obtained from the analysis of the *I-V* relations of five additional cells from three tissues regardless of the clamping protocol used. The implications of these data with respect to this curve will be discussed below.

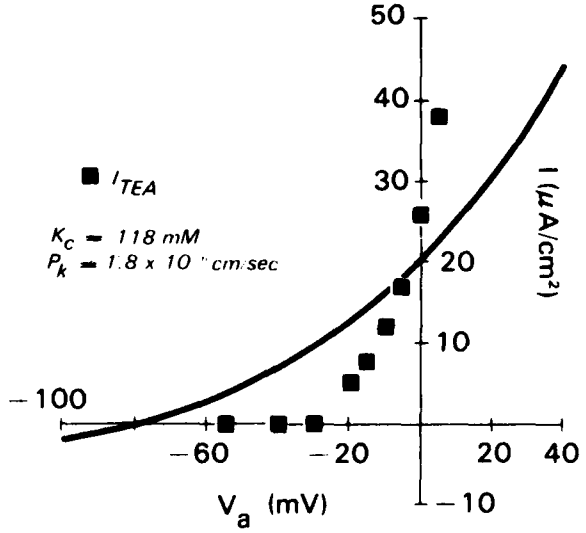

FIG. 10. *I-V* relation of TEA-sensitive pathway calculated from subtraction of two curves shown in Fig. 9. Curve is computer-generated best fit of data to Goldman constant-field equation giving values for P_K and K_c shown. See text for definitions.

DISCUSSION

Interpretation of data. The results of this study indicate that a voltage-dependent K^+ conductance resides in the apical membrane of guinea gallbladder epithelial cells. This is supported by the observations that *1*) depolarization of the apical membrane is accompanied by a decrease in the fractional resistance of the apical membrane, *2*) the change in fractional resistance can be inhibited by classical K^+-channel blockers Ba^{2+}, TEA, and pH, *3*) TEA has no effect when applied from the basolateral side, and *4*) the *I-V* relation of the TEA-sensitive pathway cannot be fit by the Goldman constant-field equation.

There are several issues central to this interpretation that must be addressed. First, does the fractional resistance reflect changes in cellular membrane resistance rather than paracellular resistance? As discussed by Boulpaep and Sackin (2), changes in fractional resistance may reflect differences in the relative values of junctional and lateral intercellular space resistances rather than cellular resistances. Although this issue was not directly addressed in this study, several lines of evidence support a cellular origin of changes in fractional resistance. Clamping the transepithelial potential to positive or negative values had little effect on transepithelial resistance. In a leaky tissue such as this, the transepithelial resistance mainly reflects the resistance of the paracellular pathway. In addition, although TEA blocked changes in f_{Ra} observed with clamping, it had little effect on transepithelial resistance. Finally, changes in f_{Ra} were blocked by classical inhibitors of membrane K^+ conductances, TEA and Ba^{2+}. Thus the changes in f_{Ra} observed in this study most likely have a cellular rather than a paracellular origin. A similar conclusion was reached for changes in f_{Ra} with voltage in *Necturus* gallbladder by Garcia-Diaz et al. (7). However, because in *Necturus* gallbladder voltage clamping changed transepithelial resistance by 50%, these investigators used La^{3+} to block

[2] In the analysis of Na conductance in rabbit colon (30), the *I-V* relation was analyzed for conformity to the Goldman constant-field equation using values of permeability and intracellular ion activity from fit of the equation to I when $V_a = E_i$ (the reversal potential or zero current) and $V_i = 0$. This approach was not used in the present study as V_a at which the TEA-sensitive current reversed was not clear. The data suggest that this conductance is essentially zero around the negative potentials at which I_K is expected to reverse in these cells (~−75 mV) and thus current is negligible at hyperpolarized potentials and within the noise of the measurement.

changes in transepithelial resistance with clamping, yet still observed changes in fractional resistance.

Second, does the relation between f_{Ra} and V_a reflect a voltage-dependent conductance change or Goldman rectification through a voltage-independent pathway? To answer this question, the *I-V* relation of the TEA-sensitive pathway was analyzed for fit to the Goldman constant-field equation for voltage-independent K^+ movement across the apical membrane. *I-V* relations were determined from differences in transepithelial current in the presence and absence of the inhibitor, TEA. As discussed by Lapointe et al. (21), this approach is generally not applicable to the study of ion transport across "leaky" epithelia. The preponderance of transepithelial current flow through paracellular rather than cellular pathways can preclude the determination of transcellular current flow. However, fortuitously, this does not appear the case for the TEA-sensitive pathway in guinea pig gallbladder. Although it was difficult to reliably determine ΔI_t at hyperpolarized potentials, the reduction of I_t by TEA was substantial within the range of voltages at which the TEA-sensitive conductance appears activated (< -30 mV). At very depolarized values of V_a, in some cases, TEA reduced I_t by ~80 $\mu A/cm^2$. Thus, although there may be some uncertainty at hyperpolarized regions of the *I-V* curve, this is not the case for that portion of the curve of particular interest.

Central to the analysis of these *I-V* relations are the criteria that *1*) TEA affects only a transcellular pathway, *2*) the *I-V* relation is instantaneous with respect to changes in ionic composition, and *3*) that other conductive pathways are not affected by the inhibitor. All of these criteria were met in the study. As noted earlier, TEA predominantly affects the transcellular pathway. Neither voltage nor TEA had much effect on transepithelial resistance with changes in transepithelial resistance being < 10%. The error introduced in the analysis by this change is small. In addition, TEA has previously been shown to block membrane K^+ conductances in other epithelia with little effect on paracellular transport (7, 11).

The *I-V* relations were obtained under conditions that appeared to be instantaneous with respect to changes in intracellular composition. One of the clamping protocols used was essentially identical to that employed by Thompson et al. (30) in which the sequence is bipolar (in *protocol 2*, the potential was rapidly clamped to alternately a positive or negative voltage from 0). Such a sequence would not be expected to cause shifts in intracellular composition. Although the other protocol employed was unipolar (in *protocol 1*, the clamping voltage became progressively positive or negative without returning to 0) and more prone to produce changes in intracellular composition, the results obtained were essentially identical, perhaps due to the rapidity with which the clamping sequence was accomplished. The *I-V* relation, however, was not instantaneous with respect to changes in membrane voltage. Depolarizing the apical membrane beyond -30 mV produced a progressive increase in the time required for a steady-state voltage to be reached (~25 ms). Similar changes were observed previously for *Necturus* gallbladder under current clamp by Reuss and Finn (27) and voltage-clamp conditions by Garcia-Diaz et al. (7). Reuss and Finn (27) suggested that these changes were related to polarization effects at the membrane (changes in ionic composition in extracellular compartments). Such an explanation would bring into question the appropriateness of the data analysis presented here. However, as discussed by Garcia-Diaz et al. (7) and Garcia-Diaz and Essig (6) for *Necturus* gallbladder and more recently for *Necturus* small intestine by Lapointe et al. (21), the voltage transients observed here are more likely capacitative (charging of linear RC elements). The apparent increase in the time constant results from the voltage-dependent decline of the apical membrane resistance and a subsequent decrease in the ratio of apical to basolateral membrane time constants. This does not adversely affect the interpretation of the data provided that values of V_a and f_{Ra} are taken after the transients, as was the case.

It is also unlikely that the addition of TEA affects conductive pathways other than that of the apical membrane K^+ conductance. TEA only blocked the conductance associated with depolarization. The inhibitor had no effect on basal membrane potential and little effect on f_{Ra}. Thus driving forces for other ion flows should be unchanged and the *I-V* relation of the transcellular TEA-sensitive pathway approximate that of the apical membrane without requiring corrections employed by others (30).

Thus because the *I-V* relation of the TEA-sensitive pathway met the necessary criteria described above, analysis of this relation with respect to the Goldman constant-field equation is appropriate. Using reasonable values for apical membrane potassium permeability and intracellular potassium activity , the TEA-sensitive current could not be fit by this equation. This was particularly evident for the dramatic increases in current observed at V_a corresponding to values at which f_{Ra} was noted to decrease. Thus the changes in current and f_{Ra} observed with voltage are consistent with activation of a voltage-dependent K^+ conductance. Garcia-Diaz et al. (7) reached a similar conclusion for *Necturus* gallbladder, however, these investigators did not analyze the *I-V* relations of this pathway.

Nature of voltage-dependent K^+ conductance and its relation to those in other epithelia. To gain additional information concerning the nature of the pathway responsible for the voltage dependence of the apical membrane conductance, two series of experiments were performed. First, the efficacy of several K^+-channel blockers that have been shown to block different types of K^+ channels (22) was assessed. In addition to TEA, both Ba^{2+} and decreased pH (5.0) blocked changes in fractional resistance with voltage. Quinidine and 4-AP had no effect on the voltage-dependent conductance. Ba^{2+} and pH also had effects on basal potential and fractional resistance consistent with blocking basal K^+ conductance, whereas TEA, quinidine, and 4-AP did not. Thus TEA appears to specifically block the voltage-dependent K^+ conductance with little effect on the K^+ conductance comprising the basal K^+ conductance of the membrane, whereas Ba^{2+} and pH have effects on both. This raises the possibility that at least two different types or states

of K^+ conductance reside in the apical membrane.

In a second series of experiments, the effect of the Ca^{2+} ionophore, ionomycin, was determined. A shift in the voltage dependence was observed such that changes in fractional resistance occurred at more hyperpolarized potentials. Thus the voltage-dependent conductance also appears to be calcium sensitive.

This conductance was localized to the apical membrane. There was no effect of TEA when applied from the serosal side. In a previous study (15), serosal Ba^{2+} and quinidine were observed to inhibit basolateral membrane K^+ conductance as was also observed for turtle colon (8, 29). These pharmacological differences suggest that the individual conductances contributing to the K^+ conductance of the serosal membrane are distinct from those of the apical membrane.

Given the pharmacology of the voltage-dependent conductance reported in the present study, the membrane voltage at which the conductance appears activated (−30 mV) and its calcium sensitivity the data suggest that activation of channels generally referred to as "maxi-K^+" channels underlie the observed changes in fractional resistance with membrane voltage. Although this awaits confirmation, these channels have been observed in the cell membranes of several other epithelia (3, 19, 22) including the apical membrane of Triturus gallbladder (23). It is distinctly different from that described recently by Palmer (24) for the apical membrane of toad urinary bladder that is blocked by Ba^{2+}, pH and quinidine, but not TEA, and activated at V_a exceeding 50 mV.

The physiological significance of a voltage-dependent K^+ conductance in the apical membrane of guinea pig gallbladder epithelial cells is presently unclear. The lack of an effect of TEA on basal V_a and f_{Ra}, or membrane hyperpolarization on f_{Ra} suggest that in contrast to *Necturus* gallbladder (7), this conductance does not generally contribute to the basal K^+ conductance of these cells. The voltage sensitivity of the conductance indicated by this study, however, suggests that it would become significant at membrane potentials less than −30mV. Activation of such a conductance would partially repolarize the membrane, reestablishing the membrane potential and the driving force for various ion movements. Although it is unlikely that the apical membrane would be depolarized to this potential under physiological conditions, in the presence of increased intracellular Ca^{2+} the conductance would be activated at more hyperpolarized potentials. Guinea pig gallbladder secretes fluid and electrolytes in the presence of secretagogues such as prostaglandin (16). HCO_3^- secretion has been observed to be accompanied by K^+ secretion. Although the electrophysiological response of this tissue to secretagogues has not been studied, the notion that the voltage-dependent conductance is involved in this secretory response is attractive. Along these lines, in preliminary experiments, TEA was observed to increase the short-circuit current elicited by prostaglandin in guinea pig gallbladder (unpublished data). Basolateral membrane Ca^{2+}-activated, voltage-dependent K^+ channels have been observed to be involved in the secretory response of several secretory epithelia including lacrimal, pancreatic, and salivary glands (see Ref. 26). Determination of the role of similar channels in the apical membrane of epithelial cells, however, has been more elusive (5).

In summary, the present study reveals a voltage-dependent K^+ conductance in the apical membrane of guinea pig gallbladder epithelial cells. In addition, the conductance appears to be activated by Ca^{2+}. Future studies on the mode of regulation of this conductance by voltage and Ca^{2+} with respect to its physiological role should yield valuable information concerning the regulation of transport processes in epithelial cells.

NOTE ADDED IN PROOF

Stoddard and Reuss (29a) have very recently reevaluated apical membrane potential and fractional resistance in *Necturus* gallbladder under current clamp conditions. They also conclude that the results (which are qualitatively similar to those reported here) reflect a voltage-sensitive K conductance in the apical membrane.

I gratefully acknowledge Dr. T. Pellmar for helpful discussions, Dr. K. Zbicz for data acquisition and analysis programming, and Drs. Gallin and Livengood for critical reading of the manuscript.

This work was supported by the Armed Forces Radiobiology Research Institute, Defense Nuclear Agency, under work unit 00107. Views presented in this paper are those of the author; no endorsement by the Defense Nuclear Agency has been given or should be inferred.

Research was conducted according to the principles enunciated in the "Guide for the Care and Use of Laboratory Animals" [DHEW Publication No. (NIH) 80-23, Revised 1978, Office of Science and Health Reports, DRR/NIH, Bethesda, MD 20205].

Received 9 February 1988; accepted in final form 14 July 1988.

REFERENCES

1. BOLIVAR, J. J., AND M. CEREIJIDO. Voltage and Ca^{2+}-activated K^+ channel in cultured epithelial cells (MDCK). *J. Membr. Biol.* 97: 43–51, 1987.
2. BOULPAEP, E. L., AND H. SACKIN. Electrical analysis of intraepithelial barriers. *Curr. Top. Membr. Transp.* 13: 169–197, 1980.
3. CHRISTENSEN, O., AND T. ZEUTHEN. Maxi K^+ channels in leaky epithelial are regulated by intracellular Ca, pH, and membrane potential. *Pfluegers Arch.* 408: 249–259, 1987.
4. CREMASCHI, D., G. MEYER, AND C. ROSSETTI. Bicarbonate effects, electromotive forces and potassium effluxes in rabbit and guinea-pig gallbladder. *J. Physiol. Lond.* 335: 51–64, 1983.
5. FRINDT, G., AND L. G. PALMER. Ca-activate K^+ channels in apical membrane of mammalian CCT, and their roles in K^+ secretion. *Am. J. Physiol.* 252 (*Renal Fluid Electrolyte Physiol.* 21): F458–F467, 1987.
6. GARCIA-DIAZ, J. F., AND A. ESSIG. Capacitative transients in voltage-clamped epithelia. *Biophys. J.* 48: 519–523, 1985.
7. GARCIA-DIAZ, J. F., W. NAGEL, AND A. ESSIG. Voltage-dependent K conductance at the apical membrane of *Necturus* gallbladder. *Biophys. J.* 43: 269–278, 1983.
8. GERMANN, W. J., M. E. LOWY, S. ERNST, AND D. C. DAWSON. Differentiation of two distinct K conductances in the basolateral membrane of turtle colon. *J. Gen. Physiol.* 88: 237–251, 1986.
9. GITTER, A. H., K. W. BEYENBACH, C. W. CHRISTINE, P. GROSS, W. W. MINUTH, AND E. FROMTER. High-conductance K^+ channel in apical membrane of principal cell cultured from rabbit renal cortical collecting duct anlagen. *Pfluegers Arch.* 498: 282–290, 1987.
10. GOGELEIN, H., AND R. GREGER. A voltage-dependent ionic channel in the basolateral membrane of late proximal tubules of the rabbit kidney. *Pfluegers Arch.* 407, *Suppl.* 2: S142–S148, 1986.
11. GOGELEIN, H., AND W. VAN DRIESSCHE. Noise analysis of the K^+ current through the apical membrane of *Necturus* gallbladder. *J. Membr. Biol.* 3: 243–254, 1981.
12. GREGER, R., F. [illegible]LATTER, AND H. GOEGELEIN. Chloride channels in the luminal membrane of the rectal gland of the dogfish (*Squalus acanthias*). properties of the "larger" conductance channel. *Pfluegers Arch.* 409: 114–121, 1987.

13. GUGGINO, S. E., W. B. GUGGINO, N. GREEN, AND B. SACKTOR. Ca-activated K^+ channels in cultured medullary thick ascending limb cells. *Am. J. Physiol.* 252: (*Cell Physiol.* 21): C121–C127, 1987.
14. GUNTER-SMITH, P. J. Voltage-sensitive conductance in guinea pig gallbladder epithelial cells (Abstract). *Federation Proc.* 46: 1269, 1987.
15. GUNTER-SMITH, P. J. Serosal membrane conductances and the effect of reducing bath Na in guinea pig gallbladder (Abstract). *J. Gen. Physiol.* 88: 26a, 1986.
16. HEINTZE, K., K.-U. PETERSEN, S. H. SAVERYMUTTER, AND J. R. WOOD. Effects of bicarbonate on fluid and electrolyte transport by the guinea pig gallbladder: a bicarbonate-Cl exchange. *J. Membr. Biol.* 45: 43–59, 1979.
17. HUNTER, M., A. G. LOPES, AND E. BOULPAEP. Regulation of single potassium ion channels from the apical membrane of rabbit collecting tubule. *Am. J. Physiol.* 251 (*Renal Fluid Electrolyte Physiol.* 20): F725–F733, 1986.
18. HVIID-LARSEN, E., AND B. E. RASMUSSEN. Membrane potential plays a dual role for chloride transport across toad skin. *Biochim. Biophys. Acta* 728: 455–459, 1983.
19. KOLB, H. A., C. D. A. BROWN, AND H. MURER. Identification of a voltage-dependent anion channel in the apical membrane of a Cl-secretory epithelium (MDCK). *Pfluegers Arch.* 403: 262–265, 1985.
20. KOLB, H. A., C. D. A. BROWN, AND H. MURER. Characterization of a Ca-dependent Maxi K channel in the apical membrane of a cultured renal epithelium (JTC-12.P3). *J. Membr. Biol.* 92: 207–215, 1986.
21. LAPOINTE, J.-Y., R. L. HUDSON, AND S. G. SCHULTZ. Current-voltage relations of sodium-coupled sugar transport across the apical membrane of *Necturus* small intestine. *J Membr. Biol.* 93: 205–219, 1986.
22. LATORRE, R., AND C. MILLER. Conductance and selectivity in potassium channels. *J. Membr. Biol.* 71: 11–30, 1983.
23. MARUYAMA, Y., H. MATSUNAGA, AND T. HOSHI. Ca^{2+}- and voltage activated K^+ channel in the apical membrane of gallbladder epithelium from *Triturus*. *Pfluegers Arch.* 406: 563–567, 1986.
24. PALMER, L. G. Apical membrane K conductance in the toad urinary bladder *J. Membr. Biol.* 92: 217–226, 1986.
25. PALMER, L. G. Patch clamp technique in renal physiology. *Am. J. Physiol.* 250 (*Renal Fluid Electrolyte Physiol.* 19): F379–F385, 1986.
26. PETERSEN, O. H. Calcium-activated potassium channels and fluid secretion by exocrine glands. *Am. J. Physiol.* 251 (*Gastrointest. Liver Physiol.* 14): G1–G13, 1986.
27. REUSS, L., AND A. L. FINN. Mechanisms of voltage transients during current clamp in *Necturus* gallbladder. *J. Membr. Biol.* 37: 299–319, 1977.
28. REUSS, L., AND A. L. FINN. Electrical properties of the cellular transepithelial pathway in *Necturus* gallbladder. II. Ionic permeability of the apical cell membrane. *J. Membr. Biol.* 25: 141–161, 1975.
29. RICHARDS, N. W., AND D. C. DAWSON. Single potassium channels blocked by lidocaine and quinidine in isolated turtle colon epithelial cells. *Am. J. Physiol.* 251 (*Cell Physiol.* 20): C85–C89, 1986.
29a. STODDARD, J. S., AND L. REUSS. Voltage- and time dependence of apical membrane conductance during current clamp in *Necturus* gallbladder epithelium. *J. Membr. Biol.* 103: 191–204, 1988.
30. THOMPSON, S. M., Y. SUZUKI, AND S. G. SCHULTZ. The electrophysiology of rabbit descending colon. I. Instantaneous transepithelial current-voltage relations and the current-voltage relations of the Na-entry mechanism. *J. Membr. Biol.* 66: 41–54, 1982.
31. VAN DRIESSCHE, W., AND W. ZEISKE. Ionic channels in epithelial cell membranes. *Physiol. Rev.* 65: 833–903, 1985.
32. WILLS, N. K., AND A. ZWEIFACH. Recent advances in the characterization of epithelial ionic channels. *Biochim. Biophys. Acta* 906: 1–31, 1987.

From: PROSTAGLANDIN AND LIPID METABOLISM
IN RADIATION INJURY
Edited by Thomas L. Walden, Jr. and Haywood N. Hughes
(Plenum Publishing Corporation, 1987)

EFFECT OF PGE_2 ON RADIATION RESPONSE OF CHINESE HAMSTER V79 CELLS *IN VITRO*

E. V. Holahan[1], W. F. Blakely[1], and T. L. Walden[2]

[1]Radiation Sciences Department
[2]Radiation Biochemistry Department
Armed Forces Radiobiology Research Institute
Bethesda, Maryland 20814-5145

ABSTRACT

Several recent investigations have reported that 16,16-dimethyl prostaglandin E_2 ($DiPGE_2$) can protect murine intestinal epithelial cells and hematopoietic stem cells (CFU-S) *in vivo* from ionizing radiation. It has been postulated that PGE_2 may also increase radiation resistance *in vitro* by stimulating free radical scavenging or repair systems for oxidative damage. This study reports on the effect of PGE_2 in modifying radiation sensitivity in an *in vitro* mammalian cell line.

Chinese hamster V79A03 cells were cultured as monolayers in 6 ml of α-MEM medium supplemented with Earle's salts, 25 mM HEPES buffer, and 10% fetal bovine serum. Exponentially growing cells were incubated in medium containing 14 μM (5 μg/ml) PGE_2 for either 2 hr (acute) or >3 weeks (chronic) before exposure to graded doses of 250 kVp X rays. Cells were assayed for variations in intracellular levels of cyclic 3',5'-adenosine monophosphate (cAMP), total protein, and glutathione (GSH), and radiation sensitivity was measured by cell survival before and after PGE_2 treatment.

An acute (2-hr) exposure induced a 25% increase in cAMP content with no significant change in intracellular GSH or protein and no effect on cell survival after exposure to radiation. Chronic exposure to PGE_2 increased intracellular GSH, protein, and cAMP levels by 82%, 3%, and 74%, respectively. However, no increase in radiation resistance was apparent following chronic exposure to PGE_2. Chronic PGE_2 exposures marginally increased the doubling time of the cells (10 versus 11 hr), although this perturbation was insufficient to alter radioresponse as a result of cell cycle perturbations. Consequently, the increase in the *in vivo* radiation response associated with PGE_2 treatment may not be the result of an intracellular response. Instead, the increased radiation resistance observed *in vivo* may be due to modifications such as localized tissue or organ system hypoxia.

INTRODUCTION

Prostaglandins are synthesized from arachidonic acid by most vertebrate tissues and certain invertebrate tissues. These prostaglandins modulate a number of humoral functions and possess a number of pharmacological actions whose physiological significance is only recently being deduced (for reviews, see references 1 and 2). Prostaglandin E_1 stimulates adenyl cyclase activity in a number of fibroblastic tissues, resulting in elevated cAMP levels (3-6). These increases can occur within 10 min of prostaglandin administration, and they remain elevated for up to 5 hr (4). Prostaglandin E_1 also is an effective radioprotective agent for cells irradiated *in vitro* (6,7). Prostaglandin E_1, when administered before irradiation, can stimulate a four- to fivefold increase in cAMP levels and decrease radiation sensitivity by increasing the shoulder of the radiation survival curve (7). Furthermore, Hanson et al. have demonstrated that a prostaglandin E_2 analogue, $DiPGE_2$, can also radioprotect murine intestinal epithelial cells (8,9) and hematopoietic stem cells (CFU-S) *in vivo* (9) by increasing the shoulder and decreasing the slope of the radiation survival curve if the analogue is injected before and not after irradiation.

The PGE-stimulated increase in adenyl cyclase and cAMP might be responsible for the decrease in mammalian cell radiosensitivity (6). Increased glutathione synthesis, which is coupled to the gamma-glutamyl amino acid transport system and whose biosynthesis is ATP dependent (10), may also contribute to the increased radioprotection observed *in vivo* and *in vitro*. We have postulated that the prostaglandin-induced increase in cAMP may also stimulate glutathione synthesis and thus confer a measurable amount of resistance to ionizing radiation. To test this hypothesis, we examined the effects of PGE_2 on the radiosensitivity of exponentially growing Chinese hamster fibroblasts.

MATERIALS AND METHODS

Chinese hamster V79A03 cells were cultured as monolayers on plastic in alpha MEM medium with Earle's salts and 25 mM HEPES buffer supplemented with 10% fetal bovine serum (Armour Pharmaceuticals, Tarrytown, NY), 14 mM sodium bicarbonate, 2 mM L-glutamine, and antibiotics. The cells were maintained at 37°C in a humidified incubator with a 3%-CO_2 and 97%-air mixture. For experiments in which asynchronous cells were treated, exponentially growing cells were trypsinized from monolayer culture, plated into 25-cm^2 flasks containing medium (6 ml at 37°C and pH 7.4), and incubated for an additional 18 to 24 hr before treatment (microcolony size of 1.5-2.2 cells per colony). The PGE_2 content of the medium supplemented with 10% fetal bovine serum was 38 pM (13.56 pg/ml). The number of cells inoculated into six replicate flasks was varied to yield 50-100 colonies per flask after treatment.

Except where indicated, the cells were incubated at 37°C with 14 μM (5 μg/ml) PGE_2 (Upjohn Co., Kalamazoo, MI) in medium for 2 hr. For chronic exposure to PGE_2, the cells were continuously subcultured every 48-72 hr for 3-5 weeks

in medium containing 5 μg/ml PGE_2 without inducing any morphological changes. The medium was exchanged with fresh medium containing 5 μg/ml PGE_2 2 hr before either irradiation or cell harvesting for cAMP or GSH assays.

The cells were irradiated on a rotating Plexiglas holder with a Phillips industrial X-ray machine (Philips GMBH, Hamburg, Germany) at room temperature (17°-21°C). The irradiation conditions were 1.65 Gy/min with an effective energy of 80 keV (SSD = 43 cm, 250 kVp, 1 HVL = 1.0 mm Cu, 15 mA).

After drug and/or irradiation treatment, the cells were incubated for 8-10 days to allow macrocolony formation. The colonies were fixed to the flasks with methanol and stained with 0.5% crystal violet. Cell survival was adjusted for the plating efficiency and the average microcolony size at the time of treatment (11). The standard error of the mean is indicated when it is larger than the datum point. All curves have been fit by eye.

For the determination of intracellular glutathione content, a number of additional 100-mm petri dishes were inoculated with 2-5 x 10^6 cells as described above. Following the various drug and/or irradiation treatments, the cells were rinsed with cold phosphate-buffered saline (PBS) and removed from the dishes by scraping the growth surface with a rubber policeman. The harvested cells were rinsed twice with cold PBS and then frozen in 0.5 ml of 0.6% sulfosalicylic acid. The cells frozen in sulfosalicylic acid were later thawed and assayed for total GSH content (oxidized and reduced) by the GSH reductase procedure (12). GSH content was expressed as nmoles/million cells and as nmoles/mg protein. Control values measured for 12 experiments ranged from 1.0 to 7.55 nmoles/million cells (0.30-2.32 μg GSH/million cells).

For cAMP determinations, cells (4-5 x 10^6) were harvested as described, and the cellular proteins were precipitated using cold trichloroacetic acid. The trichloroacetic acid was removed with ether, and the cAMP content was measured using a cAMP (^{125}I) radioimmunoassay kit (Dupont-New England Nuclear, Boston, MA). All samples were measured in triplicate with control values varying between 1.6 and 3.5 pmole cAMP/million cells for three separate experiments.

The stability of the PGE_2 in the tissue culture medium was determined by monitoring the radiolabeled products formed in the medium containing tritiated PGE_2. Briefly, the pH of a sample was adjusted to 3.0 with acetic acid followed by the addition of two volumes of ethyl acetate. The upper organic phase containing PGE_2 metabolites was removed, evaporated, and then resuspended in buffer containing 36% acetonitrile (v/v) and 64% phosphoric acid (pH 3.0). The PGE_2 samples were analyzed by reverse-phase high-performance liquid chromatography using a 5-micron Ultrasphere C-18 column (Beckman, San Ramon, CA), 4.6 x 250 mm. The samples were eluted from the column (1 ml/min) using the isocratic buffer. Labeled PGE_2 metabolites were detected using a radiation flow-through monitor (RAMOND-D, IN/US, Fairfield, NJ) and identified by coelution with known standards.

RESULTS

The stability of PGE_2 in medium alone and in medium when exposed to metabolically active V79 cells was monitored using tritium-labeled PGE_2. Radiolabeled medium was incubated at 37°C for 0 or 24 hr in the presence of 1.0-10 x 10^5 cells. After each exposure (indicated in Figure 1), medium samples were analyzed for PGE_2 metabolites. All of the samples analyzed contained 10%-25% PGA_2 as well as PGE_2. Only when the PGE_2 was exposed to 1 x 10^6 cells or more for a minimum of 24 hr were metabolites of PGE_2 detectable. 15-Keto PGE_2 (peak II), 13,14-dihydro-15-keto PGE_2 (peak III), and PGA_2 (peak IV) were the major metabolites observed. No other PGE_2 metabolites were detected, nor was PGE_2 converted to $PGF_{2\alpha}$. PGE_2 was stable at 37°C in cell-free medium containing 10% fetal bovine serum for up to 1 week.

An acute exposure to PGE_2 (14 μM) did not confer radioprotection *in vitro* (Figure 2). Exponentially growing cells were incubated for 2 hr in medium with PGE_2 before irradiation, but the radiosensitivity of the cells was not modified. In addition, when the concentration and pretreatment time were increased to 30 μM and 8 hr, respectively, no modification in radiation resistance was observed (data not shown).

The intracellular content of glutathione and cAMP was measured after the acute exposure to PGE_2 to determine if an increase in intracellular sulfhydryl content might increase the cellular free radical-scavenging capability after radiation exposure. A small increase in GSH and cAMP content was observed after an acute PGE_2 exposure (Table 1), but no increase in the GSH:protein ratio was evident.

In order to mimic the environmental conditions that PGE_2-secreting tumor cells might create (13), cells were continuously subcultured in medium containing PGE_2 for a minimum of 3 weeks. Continuous exposure to PGE_2 marginally increased the doubling time of the cells from 10.5 to 11 hr but did not alter the plating efficiency of the cells. The tissue culture medium was replaced with fresh medium in order to remove metabolite by-products of PGE_2 that might interfere with any radioprotection that might be induced. The data in Figure 3 indicate that chronic exposure to PGE_2 does not confer any additional radioprotection to the cells.

The intracellular GSH and cAMP contents were also measured after the chronic exposure to PGE_2 (Table 2). Under these conditions, glutathione and cAMP contents increased 82% and 75%, respectively, with no appreciable increase in cellular protein.

DISCUSSION

Prostaglandin-induced radioprotection of hematopoietic and intestinal stem cells *in vivo* was expressed as an increase in the D_o and shoulder of the radiation survival

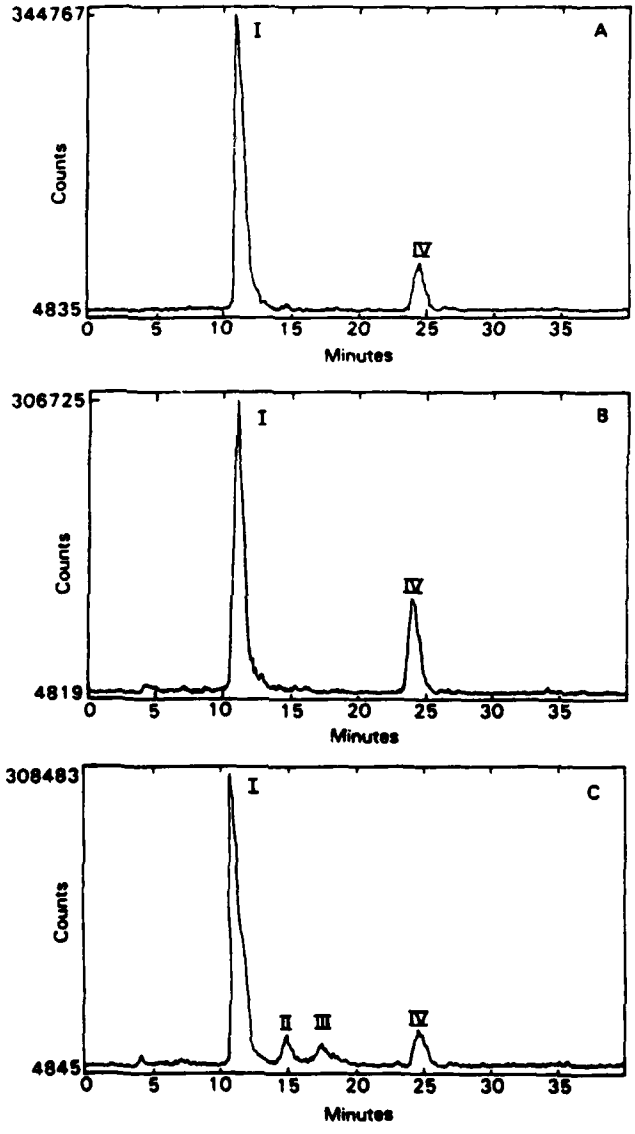

Fig. 1. PGE_2 stability in tissue culture medium as measured by HPLC chromatography. PGE_2 (5 μg/ml) was incubated at 37°C in presence of 0 cells (panel A), 1.0×10^5 cells (panel B), or 1.0×10^6 cells (panel C) for 24 hr. Four products eluted from chromatography columns were peak I: PGE_2 (11.5 min); peak II: 15-keto PGE_2 (13.8 min); peak III: 13,14-dihydro-15-keto PGE_2 (16.9 min); and peak IV: PGA_2 (24.1 min).

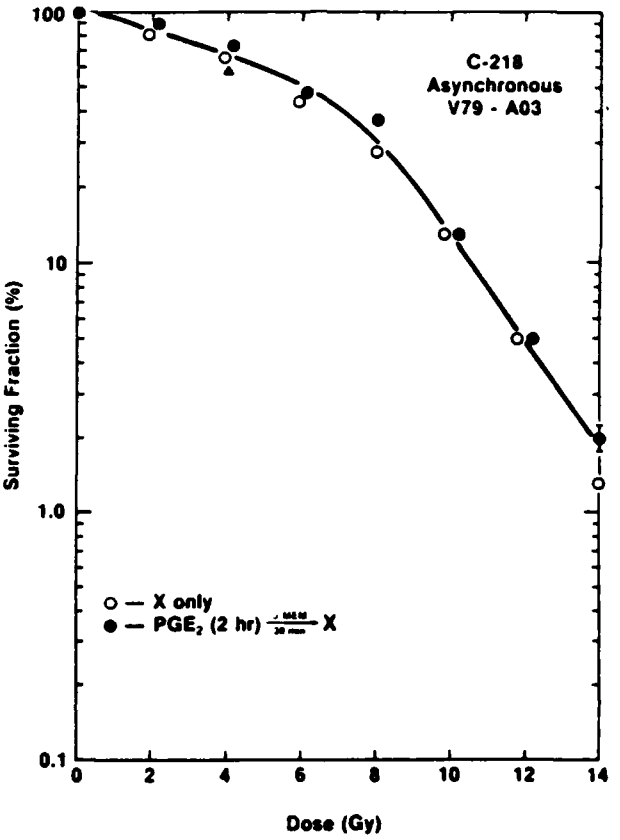

Fig. 2. Effect of PGE_2 on radiation response of Chinese hamster V79 cells. Cells were inoculated into flasks, incubated for 18 hr, and then exposed (2 hr) to either 0 μM (○) or 14 μM (●) PGE_2 before X irradiation. Each datum point represents mean survival of six replicate flasks.

Table 1. Effect of Acute PGE_2 Exposure on Intracellular cAMP and GSH Content[1]

	nmoles GSH/ 10^6 cells	μg protein/ 10^6 cells	nmoles GSH/ mg protein	pmoles cAMP/ 10^6 cells
Control	1.36 ± 0.07	164 ± 11	8.29 ± 0.31	2.0 ± 0.14
PGE_2	1.52 ± 0.10	178 ± 8	8.54 ± 0.55	2.5 ± 0.18
Relative Change	1.12	1.08	1.02	1.25

[1]Reported values represent mean of at least two separate measurements from each of three different experiments.

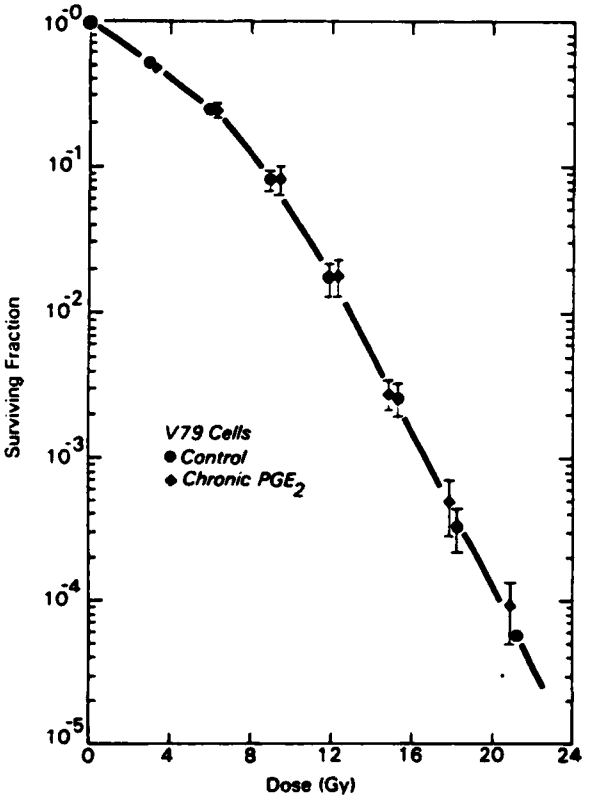

Fig. 3. Effect of chronic exposure to PGE_2 on radiation response of Chinese hamster cells. Exponentially growing cells were continuously subcultured for 3-5 wk in medium containing 5 μg/ml PGE_2. Two hr before irradiation, medium was exchanged with fresh medium containing PGE_2 (◆) and compared with survival of cells not exposed to PGE_2 (●). Datum points represent mean survival of four experiments, each with at least five replicate flasks per radiation exposure.

Table 2. Effect of Chronic PGE_2 Exposure on Intracellular cAMP and GSH Content[1]

	nmoles GSH 10^6 cells	μg protein 10^6 cells	nmoles GSH mg protein	pmoles cAMP 10^6 cells
Control	6.1 ± 0.53	163 ± 18	37.8 ± 2.7	2.0 ± 0.14
PGE_2	11.1 ± 1.33	169 ± 6.5	65.8 ± 7.1	3.5 ± 0.02
Relative Change	1.82	1.03	1.74	1.75

[1]Reported values represent mean of at least two different measurements from each of three different experiments.

curve (8,9). The *in vivo* radioprotection was postulated to result from a rapid increase in intracellular sulfhydryl compounds, rather than direct free radical scavenging by $DiPGE_2$, localized hypoxia, or a drug-induced cell cycle redistribution.

In this study we exposed Chinese hamster cells to concentrations of PGE_2 that were significantly greater than the serum concentrations of the C3H mice used in the *in vivo studies* (8,9), to determine if the radioprotective activity had a cellular or molecular mechanism of action. PGE_2 (C20:H32:05) does not contain any sulfhydryl moieties, and although it may interact with free radicals by attacking unsaturated bonds, it is unlikely that this proceeds at a significant rate. Exposure of cells to PGE_2, either acutely or chronically, failed to stimulate any increased radiation resistance (Figures 2 and 3). Under both conditions, the PGE_2 was not metabolically degraded (Figure 1), an increase was seen in the cellular cAMP content (Tables 1 and 2), and a significant increase in glutathione content was demonstrated after chronic PGE_2 exposure (Table 2).

The increase in cellular GSH may have been induced by chronic exposure to PGE_2, but it is also possible that the increased level of GSH may have been stimulated by a PGA_2 contaminant that could also have been introduced to the medium or the conversion of PGE_2 to PGA_2 in a slightly acidic medium environment. Millar and Jinks (14) demonstrated that exposure to 10 μg/ml PGA_2 for 46 hr could stimulate a 64% increase in the amount of GSH that could be isolated from V79-753B cells. However, this PGA_2-induced stimulation of GSH synthesis did not modify radiation sensitivity. Russo and Mitchell (15) also reported the failure of elevated GSH levels to alter radiosensitivity in a V79 cell line. Oxo-thiazolidine-4-carboxylate (10 mM) stimulated GSH levels to 200%-300% above controls. No decrease in radiosensitivity was observed, suggesting that GSH-mediated free radical scavenging and/or $GSH^{\cdot}$ peroxidase-mediated detoxification of hydrogen peroxide were operating at maximum velocity. In contrast, GSH exogenously supplied to a human lymphoid has been shown to confer some radioprotection (16). It appears that the radiation resistance of V79 cells may not be easily manipulated by simply varying cellular GSH content. While the increased radiation resistance observed for mouse stem cells *in vivo* might be the result of increased GSH content, PGE_2 exposure induced no additional radioresistance in V79 cells *in vitro*.

Another popular hypothesis regarding prostaglandin-induced radiation resistance involves the stimulation of cAMP content. Although the specific mechanism has not been deduced, variations in intracellular cAMP have been temporally correlated with changes in radiation resistance (6,7,17,18). This does not appear to be the case with our V79 cells. The chronic exposure to PGE_2 increased cAMP by 75% (Table 2), had no effect on radiation resistance (Figure 3), and increased the cell doubling time by approximately 30 min compared to the control cells. Although these data are not entirely inconsistent with other reports, it does appear that cAMP may be the important prostaglandin (E_1 and E_2) second messenger and not the only factor involved for radioprotection.

ACKNOWLEDGMENTS

The authors thank E. J. Golightly, J. J. Raymond, M. A. Behme, D. P. Dodgen, and C. L. Hollies for their excellent technical support and Dr. L. K. Steel for the serum PGE_2 measurements. Supported by the Armed Forces Radiobiology Research Institute, Defense Nuclear Agency, under Research Work Unit 4640-B5104. The views presented in this paper are those of the authors; no endorsement by the Defense Nuclear Agency has been given or should be inferred.

REFERENCES

1. Samuelsson, B., Granstrom, E., Green, K., Hamberg, M., and Hammarstrom, S. Prostaglandins. Ann. Rev. Biochem. 44: 669-695, 1975.
2. Samuelsson, B., Goldyne, M., Granstrom, E., Hamberg, M., Hammarstrom, S., and Malmsten, C. Prostaglandins and thromboxanes. Ann. Rev. Biochem. 47: 997-1029, 1978.
3. Makman, M. H. Conditions leading to enhanced response to glucagon, epinephrine, or prostaglandins by adenyl cyclase of normal and malignant cultured cells. Proc. Nat. Acad. Sci. USA 68: 2127-2130, 1971.
4. Maganiello, V., and Vaughan, M. Prostaglandin E_1 effects on adenosine 3':5'-cyclic monophosphate concentration and phosphodiesterase activity in fibroblasts. Proc. Nat. Acad. Sci. USA 69: 269-273, 1972.
5. Penit, J., Cantau, B., Huot, J., and Jard, S. Adenylate cyclase from synchronized neuroblastoma cells: Responsiveness to prostaglandin E_1, adenosine, and dopamine during the cell cycle. Proc. Nat. Acad. Sci. USA 74: 1575-1579, 1977.
6. Lehnert, S. Modification of postirradiation survival of mammalian cells by intracellular cyclic AMP. Radiat. Res. 62: 107-116, 1975.
7. Prasad, K. N. Radioprotective effect of prostaglandin and an inhibitor of cyclic nucleotide phosphodiesterase on mammalian cells in culture. Int. J. Radiat. Biol. 22: 187-189, 1972.
8. Hanson, W. R., and Thomas, C. 16,16-dimethyl prostaglandin E_2 increases survival of murine intestinal cells when given before photon irradiation. Radiat. Res. 96: 393-398, 1983.
9. Hanson, W. R., and Ainsworth, E. J. 16,16-dimethyl prostaglandin E_2 induces radioprotection in murine intestinal and hematopoietic stem cells. Radiat. Res. 103: 196-203, 1985.
10. Meister, A., and Anderson, M. E. Glutathione. Ann. Rev. Biochem. 53: 711-760, 1983.
11. Sinclair, W. K., and Morton, R. A. X-ray and ultraviolet sensitivity of synchronous chinese hamster cells at various stages of the cell cycle. Biophys. J. 5: 1-25, 1965.
12. Tietz, F. Enzymatic method for quantitative determination of nanogram amounts of total and oxidized glutathione: Applications to mammalian blood and other tissues. Anal. Biochem. 27: 502-522, 1969.

13. Seyberth, H. W., Segre, G. V., Morgan, J. L., Sweetman, J. R., Potts, J. T., and Oates, J. A. Prostaglandins as mediators of hypercalcemia associated with certain types of cancer. N. Engl. J. Med. 293: 1278-1283, 1975.
14. Millar, B. C., and Jinks, S. Do prostaglandins affect cellular radiosensitivity in vitro? Int. J. Radiat. Biol. 46: 367-373, 1984.
15. Russo, A., and Mitchell, J. B. Radiation response of Chinese hamster cells after elevation of intracellular glutathione levels. Int. J. Radiat. Oncol. Biol. Phys. 10: 1243-1247, 1984.
16. Jensen, G. L., and Meister, A. Radioprotection of human lymphoid cells by exogenously supplied glutathione in mediated γ-glutamyl transpeptidase. Proc. Nat. Acad. Sci. USA 80: 4714-4717, 1983.
17. Lehnert, S. Intracellular cyclic AMP levels and radiosensitivity in synchronized V-79 cells. Radiat. Res. 64: 394-398, 1975.
18. Chirkov, Y. Y., and Sobolev, A. S. Prostaglandin E_1: cAMP level and radiosensitivity of cultured B-82 cells. Strahlentherapie 160: 521-522, 1984.

Life Sciences, Vol. 43, pp. 59-66
Printed in the U.S.A.

Pergamon Press

ATTENUATION OF A RADIATION-INDUCED CONDITIONED TASTE AVERSION AFTER THE DEVELOPMENT OF ETHANOL TOLERANCE

Walter A. Hunt[1] and Bernard M. Rabin[1,2]

[1]Behavioral Sciences Department
Armed Forces Radiobiology Research Institute
Bethesda, MD 20814-5145
and
[2]Department of Psychology
University of Maryland Baltimore County
Catonsville, MD 21228

(Received in final form May 9, 1988)

Summary

An attempt to reduce a radiation-induced conditioned taste aversion (CTA) was undertaken by rendering animals tolerant to ethanol. Ethanol tolerance, developed over 5 days, was sufficient to block a radiation-induced taste aversion, as well as an ethanol-induced CTA. Several intermittent doses of ethanol, which did not induce tolerance but removed the novelty of the conditioning stimulus, blocked an ethanol-induced CTA but not the radiation-induced CTA. A CTA induced by doses of radiation up to 500 rads was attenuated. These data suggest that radioprotection developing in association with ethanol tolerance is a result of a physiological response to the chronic presence of ethanol not to the ethanol itself.

Animals have developed over the course of evolution mechanisms to help prevent accidental poisoning. In addition to emesis during which presumably tainted food is expelled from the stomach, animals are also capable of avoiding potentially toxic substances after a single ingestion of quantities less toxic than those required to induce vomiting. This is done through a process called the conditioned taste aversion (CTA). A CTA develops when the animal associates the taste of novel tasting food with a physiological response, possibly illness, and then subsequently avoids further ingestion of that food. In a laboratory setting, a CTA is typically induced by pairing a normally preferred but novel tasting fluid with exposure to a toxin. The animal will then avoid drinking the fluid.

The CTA has been extensively studied and a specific nucleus of the brain stem, the area postrema, has been demonstrated to play an important role in the development of a CTA to a broad range of unrelated toxins. These toxins include ionizing radiation, lithium chloride, copper sulfate, paraquat, amphetamine, and ethiofos (WR-2721). The area postrema is sufficiently important that if lesions are placed in this nucleus, the development of a CTA to these toxins is blocked (1-6). Not all toxin-induced CTAs are mediated by the area postrema. For example, CTAs induced by ethanol and morphine are not blocked by lesions of the area postrema (7).

0024-3205/88 $3.00 + .00

The biological mechanisms by which toxins induce a CTA mediated by the area postrema are not well understood. Toxins generally are not likely to act directly on specific receptors in this area of the brain, since toxins are usually foreign substances, and specific receptors for each possible toxin are not expected to have evolved. The area postrema is a highly vascularized nucleus in the brain stem and has a poorly developed blood-brain barrier (8). With this characteristic, it can monitor the blood for the presence of toxins (9). However, in order to effectively detect most toxins, an intermediary mechanism in the induction of CTAs involving one or more secondary mediators has been postulated (10,11). Basically, the theory suggests that a toxin primarily acts peripherally, rather than centrally, to stimulate the release of such a mediator into the blood, which, in turn, circulates to the area postrema, where it interacts with a specific receptor. If this interaction occurs following consumption of a novel tasting fluid, a CTA is then initiated.

Several approaches have been taken to block the development of a CTA. One approach involves preexposure to a toxin different from the one used to induce a CTA. If both toxins act by similar mechanisms, then the novelty of the CTA-inducing stimulus will be lost and a CTA will not develop, a process of behavioral conditioning. A recent study from our laboratory has employed this approach (12). However, the results provided mixed results. Preexposure to lithium chloride could block a CTA induced by ionizing radiation or ethanol, but preexposure with the latter toxins could not block a lithium chloride-induced CTA.

Another approach is to intervene in the interaction of the toxin or secondary mediator with receptors in the neural circuitry involved with the acquisition of a CTA. These receptors could be located in the area postrema or other parts of the brain. Biogenic amines have been the primary focus of the available studies. The results obtained using drugs that modify transmitter-receptor interactions or placing lesions in relevant areas of the brain have depended on the toxin used but have produced variable results. For example, although catecholamines appear to be involved in amphetamine-induced CTAs, they are not involved in lithium chloride- nor radiation-induced CTAs (see review of Rabin and Hunt (11) for details).

A third approach to block a CTA might be to interrupt the physiological consequences of stimulating receptors by a toxin or secondary mediator, rather than attempting to block the action of a toxin directly at receptors. Many mechanisms are activated after receptors are stimulated and if these mechanisms could be desensitized so that their responsiveness to the presence of a toxin is reduced, the behavioral consequences of exposure to the toxin might also be reduced. The present experiments were undertaken to test this possibility.

The procedure selected to desensitize neurons was to render them tolerant to the nonspecific toxin ethanol. The use of ethanol tolerance has one major advantage over the use of tolerance induced by other drugs. The induction of ethanol tolerance can reduce nonspecifically the sensitivity to a variety of different classes of drugs. Chronic ethanol administration is known not only to induce cross-tolerance to other depressants, such as gaseous anesthetics, barbiturates, and benzodiazepines, but also to reduce the sensitivity to other drug classes, such as dopamine agonists and antagonists (13-16), γ-aminobutyric acid agonists and antagonists (17), and in some cases opiates (18-19). With this relatively nonselective desensitization in the presence of ethanol tolerance to the effects of a number of drug types, the probability of reducing toxin-induced CTAs might be improved.

In these experiments ionizing radiation was used as the toxin to avoid drug interactions with ethanol. Also, both toxins exert similar effects on a number of neural mechanisms, increasing the likelihood of developing cross-tolerance. For example, radiation and ethanol induce hypothermia (20,21), stimulate striatal potassium-stimulated dopamine release in vitro (22,23), reduce the concentrations of striatal dopamine metabolites (24,25), and inhibit voltage-dependent sodium and calcium channels (26-29). Since ethanol itself can induce a CTA (30,31), the effect of tolerance on this end-point was assessed for comparison with the radiation-induced CTA.

Methods

Male Sprague-Dawley Crl:CD(SD)BR rats (Charles River Breeding Laboratories, Kingston, NY) weighing 200-300 g were used in these experiments. Rats were quarantined on arrival and screened for evidence of disease by serology and histopathology before being released from quarantine. The rats were housed individually in polycarbonate isolator cages (Lab Products, Maywood, NJ) on autoclaved hardwood contact bedding ('Beta Chip' Northeastern Products Corp., Warrensburg, NY) and were provided commercial rodent chow ('Wayne Rodent Blok' Continental Grain Co., Chicago IL) and acidified water (pH 2.5 using HCl) ad libitum to reduce Pseudomonas infections. Animal holding rooms were kept at $21 \pm 1^{\circ}$ C with $50 \pm 10\%$ relative humidity on a 12-hr, light:dark lighting cycle with no twilight (lights on at 7 AM; off at 7 PM).

The animals were rendered ethanol-tolerant by giving them doses of ethanol twice daily (morning and afternoon) for 5 days. Ethanol was administered orally as a 20% (w/v) aqueous solution using a pediatric feeding tube. The initial dose was 4 g/kg and increased toward the end of the 5-day period to 6 g/kg, as the responsiveness to a dose of ethanol decreased. The second dose each day was determined based on the degree of intoxication as described by Majchrowicz (32). The higher the degree of intoxication, the lower the dose of ethanol administered. Control groups were given an amount of water equivalent to that received by the experimental groups. Tolerance was demonstrated 5 days after the last dose of ethanol by comparing sleep-times induced by a single dose (3-g/kg, ip) of ethanol obtained from the ethanol-tolerant and control groups. The sleep-time was the period during which the animal lost its righting reflex.

After the last dose of ethanol, the animals were deprived of water for 23.5 hr per day for five days. On each of those days, they were given water for only a 30-min period during the early light phase of the diurnal cycle (8-11 AM). On the fifth day after the last dose of ethanol (the conditioning day), the animals were presented with a 10% sucrose solution. After they were permitted to consume the fluid for 30 min and the amount consumed recorded, the animals were exposed to varying doses of ionizing radiation or to a 4-g/kg, oral dose (via intubation) of ethanol. Two days later on the test day, the 10% sucrose solution was presented again for a 30-min period, and the amount of fluid consumed was recorded. A CTA was defined as a statistically significant reduction in the intake of the 10% sucrose solution on the test day.

Irradiated animals were exposed to a single bilateral dose of gamma radiation from a ^{60}Co source at a rate of 40 rads/min. Radiation dosimetry was performed using paired, 50-ml ion chambers. Delivered dose was expressed as a ratio of the dose measured in a tissue-equivalent plastic phantom enclosed in a restraining tube, to that measured free in air.

Results

Exposure to either ionizing radiation (100 rads) or ethanol (4 g/kg, po) resulted in the development of a CTA in control animals (Fig. 1). As expected, when animals were rendered tolerant to ethanol (as demonstrated by reduced sleep-times in Table 1), they were resistant to the acquisition of an ethanol-induced CTA. However, ethanol-tolerant animals were also resistant to a radiation-induced CTA as well (Fig. 1). No significant difference in sucrose consumption was found on the test day for either toxin.

The attenuation of a radiation-induced CTA in ethanol-tolerant rats might suggest that radiation and ethanol are experienced as similar stimuli by the animal. Consequently, this attenuation could be due to the lack of novelty of the experience of the toxin, and such a lack in itself would block the acquisition of a CTA. To test this possibility, animals were given single doses of ethanol on 3 days prior to the conditioning day on which they were exposed to either ethanol or ionizing radiation. Single doses of ethanol were administered 2, 5, and 8 days before the conditioning day. This procedure was not sufficient to induce tolerance (Table 1). Under these experimental conditions, although several doses of ethanol were sufficient to block an ethanol-induced CTA, they were not sufficient to block a radiation-induced CTA (Fig. 2) (cf. ethanol/rad groups in Fig. 1 with ethanol/rad groups in Fig. 2).

In another set of experiments to determine if ethanol tolerance could block the CTA induced by higher doses of radiation, animals were exposed to 100-, 300-, or 500-rad doses of radiation and the presence of a CTA was assessed in the manner described above. Increasing doses of radiation as expected intensified the CTA in a dose-dependent manner in nontolerant animals with the maximum CTA being observed after a dose of 500 rads (Fig. 3). When animals were rendered ethanol-tolerant, a similar dose-response effect was observed, but revealed a reduced sensitivity to radiation at all doses. The degree to which ethanol-tolerance could confer radioprotection depended somewhat on the intensity of the CTA. Although the dose required to reduce the consumption of the 10% sucrose solution by 50% (ED_{50}) was 2.5 times greater for the ethanol-tolerant rats, it was 3.4 times greater for the ED_{40} but only 2.0 times greater for the ED_{70} (Fig. 3). In effect, ethanol tolerance had the most beneficial effects after exposure to the lower doses of radiation.

Discussion

The present results indicate that short-term chronic administration of ethanol sufficient to render animals tolerant to the depressant effects of ethanol can attenuate a radiation-induced CTA. This attenuation could be observed over a range of doses from 100 to 500 rads.

There are three possible mechanisms by which ethanol treatment could have a radioprotectant effect. One mechanism could involve a competitive interaction between ethanol and radiation (possibly via a secondary mediator) on the sites in the brain where CTAs are initiated. This possibility appears unlikely. Although radiation and ethanol have some actions in common, as discussed earlier, radiation acts, at least indirectly, on the important center of CTA induction, the area postrema (2,3), while ethanol does not (7). Thus, the radioprotectant effect apparently does not result from a direct action of ethanol per se on the systems responsible for the induction of CTAs, but rather from the response of the animal to the continuous presence of ethanol.

TABLE 1

SLEEP-TIMES (MIN) AS A FUNCTION OF ETHANOL TOLERANCE AND PREEXPOSURE PROCEDURES

	N	PRETREATMENT	POSTTREATMENT
TOLERANCE			
Ethanol	15	100.07 ± 8.06*	61.40 ± 5.15**
Water	14	105.64 ± 7.88	124.57 ± 10.26**
PREEXPOSURE			
Ethanol	12	114.83 ± 8.26	100.58 ± 11.67
Water	11	110.73 ± 10.68	112.45 ± 17.40

* Mean ± standard error of the mean.
** Significantly different from pretreatment mean, $p < 0.05$, based on Student's t-tests.

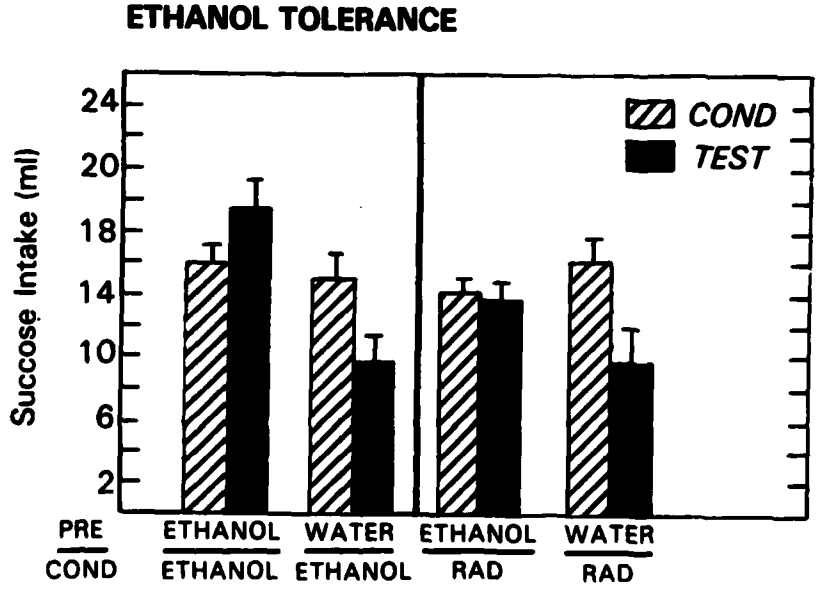

FIG. 1

The effect of ethanol tolerance on an ethanol and radiation-induced CTA. Each pair of bars represents the sucrose intake on the conditioning and test days under different experimental conditions. Animals were pretreated chronically with either ethanol or water for 5 days. A 100-rad dose of ionizing radiation or a 4-g/kg dose of ethanol could induce a CTA in non-ethanol-tolerant animals but not in tolerant ones. Statistical analyses were performed using the paired t-test; 0.05 was the level of significance. No CTA developed when water was substituted for sucrose or when animals were sham-irradiated (data not shown).

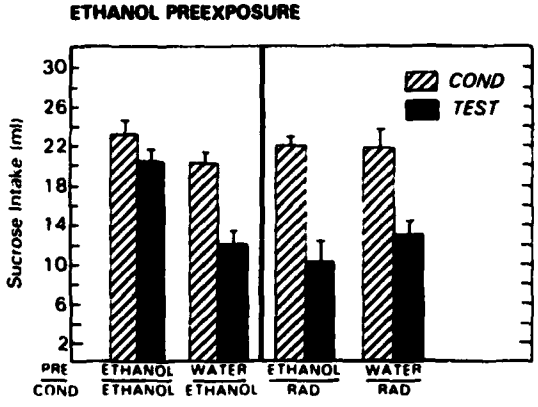

FIG. 2

The effect of ethanol preexposure on an ethanol and radiation-induced CTA. Each pair of bars represents the sucrose intake on the conditioning and test days under different experimental conditions. Animals were administered a single dose of ethanol on 3 separate days. Preexposure to ethanol blocked an ethanol-induced CTA but not a radiation-induced CTA. Statistical analyses were performed using the paired t-test; 0.05 was the level of significance. No CTA developed when water was substituted for sucrose or when animals were sham-irradiated (data not shown). In these experiments, the animals were water deprived for 10 days prior to the conditioning day to maximize the chance of finding an effect of preexposure. As a result, they consumed more fluid on the conditioning day than the ethanol-tolerant animals deprived of water for only 5 days.

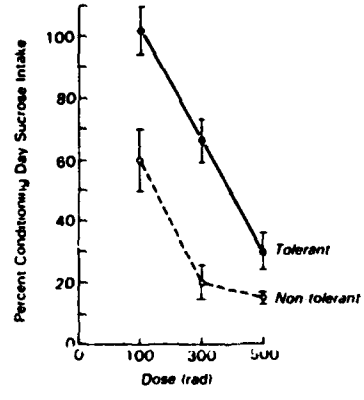

FIG. 3

The effect of increasing doses of radiation on sucrose intake in ethanol-tolerant and non-tolerant animals expressed as a percentage calculated by dividing the intake on the test day by the intake on the conditioning day. Ethanol-tolerant animals were less sensitive to the induction of a radiation-induced CTA at all doses examined ($p < 0.001$, based on an analysis of variance, $F = 32.0$, $df = 1,56$).

If the stimuli underlying the acquisition of radiation- and ethanol-induced CTAs were similar, the novelty of the radiation stimulus would be reduced by prior experience with an ethanol stimulus and, consequently, the intensity of a radiation-induced CTA would be attenuated. The lack of involvement of the area postrema in the induction of both CTAs and the results in Fig. 2 argue against this possibility of a preexposure effect. The administration of several doses of ethanol prior to the pairing of the sucrose with radiation was not sufficient to block the subsequent radiation-induced CTA. Also, in a more extensive study ethanol preexposure was unable to block a CTA induced by lithium chloride nor amphetamine (12). Only an ethanol-induced CTA could be blocked by ethanol preexposure.

The development of tolerance to ethanol appears to be the best explanation of the radioprotectant effect observed. Tolerance to a drug is defined as the progressive decline in the effect of a given dose to induce a given response or as the need to increase the dose to maintain the response. There are several types of ethanol tolerance that can be studied in experimental animals, including environmentally conditioned, metabolic, and cellular tolerance. However, the first two types of tolerance are not pertinent to the present experiments. Environmentally conditioned tolerance can occur when animals are tested for sensitivity and tolerance to ethanol and chronically treated under the same experimental and environmental conditions (33). They are, in effect, conditioned by environmental cues to compensate for the depressant effect of ethanol. Since sleep-times in our studies were performed after a different route of administration of ethanol than was used to induce tolerance, and since irradiations were performed in a different environment, environmentally conditioned tolerance would not play a role in the results obtained. Metabolic tolerance is a result of an increased rate of ethanol metabolism, a process not relevant to radiation exposure. Cellular tolerance is expressed as a reduced responsiveness of physiological processes to the presence of ethanol and correlates with the development of behavioral tolerance. Since behavioral and cellular tolerance to ethanol results from a reduction in the ability of ethanol to disrupt the structure and function of cellular membranes (34,35) and affected mechanisms become cross-tolerant to the actions of other drugs, the responsiveness of these mechanisms may also be reduced to the actions of a toxin not a chemical substance, such as ionizing radiation. This process may be the basis of the radioprotective effect of ethanol tolerance.

The induction of cellular tolerance to ethanol is a general way to desensitize a variety of systems, presumably nonspecifically. As pointed out earlier, the actions of a number of unrelated classes of drugs are less effective in ethanol-tolerant animals. It would appear from the present results that the ability to induce a CTA after exposure to ionizing radiation is also reduced in ethanol-tolerant animals. The usefulness of this approach to block the development of a CTA might depend on its ability to block CTAs induced by other toxins. Preliminary results indicate that ethanol tolerance also attenuates a CTA induced by lithium chloride. Further research is in progress.

Acknowledgements

This research was supported by the Armed Forces Radiobiology Research Institute, Defense Nuclear Agency, under work unit B4123. Views presented in this paper are those of the authors; no endorsement by the Defense Nuclear Agency has been given nor should be inferred. Research was conducted according to the principles enunciated in the 'Guide for the Care and Use of Laboratory Animal Resources, National Research Council.' The authors acknowledge the support of the Computer Science Center at the University of Maryland Baltimore County.

References

1. M.S. DEY, R.I. KRIEGER, and R.C. RITTER, Toxicol. Appl. Pharmacol. 87 212-221 (1987).
2. K.-P. OSSENKOPP, Behav. Brain Res. 7 295-305 (1983).
3. B.M. RABIN, W.A. HUNT, and J. LEE, Radiat. Res. 93 388-394 (1983).
4. B.M. RABIN, W.A. HUNT, and J. LEE, Neurobehav. Toxicol. Teratol. 8 83-87 (1986).
5. B.M. RABIN, W.A. HUNT, and J. LEE, Pharmacol. Biochem. Behav. 27 677-683 (1987).
6. S. RITTER, J.L. MCGLONE, and K.W. KELLY, Brain Res. 201 501-506 (1980).
7. W.A. HUNT, B.M. RABIN, and J. LEE, Alcohol, 4 169-173 (1987).
8. E.W. DEMSEY, J. Comp. Neurol. 150 177-200 (1970).
9. H.L. BORISON, Life Sci. 14 1807-1817 (1974).
10. E.L. HUNT, H.W. CARROLL, and D.J. KIMELDORF, Science, 150 1747-1748 (1965).
11. B.M. RABIN and W.A. HUNT, Neurosci. Biobehav. Rev. 10 55-65 (1986).
12. B.M. RABIN and W.A. HUNT, Abst. Soc. Neurosci. (1987).
13. R.F. BLACK, P.L. HOFFMAN, and B. TABAKOFF, Alcoholism: Clin. Exp. Res. 4 294-297 (1980).
14. P.L. HOFFMAN and B. TABAKOFF, Nature 268 551-553 (1977).
15. B. TABAKOFF and P.L. HOFFMAN, J. Neurochem. 31 1223-1229 (1978).
16. B. TABAKOFF, P.L. HOFFMAN, and R.F. RITZMANN, Life Sci. 23 643-648 (1983).
17. S. URWYLER and B. TABAKOFF, Alcoholism: Clin. Exp. Res. 4 232 (1980).
18. P.L. HOFFMAN, S. URWYLER, and B. TABAKOFF, J. Pharmacol. Exp. Ther. 222 182-189 (1982).
19. B. TABAKOFF, S. URWYLER, and P.L. HOFFMAN, J. Neurochem. 37 518-521 (1981).
20. S.B. KANDASAMY, W.A. HUNT, and G.A. MICKLEY, Radiat. Res. in press.
21. G. FREUND, Life Sci. 13 345-349 (1973).
22. W.A. HUNT, T.K. DALTON, and J.H. DARDEN, Radiat. Res. 80 556-562 (1979).
23. J.H. DARDEN and W.A. HUNT, J. Neurochem. 29 1143-1145 (1977).
24. W.A. HUNT and T.K. DALTON, in preparation.
25. W.A. HUNT and E. MAJCHROWICZ, Pharmacol. Biochem. Behav. 18 Suppl. 1, 371-374 (1983).
26. H.N. WIXON and W.A. HUNT, Science 220 1073-1074 (1983).
27. M.J. MULLIN and W.A. HUNT, Life Sci. 34 287-292 (1984).
28. S.B. KANDASAMY and W.A. HUNT, in preparation.
29. S.W. LESLIE, E. BARR, J. CHANDLER, and R.P. FARRAR, J. Pharmacol. Exp. Ther. 225 571-575 (1983).
30. R.F. BERMAN and D.S. CANNON, Physiol. Behav. 12 1041-1044 (1974).
31. P.J. KULKOSKY, J.L. SOCKEL, and A.L. RILEY, Pharmacol. Biochem. Behav. 13 77-80 (1980).
32. E. MAJCHROWICZ, Psychopharmacologia 43 245-254 (1975).
33. C.L. MELCHIOR and B. TABAKOFF, J. Pharmacol. Exp. Ther. 219 175-180 (1981).
34. J.H. CHIN and D.B. GOLDSTEIN, Science 196 684-685 (1977).
35. W.A. HUNT, Alcohol and Biological Membranes, Guilford Press, New York (1985).

Laboratory Animal Science

Vol 38, No 5
October 1988

A Tethered-Restraint System for Blood Collection from Ferrets

Robert K Jackson, Victor A Kieffer, Jerome J Sauber and Gregory L King

The laboratory ferret, *Mustela putorius furo*, recently has come into prominence as a laboratory animal for use in biomedical research. Our laboratory has adopted the use of this species because the ferret's emetic response to radiation occurs at a lower dose and has a more rapid onset than that of dogs (1, 2, 3). One approach for determining the physiological basis of this response is to measure serum levels of various circulating substances before and after irradiation. However, blood collection from the ferret can be difficult because the lack of easily accessible veins and seasonal accumulation of subcutaneous body fat.

Previously described methods for blood collection in this species (toenail clip, retro-orbital or cardiac puncture, caudal tail or jugular venipuncture and bleeding from the ventral tail artery) all require chemical or physical restraint (4). These restraint methods are not well suited for studies in which an active response is to be observed during blood withdrawal or drug administration. Sedation inhibits radiation-induced emesis in other species (1, 2) and sling-restraint interferes with radiation-induced emesis in the ferret (5). Therefore, we developed a means by which ferrets could be restrained which would have minimal effect on the emetic response.

This report describes a method of tethered-restraint for the ferret in which an in-dwelling venous jugular catheter is implanted for withdrawing blood samples. No interference with the animal's normal activities occurs during the sampling procedure. Each animal is conditioned to the tethered-restraint prior to surgical placement of the catheter. The technique provides a minimally stressful method of restraint. A similar tethering system has been used successfully on several other animal species, such as non-human primates (6) and rats (7).

Thirty-three commercially obtained adult male, fitch (sable), castrated and descented ferrets (1 to 1.5 kg), were used[1]. All animals were housed in modified stainless-steel rabbit or cat cages and fed dried cat or ferret diet *ad libitum*. The animal quarters were maintained at

From the Department of Veterinary Science (Jackson, Sauber) and Physiology (Kieffer, King), Armed Forces Radiobiology Research Institue, Bethesda, MD 20814.

Laboratory Animal Science
Copyright' 1988
by the American Association for Laboratory Animal Science

Vol 38, No 5
October 1988

the following temperature, relative humidity and photocycle respectively: 15–21°C, 45–55% and 12 hours light/12 hours dark.

Each animal was caged individually and fitted with a modified guinea pig harness and tether produced by Alice King Chatham Medical Arts (8)[2]. The harness fit around the animal's upper torso and was attached to a stainless-steel flexible-spring tether through which the catheter was threaded. The distal end of the tether was connected to a miniature fluid swivel which was attached to the catheter and was clamped to the cage top. The only rotation occurred between the swivel shaft and the housing of the swivel. This arrangement prevented twisting or kinking of the catheter. The system restricted movement somewhat, but did not interfere with normal activity once the animal became accustomed to tethered-restraint (Figure 1).

The catheter material was flexible tubing, type MRE-040, 0.040" (.88 mm) o.d. × .025" (.55 mm) i.d., approximately 90 cm in length[3]. One end was beveled for insertion into the jugular vein while the end to be exteriorized was sealed with a stainless-steel 23 ga. pin. A collar of a 5–10 mm piece of slightly larger diameter polyethylene tubing (1.36 mm o.d. × 0.99 mm i.d.) was glued around the catheter 10 cm from the beveled end with a silicone sealant and allowed to dry overnight. Catheters were gas sterilized.

Conditioning to tethered-restraint began after the ferret's arrival and acclimation to its new environment. Ferrets were first fitted to the harness alone, followed by the addition of the tether. Each animal was fitted with a small or medium size jacket designed for guinea pigs. The larger size of the ferret necessitated the enlargement of the leg openings by cutting four small slits radially around the inner edges. This modification helped prevent irritation caused by normal motion of the legs. To fit the jacket, the ferrets were held by the skin of the neck while the forepaws were fed through the leg openings. The jacket was then pulled snugly to the back where a 4 × 7 cm piece of Velcro® held the ends together. The jacket, composed of lightweight nylon, was laced by a string to clasps on each side.

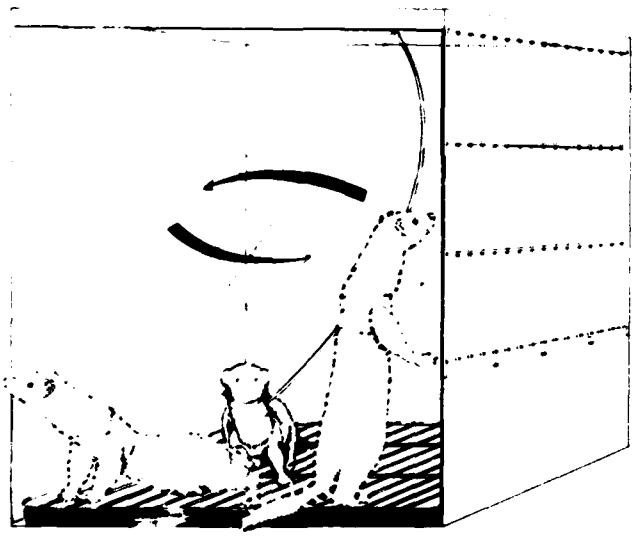

Figure 1 The length of the tether is sufficient to allow the ferret access to all areas of the cage. The system restricts movement somewhat, but does not interfere with normal activity once the ferret has become accustomed to tethered-restraint.

Conditioning was for short periods of time initially and progressed until the animal tolerated continuous tethered-restraint. Full adaptation was defined by a normal pattern of activity which included grooming, eating, sleeping and inquisitive behavior. During the initial fitting and conditioning each animal was observed for the first hour. For conditioning periods longer than 1 hour, ferrets were monitored intermittently. At the first signs of distress the animal was removed from the restraint apparatus. Those animals that did not adapt (e.g., tolerance time to restraint lessened rather than lengthened) were removed from the study. Animals did not undergo catheterization until accustomed to at least 24 hour restraint. All pre-operative conditioning procedures required individual housing of the ferrets.

On first fitting the nylon jackets to the ferrets, there was some initial discomfort as evidenced by rolling over and scratching at the jacket. This initial response subsided within a few minutes. Of the 33 animals in the study, only one animal was withdrawn because it would not tolerate the jacket.

During the next stage of conditioning, animals were tether-restrained for 4 days with periods of restraint progressing from 1 to 8 hours. Those animals that adapted rapidly were tethered for 5 to 6 hours on day two. By days three to five, each animal was tether-retrained for at least one 24 hour period. Tethered-restraint did not interfere with normal eating, sleeping or exploratory behavior, thus meeting the criteria for full adaptations.

Twelve to sixteen hours prior to surgery each animal was assessed for the status of its general health and food was withheld. Each animal was preanesthetized with an IM injection of ketamine hydrochloride (30 mg/kg) and acetylpromazine maleate (25 mg/kg). This placed the overall injected dose of both preanesthetic compounds within the middle of the recommended dosage ranges (i.e., 20–35 mg/kg ketamine and 0.2–0.35 mg/kg acetylpromzine) for the ferret (4).

Early in the study, induction and maintenance of a surgical plane of anesthesia was accomplished by masking the animal and gassing with 0.75 – 1.25% halothane in 0.8 L/min of N_2O and 0.4 L/min of O_2. Respirations and mask placement/retention over the snout were monitored visually throughout the procedure. In more recent procedures, ferrets were intubated using a 3.0 I.D.x4.3 O.D. endotracheal tube and maintained on 1.0 – 1.5% isoflurane in 0.5 L/min of O_2 using a Bickford PC-2, pediatric, non-rebreathing system[4].

The use of gas anesthesia helped to maintain a safe plane of surgical anesthesia and to ensure rapid postoperative recovery. Altering the anesthetic technique to the use of isoflurane, intubation, and a pediatric, non-

Laboratory Animal Science

Vol 38, No 5
October 1988

rebreathing system enhanced the ability to control the plane of anesthesia and further shortened the recovery period. N_2O has been used for jugular catheterization in the ferret (9) and no complications were noted with it in our study. Nevertheless, its use was discontinued due to the risk of expansion of any possible air embolism secondary to the jugular cutdown procedures.

One death occurred due to a presumed hypersensitivity reaction to the pre-anesthetic medications. This particular 1.1 kg ferret received the calculated pre-anesthetic dose of ketamine and acetylpromazine, was returned to the holding cage in the surgical preparation area and expired prior to retrieval for surgical preparation. Attempts to resuscitate the animal were unsuccessful.

The surgical approach to the jugular vein in the ferret did not offer significantly from the approach in the dog and cat, and various techniques have been described previously in the ferret (10, 11). The saline-filled catheter was inserted through the jugular incision and advanced until the collar passed just beyond the incision site. Cannula patency was tested by drawing blood into the catheter and then flushing with approximately 1 ml of heparinized saline (10 mg/1000 ml). Once the catheter was determined to be patent, it was sealed with a sterile stainless-steel pin. The catheter was secured in place by tying two silk ligatures on either side of the collar. The distal end of the catheter exited through a dorsal midline incision between the scapulae. In our experience, subcuticular sutures are better tolerated than skin sutures in the ferret, and minimize the chance for catheter complications secondary to handling the animal to remove non-absorbable skin sutures. After closing both incisions, the exposed end of the catheter was threaded through the sterile flexible tether. The harness was fitted and fastened, and the catheter uncapped and attached to the sterile, sealed swivel.

Post surgically, each animal was ventilated briefly with 100% O_2, and then allowed to breathe room air before being returned to its cage. The swivel was attached to the overhead clamp and the tether's length (53 cm) allowed the ferret access to the entire cage interior. Animals were monitored constantly until sufficiently recovered to maintain sternal recumbancy. All animals recovered from the effects of the anesthesia within an hour and were eating and active by the end of the day. They were observed frequently over the next 24 hours to ensure complete recovery from anesthesia and to monitor for excessive bleeding. Each animal was also checked for possible seroma or hematoma formation in dependent areas and for proper jacket fit.

The catheter was checked daily to ascertain its patency by aspirating until blood was visualized and then flushing with approximately 1.0 ml of sterile heparinized saline solution. Sterile gloves were worn and aseptic techniques used for this procedure (e.g., sterile syringes and needles).

Within 24 to 48 hours after recovery from surgery, blood was drawn for control samples. One to two days after control samples were drawn, the animals were irradiated and additional blood samples were taken. Aseptic technique was used to withdraw all samples. Sampling was done from outside the cage by manipulating the distal end of the catheter where the tether attached to the swivle assembly, thus avoiding the need to handle the ferret. During sampling, no more than 4 ml of blood was drawn at any one time. An equal volume of normal saline was infused afterward to maintain the intravascular blood volume.

Of the 32 animals adapted to tethered-restraint and implanted with catheters, blood samples were drawn successfully from 30. Of these, both control (pre-irradiation) and experimental (post-irradiation) samples were drawn from 25, while control samples only were collected from five. With one exception, control blood samples were taken at 1 to 2 days postoperatively, and experimental samples were drawn 2 to 9 days postoperatively. In the one case, the control sample was taken at day 18 postoperatively and the experimental sample drawn at day 21. The volume of blood taken during a single withdrawal ranged from 2 to 4 ml.

We were unable to obtain any blood from two ferrets. In these two cases, the problem was attributed to clotting at the end of the catheter, and was confirmed at necropsy. The clotting presumably resulted from occlusion of the jugular and subsequent loss of blood flow around the catheter tip. This problem was corrected by lengthening the intravascular portion of the catheter to 10 cm, so that its tip would rest where the left and right jugular veins join to form the precava. With the remaining five animals, complications arose while drawing the experimental sample. In one of these animals, the catheter had become crimped in the subcutaneous tunnel. In another, the catheter was not blocked at necropsy although it was impossible to flush or withdraw *in situ*. The probable cause was thought to be a fibrin tag acting as a one way valve. No necropsy was performed on the other three animals.

At the conclusion of the experiment, each animal was euthanatized with an IV injection of T-61® (0.3 ml/kg)[5].

The principal conclusion to be drawn from these studies is that the ferret is amenable to tethered-restraint. This is evidenced by the 97% success rate ($n = 32/33$) for adaptation after conditioning. Restriction of movement induced by the tether is minimal. All animals exhibited normal behavior patterns of sleeping, eating, grooming and exploration. Alternative restraint systems, such as a lucite tube (12) or a sling (5) prevent such activity.

A major advantage of tethered-restraint is the apparent lack of stress that has been observed as compared with other means of physical restraint. Tether-restrained ferrets exhibited no observable difference in activity levels or behavioral traits from non-restrained animals. In addition, the emetic responses of the tethered ferrets did not differ in latency from those of non-restrained ferrets (3). From these observations, it appears that the stress of tethered-restraint in the ferret is no greater that of single housing them in standard laboratory animal caging.

Laboratory Animal Science
Copyright 1988
by the American Association for Laboratory Animal Science

Vol 38, No 5
October 1988

Given the small diameter of ferret veins and the difficulty with locating them (10), intermittent venipuncture of these vessels (12) requires periods of restraint that add to the stress of venipuncture and may alter physiologic parameters under study. Even the jugular catheterization technique described by Greener and Gillies (11) requires a degree of physical restraint during sampling. The conditioning of ferrets to tethered-restraint should minimize stress-induced changes in levels of numerous circulating hormones, vasoactive compounds and hemotological components (13, 14). Additionally, it allows the investigator to administer compounds and withdraw samples unassisted.

The major complications arising from this study have been associated with catheter length. In two early cases, the catheter blocked with clotted blood. This problem was corrected by lengthening the indwelling portion of the catheter so that its tip would extend into the precava, thus maintaining blood flow away from the end. Once this problem was corrected, the overall success rate for blood withdrawal from the remaining ferrets was 83% (n = 25/30). The one instance in which blood was drawn 18 and 21 days postoperatively suggests this method may be amenable for chronic studies and warrants additional investigation.

Other complications resulted from the lack of precise postoperative fitting of the jacket. If the jacket fit too snugly, postoperative edema occurred and skin irritation around the neck and axillary regions resulted. If the jacket fit too loosely, the animals could remove the jacket and possibly dislodge the catheter. Careful monitoring and adjustment of the jackets for the first 24 hours prevented these problems.

In conclusion, we find that ferrets easily adapt to the tethered-restraint system, and that the behavior of tethered ferrets is not discernibly different from non-tethered ferrets. Additionally, tethered-restraint allows blood samples to be drawn by one person, reduces the stress normally associated with other means of physical restraint, and avoids the need for tranquilization or sedation during sampling.

Acknowledgements

This research was supported by the Armed Forces Radiobiology Research Institute, Defense Nuclear Agency, under work unit 00167. Views presented in this paper are those of the authors. No endorsement by the Defense Nuclear Agency has been given nor should be inferred. Research was conducted according to the principles enunciated in the "Guide for the Care and Use of Laboratory Animals" prepared by the Institute of Laboratory Animal Resources, National Research Council.

Correspondence concerning this manuscript should be sent to G.L. King, Ph.D., Department of Physiology, Armed Forces Radiobiology Research Institute, Bethesda, MD 20814.

References

1. Mattsson JL, Cordts RE, Yochmowitz MG, *et al.* Prevention of radiation emesis in dogs by a combination of drugs. *Int J Radiation Oncology Biol Phys* 1984; 10:1067–72.

2. Cooper JR, Mattsson JL. Control of radiation-induced emesis with promethazine, cimetidine, thiethylperazine, or naloxone. *Am J Veterinary Res* 1979; 40:1057–61.

3. King GL. Characterization of radiation-induced emesis in the ferret. *Rad Research* 1988; 114:599–612.

4. Moody KD, Bowman TA, Lang CM. Laboratory management of the ferret for biomedical research. *Lab Anim Sci* 1985; 35:272–79.

5. Tuor UI, Kondysar M, Harding RK. Emesis, radiation exposure and local cerebral blood flow in the ferret. *Rad Research* 1988; 114:537–49.

6. McNamee GA, Wannenmacher RW, Dintermann RE, *et al.* A surgical procedure and tethering system for chronic blood sampling, infusion, and temperature monitoring in caged nonhuman primates. *Lab Anim Sci* 1984; 34(3):303–07.

7. Dons RF, Havlik R. A. multilayered cannula for long-term blood sampling of unrestrained rats. *Lab Anim Sci* 1986; 36(5):544–45.

8. Chatham AK. Jacket and swivel tethering systems. *Lab Anim* 1985; 14(8):29–33.

9. Miner WD, Sanger GJ, Turner, DH. Evidence that 5-hydroxytryptamine receptors mediate cytotoxic drug and radiation-evoked emisis. *Br J Cancer* 1987; 56:159–62.

10. Florczyk AP, Schurig JE. A technique for chronic jugular catheterization in the ferret. *Pharm Biochem Behav* 1981; 14:255–57.

11. Greener Y, Gillies B. Intravenous infusion in ferrets. *Lab Anim* 1985; 14(6):41–44.

12. Bleakley SP. Simple technique for bleeding ferrets (*Mustela putorius furo*). *Laboratory Animals* 1980; 14:59–60.

13. Frederickson RCA, Geary LE. Endogenous opioid peptides: review of physiological, pharmacological and clinical aspects. *Prog Neurobiology* 1982; 19(1/2):19–70.

14. Wannenmacher Jr RW, Hadick CL, Beisel WR. Nutrition and infection interrelations in the monkey. *In* Hayes KC, ed. *Primates in Nutritional Research*. New York: Academic Press, 1979; 315–40.

Footnotes

[1]Marshall Research Animals, Inc., North Rose, NY
[2]Alice King Chatham Medical Arts, Los Angeles, CA
[3]Microrenathane®; Braintree Scientific, Inc., Braintree, MA
[4]A.M. Bickford, INC., Wales Center NY
[5]T-61®; American Hoechst Division, Somerville, NJ

RADIATION RESEARCH 114, 599–612 (1988)

Characterization of Radiation-Induced Emesis in the Ferret

GREGORY L. KING

Department of Physiology, Division of Neurophysiology, Armed Forces Radiobiology Research Institute, Bethesda, Maryland 20814-5145

KING, G. L. Characterization of Radiation-Induced Emesis in the Ferret. *Radiat. Res.* **114**, 599–612 (1988).

Forty-eight ferrets (*Mustela putorius furo*) were individually head-shielded and radiated with bilateral ^{60}Co γ radiation at 100 cGy min^{-1} at doses ranging between 49 and 601 cGy. The emetic threshold was observed at 69 cGy, the ED_{50} was calculated as 77 cGy, and 100% incidence of emesis occurred at 201 cGy. With increasing doses of radiation, the latency to first emesis after radiation decreased dramatically, whereas the duration of the prodromal period increased. Two other sets of experiments suggest that dopaminergic mechanisms play a minor role in radiation-induced emesis in the ferret. Twenty-two animals were injected either intravenously or subcutaneously with 30 to 300 μg/kg of apomorphine. Fewer than 50% of the animals vomited to 300 μg/kg apomorphine; central dopaminergic receptor activation was apparent at all doses. Another eight animals received 1 mg/kg domperidone prior to either 201 (n = 4) or 401 (n = 4) cGy radiation and their emetic responses were compared with NaCl-injected-irradiated controls (n = 8). At 201 cGy, domperidone significantly reduced only the total time in emetic behavior. At 401 cGy, domperidone had no salutary effect on radiation-induced emesis. The emetic responses of the ferret to radiation and apomorphine are compared with these responses in other vomiting species.

INTRODUCTION

Emesis, along with fatigue, is the most prominent human response to low-level (100–1000 cGy) radiation exposure, and its occurrence signifies the prodromal phase of the acute radiation syndrome (*1*). To better understand the mechanism underlying the emetic response, the canine and the nonhuman primate have been used as the primary animal models. It has been suggested that the canine may be the more suitable animal model for comparison with man (*2, 3*), given their similar emetic sensitivities to apomorphine (ED_{100} for man, 50 μg/kg (*4*); for canine, 10–15 μg/kg (*5, 6*)) and radiation (ED_{50} for man, 214–230 cGy (*7, 8*); for canine, 258 cGy (*3*)), and their similar thresholds for radiation-induced emesis (man, 180 cGy MLT (*9*); canine, 150–170 cGy MLT (*3, 10*)). Nonhuman primates have a radiation ED_{50} of 446 cGy (*11*) and do not vomit in response to apomorphine (*12*). Cats are seldom used since they require large doses of both apomorphine (*13*) and radiation to induce emesis (*14, 15*).

Recently, however, the ferret (*Mustela putorius furo*) has been proposed as a new animal model for the study of radiation-induced emesis. Gylys (*16, 17*) and Andrews (*18, 19*) and their co-workers have reported some details of the ferret emetic response to radiation. The emetic threshold for radiation in ferrets lies somewhere between 75

0033-7587/88 $3.00

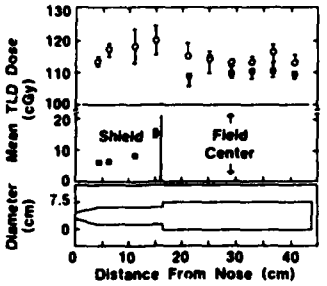

FIG. 1. ^{60}Co dosimetry results from ferret "phantom." Lower panel: Schematic of lucite cylinder or phantom which approximates shape of the ferret. Lithium fluoride thermoluminescent dosimeters (TLDs) were placed at fixed intervals along its central core. All radiations were specified at a 100-cGy dose at 100 cGy min^{-1}. Upper panel: Mean TLD dose recorded along central axis of phantom with (■) or without (○) head-shielding. Error bars represent standard error of the mean. See text (Methods) for more details.

and 100 cGy (J. A. Gylys and C. J. Davis, personal communication). Ferrets also vomit in response to apomorphine and several other compounds (*20, 21*).

This paper reports, in detail, the ferret emetic response to low-level (100–600 cGy) radiation. In addition, this paper describes the ferret emetic response to apomorphine, a dopamine receptor agonist, and the refractoriness of radiation-induced emesis to domperidone, a peripheral dopamine receptor antagonist. These results have been communicated in part as an abstract to the Society for Neuroscience (*22*).

METHODS

Animals

Adult male, fitch (sable), castrated, and descented ferrets (1–1.5 kg) were obtained from Marshall Farms (North Rose, NY) and used for all studies reported herein. All animals were housed in stainless-steel modified rabbit or cat cages and provided commercial cat feed and water *ad libitum*. Only those with an indwelling jugular catheter were housed individually. The animal quarters were maintained, respectively, at the following temperature, relative humidity, and photocycle: 15–21°C, 45–55%, and 12 h light/12 h dark.

Radiation Studies

Dosimetry and Radiation Exposure

Dosimetry with lithium fluoride thermoluminescent dosimeters (TLDs) was performed on a "phantom" ferret (Fig. 1), a lucite cylinder which approximates body tissue in absorption and scatter of radiation (*23*). The phantom length and diameters were modeled on the average body length and circumference values measured from 11 ferrets weighing an average (±SEM) of 1.26 ± 0.16 kg (*circumference:* head = 15.9 cm, chest = 19.6 cm, lower abdomen = 28.9 cm). TLDs were placed at the following distances (in cm) from the rostral end of the phantom (distance from nose in Fig. 1): 4, 6, 10.7, 14.5, 20.6, 24.6, 28.6, 32.6, 36.6, and 40.6. All dosimetry trials were run at a dose of 100 cGy at 100 cGy min^{-1}. This dose rate compares well to the 125 cGy min^{-1} used by C. J. Davis (personal communication) and the 138 cGy min^{-1} used by Gylys and co-workers (*18, 19*). Trials on the phantom were performed either with (n = 8) or without (n = 4) head-shielding, provided by a layer of 5 × 10 × 20-cm lead bricks stacked around the "head" of the phantom. Irradiation was provided by a bilateral ^{60}Co source and delivered at a source–midline distance of 292 cm. Measurements of dose rate were taken with an ion chamber at the source midline. Results from free-in-air and source–midline measurements gave a TAR (tissue to air ratio) of 0.90.

Figure 1 shows the results from this dosimetry. Without shielding, the mean TLD recorded dose for the head was 117.6 ± 1.8 cGy (mean ± SEM), a value similar to that received by the phantom "body" (114.4 ± 0.8 cGy). Conversely, the recorded dose for the shielded head was 7.8 cGy, with some increase near the "shoulder" (16.1 cGy). The head-shielded mean-total-midline or body dose was 111.46 ± 1.02 cGy, a value not significantly different from the unshielded body dose. The average absorbed TLD dose, however, was 11 cGy greater than that specified for each radiation run. All dose values reported here were adjusted to reflect this difference. The ±SEM values for the total midline–body dose received by the head-shielded phantom were ±1 cGy (vide supra). Given this, it was deemed appropriate to ascribe (and thus report) the precise dose values calculated for each animal.

For radiation exposure, each animal was individually transported to the ^{60}Co facility in a Plexiglas box covered with an environmental filter and then transferred to a hollow Plexiglas tube, capped on both ends and drilled with ventilation ports (modified from (*24*)). Two tubes of different diameters were used (8.2 or 9 cm); the smaller tube was for animals weighing 1–1.2 kg. This prevented turning by the animal and maintained head-shielding. The tubes were placed on a platform centered between the ^{60}Co sources and oriented with the gut in the field center. Each animal was irradiated, transferred back to the filtered box, and returned to the laboratory for a 2-h observation period. The tubes did not disrupt the uniformity of the radiation field.

Apomorphine Studies

Intravenous Cannulation

Catheter construction. The catheter material was flexible tubing (Micro-Renathane, type MRE-040, 0.102 cm o.d. × 0.064 cm i.d., Braintree Scientific, Inc., Braintree, MA) approximately 30 cm long. (One end is beveled for insertion into the jugular, the other is sealed with a stainless-steel 23-gauge pin and exteriorized through the neck.) A 5- to 10-mm piece of slightly larger diameter polyethylene tubing (Intramedic PE-160, 0.16 cm o.d. × 0.11 cm i.d., Becton–Dickinson and Co., Parsippany, NJ) was glued around the catheter 10 cm from the beveled end with a silicone sealant and allowed to dry overnight. Each catheter was then gas sterilized.

Surgical and postoperative procedures. All catheter implantations were done under sterile conditions. Twelve to sixteen hours prior to surgery each animal was observed to be healthy and then placed on nothing per os except for H_2O.

Each animal was preanesthetized with an im injection (0.3 ml) of a 10:1 combination of 100 mg/ml ketamine hydrochloride (Vetalar, Park-Davis) and 10 mg/ml acetylpromazine maleate (Acepromazine Maleate Injection, Tech America). After shaving and cleansing both the neck and dorsal thorax with a povoiodine scrub, a 2- to 3-cm incision was made parallel to the right jugular vein, which was then isolated by blunt dissection. The vein was ligated cranially; the catheter was then inserted through a more caudal, transverse incision and secured with ligature on either side of the collar. Each animal was then rotated into a lateral recumbancy position, the ventral neck incision was covered with sterile gauze, and a short incision was made dorsally in the center of the neck. A subcutaneous tunnel for the catheter was made from this site to the ventral incision. Some slack in the catheter was left near the jugular to prevent "fouling" by head and neck movement during normal activity. Both incisions were closed with a subcuticular, simple-continuous suture pattern. The catheter was shortened to leave 2–3 cm exposed, flushed with heparinized saline, and resealed. Anesthesia was maintained throughout the surgical procedure by inhalation of 0.75–1.25% halothane in 0.8 liter/min N_2O and 0.4 liter/min O_2. Respirations, mask placement, and mask retention were monitored visually throughout the procedure. Strict adherence to aseptic surgical techniques has precluded the necessity for antibiotics; there have been no problems from infection with implanted jugular catheters for up to 25 weeks.

Postsurgically, each animal was ventilated for a few minutes with 100% O_2, then allowed to breathe room air and returned to its cage. Animals were monitored frequently over a 24- to 48-h period to ensure uneventful recovery from anesthesia. The catheter was flushed 6 days/week, with approximately 0.3–0.6 ml heparinized sterile saline. Mild restraint is required for this procedure, but the ferrets adapt very quickly (see also (*25*)).

Injections and Behavioral Observations

For *intravenous* apomorphine administration, a bolus of sterile heparinized saline (0.3–0.6 ml) was first injected to flush the catheter, followed by sterile apomorphine (0.3–0.9 ml; 10–300 μg/kg), which was in turn followed by sterile saline (0.3–0.6 ml). The catheter was then recapped. Intravenous apomorphine testing began 6–7 days postoperatively. For *subcutaneous* injections, each animal was gripped and held at the scruff of the neck and apomorphine was injected along the thorax. Apomorphine HCl (Sigma Chemical Co.) was made fresh daily and injected at no less than 48-h intervals. All doses were delivered on a microgram per kilogram basis, according to the animal's weekly weight, and never exceeded 1 ml in volume. The dosing procedure for each animal began at a single value and was lowered or raised, depending on whether there was an emetic or retching response.

Domperidone vs Radiation-Induced Emesis

For this series of experiments, naive animals were ip injected with 1.0 mg/kg of domperidone (R 33,812; Janssen Pharmaceutica, Inc.) approximately 30 min prior to either 201 (n = 4) or 401 cGy (n = 4) ^{60}Co radiation. Domperidone was prepared and injected as a suspension made from a 2% carboxymethyl cellulose vehicle in NaCl. Eight other animals were injected ip with NaCl only and exposed to 201 (n = 4) or 401 (n = 4) cGy radiation. Animals were observed and notations were made as described below.

At the termination of the postradiation observation period or when a catheter became permanently occluded, animals were anesthetized with sodium pentobarbital (ip, 35–50 mg/kg) and euthanized with T-61 (ip, 0.3 ml/kg, American Hoechst Division).

Data Analysis

After each radiation the following events were recorded for 2 h, along with the time of their occurrence:

(1) emesis and/or retch (nonproductive emesis),

(2) defecations and/or diarrhea, and

(3) other behaviors or responses that might be considered a consequence of radiation exposure.

From these data the latency to and duration of the entire prodromal emetic period and individual emetic or retching episodes were calculated. No objective physiological measure was used to discriminate between emesis and retching, e.g., record of changes in intrathoracic pressure (*26*). For this study, the *prodromal (emetic) period* for each animal is defined as that period of time which begins with the onset of first emesis or retch and ends with the termination of the final emesis or retch. This time frame becomes equivalent to the prodromal phase of acute radiation sickness (*1*). Each prodromal period consisted of distinct emetic or retching *episodes;* an episode was considered emetic if emesis occurred within a series of retches. An interepisode interval consisted of ≥4 min between the last emetic or retching movement of an episode and the first movement of the next episode. All emetic episodes were timed from the end of ^{60}Co radiation.

To determine the ED_{50} for radiation-induced emesis, the percentage of responding animals was analyzed by a Weibull nonlinear fit routine (BMDP 3R) and linear- and log-probit analyses, each with two parameters. A χ^2-test was used to determine the goodness-of-fit for each analysis. Linear regression analysis was used to determine the degree to which any single variable (e.g., latency to the first episode) was linearly related to radiation dose. To compare the effects of domperidone with NaCl on radiation-induced emesis, a standard Student's t test and a Mann–Whitney test were used. Except where noted, all values are reported as means ± SEM. A significant difference was assumed if $P < 0.05$.

RESULTS

Radiation-Induced Emesis

For these studies a total of 48 naive animals were head-shielded and individually radiated at one of the following doses (in cGy): 601 (n = 6), 401 (n = 6), 201 (n = 6),

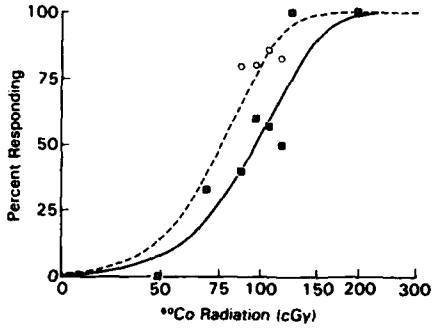

Dose (Gy)	0.49	0.69	0.88	0.98	1.08	1.17	1.27	2.01
Emesis	0/2	1/3	2/5	4/5	4/7	3/6	2/2	6/6
Emesis and/or Retching	0/2	1/3	4/5	4/5	6/7	5/6	2/2	6/6

FIG. 2. Weibull distribution of ferret emetic response to ^{60}Co radiation. Population dose response (as calculated by the Weibull model) of the percentage of animals responding to distinct radiation doses with episodes of either emesis only (■) or emesis and retching (nonproductive emesis (○)). Overlapping data are indicated by the (◘). Dashed and solid lines are fit by computer program. Lower table: Number of animals in each group responding to distinct radiation doses (upper ribbon of panel).

and $n = 30$ for steps between 49 and 127 cGy (see Fig. 2). Seven other naive animals were sham-irradiated at either 101, 201, or 401 cGy. These animals were tube-restrained and placed on the platform for times equivalent to radiation at 100 cGy min^{-1}. No emesis or retching was observed in this latter group. It is possible that tube restraint affected some of the emetic variables. Since all irradiated and sham-irradiated animals were restrained in a similar fashion, tube restraint was not a confounding variable.

Dose–response Curve and ED_{50}

Figure 2 illustrates a Weibull distribution of the percentage of animals vomiting, or vomiting and retching, in response to the lower radiation doses. The table below the figure shows the raw data for these calculations. This distribution gives an ED_{50} for emesis alone at 98 cGy, slightly more than the 90 cGy reported by C. J. Davis (personal communication). Including nonproductive emesis or retching as an episode, and therefore part of the prodromal period, at lower doses shifts the dose–response curve to the left and steepens it. The ED_{50} thus becomes 77 cGy. The *observed* threshold dose for emesis is 69 cGy, comparable to the 75-cGy threshold found by C. J. Davis (personal communication), who used whole-body radiation on ferrets of both sexes, different strains, and all ages.

Table I compares the ED_{50} and other quantile doses calculated by the Weibull distribution with the values for these doses calculated by a linear- and log-probit. As seen here the ED_{50} and other quantile dose values generated by each method are similar. The ED_{50}, produced by including retching as an episode, is lower in all analyses, and all quantile doses are similar. Ninety-five percent confidence limits were not

TABLE I

Ferret Emesis and Retching Incidence in Response to Radiation

Model	*Emesis*	*Quantile dose (cGy)*		
		ED_{10}	ED_{50}	ED_{90}
Weibull	Only	54	98	151
		[19, 90]	[81, 119]	[110, 209]
	With retching	45	77	114
		[23, 86]	[59, 101]	[93, 140]
Probit	Only	40	95	150
		[—]	[—]	[—]
	With retching	44	79	113
		[-, 62]	[20, 93]	[98, 182]
Log probit	Only	59	96	158
		[-, 77]	[67, 119]	[126, 561]
	With retching	52	77	114
		[-, 69]	[41, 91]	[97, 218]

Note. Brackets indicate 95% confidence limits.

generated by the linear-probit method when retching was excluded from analysis. A χ^2 analysis for goodness-of-fit showed the population to be normally distributed for each analytical method ($\alpha > 0.05$). A straight line was a good fit for both probit analyses.

Emetic Latency, Duration, and Frequency

Of all the variables, the one most highly correlated with and linearly related to the radiation dose was the sum total of time spent in emetic behavior during the prodromal period. As seen in Table II, these raw data had a 0.87 correlation with the radia-

TABLE II

Correlation of Emetic Response Variables with Radiation Dose

Response variable	*Correlation coefficient*[a]
Total emetic time	0.8661
Prodromal period	0.7913[b]
Latency to first episode	−0.7649[b]
Total expulsions	0.7464
Total bouts	0.6468
Total defecations	0.5419[b]

[a] Linear regression analyses show that all variables are a linear function of dose ($P < 0.005$) and that the slope of each function is significant ($P < 0.005$). $df = 39$.

[b] Robust (bisquare) regression used; all others done with least-squares calculation.

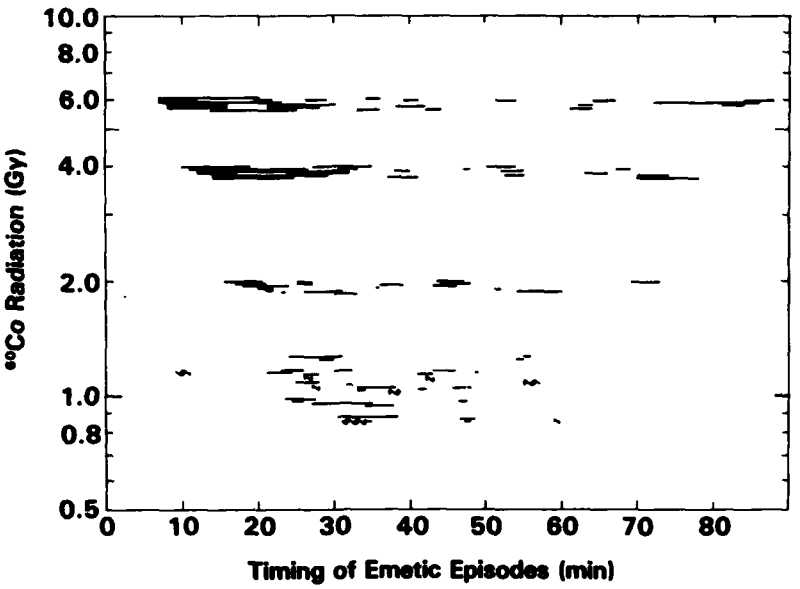

FIG. 3. Timing of individual emetic episodes during the prodromal period following ^{60}Co radiation. Each line represents the duration of a single emetic episode from an individual animal. The latency to each episode was calculated from T_0 = time that ^{60}Co ended. For each radiation dose, emetic responses are arrayed according to the shortest latency to onset. Wavy lines (e.g., 1.2 Gy at 10 min) represent episodes of retching without emesis. Although the animals were observed for 2 h, the prodromal period had ended by 90 min at the highest radiation dose tested.

tion dose. As expected, both the prodromal period and latency to first emesis were also correlated with and linearly related to radiation dose (see Table II).

Figure 3 summarizes the raw emetic data obtained from all animals, e.g., the latency to and duration of each emetic and retching episode in each animal plotted vs the radiation dose. The responses are arrayed according to the earliest onset of the first episode. (Eight episodes were retches only.) With increasing doses of radiation, (1) the delay to onset of the prodromal period diminishes, (2) the duration of the prodromal period increases, and (3) the number of distinct episodes within the prodromal period increases. At 69 cGy, for example, one ferret (of three, see Fig. 2) had a single brief episode, lasting 0.5 min, with two expulsions (data not expressed). In contrast, at 601 cGy, one animal had seven episodes, lasting 2–5 min each, with 15 expulsions. The entire prodromal period for this latter animal lasted almost 1.5 h. For comparison, the duration of the prodromal period in the dog in response to 600 cGy (at 100 cGy min^{-1}) is also about 1.5 h, with four or five episodes (*27*).

Figure 4 is a graph of the mean latencies of the first three emetic episodes within the prodromal period vs the radiation dose. The latency decreases dramatically from 40 min at 68.9 cGy to 8.5 min at 601 cGy. The latency values reported here are consistent with Davis' report (for example, 44 min latency at 75 cGy, an average 16 min latency for 200 plus 400 cGy). The hatched bars attached to the episode 1 laten-

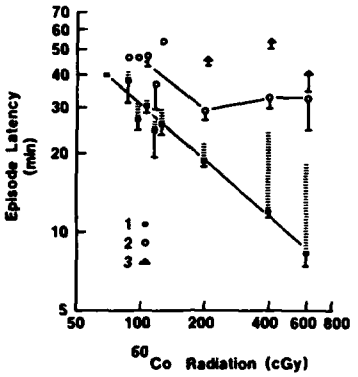

FIG. 4. Mean latencies to first three emetic episodes following ^{60}Co radiation. Hatched bars attached to mean latencies of the first emetic episode represent the mean duration of that episode. Error bars represent standard error of the mean. Solid line through first latencies is computer generated best fit of a straight line; others are drawn by hand.

cies represent the mean duration for that first episode. The duration of episode 1 increases dramatically from 4 min at 98 cGy to 10–12 min at 401 and 601 cGy.

Behavioral Observations

The behavioral and emetic responses of the ferret to low-dose radiation differ from those responses reported for other species. The ferret does not demonstrate the prodromal signs shown by the dog (*28*), e.g., yawning, salivation, licking of the nose, and standing with its head lowered, or the monkey (*11, 29*), e.g., general malaise, yawning, grimacing, and exaggerated oral movements. The ferret does, however, show a lip-licking behavior similar to that of the feline emetic response to β-endorphin (*30*) and also claws at the roof of its mouth. In addition, a very active "burrowing" behavior frequently occurs prior to emesis. The lip-licking, clawing, and burrowing behaviors are somewhat predictive for emesis at lower radiation doses, but no statistical correlation was attempted. All ferrets show a characteristic posture during retching and emesis, regardless of emetic agent. The animals will arch their back, with fore- and hindlegs drawn together, in an inverted "u"-shape.

At the lower doses ($\leq$201 cGy) of radiation, the ferrets tend to vomit toward that area in which they defecate. At higher doses (401–601 cGy), retching may not precede vomiting, vomiting may be projectile, and the animals are less discriminate about their site of vomition. At these higher doses the animals are lethargic between episodes, rather than active, and mucous-filled diarrhea frequently occurs.

Apomorphine-Induced Emesis

For these studies 22 animals were used, 5 of which received apomorphine iv only and 5 sc only. The 12 other animals received both iv and sc injections for comparison between the responses within the same animal. The doses injected were 10, 30, 100, and/or 300 μg/kg. Two animals received a single sc dose of apomorphine (300 μg/

TABLE III

Ferret Emesis/Retching Response to iv or sc Apomorphine

Route	Dose (μg/kg)	No. responding / No. tested	Percentage responding	Mean episode latency (min)
iv	10	0/1	0	—
	30	2/15	13	3.0
	100	6/17	35	4.9
	300	6/15	40	12.2
sc	30	0/15	0	—
	100	7/15	47	6.9
	300	5/16	31	10.2

kg); all others received two or three different doses. No animal was tested twice at the same dose and all dosing occurred at ≥48-h intervals.

The results from these studies are shown in Table III. No distinction is made between retching and emesis in the table. As seen here, no single dose of apomorphine was 100% effective in producing either emesis or retching, regardless of administration route. Vomiting or retching might occur in response to a single dose administered via one route but not the other. Three animals showed neither emesis nor retching, regardless of administration route.

The 100 μg/kg dose produced the largest percentage response (47%). Individual responses varied markedly, with an animal responding to one dose, yet not to a higher dose. Subcutaneous injection also produced a bell-shaped distribution for the number of episodes per animal (30 μg/kg, 1; 100 μg/kg, 1–7; 300 μg/kg, 1–2), whereas iv injection produced a single episode at all doses. The episodes were of very short duration, ranging from 10 s to 2 min, and the latency to the first episode increased with increasing dose. Although this increased latency is not usually predicted for dose–response behavior, the latency differences were not significantly different. Multiple episodes were seen with 100 and 300 μg/kg sc doses. Emetic and retching responses to apomorphine were also preceded by lip-licking and burrowing behavior.

Behavioral actions suggesting central nervous dopaminergic activation were pronounced in 60% of the animals. These occurred regardless of administration route or presence of an emetic response and also varied across animals and drug doses. These behavioral actions appeared at doses as low as 30 μg/kg. The behaviors included leaping, jumping, twisting, and some aggressive display. Sedation was also observed, exemplified by head-rocking and ptosis, but neither the activation nor the sedation responses appeared dose related.

Domperidone vs Radiation-Induced Emesis

Table IV shows the effect of domperidone on several emetic parameters (described in Table II) following either 201 or 401 cGy radiation and compares these values with those obtained from the NaCl-injected-irradiated control group. After 201 cGy, domperidone significantly reduced only the total time in emetic behavior. Domperi-

TABLE IV

Domperidone (1 mg/kg) Effect on Mean Emetic Responses to 201 and 401 cGy Radiation

	NaCl	*Domperidone*
201 cGy		
Latency to first episode (min)	28.0 ± 4.7*	35.3 ± 3.5
Prodromal period (min)	25.8 ± 6.4	12.2 ± 6.8
Total emetic time (min)	9.0 ± 2.0**	2.6 ± 1.2**
Total expulsions	4.5 ± 1.5*	2.0 ± 1.4
401 cGy		
Latency to first episode (min)	12.8 ± 0.6	12.0 ± 1.1
Prodromal period (min)	56.2 ± 5.8	48.1 ± 6.1
Total emetic time (min)	17.5 ± 3.2	11.3 ± 0.9*
Total expulsions	4.0 ± 2.1	8.0 ± 1.2
n	4	4

* $P < 0.05$; Wilk–Shapiro test for normality.
** $P < 0.05$; pooled variance *t*-test.

done had no beneficial effect on radiation-induced emesis following 401 cGy. Although not shown in the table, the nondrug control groups showed significant differences between two variables. For the nontreated group at 201 cGy, the mean emetic latency was 19.1 ± 1.1 min. For this group at 401 cGy, the mean total number of expulsions was 12.3 ± 2.7 min. (Compare these values with those for the NaCl-injected control group in Table IV.) These latter differences may be a response to the stress of handling or injection or may simply be due to the small sample size in the groups ($n = 4$).

DISCUSSION

The principal finding from these studies is that the ferret, like man, canines, and nonhuman primates, shows an emetic response to relatively low doses of radiation. However, the ferret is unique in that this prodromal response appears at much lower doses than in the other species and also occurs much sooner after radiation. In addition, like man, canine, and feline, the ferret vomits in response to apomorphine, a dopaminergic agonist. The ferret emetic response to apomorphine is quite variable, however, and the lack of domperidone antagonism of radiation-induced emesis emphasizes the differences among species.

Radiation-Induced Emesis in the Ferret

The observed threshold and calculated ED_{50} values for radiation-induced emesis in the ferret are similar to the values observed by others. The 69-cGy threshold value reported here is closer to the 75-cGy value reported by C. J. Davis (personal communication) and less than the 100-cGy value reported by J. A. Gylys (personal communication). The 90-cGy ED_{50} value reported by Davis falls within the range of calculated ED_{50} values (77–98 cGy, see Table I) reported here. The 125-cGy ED_{100}

reported by Davis also falls within the range of calculated ED_{90} values herein (113–158 cGy).

The Weibull, probit, and log-probit mathematical models are generally used to describe the dose–response relationship of mortality from hematological depression after radiation (*31*). The emetic data in the ferret described in this report are fit well by all three models, as seen by the similar quantile doses generated by all three (see Table I). The inclusion of retching as an emetic episode within the prodromal period lowers the calculated quantile dose values, yet the quantile doses remain very similar across models. The value obtained from the Weibull distribution was chosen to represent the ED_{50} value because this distribution appears to be the most flexible mathematical model of the three. In addition, the other two models fail to generate reasonable 95% confidence limits (see Table I).

Since the inclusion of retching episodes within the prodromal period lowers the quantile dose values, this suggests that some error can be introduced by their exclusion. For example, some nonhuman primate studies have differentiated between retching and emesis, or excluded retching, because of the problems associated with food that is regurgitated into cheek pouches and later swallowed (*11, 32*). However, ferrets do not store food in cheek pouches. Given this observation, and the fact that retching differs from emesis only in its opposite intrathoracic pressure developed against an open rather than closed glottis (*25*), retching is included as an emetic episode to calculate the ED_{50} (e.g., 77 cGy).

Compared with other species, the observed threshold and calculated ED_{50} values for radiation-induced emesis in the ferret are lower. As reported here, these values are 69 and 77 cGy, respectively. For the canine, the threshold is near 150–170 cGy (*3, 10*) and the ED_{50} is 258 cGy (*3*). For the nonhuman primate these values are, respectively, 400 and 446 cGy (*11*). For man these values are, respectively, 170–180 cGy (*9*) and 230 cGy (*8*).

The latency of radiation-induced emesis in the ferret is also dramatically shorter than that observed in other species. This is emphasized when the emetic latency to a single radiation dose at a fixed dose rate is compared across species. Using the 100 cGy min^{-1} dose rate employed here and a dose of 600 cGy, the following latencies to emesis occur: ferret—8.5 min (see Fig. 3), nonhuman primate—45 min (*33*), and canine—100 min (*27*). The latter two doses were free in air, rather than absorbed. At 45 cGy min^{-1}, with doses ranging from 100 to 600 cGy, man vomits in about 52–63 min (*34*). The duration of the prodromal period, as measured by the occurrence of emesis and/or retching, lasts 1–1.5 h for all species.

Dopaminergic Receptor Activation in Ferret Emesis

The dopaminergic response of the ferret markedly differs from that of other species. Clearly man (*4*) and canine (*5, 6, 27*) vomit in response to low doses of apomorphine. Nonhuman primates require a near-lethal dose to demonstrate emesis (*12, 35*). Felines require much greater doses than do canines and their response is inconsistent (*13, 36*), like that of the ferret.

The variable emetic response to low doses of apomorphine in the ferret, like that reported here, has been reported by others (*21, 19*). In a similar fashion, Andrews and

co-workers (*21*) have found a "bell-shaped" dose–response curve for apomorphine-induced emesis and a longer latency to greater doses than to lower doses. In contrast, however, Andrews finds 100 μg/kg apomorphine (sc) to be 100% emetic. Andrews also finds that 5 mg/kg apomorphine (iv) produces no emesis or retching whereas Floryczk *et al.* (*20*) report this dose (also iv) produces 100% emesis. Such differences may be attributed to strain, although the American laboratory ferret is descended from the English species. Alternatively, the differences could be in response to hormonal or other changes induced by castration or rabies vaccination, neither of which is done in the United Kingdom.

The 5 mg/kg doses of apomorphine (*20*) produced a dopaminergic excitability lasting for up to 4 h, clearly suggesting CNS involvement. The cat also shows this hyperactivity (*28*). That the excitability can also occur following lower doses, as reported here, implies a complex action of apomorphine in the ferret. The precise determinants of this action are poorly understood.

Given the variable sensitivity of ferrets to apomorphine, it is not surprising that 1 mg/kg domperidone does not antagonize radiation-induced emesis in this species. The weak antagonism of even higher doses (3–6 mg/kg) against radiation-induced emesis in the ferret (*16, 17*) may result from domperidone's progastrokinetic action (*37*). In man, domperidone is an effective antiemetic for radiation at maintained doses of less than 1 mg/kg (*38–40*). This is also true for the canine at 0.6–1.0 mg/kg (*41, 42*). In the nonhuman primate, however, 1 mg/kg does not alter radiation-induced emesis (*43*). This once again emphasizes the differences among the species and raises the issue of whether the presence of an emetic response to dopaminergic compounds is a reliable predictor of the emetic response to radiation.

The Ferret as an Animal Model for Radiation-Induced Emesis

In summary, the ferret emetic response to radiation differs from that in other species with regard to both its lower threshold and earlier onset. Such sensitivity to radiation can be a valuable tool for investigators. The ferret has only recently been introduced as an animal model to study emesis per se. Thus it remains to be seen which central and peripheral factors contribute to emesis in this species. It is clear that dopaminergic mechanisms have little, if any, role in radiation-induced emesis in the ferret. The degree to which serotonergic mechanisms are involved in radiation-induced emesis (*17*), as they are in cytotoxin-induced emesis, is poorly understood (*44–47*). The role of the peripheral nervous system in radiation-induced emesis in the ferret has been partially described by Andrews and others (*16, 17*), who have found vagotomy to delay the first emetic episode to 600 cGy radiation. Whether area postrema lesions alter this emetic response is unknown.

ACKNOWLEDGMENTS

I thank R. Jackson and J. Sauber of the Veterinary Medicine Department for their expert assistance in the surgical protocols, W. Jackson for his assistance with the statistical analyses, and V. Kieffer for his excellent technical assistance for the entire project. Views presented in this paper are those of the author; no endorsement by the Defense Nuclear Agency has been given or should be inferred. All research was conducted according to the principles enunciated in the "Guide for the Care and Use of Laboratory Animals" prepared by the Institute of Laboratory Animal Resources, National Research Council.

RECEIVED: August 31, 1987; REVISED: December 15, 1987

REFERENCES

1. R. W. YOUNG, Acute radiation syndrome. In *Military Radiobiology* (J. J. Conklin and R. I. Walker, Eds.), pp. 165–190. Academic Press, New York, 1986.
2. J. H. BARNES, The physiology and pharmacology of emesis. *Mol. Aspects Med.* **7**, 399–508 (1984).
3. J. L. MATTSSON, R. E. CORDTS, M. G. YOCHMOWITZ, and K. A. HARDY, Prevention of radiation emesis in dogs by combination of drugs. *Int. J. Radiat. Oncol. Biol. Phys.* **10**, 1067–1072 (1984).
4. J. D. PROCTOR, C. N. ATHANASSIOS, E. F. EVANS, and A. J. WASSERMAN, An apomorphine-induced vomiting model for anti-emetic studies in man. *J. Clin. Pharmacol.* **18**, 95–99 (1978).
5. D. O. CARPENTER, D. B. BRIGGS, and N. L. STROMINGER, Peptide-induced emesis in dogs. *Behav. Brain Res.* **11**, 277–281 (1984).
6. I. M. LANG, S. K. SARNA, and R. E. CONDON, Gastrointestinal motor correlates of vomiting in the dog: Quantification and characterization as an independent phenomenon. *Gastroenterology* **90**, 40–47 (1986).
7. C. C. LUSHBAUGH, F. COMAS, E. L. SANGER, M. JACOBS, R. HOFSTRA, and G. A. ANDREWS, Radiosensitivity of man by extrapolation from studies of total-body irradiation patients. *Radiat. Res.* **27**, 487–488 (1966).
8. C. C. LUSHBAUGH, Reflections on some recent progress in human radiobiology. *Adv. Radiat. Biol.* **3**, 277–315 (1980).
9. C. C. LUSHBAUGH, Human radiation tolerance. In *Space Radiation Biology and Related Topics* (C. A. Tobias and P. Todd, Eds.), pp. 475–522. Academic Press, New York, 1974.
10. J. R. COOPER and J. L. MATTSON, Control of radiation-induced emesis with promethazine, cimetidine, thiethylperazine, or naloxone. *Am. J. Vet. Res.* **40**, 1057–1061 (1979).
11. J. L. MATTSSON and M. G. YOCHMOWITZ, Radiation-induced emesis in monkeys. *Radiat. Res.* **82**, 191–199 (1980).
12. D. C. BROWNE and R. SPARKS, Vomiting mechanisms: A clinical study of thiethylperazine. *South. Med. J.* **54**, 953–961 (1961).
13. S. C. WANG, Emetic and antiemetic drugs. In *Physiological Pharmacology*, Vol. 2, pp. 255–328. Academic Press, New York, 1965.
14. H. L. BORISON, Site of emetic action of x-irradiation in the cat. *J. Comp. Neurol.* **197**, 439–453 (1957).
15. H. L. BORISON, L. E. MCCARTHY, E. B. DOUPLE, J. JOHNSON, and R. BORISON, Acute radiation-induced vomiting in area postrema-ablated cats. *Radiat. Res.* **109**, 430–439 (1987).
16. J. A. GYLYS and J. S. GIDDA, Radiation-induced emesis in ferrets: An experimental model of emesis. *Gastroenterology* **90**, 1446 (1986).
17. J. A. GYLYS, R. N. WRIGHT, W. D. NICOLOSIA, J. P. BUYNISKI, and R. R. CRENSHAW, BMY 25801, an anti-emetic agent free of D_2 dopamine receptor antagonist properties. *J. Pharmacol. Exp. Ther.*, in press, **244**, 830–837 (1988).
18. P. L. R. ANDREWS, C. J. DAVIS, and J. HAWTHORN, Abdominal vagotomy modifies the emetic response to radiation in the ferret. *J. Physiol. (London)* **378**, 16P (1986). [Abstract]
19. P. L. R. ANDREWS, J. HAWTHORN, and G. J. SANGER, The effect of abdominal visceral nerve lesions and a novel 5HT-M receptor antagonist on cytotoxic and radiation induced emesis in the ferret. *J. Physiol. (London)* **386**, 47P (1986). [Abstract]
20. A. P. FLORCZYK, J. E. SCHURIG, and W. T. BRADNER, Cisplatin-induced emesis in the ferret: A new animal model. *Cancer Treat. Rep.* **66**, 187–189 (1982).
21. P. L. R. ANDREWS, C. J. DAVIS, D. G. GRAHAME-SMITH, and L. B. MASKELL, Apomorphine-induced vomiting in the ferret; anomalies of response to dose and route of administration. *Br. J. Pharmacol. Proc. Suppl.* **89**, 860P (1986). [Abstract]
22. G. L. KING, Radiation- and drug-induced emesis in the ferret. *Soc. Neurosci. Abstr.* **13**, 997 (1987). [Abstract]
23. Task Group 21 of AAPM, A protocol for the determination of absorbed dose from high energy photon and electron beams. *Med. Phys.* **10**, 741–771 (1983).
24. J. L. CURL and J. S. CURL, Restraint device for serial blood sampling of ferrets. *Lab Anim. Sci.* **35**, 296–297 (1985).
25. A. P. FLORCZYK and J. E. SCHURIG, A technique for chronic jugular catheterization in the ferret. *Pharmacol. Biochem. Behav.* **14**, 255–257 (1981).

26. L. E. McCarthy and H. L. Borison, Respiratory mechanics of vomiting in decerebrate cats. *Am. J. Physiol.* **226**, 738–743 (1974).
27. R. K. Harding, H. Hugenholtz, M. Keaney, and J. Kucharczyk, Discrete lesions of the area postrema abolish radiation-induced emesis in the dog. *Neurosci. Lett.* **53**, 95–100 (1985).
28. H. L. Borison and S. C. Wang, Physiology and pharmacology of vomiting. *Pharmacol. Rev.* **5**, 193–230 (1953).
29. E. Eldred and W. V. Trowbridge, Radiation sickness in the monkey. *Radiology* **62**, 65–73 (1954).
30. D. H. Catlin, R. George, and C. Hao, β-endorphin: Pharmacologic and behavioral activity in cats after low intravenous doses. *Life Sci.* **23**, 2147–2154 (1978).
31. M. D. Morris and T. D. Jones, *A Comparison of Dose–Response Models for Death from Hemotological Depression*, pp. 1–12. IACAO DNA 85-903 and DE-AC05-840R21400, 1987.
32. G. R. Middleton and R. W. Young, Emesis in monkeys following exposure to ionizing radiation. *Aviat. Space Environ. Med.* **46**, 170–172 (1975).
33. M. G. Yochmowitz, J. L. Mattsson, and V. L. Bewley, *Radiation Emesis Repository (1971–1977): An Analysis.* SAM-TR-78-26, USAF School of Aerospace Medicine, 1978.
34. G. A. Grant, A. B. Cairnie, R. K. Harding, N. T. Gridgeman, and W. D. Rider, A predictive study of the incidence of vomiting in irradiated military personnel. Rep. No. 817, Defence Research Establishment, Ottawa, 1979.
35. K. R. Brizzee, L. M. Neal, and P. M. Williams, The chemoreceptor trigger zone for emesis in the monkey. *Am. J. Physiol.* **180**, 659–662 (1955).
36. D. Bieger, A. Weerasuriya, and C. H. Hockman, The emetic action of L-DOPA and its effect on the swallowing reflex in the cat. *J. Neural Trans.* **42**, 87–98 (1978).
37. J. Brugmans, Domperidone (R 33,812): An appraisal of the literature. In *Treatment of Cancer Chemotherapy-Induced Nausea and Vomiting* (D. S. Poster, J. S. Penta, and S. Bruno, Eds.) pp. 174–194. Masson, New York, 1984.
38. J. Bernier and J. Huy, Domperidone in the symptomatic treatment of radiotherapy-induced nausea and vomiting. *Postgrad. Med. J.* **55**, 50–54 (1979).
39. M. Endoh, Clinical evaluation of domperidone in nausea and epigastric discomfort following radiation. *Igaku to Yakugaka* **9**, 984–990 (1983).
40. A. Reyntjens, Domperidone as an anti-emetic; summary of research reports. *Postgrad. Med. J. Suppl.* **55**, 50–54 (1979).
41. A. Dubois, J. P. Jacobus, M. P. Grissom, R. R. Engs, and J. J. Conklin, Altered gastric emptying and prevention of radiation-induced vomiting in dogs. *Gastroenterology* **86**, 444–448 (1984).
42. D. O. Carpenter, D. B. Briggs, A. P. Knox, and N. L. Strominger, Radiation-induced emesis in the dog: Effects of lesions and drugs. *Radiat. Res.* **108**, 307–316 (1986).
43. E. Danquechin Dorval, G. P. Mueller, R. R. Engs, A. Durakovic, J. J. Conklin, and A. Dubois, Effect of ionizing radiation on gastric secretion and gastric motility in monkeys. *Gastroenterology* **89**, 374–380 (1985).
44. B. Costall, A. M. Domeney, R. J. Naylor, and F. D. Tattersall, 5-Hydroxytryptamine m-receptor antagonism to prevent cisplatin-induced emesis. *Neuropharmacology* **25**, 959–961 (1986).
45. W. D. Miner and G. J. Sanger, Inhibition of cisplatin-induced vomiting by selective 5-hydroxytryptamine M-receptor antagonism. *Br. J. Pharmacol.* **88**, 497–499 (1986).
46. B. Costall, A. M. Domeney, S. J. Gunning, R. J. Naylor, F. D. Tattersall, and M. B. Tyers, GR38032F: A potent and novel inhibitor of cisplatin-induced emesis in the ferret. *Br. J. Pharmacol.* **90**, 90p (1987). [Abstract].
47. D. Cunningham, J. Hawthorn, A. Pople, J.-C. Gazet, H. T. Ford, T. Challoner, and R. C. Coombes, Prevention of emesis in patients receiving cytotoxic drugs by GR38032F, a selective 5-HT_3 receptor antagonist. *Lancet* **27**, 1461–1462 (1987).

Toxicology Letters, 43 (1988) 219–233
Elsevier

TXL 02046

Flow cytometry techniques in radiation biology

Kenneth F. McCarthy and Martha L. Hale

Radiation Biochemistry Department, Armed Forces Radiobiology Research Institute, Bethesda, MD (U.S.A.)

(Received 20 February, 1988)
(Revision received 23 May, 1988)
(Accepted 23 June, 1988)

Key words: Radiation; Flow cytometry; Hematopoietic stem cells

SUMMARY

Hematopoietic stem cells (HSC) are present in the marrow at a concentration of approximately 2–3 HSC per 1000 nucleated marrow cells. In the past, only clonogenic assays requiring 8–13 days and ten irradiated recipient rodents were available for assaying HSC. Because of the importance of HSC in the postirradiation syndrome, we have developed a new rapid method based on flow cytometry not only to assay but also to purify and characterize HSC. This new method makes extensive use of monoclonal antibodies conjugated to fluorescent phycobiliproteins through the sulfhydryls of the hinge region of the IgG molecule. An optical bench arrangement with a dye laser and an argon laser was used for dual excitation of the phycobiliprotein-monoclonal antibody conjugates and various cellular and DNA probes. Using 4′,6-diamidino-2-phenylindole dihydrochloride (DAPI) exclusion to identify viable cells, it was possible to follow regeneration of postirradiated rat marrow HSC.

INTRODUCTION

Considerable evidence exists that all blood cells are derived from HSC. These cells are of interest to radiobiologists because they are highly sensitive to low doses of ionizing radiation [1]. In the rodent HSC, as measured by the CFU-S assay, are characterized by a D_0 of 0.8–1.0 Gy. As such, doses greater than 9 Gy effectively

Address for correspondence: Dr. K.F. McCarthy, Department of Radiation Biochemistry, Armed Forces Radiobiology Research Institute, Bethesda, MD 20814-5145, U.S.A.

Abbreviations: HSC, hematopoietic stem cells; DAPI, 4′,6-diamidino-2-phenylindole dihydrochloride; FITC, fluorescein isothiocyanate; PhyB, phycoerythrin B; PhyR, phycoerythrin R; APC, allophycocyanin; MMB, maleimidobutyryl biocytin; TBR, total body irradiation; FDA, fluorescein diacetate; PI, propidium iodide; CFU, colony-forming unit; FACS, fluorescence-activated cell sorting; UV, ultraviolet; NBR, Norway Black Rat; WGA, wheat germ lectin; PMT, photomultiplier tube.

sterilize the HSC compartment. If not rescued by bone marrow grafting, the lethally irradiated individual will eventually die, primarily from bleeding and sepsis, due to the inability to replenish blood cells from HSC. Therefore, it is of importance to understand how radiation damages these HSC in order to prevent this damage or to devise methods by which the damaged HSC may be replaced in the irradiated individual.

The major difficulty in studying directly the interaction of ionizing radiation with the HSC is the scarcity of these cells in the marrow and the lack of a distinguishing feature necessary for their accurate and rapid identification. In the rat, HSC comprise less than 0.3% of the total marrow hematopoietic cells [2,3]. In the past, efforts to isolate the HSC used physical techniques such as density gradient centrifugation in isotonic media, sedimentation velocity, elutriation, electrophoresis, nylon wood filtration, and plastic adherence. These techniques usually result in purification of less than 10-fold, which is well short of the 300-fold-plus

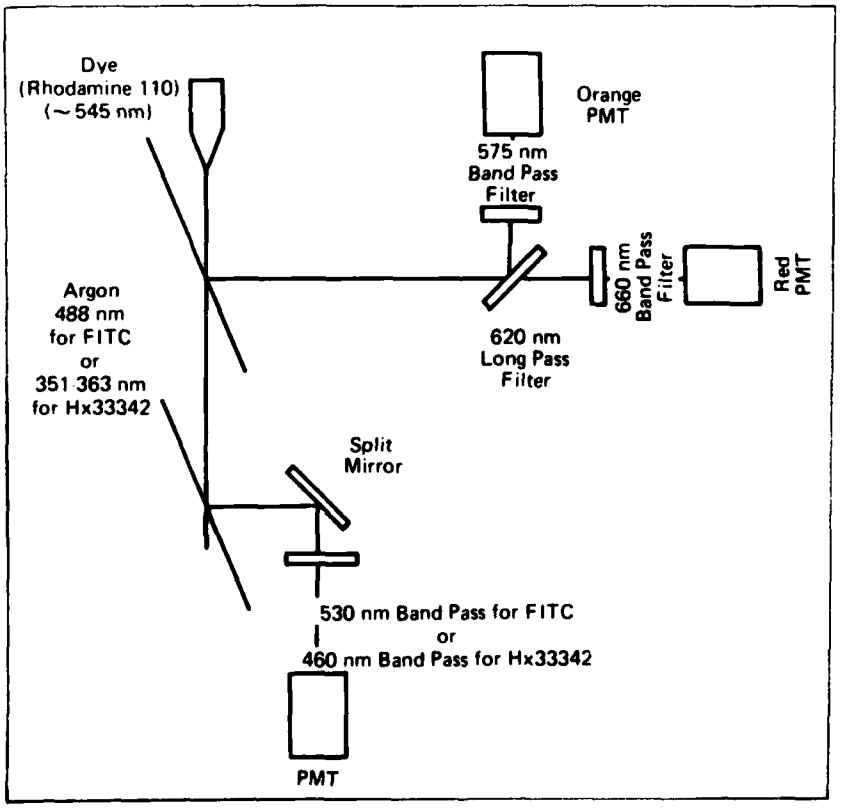

Fig. 1. Optical bench arrangement of 4-parameter light-activated cell sorter.

purification necessary to generate a pure HSC population. For this reason this laboratory and others [4] have made extensive use of the techniques of flow cytometry and/or fluorescence-activated cell sorting (FACS) [5] for the isolation and identification of HSC.

MATERIALS AND METHODS

Flow cytometry and sorting

Flow cytometry measurements and cell sorts were performed on a dual laser Becton Dickinson FACS II cell sorter interfaced to a Consort 40 computer system. The optical bench arrangement of the dual lasers is shown in Fig. 1.

Phycobiliproteins

Studies on the isolation and characterization of HSC have made extensive use of a new class of fluorescent proteins referred to as phycobiliproteins [6]. These fluorescent proteins are isolated from cyanobacteria (blue-green algae) and red algae. They show maximum absorbance in the 470–650 nm region, and fluorescence emission bands begin in the orange (550 nm) and extend into the far red. The molar fluorescence intensity of phycoerythrins is up to 20 times that of fluorescein isothiocyanate (FITC). Several different proteins are included in the phycobiliprotein family. We have used primarily phycoerythrin B (PhyB) and allophycocyanin (APC). The excitation and emission spectra of these two phycobiliproteins are shown in Fig. 2.

Lasers and optical bench arrangement

Because both phycoerythrin R (PhyR) and FITC have an absorbance maximum between 490 and 496 nm but emit at different wavelengths (in green and orange, respectively), most dual parameter immunofluorescence work is performed using the strong 488.0 nm spectral line of the argon laser to excite both PhyR- and FITC-conjugated monoclonal antibodies bound to cell surface determinants. However, we have chosen to label two different monoclonals with two different phycobiliproteins rather than one phycobiliprotein and FITC [3]. We have found that excitation for both APC and PhyB can be performed effectively with the krypton laser tuned to the 530.9 nm spectral line, by an argon laser tuned to the 528.7 nm spectral line, or by a dye laser (rhodamine 110) tuned to approximately 545 nm. Further, we have shown that APC can also be excited with the 488.0 argon laser spectral line, allowing 3-parameter immunofluorescence studies (APC, PhyB, and FITC) to be performed with a single laser. However, it was determined that the best results are obtained when the dye laser is used as the primary laser and the argon laser (tuned to the 488

nm or UV spectral lines) is used as the delayed or secondary laser. This optical bench arrangement allowed us to not only identify the HSC with the dye laser but also to analyze and characterize the HSC with the argon laser.

Conjugation of monoclonal antibodies to phycobiliproteins

It was found previously [2] that incubation of marrow cells with the monoclonal antibody Ox7 restricted the generation of splenic hematopoietic colonies (see section HSC assays), presumably due to initiation of in vivo cellular cytotoxic events by the Fc region of the bound IgG molecule. This problem can be avoided by digesting the

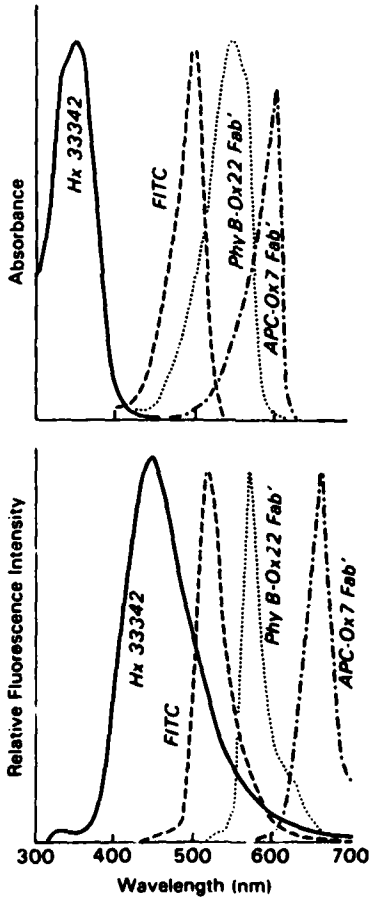

Fig. 2. Excitation and emission spectra of several compounds. Hx33342 is a DNA-specific dye used to generate cell cycle DNA histograms. Absorption and emission fluorescence spectra were determined on a model SLM-8000 fluorescence spectrophotometer. Spectra are normalized at peak amplitude and are uncorrected

monoclonal antibody with pepsin, which produces the $F(ab')_2$ fragment. The $F(ab')_2$ fragment is then reduced with Cleland's reagent, and the Fab' with its free sulfhydryl is linked through a thioether bond to the maleimide-phycobiliprotein conjugate. Although time consuming, this technique has proven to be a reliable method of conjugating monoclonal IgG to phycobiliproteins. The following monoclonal antibodies have all been conjugated to either PhyR, PhyB, or APC using this technique: W3/13, Ox22, Ox7, W3/25, Ox19, Ox8, and My10 [2,3]. These conjugates generate a more intense signal than can be achieved using the sandwich technique, which uses FITC-antimouse IgG antibody as the second antibody. There are other benefits of this technique. The Fab'-phycobiliprotein conjugates have a long shelf life (greater than a year) when stored at 4°C in 0.01% sodium azide. There is an absence of binding to Fc receptors, they are stable when shipped through the mail, and it is easy to perform 3-parameter immunofluorescence studies by using FITC-antimouse IgG Fc-specific antibody as the second reagent in the sandwich technique [7].

A variation of the conjugation technique described above is as follows. Maleimidobutyryl biocytin (MMB) is substituted for the maleimidephycobiliprotein, the result being biotinylation of the free Fab' sulfhydryl group. Following incubation of cells with the biotinylated Fab' antibody, avidin conjugated to either FITC or phycobiliprotein is added [3]. Unfortunately, this technique does not work with all monoclonal antibodies. For example, it works well with Ox8 but not with W3/13 or Ox22.

Animals

Lewis rats (male, 6–8 weeks old) were obtained from Charles River Labs (Kingston, NY) and were quarantined on arrival and screened for evidence of disease before being released from quarantine. They were maintained in an AAALAC-accredited facility in plastic Micro-isolator cages on hardwood chip contact bedding and were provided with commercial rodent chow and acidified tap water ad libitum. The rats were on a 12 h light/dark full spectrum with no twilight. Total body irradiation (TBR) was delivered with an opposing ^{60}Co radiation source as described previously [3]. Rats were killed by exsanguination while under methoxyfurane inhalation anesthesia. Irradiated rats were given 1 mg/ml tetracycline in their drinking water. Rats were cared for according to principles enunciated in the Guide for the Care and Use of Laboratory Animals Resources, National Research Council.

HSC assays

Three different HSC assays were used to measure the degree of HSC purification. They were the CFU-S assay [2], the 30-day survival of lethally irradiated recipient

rats [3], and the intrathymic injection of histocompatible, T-cell allotype disparate donor stem cells [7]. The CFU-S assay was performed as follows: irradiated rats (9 Gy ^{60}Co TBR, 0.4 Gy/min) were grafted by intravenous injection of bone marrow cellular suspensions or purified HSC. In the rat, approximately 3–10% of the stem cells seed the spleen [2], proliferate, and form discrete colonies of hematopoietic cells. The number of colonies formed is proportional to the number of HSC injected. This clonogenic assay is cumbersome: 11–13 days, and a large number of irradiated recipient animals, are required to perform this assay. The second assay involves grafting of HSC in order to protect lethally irradiated rats from the lethal effects of irradiation. Rats receive a dose of 9.5 Gy ^{60}Co TBR, 0.4 Gy/min. The rats are then grafted with either normal marrow or purified HSC. The ratio number of normal marrow cells or purified HSC required to rescue the lethally irradiated rat is used to calculate the degree of purification of HSC. This assay is generally considered to be a more accurate assay for HSC than the CFU-S assay, which appears to measure committed as well as multipotent HSC [8]. The third assay used was the direct injection of either normal or purified Lewis rat HSC into the thymus of sublethally irradiated (8 Gy ^{60}Co TBR, 0.4 Gy/min) Norway Black Rat (NBR)

TABLE I

MONOCLONAL ANTIBODIES RECOGNIZING DETERMINANTS ON RAT LYMPHOCYTES

Monoclonal antibody[a]	Antigenic determinant recognized	Cell population recognized
Ox2	Glycoprotein on thymocyte membrane	B-cells, neuronal endothelial cells, thymocytes, dendritic cells
Ox3	Polymorphic determinant on rat 1a	B-cells, some epithelial cells, dendritic cells
Ox4	Polymorphic determinant on rat 1a	B-cells, 20% of thymocytes
Ox6	Monomorphic determinant on rat 1a	B-cells, 20% of thymocytes
Ox7	Rat Thy-1.1 antigen	Thymocytes, stem cells, neuronal cells, immature B-cells
Ox8	Glycoprotein determinant on thymocyte membranes	Cytotoxic, suppressor T-cells, NK, thymocytes
Ox12	Rat kappa chains	B-cells
Ox17	α-Chain rat 1a-antigen	B-cells
Ox18	Monomorphic determinant rat class I MHC	Class I MHC (RT-1A)
Ox19	Glycoprotein on thymocytes	Thymocytes, peripheral T-cells
Ox22	High molecular weight form of leukocyte common antigen	B-cell, some T-cells
W3/13	Sialoglycoprotein of rat thymocytes	Thymocytes, peripheral T-cells, granulocytes
W3/25	Glycoprotein on helper T-cells	Helper T-cells, thymocytes

[a]Mason et al. [17].

recipient rats [9]. After an extended incubation period, the HSC proliferate and differentiate into thymocytes. The number of newly generated thymocytes is measured by the use of the allogeneic system designated as RT 7. Lewis rats express the RT 7.1 antigen on thymocytes while the histocompatible NBR rats express the RT 7.2 antigen. Using the monoclonal antibodies BC-84 and 8G6.1, which recognize RT 7.1 and RT 7.2, respectively, the number of donor thymocytes (from Lewis marrow cells) that appear 18 days postinjection is a linear function of the number of cells injected. This assay establishes the origin of the newly formed thymocytes. Further, the thymus is an avascular organ and this minimizes the escape of the injected HSC into the circulation. The main advantage of this assay is its sensitivity, as it is 50 times more sensitive than the CFU-S assay [10].

Cell preparation and staining

Rat marrow cells were prepared as described previously [3]. Staining with fluorescein diacetate (FDA) was performed according to the Hale and McCarthy method [11]. Cells were tagged with FITC-wheat germ lectin (FITC-WGA) according to the method of Visser et al. [12]. DAPI (1 mg/ml in distilled water) and propidium iodide (PI) (1 mg/ml in ethanol) were added to a cell suspension at a final concentration of 10 μg/ml and 20 μg/ml, respectively.

RESULTS

HSC characterization and isolation

The ideal solution to measuring the concentration of marrow HSC is to develop a monoclonal antibody to a membrane antigenic determinant expressed only on the HSC and no other marrow cell. Conjugation of this antibody with the appropriate fluorochrome would then allow fluorochrome-tagged HSC to be identified and separated from the remainder of the marrow by cell sorting. Unfortunately, no such unique HSC antigen has been identified to date. In order to isolate the HSC, it was necessary to label marrow hematopoietic cells with a 'cocktail' of fluorochrome-conjugated monoclonal antibodies and/or lectins and to identify the HSC by pattern recognition. A partial list of monoclonals used and their specificities is presented in Table I.

The combination of conjugated antibodies that proved to be optimum for HSC identification was APC-Ox7 Fab', PhyB-Ox22 Fab', and FITC-W3/13 IgG. A correlated dual parameter plot of marrow cells tagged with the above-mentioned antibodies and excited with a dye laser (rhodamine 110) tuned to 545 nm is shown in Fig. 3. The HSC was found exclusively in the Ox7 upper 20% positive, Ox22 negative window [3,7]. The purification of HSC as measured by the CFU-S assay, survival following lethal irradiation, and intrathymic injection are presented in

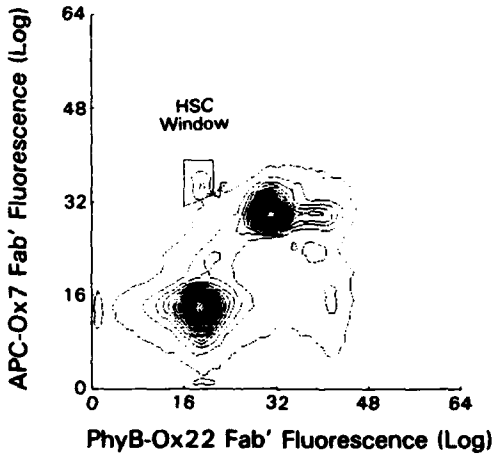

Fig. 3. Contour plot of rat marrow cells labeled with PhyB-Ox22 Fab' and APC-Ox7 Fab'. HSC were found only within the Ox7 upper 20% positive, Ox22 negative window and cells within this window accounted for 0.265% of the total marrow cell population.

Table II. There is a discrepancy between the CFU-S assay and the other two assays for measuring HSC purification. We believe this is due in part to an obligatory step of HSC lodgement in bone marrow before it can express itself in the spleen as a CFU-S assay [13]. Further, a more complex, dual laser, 3-parameter immunofluorescence study using a second argon laser tuned to 488 nm and FITC-W3/13 as the third antibody showed that the Ox7 upper 20% positive, Ox22 negative cells to be primarily W3/13 dim (80–90%) and the remainder W3/13 positive (data not shown).

Using the sandwich technique [7], it was possible to further characterize the HSC as being Ox8, W3/25, Ox6 and Ox17 negative; possibly Ox19 dim; and Ox18 very bright. The specificities of these monoclonal antibodies are given in Table I. The optical bench arrangement shown in Fig. 1 can also be used to characterize HSC with respect to lectin receptor sites and various intracellular enzyme systems. For example, the rat HSC binds FITC-WGA and is apparently characterized by a high cytoplasmic concentration of nonspecific esterases as measured by FDA uptake as shown in Figs. 4 and 5.

TABLE II

ASSAYS FOR ANALYZING PURIFICATION OF STEM CELL POPULATIONS

Route of injection	Assay system	Stem cell purification
i.v.	CFU-S	100
i.v.	Irradiated recipient survival	350
i.t.	Intrathymic adoptive transfer	282

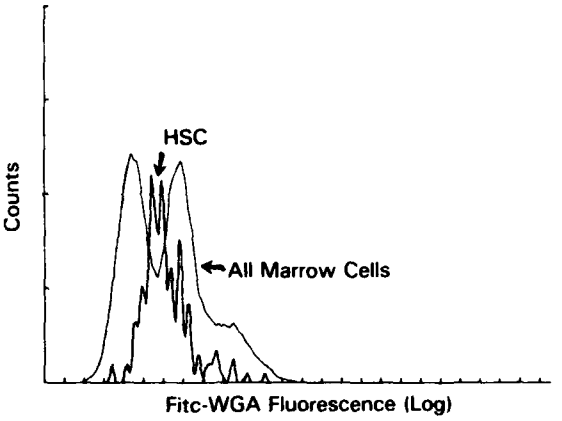

Fig. 4. Relative fluorescence distribution of marrow cells and HSC incubated with FITC-wheat germ agglutinin.

Comparison of dose survival curves generated by the CFU-S and FACS assays

HSC were assayed in irradiated rats by both the CFU-S and FACS procedures. These two assay systems generated different results as shown in Fig. 6 and reported previously [14]. One of several possible explanations for this discrepancy might be nonspecific tagging of dead and dying cells with the phycobiliprotein-monoclonal antibody conjugates so that these dead cells are scored as HSC by the FACS procedure, leading to overestimation of the concentration of viable HSC in the marrow

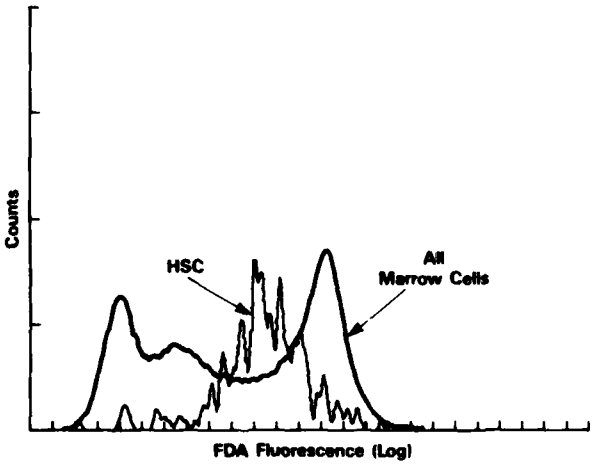

Fig. 5. Relative fluorescence distribution of marrow cells and HSC incubated with FDA.

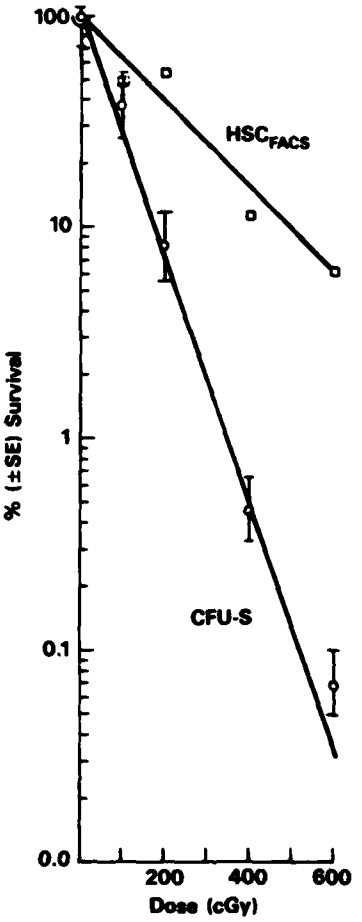

Fig. 6. Radiation dose-response curves for HSC as measured by FACS and CFU-S assays.

of postirradiated rats. Therefore, a new technique was devised for determining and enumerating viable marrow cells, including HSC, in the immediate postirradiated marrow.

DAPI staining of dead cells

The most commonly used fluorescent probe in flow cytometry for staining and gating out dead cells from immunofluorescence histograms is PI. It is an intercalating DNA dye with an absorbance maximum in the yellow and an emission maximum in the orange-red (for a more comprehensive discussion of DNA stains, see [15]). Dead cells are labeled with PI by including it in the last cell wash at a concentration of 20 μg/ml. Live cells exclude the PI while dead cells take up the stain. The

result is an intensive orange-red nuclear fluorescence emanating from the dead cells. Although the fluorescence of PI overlaps that of PhyB and PhyR, PI can be used to gate out dead cells in 2- and 3-parameter immunofluorescence studies. The orange-red fluorescence of the PI-stained dead cells is an order of magnitude brighter than the immunofluorescence from the PhyB- or PhyR-antibody-tagged viable cells and does not interfere with or alter the immunofluorescence histograms of viable cells. However, the immunofluorescence histograms of dead and dying cells cannot be determined in the presence of PI, for the PI fluorescence cannot be separated from the PhyB or the PhyR fluorescence. In order to determine the phenotype of dead cells it was necessary to use a fluorescent probe whose emission spectrum did not overlap that of FITC, Phy, or APC. Such a fluorescent probe is DAPI.

DAPI is a nonintercalating DNA-specific stain with an absorption maximum in the UV and an emission maximum in the blue [15]. Like Hx33342, DAPI can be excited with the argon laser tuned to the UV and the resulting fluorescence can be detected using the 460 nm PMT (Fig. 1). In order to demonstrate that DAPI stains only dead cells, 20 μg PI and 10 μg DAPI were added to a 1 ml solution of 5×10^6 rat marrow cells. The cells were allowed to incubate for 30 min at 4°C and then analyzed on the FACS. The PI-stained cells were excited with the dye laser and their fluorescence measured with the orange PMT, while DAPI-stained cells were excited with the UV laser and their fluorescence recorded on the violet-blue PMT. The correlated PI and DAPI fluorescences are plotted in Fig. 7. Clearly, marrow cells that stain with PI (i.e., dead cells) also stain with DAPI. Viable cells that do not stain with PI also exclude DAPI. Therefore, substituting DAPI for PI as a cell viability stain allows not only dead cells to be gated 'out' of 2-parameter im-

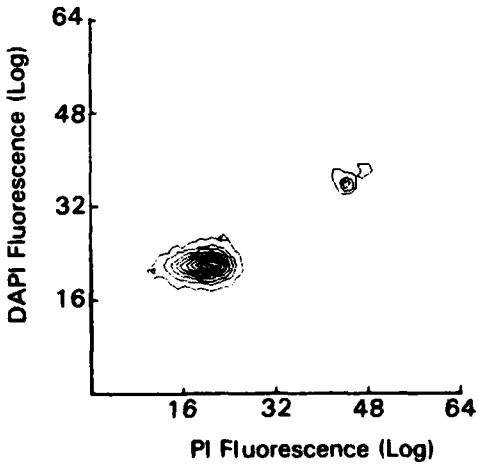

Fig. 7. Contour plot of rat marrow cells labeled with PI and DAPI.

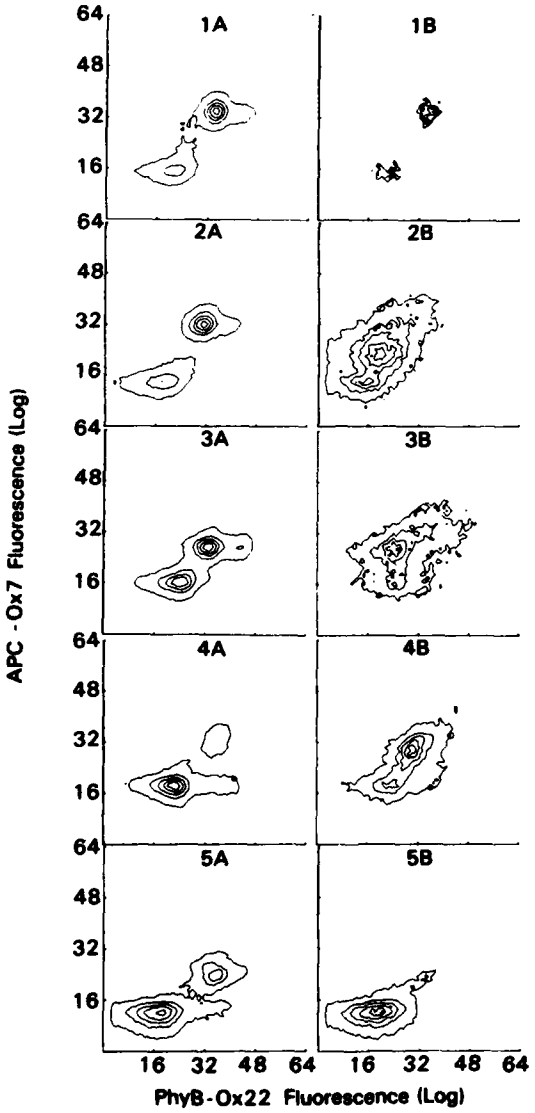

Fig. 8. Contour plots of viable (*A*) and dead (*B*) cells labeled with APC-Ox7 Fab', PhyB-Ox22 Fab', and DAPI. DAPI fluorescence was determined with the delayed or second laser and is not shown. Viable cells are DAPI negative while dead cells are DAPI positive. Time sequence from top to bottom is as follows: (1) normal marrow, (2) 3 h postirradiation, (3) 1 day postirradiation, (4) 3 days postirradiation, and (5) 5 days postirradiation. Contour maps were drawn as a percent of peak amplitude at increments of 5%, 25%, 45%, 65%, and 85%. Radiation was 2 Gy TBR ^{60}Co at a dose rate of 0.04 Gy/min.

munofluorescence work but also makes it possible to gate 'on' dead cells for the analysis of both the rate and phenotype of dying cells in the postirradiated rat marrow. Such a study is shown in Fig. 8, where the phenotypes of viable and dead cells are presented as a function of time postirradiation. The first cells to die immediately postirradiation appear to be blast cells and erythrocytic precursors, followed by lymphocytes at 1–3 days postirradiation and granulocytes at 4–5 days postirradiation. Further information on the dead cell fraction in the total marrow population and the dead cell fraction within the Ox7 upper 20% positive, Ox22 negative window or HSC window is given in Table III.

DISCUSSION

New techniques were developed for the identification of rat HSC in normal marrow by flow cytometry using a modified FACS-II instrument. When these techniques were used to monitor the concentration and regeneration of HSC in the postirradiated rat, discrepancies between the CFU-S assay and the FACS assay for determining the relative size of the postirradation HSC compartment became obvious. The results presented in the present study indicate that part of the difference

TABLE III

PERCENT DEAD CELLS INCLUDING HSC IN POSTIRRADIATED RAT MARROW

Experiment		Total cells/ femur × 10^{-7}	% Total cells $DAPI^+$	$HSC/10^5$ cells	% HSC $DAPI^+$	Corrected $HSC/10^5$ cells	HSC/femur
Control[a]							
	1	3.20	0.8	307	2.0	301	96 320
	2	4.80	0.5	408	0.2	407	195 360
Irradiated[b]							
3 h	1	2.30	23.3	1 071	63.4	392	90 409
	2	1.75	24.6	1 104	67.8	355	62 210
6 h	2	1.30	26.9	347	24.2	263	34 193
	2	1.10	23.9	416	23.8	317	34 869
24 h	1	0.80	4.7	463	14.7	395	31 595
	2	0.55	11.7	277	22.0	216	11 883
30 h	1	0.55	12.8	252	7.9	232	12 765
	2	0.32	17.6	250	16.0	210	6 720
3 days	1	2.70	19.3	78	2.6	75	20 512
	2	2.47	–	–	–	–	–
5 days	1	2.95	17.6	117	17.9	96	28 336
	2	2.40	31.2	122	45.1	67	16 074

[a]Each experiment consisted of two rats.

[b]Experiment performed on rats receiving 2 Gy ^{60}Co TBR, dose rate 0.4 Gy/min.

between these two assays can be explained by the presence of dead and dying cells in the Ox7 upper 20% positive, Ox22 negative window or the HSC window. If these cells are either dead HSC or nonspecifically phycobiliprotein-antibody-tagged dead cells, then the number of surviving HSC as determined by the FACS assay would be overestimated. However, the total difference between the phenotypic FACS assay and the clonogenic CFU-S assay cannot be fully accounted for by the presence of dead and dying cells in the HSC window. It is conceivable that the difference that remains between the two assays after subtracting out these dead and dying cells from the total number of cells found within the HSC window represents damaged irradiated HSC that do not express themselves in the CFU-S assay [14].

The present optical bench arrangement and computer support limit us to 4-parameter cellular measurements, which are a forward light scatter measurement, two immunofluorescence measurements, and a DAPI-DNA fluorescence measurement. Therefore, enumeration of dead cells could be undertaken only in the Ox7 upper 20% positive, Ox22 negative window and not in the Ox7 upper 20% positive, Ox22 negative, W3/13 dim window. There is the possibility, although slight, that in a 3-parameter immunofluorescence analysis of the postirradiated HSC compartment, dead cells would not appear in the Ox7 upper 20% positive, Ox22 negative, W3/13 dim window. To perform this experiment, a 5-parameter flow cytometer would be needed.

The above limitations notwithstanding, the present FACS assay of postirradiation rat marrow indicates that at least 30 h is required for removal of dead and dying HSC from the marrow. At this time the initial regeneration of the HSC compartment can be observed by both the FACS (Table III) and the CFU-S assays [16]. HSC renewal, therefore, begins while there is still extensive cell death occurring in the marrow lymphocyte and granulocyte compartments. What influence this continued hematopoietic cell death has on the stromal tissues that support hematopoiesis and on regenerating HSC is an important question to be addressed if we wish to improve therapies for rapid recovery of the postirradiated marrow.

ACKNOWLEDGEMENTS

This research was supported by the Armed Forces Radiobiology Research Institute, Defense Nuclear Agency, under Research Work Unit B3012. Views presented in this paper are those of the authors; no endorsement by the Defense Nuclear Agency has been given or should be inferred. Research was conducted according to the principles enunciated in the 'Guide for Care and Use of Laboratory Animals' prepared by the Institute of Laboratory Animal Resources, National Research Council.

REFERENCES

1 Till, J.E. and McCulloch, E.A. (1961) A direct measurement of the radiation sensitivity of normal mouse bone marrow cells. Radiat. Res. 14, 213–222.

2 McCarthy, K.F., Hale, M.L. and Fehnel, P.L. (1985) Rat colony-forming units is Ox7 positive, W3/13 positive, Ox1 positive, and Ox22 negative. Exp. Hematol. 13, 847–854.

3 McCarthy, K.F., Hale, M.L. and Fehnel, P.L. (1987) Purification and analysis of rat hematopoietic stem cells by flow cytometry. Cytometry 8, 296–305.

4 Van der Engh, G. and Visser, J. (1984) Flow cytometry in experimental hematology. In: S.J. Baum (Ed.), Current Methodology in Experimental Hematology, Karger, New York, pp. 42–62.

5 Herzenberg, L.A., Sweet, R.G. and Herzenberg, L.A. (1976) Fluorescence-activated cell sorting. Sci. Am. 234, 108–117.

6 Glazer, A.N. and Stryer, M.P. (1984) Phycofluor probes. Trends Biochem. Sci. 9, 423–427.

7 Hale, M.L., Griener, D.L. and McCarthy, K.F. (1987) Characterization of rat prothymocyte with monoclonal antibodies recognizing rat lymphocyte membrane antigenic determinants. Cell. Immunol. 107, 188–200.

8 Magli, M.C., Iscove, N.N. and Odartchenko, N. (1982) Transient nature of early hematopoietic spleen colonies. Nature 295, 527–529.

9 Griener, D.L., Goldschneider, I. and Lubaroff, D.M. (1984) Identification of thymocyte progenitors in the hematopoietic tissues of the rat. I. A quantitative assay system for thymocyte regeneration. Thymus 6, 181–199.

10 Goldschneider, I., Komschlies, K.L. and Greiner, D.L. (1986) Studies of thymocytopoiesis in rats and mice. I. Kinetics of appearance of thymocytes using a direct intrathymic adoptive transfer assay for thymocyte precursors. J. Exp. Med. 163, 1–17.

11 Hale, M.L. and McCarthy, K.F. (1984) Effect of sublethal ionizing radiation on rat Peyer's patch lymphocytes. Radiat. Res. 99, 151–164.

12 Visser, J.W., Bauman, J.G.J., Mulder, A.H., Eliason, J.F. and De Leeuw, A.M. (1984) Isolation of murine pluripotent hematopoietic stem cells. J. Exp. Med. 59, 1576–1590.

13 Van Zant, G. (1984) Studies of hematopoietic stem cells spared by 5-fluorouracil. J. Exp. Med. 159, 679–690.

14 McCarthy, K.F. and Hale, M.L. (1988) Measurement of the radiosensitivity of rat marrow by flow cytometry. Pharm. Ther. (in press).

15 Shapiro, H.M. (1985) Practical Flow Cytometry, Alan R. Liss, New York, pp. 84–154.

16 McCarthy, K.F. and Hale, M.L. (1988) Flow cytometry techniques for the study of irradiated hematopoietic stem cells. In: D. McCormack, C.E. Swenberg and H. Bucker (Eds.), Terrestrial Space Radiation and Its Biological Effects, Plenum Publishing Corp, New York (in press).

17 Mason, D.W., Arthur, R.P., Dallman, M.J., Green, J.R., Spickett, G.P. and Thomas, M.L. (1983) Functions of rat T-lymphocyte subsets isolated by means of monoclonal antibodies. Immunol. Rev. 74, 57–82.

Pharmacology Biochemistry & Behavior, Vol. 30, pp. 1007–1014. Pergamon Press plc, 1988. Printed in the U.S.A. 0091-3057/88 $3.00 + .00

Effects of Sublethal Doses of Ionizing Radiation on Schedule-Controlled Performance in Rats[1]

PAUL C. MELE, CAROL G. FRANZ AND JOHN R. HARRISON

Behavioral Sciences Department, Armed Forces Radiobiology Research Institute, Bethesda, MD 20814-5145

Received 9 July 1987

MELE, P. C., C. G. FRANZ AND J. R. HARRISON. *Effects of sublethal doses of ionizing radiation on schedule-controlled performance in rats.* PHARMACOL BIOCHEM BEHAV 30(4) 1007–1014, 1988.—Male rats responded under a fixed-ratio (FR) 50 or a fixed-interval (FI) 120 sec schedule of milk delivery. Separate groups were acutely exposed to 0.5, 1.5, 4.5 or 0 (FI only) Gray (Gy) of cobalt-60 gamma radiation 3 times at 43-day intervals. All rats received an acute dose of 6.5 Gy 64 days after the last of these exposures. One-half and 1.5 Gy did not alter FR or FI performance significantly. After 4.5 Gy, no observable changes in performance occurred within 1 hr of exposure. Maximal reductions in FR response rates occurred 24 hr after exposure and recovery followed over the subsequent 72 hr. Postreinforcement pause was increased and running response rate was decreased by 4.5 Gy. Similar effects were found after each 4.5 Gy exposure. In contrast, FI performance (overall response rate, postreinforcement pause, running response rate, index of curvature) was not altered reliably by 4.5 Gy. Both FR and FI response rates were reduced by 6.5 Gy beginning 24 hr after exposure; FR rates tended to be reduced more than FI rates 24–72 hr after exposure. Response rates under both schedules recovered gradually over 7 weeks. The behavioral effects of 6.5 Gy did not vary as a function of irradiation history. In contrast, irradiation history affected survival in that 4/9 rats previously exposed to 4.5 Gy died during weeks 4–5 after 6.5 Gy, whereas there were no deaths in the rats previously exposed to lower doses. Radiogenic disruption of operant performance was dose-related, reversible, noncumulative and dependent on the schedule of reinforcement.

Ionizing radiation Sublethal doses Repeated exposures FR, FI performance

IONIZING radiation became of interest nearly a century ago after Roentgen's discovery of X-rays in 1895 [35]. Since that time, both the beneficial and detrimental effects of ionizing radiation have received much attention. Human exposure to ionizing radiation above background levels has occurred through clinical treatment, the work place environment, industrial accidents, and immediate and delayed effects of nuclear weapon detonations [19]. Recent accidents at the Three Mile Island [1] and Chernobyl [2,21] nuclear power plants point to the current possibility of large-scale population exposure to radiation. The problems posed for manned space travel by ionizing radiation are receiving a growing amount of attention [4, 28, 36].

Exposure to ionizing radiation produces a dose-dependent sequella of signs and symptoms that progresses over time [19,33]. In humans, early effects of relatively low doses of radiation may include weakness, fatigue, nausea, vomiting, anorexia, and headache. These effects have a latency to onset of several hours and may last for hours, days or weeks [40]. As the dose of radiation is increased up to the 30 day LD_{50}, hemopoietic damage (loss of functional blood cells) occurs in most mammals and increases in severity for up to 4–6 weeks after expousre [33]. Further increases in dose produce lethal gastrointestinal damage within 1–2 weeks of exposure, while yet higher, supralethal doses produce cardiovascular shock, neuronal damage and death within hours or days.

Dose- and time-related changes in the behavior of animals following expousre to ionizing radiation have been studied for some time (see [18,25] for reviews). Included among the behaviors studied are locomotor activity [23,29,32], motor performance [5,13], food and water intake [29,31], conditioned taste aversion [34], maze performance [14,16], conditioned avoidance responding [12,20], and responding maintained by schedules of positive or negative reinforcement [7–11, 22, 39]. Typically, ionizing radiation depresses

[1]This work was supported by the Armed Forces Radiobiology Research Institute (AFRRI), Defense Nuclear Agency, under work unit B4158. Views presented in this paper are those of the authors; no endorsement by the Defense Nuclear Agency has been given or should be inferred. Research was conducted according to the principles enunciated in the "Guide for the Care and Use of Laboratory Animals" prepared by the Institute of Laboratory Animal Resources, National Research Council, DHEW Pub. No. (NIH) 85-23, 1985. AFRRI is fully accredited by the American Association for Accreditation of Laboratory Animal Care.

behavioral output with the magnitude and duration of effect being directly related to the dose administered. Behavioral recovery generally occurs after sublethal expousre.

The present study was conducted to more thoroughly evaluate the dose- and time-related effects of acute, sublethal exposure to ionizing radiation on schedule-controlled performance in rats. Fixed-ratio (FR) and fixed-interval (FI) schedules of reinforcement [15] were used here because it is well documented that they provide sensitive behavioral endpoints for detecting and measuring expousre to a wide variety of drugs and toxic agents [24,37]. Several studies have examined the short-term effects of one type of ionizing radiation (X-rays) on FR performance [7–9, 39]; there are no published reports to our knowledge on the effects of ionizing radiation on FI performance. Radiation-induced changes in rates and patterns of responding were evaluated for up to seven weeks after acute exposure in order to more thoroughly describe time-course effects. It was of particular interest to look for temporal relationships between the behavioral and the well documented physiological effects of ionizing radiation mentioned above. Individual animals received multiple exposures to ionizing radiation to determine whether cumulative effects might occur under the conditions used here.

METHOD

Animals

Thirty-five experimentally naive male rats [Crl: (CD(SD)BR] (VAF/Plus) were used. The rats were 90–120 days old at the start of the experiment and were maintained at approximately 80% of their free-feeding body weights. Rats were quarantined on arrival and screened for evidence of disease. They were individually housed in plastic Microisolator cages containing sterilized woodchip bedding; commercial rodent chow and acidified tap water were provided. Animal holding rooms were maintained at 21±1°C with 50±10% relative humidity using at least 10 air changes per hour of 100% conditioned fresh air. A 12-hr lighting cycle was in effect with full-spectrum lights on from 0600–1800.

Apparatus

Six operant conditioning chambers were used (Coulbourn Instruments, Inc.). The front wall of each chamber contained a response lever mounted on a microswitch, a set of three cue lights located above the lever, a house light, a Sonalert speaker and an opening that allowed access to a dipper that presented 0.06 ml of sweetened condensed milk (a 1:1 mixture of Bordens Eagle Brand and tap water). Each chamber was enclosed in a sound- and light-attenuating compartment which also contained an exhaust fan for ventilation and a speaker for the presentation of white masking noise. Control of experimental stations and recording of data were accomplished with a PDP8 computer and cumulative recorders located in an adjoining room.

Behavioral Procedure

Animals were trained to press the lever using an automated procedure that consisted of two schedules of milk delivery being in effect simultaneously. A variable-time (VT) schedule presented the dipper automatically on the average of every 60 sec, while an FR 1 schedule presented the dipper after each leverpress. Presentation of the dipper lasted for 5 sec and was signalled by a light over the dipper and the Sonalert tone; the house light and cue lights were extinguished during dipper presentation. The VT schedule was discontinued after 10 responses had been made within a single daily session. Sessions lasted for 60 min or until 100 responses had been made, whichever occurred first. After an additional one or two sessions under FR 1, 15 rats were exposed to a series of incremental FR schedules over several weeks until the final FR 50 schedule was in effect. The remaining 20 rats were exposed to an incremental series of FI schedules until the final FI 120 sec schedule was in effect. Under FI schedules, reinforcers are delivered for the first response occurring after the interval has elasped; responses occurring prior to the end of the interval have no programmed consequences. Session duration was 30 min for FR and 60 min for FI. Training was conducted until the performance of each rat was stable (no consistent trends in rates and patterns of responding from day to day over three to five consecutive weeks). After responding had stabilized the first radiation phase was begun.

Radiation Procedure

Rats were assigned to radiation dose groups (n=4–5 per group) such that group mean baseline response rates were similar within each reinforcement schedule. Animals from different dose groups were balanced across test chambers and time of day for testing to the extent possible.

Bilateral, whole-body, midline tissue doses of 4.5, 1.5, 0.5 or 0 (FI only) Gy of gamma photon radiation were delivered at a fixed rate of 2.5 Gy/min from a cobalt-60 source. Each rat received its designated dose of radiation three times at 43-day intervals. A final irradiation with 6.5 Gy was given to all rats 64 days after the third exposure. The time intervals between exposures were chosen to allow for (1) testing over at least 30 days after exposure, the conventional time period for expressing radiobiological LD_{50} data (the $LD_{50/30}$ for gamma radiation in the rat is 9.5 Gy [6]), and (2) the collection of sufficient control data prior to the next exposure.

Rats were placed in well ventilated, clear plastic restraining tubes for irradiation. Test sessions began 5 min after exposure ceased. Sham exposures, consisting of placing the animals in the tubes and transporting them to the exposure room, were conducted on at least eight occassions prior to the first irradiation. Forty-six days after the last exposure, all surviving rats were euthanized with an overdose (80 mg/kg) of IP pentobarbital. Tissue and blood samples were taken for general pathological evaluation. Rats not surviving until this time underwent pathological evaluation whenever possible.

Data Collection and Analysis

Animals were tested five days per week, Monday through Friday, throughout the first three exposure phases. Following the fourth (6.5 Gy) exposure animals were tested for 12 consecutive days and then five days per week thereafter. All exposures occurred on a Monday and rats were always tested on the immediately preceeding Sunday. Prior to each exposure control data were taken from 6–7 sessions.

Individual performance measures calculated for each session for FR and FI responding included mean overall response rate, postreinforcement pause duration and running response rate. Overall response rate was calculated by dividing the total number of responses emitted by the total session time (excluding the time the dipper was raised). The postreinforcement pause was defined as the time elapsed from the end of a dipper presentation until the first response

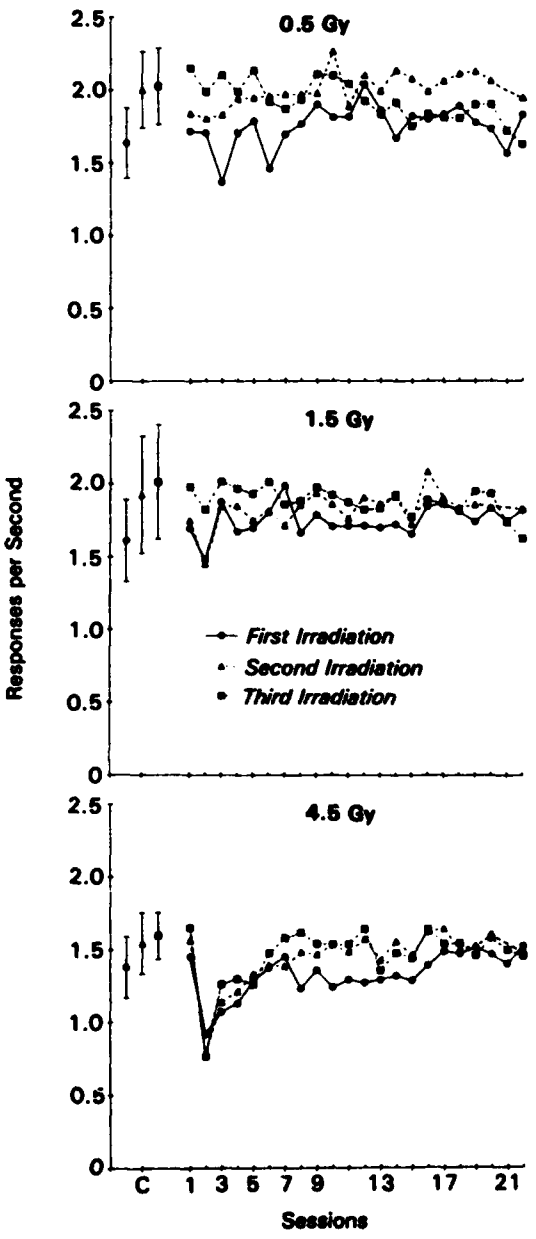

FIG. 1. Effects of gamma radiation on FR 50 response rates. Each panel represents a separate group of five rats. Each group was exposed to the indicated dose of radiation on three separate occasions at 43-day intervals. Session 1 began 5 min after exposure ceased. Subsequent sessions occurred at 24-hr intervals, Monday through Friday, over 30 days following irradiation. Points at C represent group mean control data for each of the three irradiations; vertical lines indicate ±1 SEM. Group means are based on the mean response rate of each rat across 6–7 sessions prior to irradiation.

of the next ratio or within the next interval. Running response rate was the response rate calculated with the postreinforcement pause omitted. Since responding under FI schedules typically occurs at an increasing rate as the interval times-out, the index of curvature was calculated to provide a measure of this temporal distribution of responses [17]

Performance measures were analyzed statistically using analysis of variance with the Greenhouse-Geisser correction for repeated measures [27]. Subsequent comparisons between pairs of means were performed with *t*-tests. Since virtually all of the studies examining radiation-induced changes in schedule-controlled responding have reported that response rates or frequencies were reduced following exposure, one-tailed tests were used when possible as reductions in response rates were expected. The alpha level for significance was set at 0.05.

RESULTS

Changes in FR response rates as a function of radiation dose and repeated irradiations are presented in Fig. 1. Neither 0.5 (top) nor 1.5 (middle) Gy of gamma radiation altered group mean response rates over 22 test sessions (30 days) after each of the three exposures. The only apparent effect was that the response rate of one rat was reduced below its control range 24 hr after each of the three 1.5 Gy exposures. At 4.5 Gy (bottom), changes in FR response rates were observed after each exposure. Response rates were not altered during the session which began 5 min after exposure (session 1), were reduced 24 hr later to the lowest levels observed (rates were reduced by 30–50% over the three exposures), and gradually returned to control levels by the fifth or sixth session after exposure. Following recovery, response rates remained stable throughout the remainder of each exposure phase. Changes in response rates did not vary as a function of repeated exposures. Analysis of variance performed on the response rates of each group separately (mean preirradiation control response rates and response rates from postirradiation sessions 1–10) revealed a significant effect of sessions only at 4.5 Gy; all main effects of radiation phase and radiation phase × session interactions were nonsignificant. One-tail *t*-tests revealed that sessions 2–5 differed significantly from control after the 4.5 Gy exposure.

Changes in FR postreinforcement pause after each 4.5 Gy exposure are presented in Fig. 2. Mean postreinforcement pause was not altered immediately following irradiation (session 1), but was increased two- to three-fold 24 hr later. During the third session after each exposure there was a substantial degree of recovery although the pause remained elevated above control values. Postreinforcement pause was elevated throughout the remainder of the first week of testing after exposure and returned to control levels during the second week. Changes in postreinforcement pause did not vary with repeated 4.5 Gy exposures. These effects were confirmed with an analysis of variance performed on the mean control pause and the pause from sessions 1–10 after the three 4.5 Gy exposures; the main effect of sessions was significant while the main effect of exposure phase and the interaction were nonsignificant. With the data collapsed across the three exposures, two-tail *t*-tests revealed that sessions 2–6 and 8 differed significantly from control. There were no consistent changes in postreinforcement pause after exposure to 0.5 or 1.5 Gy (not shown).

Running response rates under the FR schedule were not altered after exposure to 0.5 or 1.5 Gy of radiation. At 4.5 Gy, running rates were not altered on the day of exposure and were decreased to the lowest levels observed (by 20–40% of control over the three exposures) 24 hr later (Fig. 3). Running rates returned to control levels over the next 2–4 sessions and were stable throughout the remaining portion of each exposure phase. Analysis of variance on the running

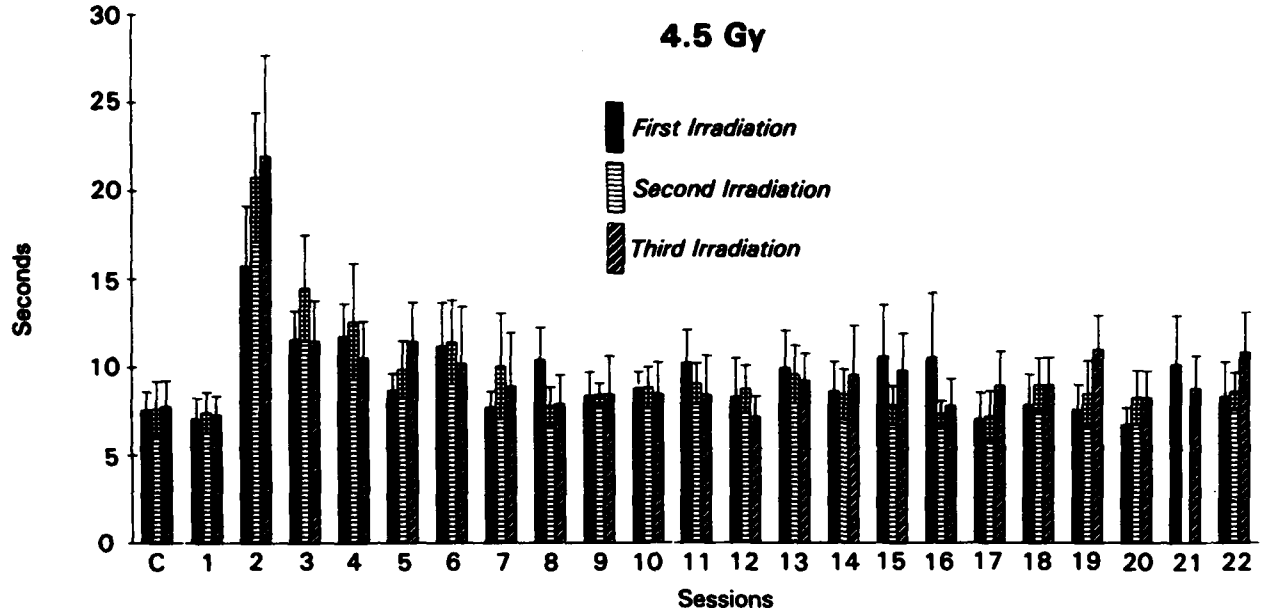

FIG. 2. Effects of 4.5 Gy of gamma radiation on FR 50 postreinforcement pause (see Fig. 1 for details).

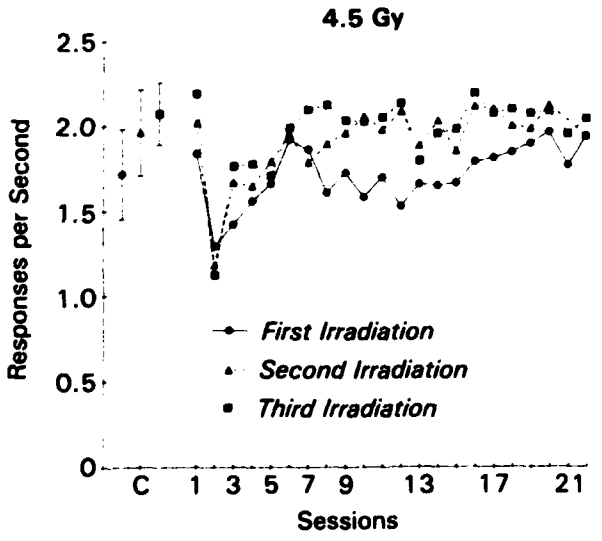

FIG. 3. Effects of 4.5 Gy of gamma radiation of FR 50 running response rates (response rates calculated with the postreinforcement pause omitted; see Fig. 1 for details).

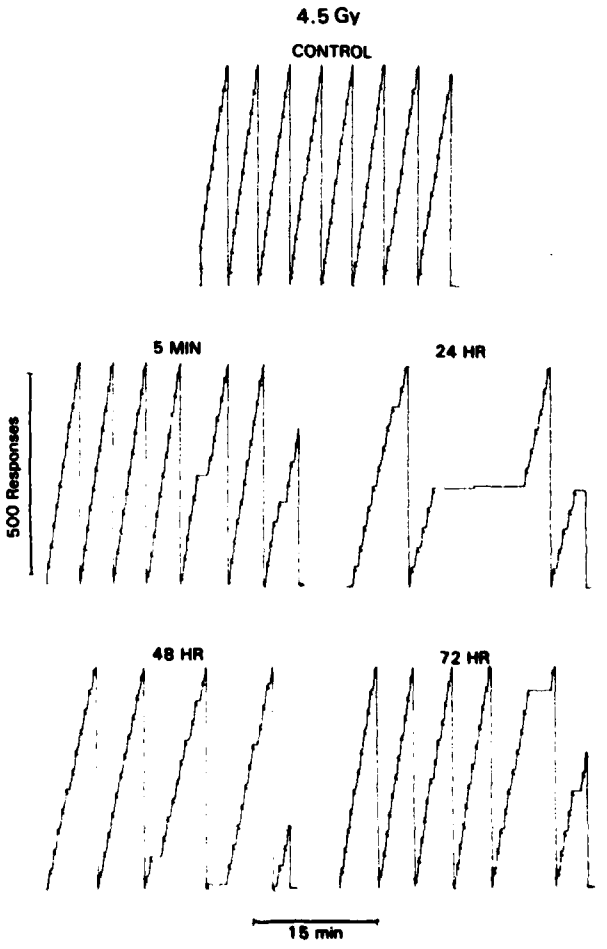

FIG. 4. Cumulative records showing the performance of one rat under the FR 50 schedule of milk presentation. Control performance prior to irradiation and performance over four successive sessions after exposure to 4.5 Gy of gamma radiation are shown. Each response stepped the pen in an incremental fashion across the page. Delivery of the milk reinforcer with the completion of the ratio is indicated by the diagonal deflections.

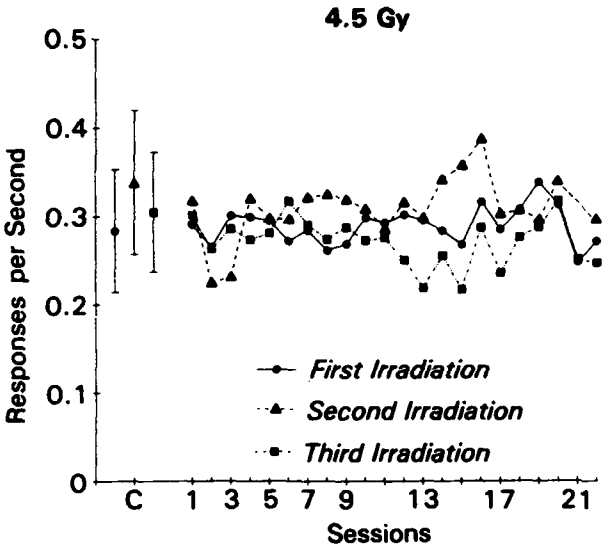

FIG. 5. Effects of 4.5 Gy of gamma radiation on FI 120 sec response rates (see Fig. 1 for details).

rates of the 4.5 Gy exposure group revealed only a significant effect of sessions, indicating that rate changes did not vary significantly as a function of repeated irradiations. One-tail *t*-tests revealed that sessions 2–4 differed significantly from control.

Sample cumulative records depicting control FR performance and performance over sessions 1–4 after exposure to 4.5 Gy are presented in Fig. 4. The overall response rate during the session that began 5 min after irradiation was within the range of control rates for this rat. At 24 hr postirradiation there was noticeable disruption in performance which included a slowing in the overall rate of responding, a lengthing of the postreinforcement pause, and an extended pause in responding. Progressive recovery of control-like performance was evident during the sessions which occurred 48 and 72 hr after exposure.

Under the FI schedule, average response rate, running response rate, postreinforcement pause and index of curvature were not altered consistently by 0.5–4.5 Gy of radiation over the three exposures (all main effects and interactions of analyses of variance were nonsignificant); response rates after 4.5 Gy are shown in Fig. 5. Individual mean control postreinforcement pauses ranged from 50 to 85 sec, while individual mean control indices of curvature ranged from 0.50 to 0.65. Fixed-interval responding did not appear to be completely unaffected by radiation, however, since the response rate of each rat in the 4.5 Gy exposure group was reduced below its control range for 24–48 hr after the second exposure.

Figure 6 presents the effects of 6.5 Gy of gamma radiation on FR response rates in rats with a history of exposure to 0.5–4.5 Gy. Response rates are presented as a percentage of mean control rates to facilitate comparison among groups. In

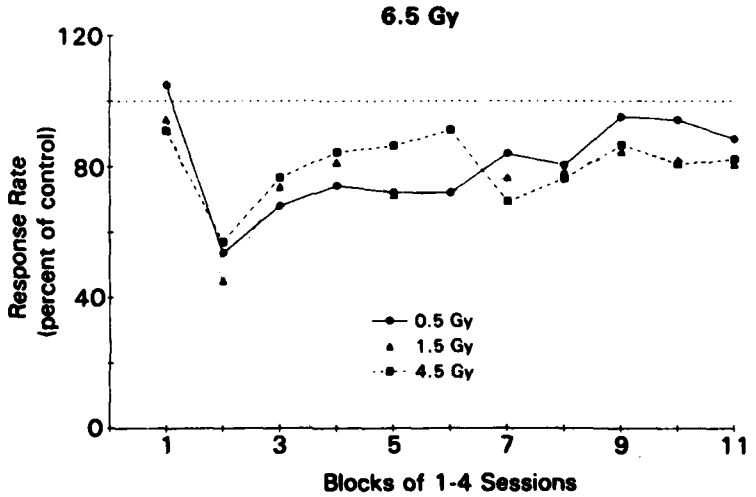

FIG. 6. Effects of 6.5 Gy of gamma radiation on FR 50 response rates. The key indicates the dose of radiation received on three separate occasions prior to exposure to 6.5 Gy. For each rat, the average response rate for a block of sessions was expressed as a percentage of the average control rate derived from 7 sessions prior to the 6.5 Gy exposure. Individual percentages were then averaged to provide group data. The first block represents the test session which began 5 min after exposure. Subsequent blocks are the mean of three sessions except for block 7 which is the mean of four sessions. For the 0.5 and 1.5 Gy exposure groups n=5. For the 4.5 Gy exposure group n=4 for blocks 1–6, n=3 for block 7, and n=1 for blocks 8–11.

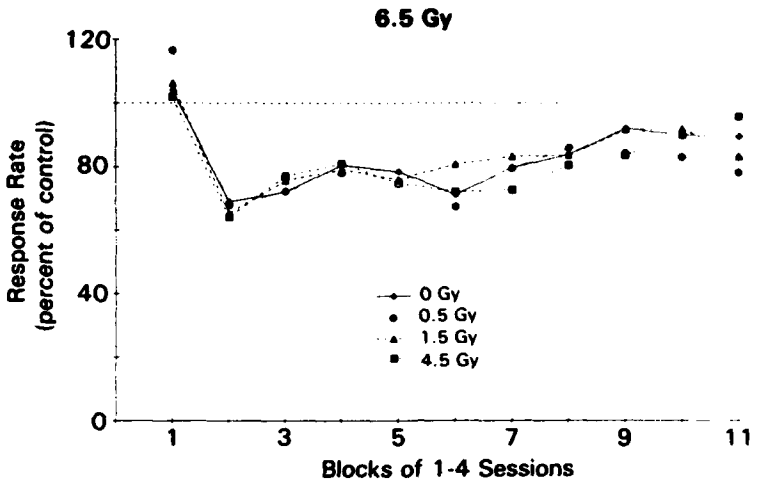

FIG. 7. Effects of 6.5 Gy of gamma radiation of FI 120 sec response rates. The key indicates the dose of radiation received on three separate occassions prior to exposure to 6.5 Gy. Each point is the mean of five rats for the 0 and 1.5 Gy exposure groups and four rats for the 0.5 Gy exposure group. For the 4.5 Gy exposure group n=5 for blocks 1–8 and n=4 for blocks 9–11 (see Fig. 6 for details).

none of the three groups of rats did 6.5 Gy alter response rates during the session that began 5 min after exposure (session block 1). Response rates were reduced in each group over the following three sessions (block 2). Response rates recovered somewhat and stabilized over the subsequent 5–6 blocks of sessions before showing additional recovery toward mean control values over the remaining blocks of sessions. Most importantly, differential radiation history did not alter the effect of 6.5 Gy on FR response rates. This was confirmed by analysis of variance on the absolute response rates which revealed that only the main effect of session block was significant. Control response rates and response rates through block 6 only were included in this overall analysis due to deaths that occurred in the 4.5 Gy exposure group during blocks 7 (one death) and 8 (two deaths). Two-tail *t*-tests on response rates collapsed across the three groups (n=14) revealed that blocks 2–6 differed from control.

Under the FI schedule, the 6.5 Gy exposure did not alter response rates on the day of irradiation in any group, while relatively stable reductions in response rates occurred over session blocks 2–7 in each group (Fig. 7). Response rates generally showed recovery over the remaining blocks of sessions. Similar to what was observed for FR responding, changes in FI response rates after exposure to 6.5 Gy of gamma radiation did not vary as a function of exposure history. The absence of any observable effect of exposure history on FI response rates is shown most dramatically by comparing the 0 Gy exposure group with the three groups that had previously been irradiated. Analysis of variance on the absolute response rates of the four FI groups (n=19) revealed only a significant effect of blocks. Because one rat in the 4.5 Gy exposure group died during session block 9, this overall comparison was restricted to the first eight blocks of sessions. Two-tail *t*-tests revealed that response rates during blocks 2–8 differed significantly from control rates.

Comparison between Figs. 6 and 7 suggests that 6.5 Gy reduced FR response rates to a greater degree than FI rates during the early postexposure period (session block 2). Response rates across the three FR groups were reduced to 51.5±4.0% (mean±SEM) of control values during block 2, while FI rates of rats with similar exposure histories (rats with a history of 0 rad exposures were excluded) were reduced to 65.7±6.1% of control. A two-tail *t*-test of these reductions in response rates revealed $p<0.07$. The 6.5 Gy dose increased FR postreinforcement pause and decreased FR and FI running rate; FI postreinforcement pause and index of curvature were not altered.

Lethality following the 6.5 Gy exposure was preceeded by a general deterioration in the condition of the animals for several days. Reduced food intake, weight loss, lowered body temperature, and paleness of the eyes which suggested failure of the hemopoietic system were observed. Prior to this each rat showed at least partial recovery from the disruption in performance seen shortly after irradiation. Pathological examination confirmed hemopoietic failure as the probable cause of death. Hemopoietic effects in surviving animals were restricted to a moderate anemia.

DISCUSSION

The effects of gamma radiation on schedule-controlled responding varied as a function of the dose and the schedule of reinforcement. At the lower doses (0.5 and 1.5 Gy) significant changes in performance were not observed. At the intermediate dose of 4.5 Gy, FR response rates were decreased after each of the three exposures, while FI response rates were not altered reliably. At the highest dose of radiation tested (6.5 Gy), both FR and FI response rates were decreased though FR rates tended to be decreased more than FI rates for several days after exposure. These findings indicate that over the range of doses used here, FR responding was more sensitive to radiogenic disruption than FI responding.

The differential effects of gamma radiation on FR and FI

performance may be due to differences in baseline response rates [24]; the higher rates under FR were disrupted at doses that did not alter or disrupted less the lower rates under FI. Effects of radiation did not appear to be solely a matter of baseline rate, however, since responding within the FI was not affected in a way that was related to the baseline rate. Under baseline conditions, responding within the FI showed the typical pattern of lower-rates early and higher-rates later in the interval. The quantitative measure of this pattern of responding, the index of curvature, was not altered by any dose of radiation even though overall response rate was reduced. This indicates that responding was decreased in a relatively uniform fashion throughout the FI. Thus, both baseline response rate and schedule of reinforcement may be important determinants of radiation-induced disruption of performance. Changes in other meausres of performance also varied in a schedule-dependent manner. The short postreinforcement pauses under FR were increased after exposure, while the longer pauses under FI were not altered. Extended pauses in responding after irradiation were generally restricted to FR. These differences contributed to the schedule-dependent changes in response rates.

At the doses of gamma radiation that produced consistent decreases in FR response rates (4.5 and 6.5 Gy), duration rather than magnitude of effect appeared to be a better indicator of dose. Averaged over the three exposures, 4.5 Gy produced maximal decreases in FR response rates to 59.0± 10.3% of control values 24 hr after exposure; recovery occurred over the next several days. Similar maximal reductions were observed 24 hr after exposure to 6.5 Gy, when FR response rates were reduced to 50.4±6.3% of control values. At this higher dose, however, FR response rates remained depressed for two additional days (response rates were reduced to 57 and 47% of control values, respectively, 48 and 72 hr after the 6.5 Gy exposore) before showing signs of recovery.

There are few previous reports on the effects of acute exposure to ionizing radiation on schedule-controlled performance. In one study, 1.0–5.0 Gy of X-rays reduced variable-interval response rates for 1–4 days while rates under a shock avoidance schedule were unaltered [22]. In another, 8.0 Gy reduced responding under an FR 1 schedule averaged over four days after exposure, whereas 2.0 and 4.0 Gy were ineffective [39]. Although neither of these studies conducted behavioral testing on the day of irradiation, the present investigation showed that performance was not altered over the immediate postexposure period after doses of 0.5–6.5 Gy. In contrast, much higher, acute doses have been shown to produce more immediate behavioral effects. Disruptions in responding under FR [8] and shock avoidance [11] schedules in rats were reported within one hour after exposure to supralethal doses (40–100 Gy), while delayed match-to-sample performance of monkeys was disrupted within minutes of supralethal irradiation [10].

Even though ionizing radiation generally depresses behavioral output, the time-course of this effect is highly dependent on the behavior examined. Here, performance changes were greatest 1–3 days after irradiation and were followed by recovery over several days or weeks. In contrast, swimming capability of rats decreased steadily over 3–4 weeks after X-irradiation and then gradually recovered [26]. Moreover, running-wheel activity of rats decreased for several days after X-irradiation, then recovered before a second, more pronounced decrease began at about day 10 postexposure [23]. These markedly different temporal relationships suggest fundamental differences in the factors underlying radiation-induced depression of schedule-controlled responding, swimming and running-wheel locomotion.

Decreased food intake is one of the earliest effects seen in humans and animals after low to moderate radiation exposure [22, 29, 40] and this may account for the disruptions in FR and FI performance observed here. However, there appear to be limitations on attempts to relate radiation-induced changes in schedule-controlled performance to a general effect on food intake, at least in the present study. At 6.5 Gy, even though most rats failed to consume their entire ration of chow on one or more days after exposure, there was little correspondence between the magnitude and time course of disruption in performance and whether or not chow was consumed. After exposure to 4.5 Gy of radiation when it was generally uncommon for any portion of the daily ration of chow to remain uneaten, the days when chow was not entirely consumed always occurred after the days when the most pronounced reductions in FR responding were found. Ionizing radiation induces a variety of subjective effects in humans that would likely disrupt ongoing behavior; these include weakness, fatigue, nausea, lethargy, headache and dizziness [40]. The performance changes reported here may provide an index of effects in animals that reflect or are in some way analogous to the subjective effects reported by humans. The use of schedule-controlled behavior in providing such an index of exposure to toxic agents has been suggested [38]. Additional research is necessary, however, to more precisely define and attempt to measure these types of effects in animals [30].

Repeated irradiations of the same animals failed to provide evidence of cumulative behavioral effects. This suggests that the 6–9 week period separating successive irradiations allowed for adequate recovery of the physiological systems underlying the behavioral effects observed here shortly after exposure. Long-term, latent physiological effects would have been expected to result in enhanced behavioral disruptions over successive irradiations. In contrast, several previous studies showed that decreases in FR responding were enhanced when rats received multiple irradiations; doses ranged from 0.5–8.0 Gy delivered every 1–7 days [7, 9, 39]. These results suggest that the dose of radiation, the time between irradiations, and the number of irradiations are important determinants of the behavioral effects of multiple exposures to ionizing radiation.

In contrast to disruption of FR and FI performance, lethality appeared to be influenced by radiation history in that all deaths that occurred after the 6.5 Gy exposure were found in the groups previously exposed to 4.5 Gy. Since no deaths occurred until 3 weeks following the 6.5 Gy exposure, there was a clear temporal separation between early, acute behavioral and later, lethal effects of radiation resulting from hemopoietic failure. Lethality was not merely the result of the total cumulative dose received, however. The total cumulative dose of 11 Gy received by the 1.5 Gy exposure groups exceeded the $LD_{50/30}$ dose of 9.5 Gy for gamma radiation in rats [6], yet no deaths occurred in these animals. The 4.5 Gy exposure groups received a total cumulative dose of 20 Gy; a single dose of this size would have been lethal to 100% of exposed animals within several days [19]. Thus, in agreement with previous data [3], dose fractionation increases the total cumulative dose that can be tolerated without producing lethality.

In summary, under the conditions used here the effects of gamma radiation on schedule-controlled performance were

found to be dose-related, reversible, noncumulative, and dependent on the schedule of reinforcement. Due to the continuing, if not increasing possibility of human exposure to ionizing radiation under a broad range of circumstances, the systematic examination of the behavioral effects of ionizing radiation should be pursued.

REFERENCES

1. Battist, L.; Peterson, H. T., Jr. Radiological consequences of the Three Mile Island accident. In: Radiation protection, vol. 2. Oxford: Pergamon Press; 1980:677–684.
2. Baverstock, K. F. A preliminary assessment of the consequences for inhabitants of the UK of the Chernobyl accident. Int. J. Radiat. Biol. 50:iii–xiii; 1986.
3. van Bekkum, D. W. Foreign bone marrow transplantation following fractional whole-body irradiation in mice. In: Ebert, M.; Howard, A., eds. Radiation effects in physics, chemistry and biology. Amsterdam: North Holland Publishing Co.; 1963:362–371.
4. Benton, E. V.; Almasi, J.; Cassou, R.; Frank, A.; Henke, R. P.; Rowe, V. Radiation measurements aboard spacelab 1. Science 225:224–226; 1984.
5. Bogo, V. Effects of bremsstrahlung and electron radiation on rat motor performance. Radiat. Res. 100:313–320; 1984.
6. Bogo, V. Behavioral radioprotection. Pharmacol. Ther., in press.
7. Brown, W. L. Response rate during X-irradiation and recovery following irradiation. J. Genet. Psychol. 108:117–120; 1966.
8. Brown, W. L.; Blodgett, H. C.; Henderson, D.; Ritter, R. M.; Pizzuto, J. S. Some effects on operant conditioning of ionizing radiation to the whole-head. J. Genet. Psychol. 108:255–261; 1966.
9. Brown, W. L; Overall, J. E.; Logie, L. C.; Wicker, J. E. Lever-pressing behavior of albino rats during prolonged exposures to X-irradiation. Radiat. Res. 13:617–631; 1960.
10. Bruner, A.; Bogo, V.; Jones, R. K. Delayed match-to-sample performance decrement in monkeys after ^{60}Co irradiation. Radiat. Res. 63:83–96; 1975.
11. Burghardt, W. F.; Hunt, W. A. Characterization of radiation-induced performance decrement using a two-lever shock-avoidance task. Radiat. Res. 103:149–157; 1985.
12. Casarett, A. P.; Comar, C. L. Incapacitation and performance decrement in rats following split doses of fission spectrum radiation. Radiat. Res. 53:455–461; 1973.
13. Cockerham, L. G.; Bogo, V.; Gosset-Hagerman, C. J. Gamma radiation produced performance decrements in rat as assessed with the accelerod. Neurosci. Lett. 49:297–300; 1984.
14. DiMascio, A.; Fuller, J. L.; Azrin, N. H.; Jetter, W. The effect of total-body X irradiation on delayed-response performance of dogs. J. Comp. Physiol. Psychol. 47:600–604; 1956.
15. Ferster, C B.; Skinner, B. F. Schedules of reinforcement. New York: Appleton-Century Crofts; 1957.
16. Fields, P. E. The effect of whole-body X radiation upon activity drum, straightaway, and maze performances of white rats. J. Comp. Physiol. Psychol. 50:386–391; 1957.
17. Fry, W.; Kelleher, R. T.; Cook, L. A mathematical index of performance on fixed-interval schedules of reinforcement. J. Exp. Anal. Behav. 3:193–199; 1960.
18. Furchtgott, E. Behavioral effects of ionizing radiations. In: Furchtgott, E., ed. Pharmacological and biophysical agents and behavior. New York: Academic Press; 1971:1–64.
19. Hobbs, C. H.; McClellan, R. O. Radiation and radioactive materials. In: Doull, J.; Klaassen, C. D.; Amdur, M. O., eds. Toxicology: The basic science of poisons. 2nd ed. New York: Macmillan; 1980:497–530.
20. Hunt, W. A. Comparative effects of exposure to high-energy electrons and gamma radiation on active avoidance behavior. Int. J. Radiat. Biol. 44:257–260; 1983.
21. International Atomic Energy Agency. Postaccident review meeting on the Chernobyl accident. Aug. 25–29, 1986, Vienna, Austria.
22. Jarrard, L. E. Effects of X-irradiation on operant behavior in the rat. J. Comp. Physiol. Psychol. 56:608–611; 1963.
23. Jones, D. C.; Kimeldorf, D. J.; Rubadeau, D. O.; Osborn, G. K.; Castanera, T. J. Effect of X-irradiation on performance of volitional activity by the adult male rat. Am. J. Physiol. 177:243–250; 1954.
24. Kelleher, R. T.; Morse, W. H. Determinants of the specificity of behavioral effects of drugs. Ergeb Physiol. 60:1–56; 1968.
25. Kimeldorf, D. J.; Hunt, E. L. Ionizing radiation: Neural function and behavior. New York: Academic Press; 1965.
26. Kimeldorf, D. J.; Jones, D. C.; Castanera, T. J. Effect of X-irradiation upon the performance of daily exhaustive exercise by the rat. Am J. Physiol. 174:331–335; 1953.
27. Kirk, R. E. Experimental design: Procedures for the behavioral sciences. Belmont: Brooks/Cole; 1968.
28. Kovalev, E. E. Radiation protection during space flight. Aviat. Space Environ. Med. 53:S16–S23; 1983.
29. Landauer, M. R.; Ledney, G. D.; Davis, H. D. Locomotor behavior in mice following exposure to fission-neutron irradiation and trauma. Aviat. Space Environ. Med. 58:1205–1210; 1987.
30. Laties, V. G. How operant conditioning can contribute to behavioral toxicology. Environ. Health. Perspect. 26:29–35; 1978.
31. Mickley, G. A.; Stevens, K. E. Stimulation of brain muscarinic acetylcholine receptors acutely reverses radiogenic hypodipsia. Aviat. Space Environ. Med. 57:250–255; 1986.
32. Mickley, G. A.; Stevens, K. E.; White, G. A.; Gibbs, G. L. Endogenous opiates mediate radiogenic behavioral change. Science 220:1185–1187; 1983.
33. Pizzarello, D. J.; Witcofski, R. L. Medical radiation biology. 2nd ed. Philadelphia: Lee & Febiger; 1982.
34. Rabin, B. M.; Hunt, W. A. Mechanisms of radiation-induced conditioned taste aversion learning. Neurosci. Biobehav. Rev. 10:55–65; 1986.
35. Roentgen, W. C. On a new kind of rays. Nature 53:274–276; 1896.
36. Rust, D. M. Solar flares, proton showers, and the space shuttle. Science 216:939–945; 1982.
37. Seiden, L. S.; Balster, R. L. Behavioral pharmacology: The current status. New York: Alan R. Liss, Inc.; 1985.
38. Weiss, B.; Ferin, J.; Merigan, W.; Stern, S.; Cox, C. Modification of rat operant behavior by ozone exposure. Toxicol. Appl. Pharmacol. 58:244–251; 1981.
39. Wicker, J. E.; Brown, W. L. The effect of gamma radiation upon operant water-reinforcement behavior. J. Genet. Psychol. 106:295–299; 1965.
40. Young, R. W. Acute radiation syndrome. In: Conklin, J. J.; Walker, R. I., eds. Military radiobiology. New York: Academic Press; 1987:165–190.

LYMPHOKINE RESEARCH
Volume 7, Number 4, 1988
Mary Ann Liebert, Inc., Publishers

RESEARCH REPORT

Comparison of In Vivo Effects of Human Recombinant IL 1 and Human Recombinant IL 6 in Mice

RUTH NETA,[1] STEFANIE N. VOGEL,[2] JEAN D. SIPE,[3] GORDON G. WONG,[4] and RICHARD P. NORDAN[5]

[1]*Armed Forces Radiobiology Research Institute, Bethesda, MD 20814*
[2]*Department of Microbiology, Uniformed Services University for the Health Sciences, Bethesda, MD 20814*
[3]*Thorndike Memorial Laboratory, Boston City Hospital and Arthritis Center, Boston University School of Medicine, Boston, MA 02118*
[4]*Genetics Institute, Cambridge, MA 01890*
[5]*Laboratory of Genetics, National Cancer Institute, Bethesda, MD 20892*

ABSTRACT

IL 1 and IL 6 share a number of biological activities, including induction of fever, neutrophilia and acute phase response, and IL 1 induces IL 6 production by fibroblasts and macrophages. Therefore, it was proposed that IL 6 mediates many of the activities of IL 1. To test this hypothesis in vivo, we assessed induction of IL 6 following IL 1α administration to mice and tested IL 6 for radioprotection and induction of early (CSF) and late (fibrinogen and SAA) acute phase reactants. IL 1α given to mice ip induced, in a dose dependent manner, detectable IL 6 in circulation, with maximal titers at 2-4 hrs. However, unlike IL 1 which is radioprotective when administered in doses above 100 ng/mouse, doses of 10-1000 ng/mouse of human recombinant IL 6 did not result in increased survival of mice following lethal irradiation. In fact, such treatment given 20 hrs before $LD_{50/30}$ doses of radiation resulted in reduced survival of mice. However, IL 6 augmented the radioprotective effect of IL 1. IL 1 in doses above 10 ng/mouse induced within 2 to 6 hrs a dose dependent increase in CSF in circulation, but IL 6 did not induce detectable levels of CSF at 2, 6 and 20 hrs after administration. Administration of IL 6 to mice produced a dose dependent increase in circulating fibrinogen and SAA. Similarly, administration of IL 1 resulted in much greater increases in levels of fibrinogen and SAA. Therefore, IL 1 is a more effective inducer of fibrinogen and SAA in mice than is IL 6. Although definitive conclusions concerning the relative roles for IL 1 and IL 6 in vivo will await availability of anti IL 1 and anti-IL 6 antibodies, our data do not support the suggestion that the above IL 1 effects can be attributed solely to IL 6.

INTRODUCTION

IL 1 is recognized as a key inflammatory mediator as evident from its ability to induce in vivo most of the inflammatory manifestations (see reviews 1,2). The use of recombinant IL 1 has eliminated previous uncertainties regarding the composition of the preparations of natural IL 1 that were used for many years for in vivo studies. Such studies were

plagued with concern that partially purified preparations contain some unidentified cytokines in addition to IL 1. Recent work has shown that administration of nanogram quantities of recombinant IL 1 to mice or rabbits results in fever, neutrophilia (3), induction of the acute phase response (4,5), changes in bone marrow population (6), and CSF release (7).

However, IL 1 is known to be induced coordinately with other cytokines (such as TNF), and to induce the production of a cascade of other cytokines such as IL-2 and CSF (8). Thus, a question can be raised as to whether the effects attributed to IL 1 are based on direct effects or due to the induction of a battery of other cytokines. Recently, IL 1 has been shown to induce the release of IL 6 by several cell types including macrophages, endothelial cells, and fibroblasts (9-11). This cytokine was initially described by a number of independent laboratories and called by different names based on various biological activities such Interferon beta 2 (IFNβ2), B Cell Stimulating Factor 2 (BSF2), and Hybridoma/Plasmocytoma Growth Factor (12-16). Upon realizing that all these activities could be attributed to the same recombinant cytokine, it was renamed IL 6.

IL 6 has been identified recently as having the activity of a hepatocyte stimulating factor (17,18), thymocyte costimulating factor (19,20) and endogenous pyrogen (11). Because of the inductive relationship between IL 1 and IL 6, it has been proposed that IL 6 is the direct mediator of a number of activities previously attributed to IL 1. To test this hypothesis, we have assessed the capacity of IL 1 to induce IL 6 *in vivo* and compared the systemic effects of direct delivery of IL 6 and IL 1 in radioprotection, in induction of early (CSF) and late (SAA, fibrinogen) acute phase reactants, and in induction of changes in bone marrow cell sizing profile. The rationale for such comparison of systemic administration of the two cytokines was based on previous findings that administration of nanogram quantities of IL 1 reproduced the effects of administration of micrograms of LPS (an IL 1 inducer) (21,22). In this report we show that although IL 1 indeed induces systemic production of IL 6, ip delivery of IL 6, up to 3 microgram quantities, does not mimic the above effects of IL 1.

MATERIALS AND METHODS

Mice. B6D2F1 mice were purchased from the Jackson Laboratory, Bar Harbor, Maine. Mice were quarantined on arrival and screened for evidence of disease before being released from quarantine. They were maintained in an AAALAC accredited facility in plastic Micro-isolator cages on hardwood chip contact bedding, provided commercial rodent chow and given acidified (HCl to a pH of 2.5) tap water *ad libitum*. Animal holding rooms were maintained at 70$\pm$2 F with 50$\pm$10% relative humidity using at least 10 air changes per hour of 100% conditioned fresh air. The mice were on a 12 hour light-dark full spectrum lighting cycle with no twilight. Mice were 8-12 weeks of age when used. All cage cleaning, handling, and injections were carried out in a laminar flow clean air unit.

Cytokines. Human recombinant IL 1α was generously provided by Dr. Peter Lomedico of Hoffman - La Roche, Nutley, NJ. The preparation, lot 1/87, was supplied in 50 mM potassium phosphate and 0.1 M NaCl (pH 6.5) buffer and used on a weight basis. Human recombinant IL 6 in 20 mM NaOAc pH 5.0, specific activity of 2×10^6 CESS units/mg, lot 1190-130 and batch 9, were received from Genetics Institute, Cambridge, MA. This material was reanalyzed in our laboratory in the hybridoma growth factor (HGF) assay (see below) and was found to possess 1.75×10^6 HGF units/mg. All reagents were diluted to the desired concentration in pyrogen-free saline just prior to a single ip injection of 0.5 ml to mice. The cytokine preparations were assayed for LPS contamination in a LAL assay and determined to contain less than 0.1 ng per maximal concentration of inoculum.

Irradiation. Mice were placed in plexiglass containers and were given whole body irradiation at 40 cGy/min by bilaterally positioned ^{60}Co elements. The number of surviving mice was recorded daily for 30 days.

Measurement of IL 6 in the serum. Mice were bled from the orbital plexus at designated times after administration of IL 1 and serum was collected following clot formation. Serum IL 6 activity was determined using the hybridoma growth factor assay described by Aarden et al. (23). This method incorporated the IL 6 - dependent hybridoma, B9, in a conventional microproliferation assay. Briefly, individual serum samples were initially treated to several 10-fold dilutions in the assay medium (RPMI 1640, 10% FCS, $5x10^{-5}$ M 2ME, and 50 ug/ml gentamycin). These samples were then two-fold serially diluted in 96-well culture plates containing 0.1 ml volume of assay medium per well. Two thousand B9 cells in 0.1 ml volume of assay medium were then added to each well (final volume 0.2 ml). The cultures were incubated at 37°C in a humidified atmosphere of 5% CO_2. After 72 hrs the cultures were pulsed with 0.5 μC ^{3}H-thymidine for 4 hrs, harvested onto glass fiber filters and counted in a liquid scintillation counter. One HGF unit was defined as the reciprocal of the dilution which yielded 50% of the maximal ^{3}H-thymidine incorporation.

Measurement of CSF activity in the serum. Mice were bled at 2, 6, and 24 hours after injection and serum was collected after clot formation by centrifugation. CSF activity was measured in pooled serum samples collected from 4-5 mice per treatment group per experiment. The bone marrow colony assay for CSF activity has been described in detail (7). Briefly, C3H/HeJ bone marrow cells were enriched for mononuclear cells by density gradient centrifugation on lymphocyte separation medium (Litton Bionetics, Charleston, SC). The cells collected from the interface of the gradient were washed and resuspended in RPMI 1640, supplemented with antibiotics, glutamine, sodium bicarbonate HEPES buffer, and 15% FCS. Three serial two-fold dilutions of each serum sample (30%, 15%, and 7.5% v/v) were prepared in this medium and 0.2 ml of each dilution was added to each of duplicate wells in a 6 well tissue culture plate. A final cell suspension was prepared in $1x10^5$ cells/ml in complete medium supplemented with 0.3% Bacto-Agar (Difco, Detroit, MI) and maintained at 41°C. One ml per well was added immediately after resuspension of the cells in the agar-medium mixture. Once solidified, the cultures were incubated at 37°C, 6% CO_2, for 6-7 days at which time colonies (more than 25 cells per colony) were counted under a dissecting microscope. Serum CSF activity was expressed as colony forming units (CFU) per ml of serum, based on colony count within the linear part of the dilution curve.

Fibrinogen assay. Assays for fibrinogen in diluted citrated plasma were performed by measuring the rate of conversion of fibrinogen to fibrin in the presence of thrombin excess. The calibration was made using the Sigma Diagnostic Kit (Sigma Chemical Co., St. Louis, MO). Measurements of fibrin clot formation were performed on a fibrometer (Becton-Dickenson, Mountain view, CA). The data are expressed as mg of fibrinogen per 100 ml of plasma.

SAA assay. SAA concentration was measured in the serum using an Elisa assay as described (24), with monoclonal rat anti-SAA antibodies prepared according to the method described by Wood et al. (25). Triplicate 200 μl aliquots of diluted serum were analyzed. SAA is expressed in terms of serum amyloid A equivalents, μg/ml, using SAA-rich LDL as a standard.

Statistical analysis. Statistical evaluation of the results was done using Chi-square analysis and z-test.

RESULTS

Induction of IL 6 with IL 1 in vivo. B6D2F1 mice were given ip injections of 1000 ng IL 1 and their sera were assessed for the presence of IL 6 at 0.5, 1, 2, 4, 8, and 24 hrs after treatment. The results (Fig.

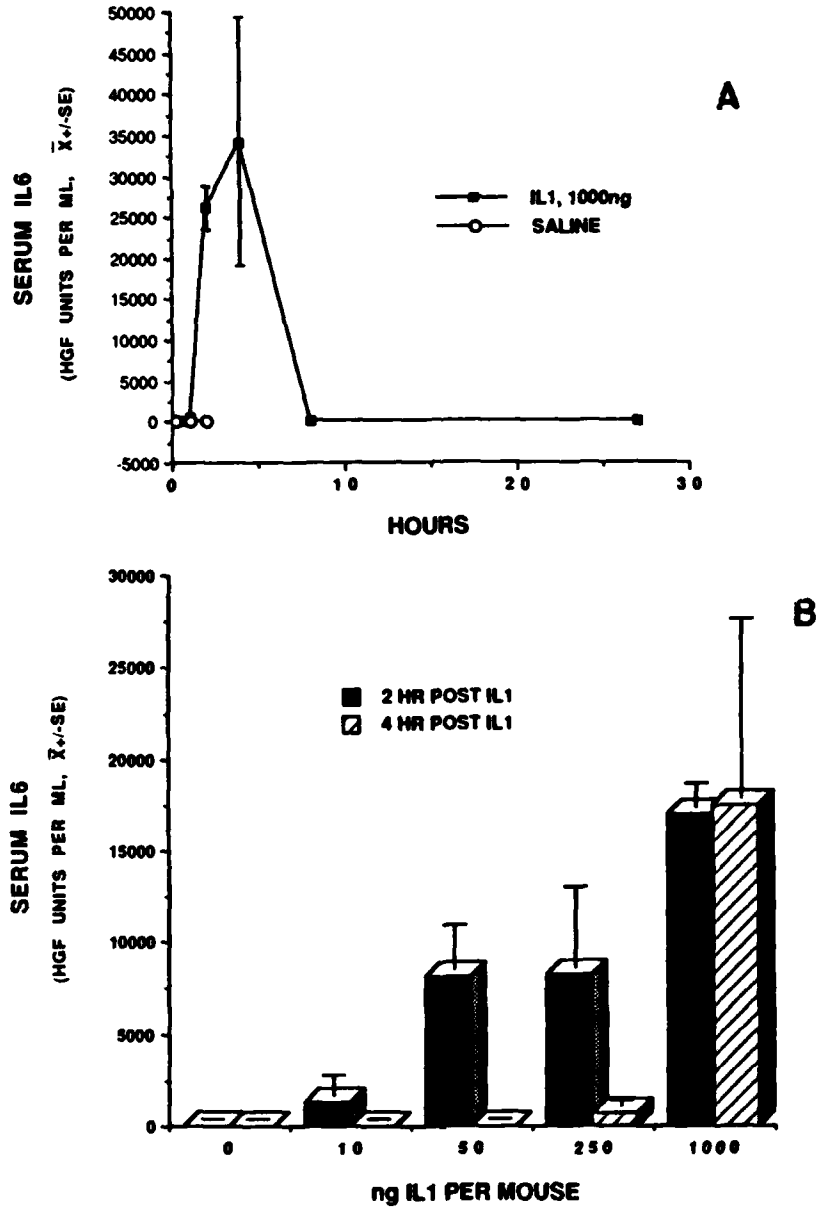

Figure 1. Serum IL 6 levels following IL 1 administration. Time response curves (A) and dose dependence (B) of induction of IL 6 with IL 1 in B6D2F1 mice (n=3 in A and 4 in B).

1) show that IL 1 treatment induced an increase of IL 6 in the circulation beginning at 1 hr, which peaked at 2-4 hrs and declined by 8 hrs after treatment (Fig. 1A). Only 1 out of 4 mice had detectable IL 6 in circulation 2 hrs following administration of 10 ng of IL 1 (Fig. 1B). All 4 mice injected with 50 ng of IL 1 had detectable IL 6 levels at 2 hrs. At these doses of IL 1 (10,50 ng) IL 6 was not detected at 4 hrs. Following 250 ng of IL 1 , low titers of IL 6 were detected at 4 hrs after injection, while 1000 ng of IL 1 resulted in high titers of IL 6 at 2 and

4 hrs. Thus, systemic administration of IL 1 induces dose dependent transient elevation of plasma levels of IL 6 in vivo in mice.

Induction of CSF in circulation. In previous experiments IL 1 in doses as low as 10 ng per mouse induced increases in circulating CSF (7). This induction of CSF by IL 1 was dose dependent, reaching a plateau at 100 to 2000 ng with the maximal titers at 2 to 4 hrs. Presently, high titers of CSF were induced with 1000 ng IL 1 at 2 hrs (6430±233), which declined by 6 hrs (2823±155), but were still detectable at 20 hrs (330±268). In contrast, IL 6 in doses ranging from 100 to 1000 ng did not induce detectable circulating CSF at 2, 6, or 20 hrs. Thus IL 6 and IL 1 differ in their ability to induce circulating CSF.

Effects on bone marrow cell size. Our previous work has shown that IL 1 increases the size distribution of the entire nucleated bone marrow cell population (6). Such increases were detectable with as little as 10 ng IL 1. Presently, 3000 ng of IL 1 ip resulted in increased numbers of large bone marrow cells at 20 and 96 hrs ($p<0.01$)(Fig.2). However, bone marrow cells from mice treated with 3000 ng of IL 6 did not show significant enlargment when compared to saline treated mice. Thus IL 1 and IL 6 differ in their effect on bone marrow cell size distribution.

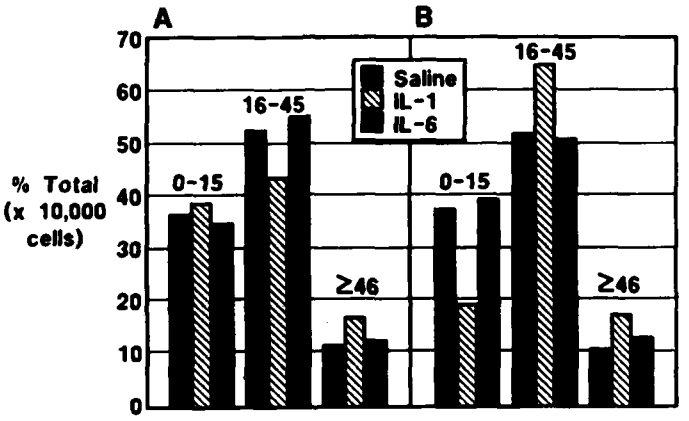

Figure 2. Effect of IL 1 and IL 6 on bone marrow cell size distribution at 20 hrs (A) or 96 hrs (B) after administration. Cells in channel 0-15 were smaller than 160 um^3, in channel 16-45 were 160-320 um^3, and above channel 46 were larger than 320 um^3. (n=3).

Comparison of IL 1 and IL 6 in radioprotection. B6D2F1 mice were given ip injections of IL 1, IL 6, or saline 20 hrs before irradition. Figure 3 summarizes the results of three experiments in which two doses of radiation were used. Following irradiation with 1000 cGy 45% of control, saline treated mice survived. IL 1 protected up to 90% of mice from death, but administration of 10-1000 ng IL 6 resulted in greatly reduced survival (only 5-15%) (Fig. 3A). Similarly, a radiosensitizing effect of IL 6 alone was also observed at 1050 cGy. In this series of three experiments, 15% of control, saline treated mice survived (Fig. 3B). However, suboptimal, non-radioprotective doses of 50 ng IL 1 combined with 1000 ng of IL 6 resulted in synergistic radioprotection ($p<0.05$). Furthermore, even at doses at which IL 1 conferred significant radioprotection (500 ng), combined injection of IL 1 and IL 6 resulted in significantly enhanced ($p<0.05$) survival of mice. Thus, unlike the finding with IL 1, treatment with IL 6 alone did not confer radioprotection. However, combined administration of IL 1 with IL 6 resulted in an enhanced radioprotective effect.

Induction of late acute phase reactants. Our previous work has shown that treatment of mice with IL 1 results in increased SAA and fibrinogen

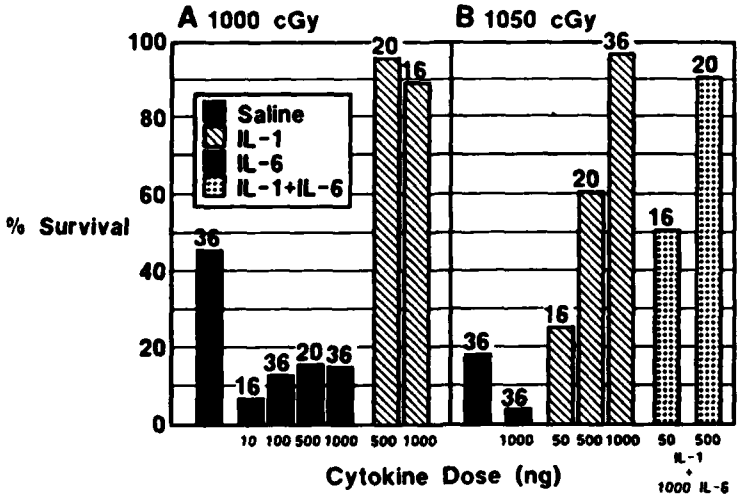

Figure 3. Effect of IL 1α and IL 6 alone and in combination on survival of irradiated mice. B6D2F1 mice were irradiated with 1000 cGy (A) or 1050 cGy (B) 20 hrs following ip administration of IL 1, IL 6, their combination, in the doses indicated, or saline. Numbers on top of the bars indicate the total number of mice/treatment.

in circulation. SAA was detected at 6 and 20 hrs and fibrinogen at 12 and 20 hrs (4,5). When compared on a weight basis with IL 1, IL 6 was a much less potent inducer of fibrinogen than IL 1 (Fig. 4). Similarly IL 6 was a less potent inducer of SAA than IL 1 at 6 and 20 hrs (Table 1).

TABLE 1
In vivo production of SAA in response to IL 1α and IL 6

Treatment	SAA concentration (μg/ml)*		
	2 hrs	6 hrs	20 hrs
Experiment 1			
saline	0.01	0.01	0.01
IL 1, 1000 ng	0.02	260	300
IL 6, 1000 ng	0.11	0.02	0.49
Experiment 2			
saline	0.05		0.05
IL 1, 1000 ng	2.2		490
IL 6, 1000 ng	0.60		1.0

*pool of sera from 3 mice were assayed in each experiment.

DISCUSSION

The foregoing results provide evidence that IL 1 induces IL 6 not only, as previously reported, in cell culture (9-11), but also systemically, as evident by its appearance in circulation. Others have shown increased levels of IL 6, at the time of graft rejection, in the serum and urine of patients receiving kidney transplants (26). Detectable levels of serum IL 6 have also been reported in febrile patients (27). This rise in IL 6 in febrile patients preceded the increase in acute phase response. The induction of release of acute phase proteins, one of the primary manifestations of inflammation, has been previously reported in

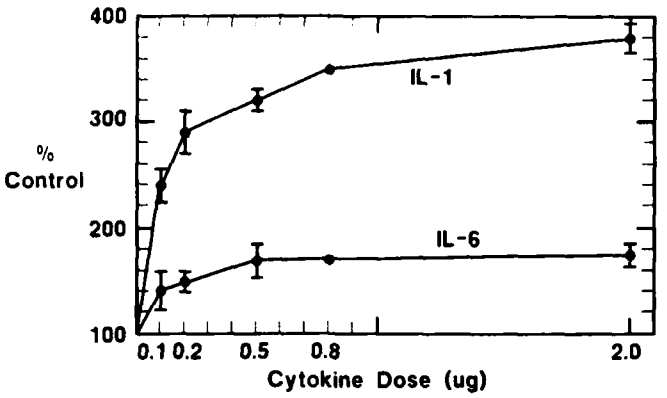

Figure 4. In vivo production of fibrinogen in response to IL 1 and IL 6. B6D2F1 mice were bled 20 hrs following administration of IL 1 or IL 6. The results are the mean of 3 experiments (±SEM), using pooled plasma from 3 mice in each experiment.

vivo (4,5) and in vitro (5,28,29) for IL 1. However, rat primary hepatocyte and human hepatocyte cell lines which produced only restricted spectrum of acute phase reactants in response to IL 1 showed much greater response to IL 6 (18). The induction of IL 6 with IL 1 in several cell types together with identification of IL 6 as a major inducer of acute phase protein synthesis, led to the belief that IL 6, rather than IL 1, may be a direct stimulator of acute phase reactants. Furthermore, based on a broad spectrum of activities of IL 6, some of which overlap with those of IL 1, it was suggested that IL 6 may mediate some of the other activities previously attributed to IL 1.

The experience from this and other laboratories showed that systemic administration of IL 1 reproduced the inflammatory manifestations produced by LPS, an IL 1 inducer. For example, systemical administration of IL 1, like LPS, stimulates the release of CSF (7). Significantly increased levels of CSF were observed after IL 1 doses as low as 10 ng per mouse. The induction of CSF with IL 1 was also demonstrated repeatedly in fibroblasts, endothelial cells, or macrophages in culture (30-33). In the present study, CSF was not detected at 2, 6, or 20 hrs following administration of as much as a 1000 ng dose of IL 6. No evidence exists that IL 6 can induce CSF in cells. Similarly, despite the reported action of IL 6 as Hematopoietin-1 (34), which parallels that attributed to IL 1 (35-37), IL 6 did not induce changes in the size of bone marrow cells characteristic of LPS and IL 1. We are aware that observations on cell size profiles of whole bone marrow populations do not preclude the effect of IL 6 on selected subtypes of such cells. The changes in cell sizes induced with IL 1 in previous studies correlated with increased cell cycling (over 25% increase in population of large cells) and with increase in GM-CFC progenitor cells (6). Thus delivery of 10-100 ng of IL 1 clearly has a much more profound effect on cells in the bone marrow than 1000 ng of IL 6.

In addition, LPS was shown more than 30 years ago to be radioprotective (38,39). Similar radioprotection was reproduced with IL 1 (40). In the present study, however, as much as 1000 ng per mouse of IL 6 did not confer radioprotection. In fact, treatment with IL 6 alone resulted in apparent radiosensitization, i.e. greater numbers of mice died of the radiation syndrome following IL 6 than saline administration. However, this effect was reversed in the presence of 50 ng of IL 1, which alone was not radioprotective, but which synergized with IL 6 in radioprotection. This result indicates that IL 6 in the presence of IL 1 is a radioprotective agent. Induction with IL 1 of bone marrow cell cycling and CSF's may

present some of the necessary prerequisites for interacting with IL 6 in radioprotection. It is difficult at present to explain the radiosensitizing effect of IL 6 in the absence of IL 1. Perhaps, as suggested by Dr. Charles Dinarello (personal communication), IL 6 suppresses endogenous production of IL 1 which may result in enhanced susceptibility to radiation.

IL 6 was also less efficacious than IL 1 in systemic induction of fibrinogen and SAA. Production of fibrinogen, α_1-antichymotrypsin, α_2-macroglobulin, and cysteine proteinase inhibitor was eliminated by the presence of anti-IFN-β2/IL 6 antibody in primary rat hepatocytes and human hepatocyte lines stimulated with supernatants which contained both IL 1 and IL 6 (18). Such treatment, however, did not eliminate α_1-acid glycoprotein or haptoglobin production. Yet the use of anti-IL 1 and anti-IL 6 antibodies in combination abrogated production of all examined acute phase proteins. Similarly, reduction of albumin synthesis was maximally reversed using the anti-IL 1 and anti-IL 6 antibodies in combination. More recent results (Dr. Jack Gauldie, personal communication) indicate that genes for SAA or α_1-acid glycoprotein may be induced with IL 1 alone, while other genes, such as fibrinogen, are not induced with IL 1. Thus our results showing less effective in vivo induction of fibrinogen with IL 6 than IL 1, may indicate that IL 1 may be necessary at the local site to induce sufficient endogenous levels of IL 6, which, in turn, may directly act to induce fibrinogen message. Final resolution of the mechanisms which function in vivo in the induction of various subclasses of acute phase reactants will depend on the selective in vivo elimination of IL 1 and IL 6 with sufficient quantities of specific antibody.

The results presented in this study, and work of others to date, already indicate that IL 1 and IL 6, although induced in sequence have diverse as well as overlapping activities, but the relative contribution of each of these cytokines to the inflammatory processes remain to be established.

ACKNOWLEDGEMENTS

We wish to thank Drs. J.J. Oppenheim and T.J. MacVittie for reviewing this manuscript and Mr. W.E. Jackson for statistical analysis of the results. This work was supported by the Armed Forces Radiobiology Research Institute, Defense Nuclear Agency, under Research Work Unit MJB3132 and USUHS protocols RO7338 and G27384. The opinions or assertions contained herein are the private views of the authors; no endorsement by the Defense Nuclear Agency has been given or should be inferred. The research was conducted according to the principals enunciated in the "Guide for the Care and Use of Laboratory Animals" prepared by the Institute of Laboratory Animal Resources, National Research Council.

REFERENCES

1. Dinarello, C.A. Rev. Infect. Dis. 6:55, (1984).

2. Durum, S., Oppenheim, J.J., and Neta R. In: Immunophysiology: Role of Cells and Cytokines in Immunity and Inflammation, eds. J.J. Oppenheim and E. Shevach, Oxford University Press, in press, (1988).

3. Dinarello, C.A., Cannon, J.G., Mier, J.W., Bernheim, H.A., LoPreste, G., Lynn, D.L., Love, R.N., Webb, A.C., Auron, P.E., Reuben, R.C., Rich, A., Wolff, S.M., and Putney, S.D. J. Clin. Invest. 77:1734, (1986).

4. Sipe J.D., Vogel, S.N., Douches, S.D., and Neta, R. Lymphokine Res., 6:93, (1987).

5. Mortensen R.F., Shapiro, J., Lin, B.F., Douches, S.D., and Neta, R. J. Immunol., 140:2260, (1988).

6. Neta, R., Sztein, M.B., Oppenheim, J.J., Gillis, S., and Douches, S.D. J. Immunol., 139:1861, (1987).

7. Vogel, S.N., Douches, S.D., Kaufman, E.N., and Neta, R. J. Immunol., 138:2143, (1987).

8. Oppenheim, J.J., Kovacs, E.J., Matsushima, K., and Durum, S.K. Immunol. Today 7:45, (1986).

9. Van Damme, J., Cayphas, S., Opdenakker, G., Bilian, A., and Van Snich, J. Eur. J. Immunol., 17:1, (1987).

10. Kohase, M., May, L.T., Tamm, I., Vilcek, J., and Sehgal, P.B. Mol. Cell. Biol., 7:273, (1987).

11. Billiau, A. Immunology Today, 8:84, (1987).

12. Zilberstein, A., Ruggieri, R., Korn, G.H., and Revel, M. EMBO. J. 5:2529, (1986).

13. Hirano, T., Yasukawa, K., Harada, H., Taga, T., Watanabe, Y., Matsuda, T., Kashiwamura, S., Nakajima, K., Koyama, K., Iwamatsu, A., Tsunasawa, S., Sakiyama, F., Matsui, Y., Takahara, Y., Taniguchi, T., and Kishimoto, T. Nature (London), 324:73, (1986).

14. Aarden, L.A., Lansdorp, P.M., and De Groot, E.R. Lymphokines, 10:175, (1985).

15. Nordan, R.P., and Potter, M. Science (Washington, DC), 233:566, (1986).

16. Van Snick, J., Cayphas, A., Vink, A., Uyttenhove, C., Coulie, M., Rubira, R., and Simpson, R.J. Proc. Natl. Acad. Sci. USA, 83:9679, (1986).

17. Andus, T., Geiger, T., Hirano, T., Northoff, H., Ganter, U., Bauer, J., Kishimoto, T., and Heinrich, P.C. FEBS Lett. 221:18, (1987).

18. Gauldie, J., Richards, C., Harnish, D., Lansdorp, P., and Baumann, H. Proc. Natl. Acad. Sci. USA 84:7251, (1987).

19. Van Damme, J., Van Beeumen, J., Decock, B., Van Snick, J., De Ley, M., and Billiau, A. J. Immunol., 140:1534, (1988).

20. Hodgkin, P.D., Bond, M.W., O'Garra, A., Frank, G., Lee, F., Coffman, R.L., Zlotnik, A., and Howard, M. J. Immunol., 141:151, (1988).

21. Neta, R., Oppenheim, J.J., and Douches, S.D. J. Immunol., 140:108, (1988).

22. Vogel, S.N., Kaufman, E.N., Tate, M.D., and Neta, R. Infect. Immun., in press, (1988).

23. Aarden, L.A., De Groot, E.R., Schaap, O.L., and Landsdorp, P.J. Eur. J. Immunol., 17:1411, (1987).

24. Zuckerman, S.H., and Surprenant, Y.M. J. Immunol. Methods, 92:37, (1986).

25. Wood, D.D., Gamon, M., and Staruch, M.J. J. Immunol. Methods, 55:19, (1982).

26. Van Oers, M.H.J., Van der Heden, A.A.P.A.M., and Aarden, L.A. Clin. Exp. Immunol., in press, (1987).

27. Nijsten, N.W.N., de Groot, E.R., Ten Duis, H.J., Klasen, H.J., Hack, C.E., and Arden, L.A. Lancet, ii:921, (1987).

28. Ramadori, G., Sipe, J.D., Dinarello, C.A., Mizel, S.B., and Colten, H.R. J. Exp. Med. 162:930, (1985).

29. Perlmutter, D.H., Goldberger, G., Dinarello, C.A., Mizel, S.B., and Colten, H.R. Science, 232:850, (1986).

30. Zucali, J.R., Dinarello, C.A., Oblon, D.J., Gross, M.A., Anderson, L., and Weiner, R.S. J. Clin. Invest. 77:1857, (1986).

31. Bagby, G.C., Dinarello, C.A., Wallace, P., Wagner, C., Hefeneider, S., and McCall, E. J. Clin. Invest., 78:1316, (1986).

32. Fibbe, W.E., Van Damme, J., Billiau, A., Voogt, P.J., Duinkerken, N., Kluck, P.M.C., and Falkenburg, J.H.F. Blood, 68:1316, (1986).

33. Lee, M. Segal, G.M., and Bagby, G.C. Exp. Hematol., 15:983, (1987).

34. Ikebuchi, K., Wong, G.G., Clark, S.C., Ihle, J.N., Hirai, Y., and Ogawa, M. Proc. Natl. Acad. Sci. USA, 84:9035, (1987).

35. Moore, M.A.S., and Warren, D.G. Proc. Natl. Acad. Sci. USA, 84:7134, (1987).

36. Mochizuki, D.Y., Eisenman, J.R., Conlon, P.G., Larsen, A.D., and Tushinski, R.J. Proc. Natl. Acad. Sci. USA, 84:5267, (1987).

37. Zsebo, K.M., Wypych, J., Yuschenkoff, V.N., Lu, H., Hunt, P., Dukes, P.P., and Langley, K.E. Blood, 71:962, (1988).

38. Ainsworth, E.J., and Chase, H.B. Proc. Soc. Exp. Biol. Med., 102:483, (1959).

39. Smith, W.W., Alderman, I.M., and Gillespie, R.F. Am. J. Physiol., 192:549, (1958).

40. Neta, R., Douches, S.D., and Oppenheim, J.J. J. Immunol., 136:2483, (1986).

Address reprint requests to:
Dr. Ruth Neta
Armed Forces Radiobiology Research Institute
Bethesda, MD 20814

Radiation-Induced Impairment of Neuronal Excitability

Radiation causes a decrease in the synaptically evoked activity of CA1 hippocampal pyramidal cells. This effect is dose and dose-rate dependent. Hydrogen peroxide, which produces hydroxyl free radicals when combined with FE^{+2}, produces similar damage. In contrast, the radioprotectant, dithiothreitol, increases the excitability of hippocampal neurons. These studies indicate that radiation can directly affect the function of central neurons.

INTRODUCTION

For the past thirty years, ionizing radiation has been known to acutely alter the electrical activity of the brain[1] as well as to produce behavioral deficits.[2] Recording from a variety of brain areas, the most striking change in electrical activity following X-radiation is the appearance of high frequency activity (spiking) in the hippocampus.[3,4] This appears within 30 minutes of exposure to 4 Gy whole body exposure and reaches a maximum after 5 to 7 hours. The spiking is sustained for almost 2 weeks.[3] Very little concomitant change in cortical activity is seen,[3,4] but the arousal threshold for the midbrain reticular formation decreases with approximately the same time course.[4] Evoked potential studies also show an alteration in brain activity following radiation exposure. Rosenthal and Timiras[5] observed that 2.5 Gy X-rays decreased the latency and reduced the size of evoked potentials in the olfactory cortex. Their observations led them to suggest that radiation reduced synaptic inhibition. Exposure to ionizing radiation tends to increase

Comments Toxicology 1988, Vol. 2, No. 4, pp. 253–263
Reprints available directly from the publisher
Photocopying permitted by license only

susceptibility to seizures. The frequency of audiogenic seizures in mice is enhanced following chronic exposure to low levels of radiation.[6] The threshold for electroconvulsive seizures is reduced in adult rats[7,8] after as little as 0.25 Gy X-irradiation.[7] Acute studies on the spinal cord of the cat[9–11] reveal that 5-50 Gy X-radiation enhances the spinal monosynaptic reflex, augments the intracellularly recorded excitatory postsynaptic potential but does not change the inhibitory postsynaptic potential.[11,12] Single unit studies in olfactory cortex[13] and in hippocampus[14] show a change in patterns of action potential generation, predominantly a depression of spontaneous and evoked activity.

Nervous system damage produced by radiation *in vivo*, as in the studies described above, is likely to be influenced by systemic effects. Exposure to ionizing radiation is accompanied by decreased blood pressure and reduced blood flow in a variety of brain regions[15–17] including the hippocampus.[18] The decrease in brain blood flow is likely to produce ischemic damage, especially in the hippocampus which is a particularly vulnerable area.[19,20] Ischemia, produced by a transient occlusion of the arterial blood supply, causes an increase in potassium and a decrease in calcium concentrations in the extracellular neuronal environment.[20] Simultaneously, neuronal activity is inhibited. Seven hours after an ischemic episode of this kind, spontaneous action potentials appear much more frequently than normal in the hippocampus but not in the cortex.[20,21] Reperfusion following ischemia is thought to produce excessive free radicals that could exacerbate the damage caused directly by radiation.[22,23]

Because the blood brain barrier is disrupted by ionizing radiation,[24,25] radiation-released mediators[26] as well as normal plasma constituents may have abnormal access to neurons. Levels of histamine, prostaglandins, β-endorphins, and neurotensin as well as other compounds are elevated by ionizing radiation.[18,26,27] Histamine is a powerful neuromodulator that increases the excitability of hippocampal neurons.[28–30] While prostaglandins do not directly alter the excitability of hippocampal pyramidal cells,[31] they may have actions in other areas of the central nervous system or even indirect actions on the metabolic or glial activity.[32] Many of the other radiation-released mediators also are known to be neuromodulators. In understanding the changes of neuronal

excitability that occur with exposure to ionizing radiation, one cannot ignore the influence of these circulating factors which can affect both neurons and glial cells. The neuronal environment is finely tuned. A disruption of this environment, as caused by an altered blood brain barrier, is likely to produce abnormal neuronal activity.

APPROACH

Analysis of the effects of radiation on the nervous system is very complex. Are the changes due to ischemia? Are they caused by higher than normal concentrations of histamine or prostaglandins? Or is radiation acting direclty on neurons in their local environment? Since radiation-induced neuronal death occurs only at doses greater than 100 Gy, classically, neurons have not been considered radiation sensitive.[32] Most of the nervous system damage has been attributed to glial cell death and vascular damage.[33,34] This analysis, however, fails to consider the complex physiological functions of neurons that are likely to be impaired by radiation and free radical attack of membrane lipids and proteins.

To study the damage produced by radiation without the complicating factors caused by systemic injury, hippocampal brain slices were used as an experimental model.[35–37] Not only has previous literature indicated a particular sensitivity of this brain region to radiation, but this model provides a complex network of neurons, accessible to analysis, that allows assessment of integrated neuronal function. Because of the laminar structure of the hippocampus, organization of the tissue is maintained in a thin slice (400–500 μm). The input and output pathways to the CA1 region can be clearly identified and selectively stimulated with metal bipolar electrodes (0.02-2 mA). Glass microelectrodes are used to record the evoked activity from the population of neurons in a defined cell body layer (orthodromic population spike, top of Fig. 1) and simultaneously from the corresponding dendritic region (dendritic response, bottom Fig. 1). Analysis of radiation- and drug-induced changes in the somatic and dendritic recordings can provide information on the efficacy of synaptic transmission (synaptic damage) and the ability of the synaptic potential to generate an action

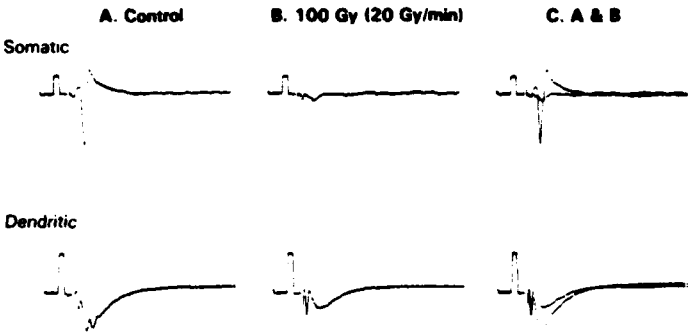

FIGURE 1 Effects of γ-radiation (100 Gy at 20 Gy/min) on population spike (somatic) and population synaptic response (dendritic) of CA1 neurons of guinea pig hippocampus. A: Recordings from a sham-irradiated slice. B: Recordings from an exposed slice. C: Superimposition of A and B. Square wave preceding all traces is a calibration pulse of 1 mV, 2 ms.

potential (postsynaptic damage). Slices can be studied before, during, and after application of radioprotectants and free radical producing agents. Radiation damage can only be tested in our system by comparing paired exposed and control slices some time after ^{60}Co radiation and sham radiation.

RADIATION DAMAGE IN AN ISOLATED NEURONAL SYSTEM

Gamma radiation (^{60}Co) can cause both synaptic and postsynaptic damage in hippocampal brain slices. The orthodromic population spike is greatly reduced by exposure. The dendritic response, the summated synaptic potential, also is decreased (Fig. 1). The decrease in the population spike is not proportionate to the decrease in the dendritic response. Even when the stimulus intensity is increased sufficiently to elicit a dendritic response in the irradiation slice comparable to that in the control slice, the resulting population spike is smaller. This indicates that while synaptic function is impaired, postsynaptic damage also is present. In contrast, however, even very high doses (200 Gy) do not alter the antidromically evoked spike. The damage to the orthodromic spike, therefore, is

not to the action potential *per se* but rather to the synaptic generation of the action potential.

The effects of radiation are dose and dose-rate dependent (Fig. 2). Increasing the dose increases the damage to the orthodromic population spike. Likewise, increasing the dose rate increases the damage to the orthodromic population spike. A dose rate of 20 Gy/min shifts to the left the dose response curve for radiation at 5 Gy/min. At 5 Gy/min, significant deficits are seen only at 75 Gy and greater. At the higher dose rate, the damage caused by 50 Gy radiation is significantly greater than at the lower dose rate. Synaptic damage and postsynaptic damage differ in their dose-rate dependence. Impairment of synaptic efficacy is more severe at higher dose rates. At 5 Gy/min it significantly contributes to the damage only at doses of 150 Gy and greater. At 20 Gy/min, however, synaptic damage is significant at 75 Gy. This dose-rate dependence suggests the existence of repair mechanisms. Lipid peroxidation, which varies inversely with dose rate, is an unlikely mechanism for synaptic damage. Impairment of postsynaptic spike generation, however, is not dose-rate dependent. It makes a significant contribution to the population spike damage at doses of 75 Gy and above, regardless of dose rate. Because of the distinction from synaptic damage, postsynaptic damage is likely to result from a different molecular mechanism.

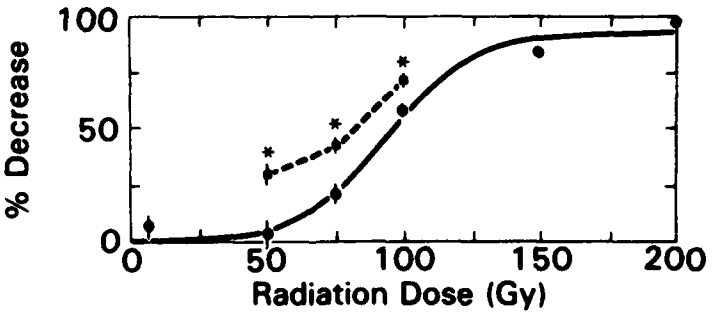

FIGURE 2 Dose response curve of effect of γ-radiation on the population spike recorded from the CA1 region of hippocampal slices. Solid line (Circles) shows effect of radiation at 5 Gy/min while dashed line (squares) shows effects of radiation at 20 Gy/min. Asterisks indicate that the effects of the two dose rates are significantly different from one another.

PEROXIDE MODEL OF FREE RADICAL DAMAGE

In an *in vitro* system, free radicals are likely to mediate the damage caused by ionizing radiation. Hydrogen peroxide or peroxide with ferrous ions can be used as a model system to generate the very reactive, hydroxyl free radicals through the Fenton reaction. Damage produced can be compared with radiation damage. Peroxide and peroxide/iron produce very similar deficits to ionizing radiation (Fig. 4A). Both synaptic efficacy and postsynaptic action potential generation are impaired following exposure to peroxide.[35] Figure

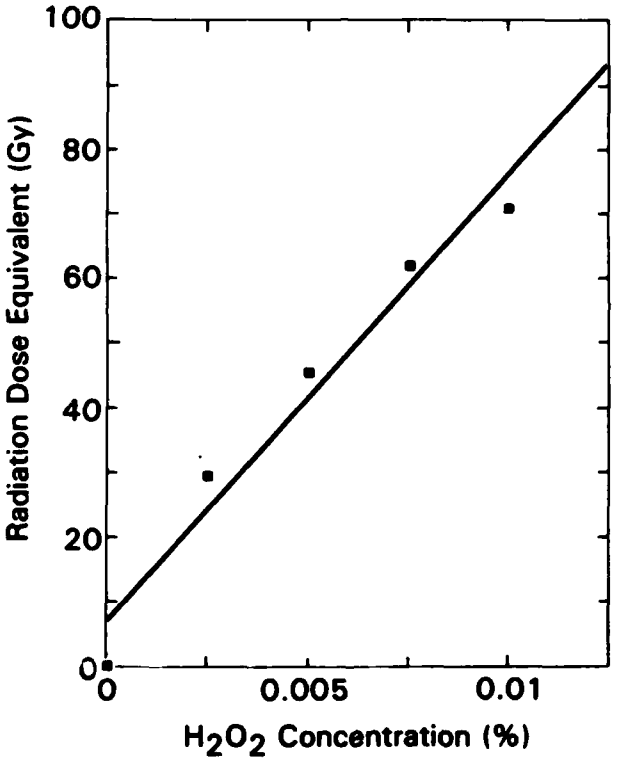

FIGURE 3 Radiation dose equivalent for peroxide damage. Concentration of hydrogen peroxide that causes a decrease in the orthodromic population spike is plotted against the radiation dose at 5 Gy/min required to elicit a similar deficit. Straight line is computer fit by linear regression.

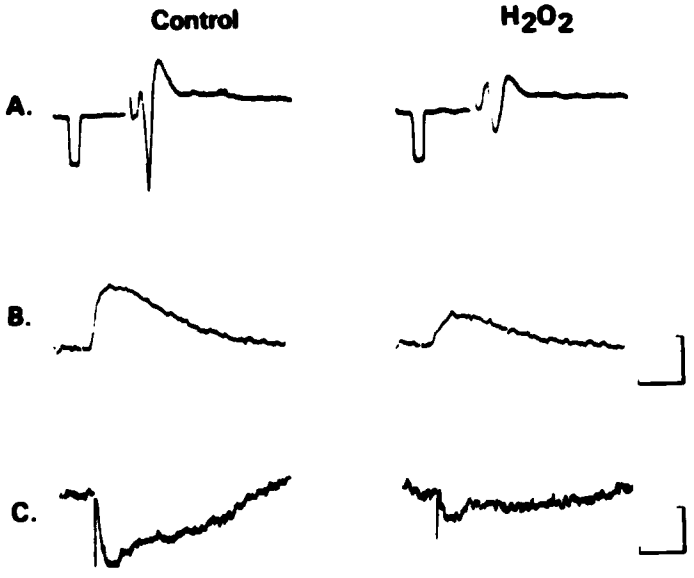

FIGURE 4 Effects of hydrogen peroxide (0.01%) on CA1 pyramidal cells of the hippocampus. A: Peroxide causes a decrease in the orthodromic population spike. Preceding calibration pulse is 1 mV, 2ms. B: Excitatory postsynaptic potential recorded intracellularly from pyramidal cell is reduced by peroxide. Calibration: 10 mV, 10 ms. C: Antidromic inhibitory postsynaptic potential is reduced by peroxide. Calibration 1 mV, 100 ms.

3 shows a curve relating peroxide concentration to a radiation dose producing similar degree of damage. A concentration of 0.005% (1.8 mM) produces the same decrease in the orthodromic population spike as approximately 45 Gy γ radiation at 5 Gy/min. The distinction should be made that peroxide damage is evaluated during exposure while radiation damage is evaluated at least 15 minutes following exposure. Peroxide damage is, at least with the lower doses, reversible. Within a half hour of removal, the effects of 0.005% peroxide or less are not functionally apparent. Higher doses of peroxide do produce decreases in the population spike that are not completely reversible within the experimental time frame. With this in mind, the peroxidative damage may actually be equivalent to much lower radiation doses.

An intracellular analysis[38] is possible using the peroxide model

for generation of free radicals. As predicted by field potential experiments, intracellularly recorded synaptic potentials are reduced by peroxide (Fig. 4B, C). Both the excitatory postsynaptic potential and the inhibitory postsynaptic potential are attenuated by peroxide. This does not result from a change in membrane resistance or membrane potential; neither is significantly affected by peroxide. Directly evoked action potentials are not altered. However, the neurons cannot sustain a train of action potentials as well as in control; that is, spike frequency adaptation is increased by exposure to peroxide.[38]

ACTIONS OF A RADIOPROTECTANT

Dithiothreitol (DTT) is a sulfhydryl reducing agent that acts as a radioprotectant.[39,40] It was tested in the hippocampal brain slice in the hope of finding an antagonist to radiation and peroxide damage. DTT has direct effects on the neural tissue.[37] Interestingly, it appears to produce damage that is the inverse of that caused by peroxide and radiation. The orthodromic population spike is increased in amplitude following a 30-minute exposure to 500 μM DTT (Fig. 5A). In addition, DTT causes the appearance of additional spikes in the field potential suggesting abnormal repetitive firing of the cells following exposure to the radioprotectant. Spontaneous burst firing also appears.[37] Analysis of the dendritic and somatic field potential recordings suggests that the synaptic potentials become much more efficient in eliciting spikes. Intracellular recordings[41] reveal that the excitatory postsynaptic potential is prolonged but the inhibitory postsynaptic potential is unaffected by DTT (Fig. 5B,C). Excitatory inputs, that normally produce only one action potential, evoke a train of spikes following exposure to DTT. Membrane resistance is not significantly altered, but membrane potential is slightly (2-8 mV) depolarized. In contrast to peroxide, DTT reduces spike frequency adaptation; the cells are more capable of sustaining a train of action potentials.

It is likely that the damage caused by DTT is a consequence of its sulfhydryl reducing properties since the oxidized form of DTT is without similar effects.[37] The hydroxyl free radical is a strong oxidizing agent and both peroxidative and radiation damage might be a consequence of oxidation of membrane constituents. Al-

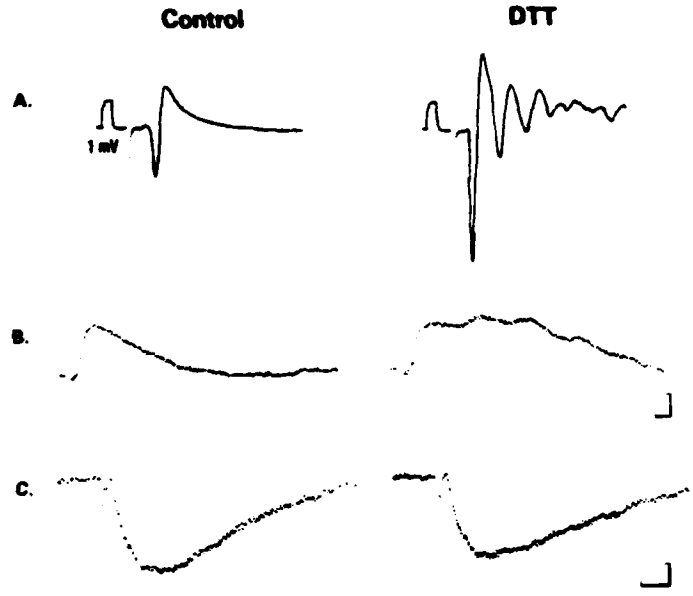

FIGURE 5 Effect of 30-minute exposure to dithiothreitol (500 μM) in CA1 neurons of hippocampus. A: DTT increases the amplitude of the population spike and elicits multiple peaks in the extracellularly recorded somatic potential. Calibration pulse preceding trace is 1 mV, 2 ms. B: Intracellularly recorded excitatory postsynaptic potential is prolonged following DTT treatment. Calibration: 2 mV, 4 ms. C: Inhibitory postsynaptic potential is unaffected by DTT. Calibration: 1 mV, 25 ms.

though DTT might not be a drug of choice to protect against radiation damage, it might be valuable as a tool to reverse the effects of free radical attack. The feasibility of this possibility needs to be further evaluated experimentally.

CONCLUSIONS

Nervous system damage caused by ionizing radiation is quite complex. Electrical activity in the brain is disrupted *in vivo* by doses as low as 200 rads. The experimental deficits described here, although experimentally elicited with higher doses, are likely to contribute to this nervous system damage. Only very slight changes

in neural properties are sufficient to disrupt the intricately balanced neuronal networks of the brain. *In vivo* the damage is compounded by ischemia and radiation-released mediators. Repair mechanisms, which *in vitro* might be adequate to functionally restore neurons, might be rendered inadequate *in vivo*. In evaluating the effects of radiation on the central nervous system, it is important to recognize the variety of contributing factors; not only is the environment changing due to altered blood flow and a damaged blood brain barrier, neuronal excitability is altered.

Disclaimer

Views presented in this paper are those of the authors; no endorsement by the Defense Nuclear Agency has been given or should be inferred. Research was conducted according to the principles enunciated in the "Guide for the Care and Use of Laboratory Animals" prepared by the Institute of Laboratory Animal Resources, National Research Council.

Acknowledgments

Supported by the Armed Forces Radiobiology Research Institute, Defense Nuclear Agency, under work unit 00105.

T. C. PELLMAR, Ph.D.
J. M. TOLLIVER, Ph.D.
K. L. NEEL, B.S.

Physiology Department
Armed Forces Radiobiology Research Institute
Bethesda, Maryland 20814-5145

References

1. D. J. Kimeldorf and E. L. Hunt, *Ionizing Radiation: Neural Function and Behavior* (Academic Press, New York, 1965).
2. V. Bogo, Comments Toxicol. **4**, 265 (1988).
3. H. Gangloff, *Effects of Ionizing Radiation on the Nervous System*, (Int. Atomic Energy Agency, Vienna, 1962) pp. 123–135.
4. T. J. Haley, *Effects of Ionizing Radiation on the Nervous System*, (Int. Atomic Energy Agency, Vienna, 1962) pp. 171–185.
5. F. Rosenthal and P. S. Timiras, Am. J. Physiol. **204**, 63 (1963).
6. D. S. Miller, *Response of the Nervous System to Ionizing Radiation. First International Symposium*, eds. T. J. Haley and R. S. Snider (Academic Press, New York, 1962) pp. 513–531.

7. T. Pollack and P. S. Timiras, Radiat. Res. **21**, 111 (1964).
8. N. M. Sherwood, G. P. Welch and P. S. Timiras, Radiat. Res. **30** 374 (1967).
9. J. R. Lott, *Effects of Ionizing Radiation on the Nervous System.* (Int. Atomic Energy Agency, Vienna, 1962) pp. 85–92.
10. M. Sato, G. M. Austin and W. R. Stahl, *Response of the Nervous System to Ionizing Radiation. First International Symposium*, eds. T. J. Haley and R. S. Snider (Academic Press, New York, 1962) pp. 561–571.
11. M. Sato, Adv. in Radiat. Biol. **7**, 181 (1978).
12. M. Sato and G. Austin, *Response of the Nervous System to Ionizing Radiation, Second International Symposium*, eds. T. J. Haley and R. S. Snider, (Little Brown and Company, Boston, 1964), pp. 279–289.
13. G. P. Cooper and D. J. Kimeldorf, Radiat. Res. **27**, 75 (1966).
14. M. H. Bassant and L. Court, Radiat. Res. **75**, 593 (1978).
15. P. H. Chapman and R. J. Young, Radiat. Res. **35**, 78 (1968).
16. L. G. Cockerham, T. J. Cervany and J. D. Hampton, Aviat. Space Environ. Med. **57**, 578 (1986).
17. R. Hawkins, Comments Toxicol. **4**, 243 (1988).
18. L. G. Cockerham, E. L. Pautler and J. D. Hampton, Federation Proc. **44**, 1357 (1985).
19. T. Kirino, Brain Res. **239**, 57 (1982).
20. R. Suzuki, T. Yamaguchi, Y. Inaba and H. G. Wagner, Prog. Brain Res. **63** 59 (1985).
21. R. Suzuki, T. Yamaguchi, C. L. Li and I. Klatzo, Acta Neuropathol. (Berl.) **60**, 217 (1983).
22. H. B. Demopoulos, E. Flamm, M. Seligman and D. D. Pietronigro, *Pathology of Oxygen*, (Academic Press, New York, 1982) pp. 127–155.
23. S. Rehncrona, B.K. Siesjo and D. S. Smith, Acta Physiol. Scand. Suppl. **492**, 135–140 (1980).
24. T. W. Griffin, J. S. Rasey and W. A. Bleyer, Cancer **40**, 1109 (1977).
25. T. Schettler and C. N. Shealy, J. Neurosurg. **32**, 89–94 (1970).
26. M. Donlon, Comments Toxicol. **4**, 205 (1988).
27. A. Dubois, Comments Toxicol. **4**, 233 (1988).
28. H. L. Haas and A. Konnerth, Nature (Lond.) **302**, 432 (1983).
29. T. C. Pellmar, J. Neurophysiol. **55**, 727 (1986).
30. M. Segal, Neurosci. Lett. **19**, 67 (1980).
31. J. E. Warnick and T. C. Pellmar, Neurosci. Lett. **70**, 295 (1986).
32. L. S. Wolfe, Adv. Neurochem. **1**, 1 (1975).
33. J. W. Hopewell, Neuropathol. Appl. Neurobiol. **5**, 329 (1979).
34. A. J. van der Kogel, Br. J. Cancer **53**, Suppl VII, 207 (1986).
35. T. C. Pellmar, Brain Res. **364**, 377 (1986).
36. T. C. Pellmar and J. M. Tolliver, *Conference on Brain Slices: Fundamentals, applications and implications*, in press (1987).
37. J. M. Tolliver and T. C. Pellmar, Brain Res. **404**, 133 (1987).
38. T. C. Pellmar, Soc. Neurosci. Abstr. **11**, 1003 (1985).
39. K. D. Held, Radiat. Res. **101**, 424 (1985).
40. J. L. Redpath, Radiat. Res. **55**, 109 (1973).
41. J. M. Tolliver and T. C. Pellmar, Soc. Neurosci. Abstr. **12**, 676 (1986).

Exp. Hematol. 16:752–757 (1988)

Experimental Hematology

Recovery of Hematopoietic Colony-forming Cells in Irradiated Mice Pretreated with Interleukin 1 (IL-1)*

Gretchen N. Schwartz, Ruth Neta, Roy M. Vigneulle, Myra L. Patchen, and Thomas J. MacVittie

Experimental Hematology Department, Armed Forces Radiobiology Research Institute, Navy Medical Command, National Capital Region, Bethesda, Maryland, USA

(Received 4 January 1988; in revised form 24 March 1988; accepted 18 April 1988)

Abstract. Data in this report determined the effect of a single injection of recombinant interleukin 1α(rIL-1) prior to irradiation of B6D2F1 mice on the recovery of colony-forming cells (CFC) at early and late times after sublethal and lethal doses of radiation. Injection of rIL-1 promoted an earlier recovery of mature cells in the blood and CFC in the bone marrow and spleen. For example, 8 days after 6.5 Gy irradiation, the number of CFU-E (colony-forming units–erythroid), BFU-E (burst-forming units–erythroid), and GM-CFC (granulocyte–macrophage colony-forming cells) per femur was approximately 1.5-fold higher in rIL-1-injected mice than in saline-injected mice. Also, 5, 9, and 12 days after irradiation, the number of both day 8 and day 12 CFU-S (colony-forming units–spleen) was almost twofold greater in bone marrow from rIL-1-injected mice. The earlier recovery of CFU-S in rIL-1-injected mice was not associated with an increase in the number of CFU-S that survived immediately after irradiation. Also, 7 months after irradiation, the number of CFU-S per femur of both saline- and rIL-1-injected mice was still <50% of normal values. Data in this report demonstrate that a single injection of rIL-1 prior to irradiation accelerates early hematopoietic recovery in irradiated mice, but does not prevent expression of radiation-induced front-end damage or long-term damage to hematopoietic tissues.

Key words: Interleukin 1α(IL-1) — Hematopoietic recovery — Colony-forming units–spleen (CFU-S) — Granulocyte–macrophage colony-forming cells (GM-CFC) — Burst-forming units–erythroid (BFU-E)

A variety of inflammatory and immunoenhancing agents administered to mice prior to irradiation increase the number of animals that survive after lethal irradiation [1–6]. For example, the radiation dose at which 50% of the mice die within 30 days (i.e., LD50/30 radiation dose) was increased by 1.0 to 3.0 Gy when agents such as bacterial endotoxins (lipopolysaccharide [LPS]) or glucans were injected 18–24 h prior to irradiation [1, 2, 5, 6]. The increase in survival was associated with an earlier recovery of mature cells in the peripheral blood [4, 5, 7, 8] and hematopoietic colony-forming cells (CFC) in the bone marrow and spleen [8–11]. The physiological mechanisms promoting the earlier recovery of CFC and mature cells in these mice are not well understood.

Macrophages are one of the primary cellular targets of inflammatory and immunoenhancing agents that are radioprotective for mice [3]. Splenic, lymph node, and peritoneal macrophages release interleukin 1 (IL-1) when stimulated in vitro, with LPS [12–14], and expression of mRNA for IL-1 was demonstrated to be maximal from 4 to 20 h after activation [12, 13]. In vivo, IL-1 activity has been detected in the plasma within 1 h after injection of LPS [15]. Recently, Neta et al. [16, 17] demonstrated that a single injection of murine or human recombinant IL-1-alpha (rIL-1) increased survival in lethally irradiated mice. Administration of rIL-1 to mice 20 h prior to their exposure to gamma radiation increased the LD50/30 radiation dose by 1.0 to 1.9 Gy [16–20].

Previous studies demonstrated that rIL-1 injection before irradiation increased the number of endogenous colony-forming units–spleen (ECFU-S) in irradiated mice [20]. However, an increase in the number of ECFU-S is not always associated with earlier bone marrow recovery or increased survival [2, 3, 5, 8]. Studies in the present report were done to determine the effect of rIL-1 injection prior to irradiation on the early and late recovery of hematopoietic colony-forming cells in B6D2F1 mice. In these studies, a single injection of rIL-1 to mice 20 h prior to lethal doses of irradiation increased the number of mice that survived beyond 30 days and promoted an earlier recovery of BFU-E (burst-forming units–erythroid) in the bone marrow. Also, rIL-1 injection before sublethal irradiation accelerated early recovery of cells in the peripheral blood and CFU-S (colony-forming units–spleen), BFU-E, CFU-E (colony-forming units–erythroid), and GM-CFC (granulocyte–macrophage colony-forming cells) in the bone marrow. However, the earlier recovery of CFU-S in rIL-1-injected mice was not associated with an increase in the number of CFU-S surviving immediately after irradiation.

Materials and methods

Mice. B6D2F1, or (C57Bl/6J × DBA/2)F1, female mice were purchased from Jackson Laboratories, Bar Harbor, Maine, and housed five to ten mice per cage. Animals were maintained on a 12-h light/

*Views presented in this paper are those of the authors; no endorsement by the Defense Nuclear Agency has been given or should be inferred.

Address reprint requests to: Dr. Gretchen N. Schwartz, American Red Cross, Department of Transplantation, Biomedical Research and Development, The Jerome H. Holland Laboratory, 15601 Crabbs Branch Way, Rockville, MD 20855, USA.

Table 1. Survival of irradiated mice pretreated with saline or rIL-1

Calculation	Radiation dose[a]	
	9.5 Gy (*n*)[b]	10.5 Gy (*n*)[b]
	% Surviving >30 days	
Saline	65 ± 13.0 (70)	7 ± 13.1 (105)
rIL-1	100 ± 0.0 (40)	85 ± 7.1 (50)
	Mean survival time (survival <30 days)	
Saline	13 ± 4.5 (12)	13 ± 2.7 (20)
rIL-1	None died (40)	16 ± 4.1 (40)

Female mice B6D2F1 12–16 weeks old administered 0.5 ml saline or 150 ng rIL-1 20 h prior to irradiation.
[a] Cobalt-60 radiation at a dose rate of 0.40 Gy/min.
[b] Total number of mice from three studies.

dark cycle and were allowed food (Wayne Rodent Blox) and HCl acidified water (pH 2.4) ad libitum. Mice 12–16 weeks old were used for these studies. Research was conducted according to the principles enunciated in the "Guide for the Care and Use of Laboratory Animals" prepared by the Institute of Laboratory Animals Resources, National Research Council.

Treatment with interleukin 1 (IL-1). Administration of 150 ng rIL-1 to mice 20 h before their exposure to gamma radiation was previously determined to be within the dose range for rIL-1-induced radioprotection [16, 17, 20]. Purified human recombinant IL-1 alpha (rIL-1), a generous gift from Dr. Steven Gillis of Immunex (Seattle, Washington), was used in these studies. The rIL-1 was supplied in a solution of phosphate-buffered saline at pH 7.2 with a specific activity of 7.5×10^6 U IL-1/mg protein, and aliquots were maintained at −70°C. Immediately before use, stock solutions of rIL-1 were diluted with pyrogen-free saline (McGaw), and 150 ng/0.5 ml was administered to normal mice by intraperitoneal injection 20 h before their irradiation. Control animals were administered 0.5 ml saline at the same time. Endotoxin (LPS) contamination in rIL-1 stock solutions was measured by the *Limulus* lysate assay. Based on these results <0.2 ng of LPS was administered per injection.

Irradiation. Mice were exposed bilaterally to gamma radiation at a dose rate of 0.40 Gy/min from a cobalt-60 radiation source and received total body doses of 1.0, 3.0, 5.0, 6.5, 9.5, or 10.5 Gy.

Hematopoietic colony-forming assays. Mice were sacrificed by cervical dislocation, and the femurs and spleens were excised. Cells were flushed from the tissues with Hanks' balanced salt solution (GIBCO) and dispersed through a 25-gauge needle until a single-cell suspension was obtained. Cell concentrations were determined by hemacytometer counts. Peripheral blood was obtained from orbital sinus using heparinized 75-μl capillary pipets.

CFU-S (colony-forming units–spleen) determinations were done basically as described by Till and McCulloch [21]. Recipient mice were exposed to 10.5 Gy radiation. This dose was sufficient to reduce background day-8 and day-12 macroscopic colonies to an average of < 1 per spleen. Cell suspensions were diluted to give 5×10^4 to 1×10^6 cells in 0.2–0.5ml media and injected into a caudal vein of each mouse. After 8 or 12 days, the spleens were removed, placed into Bouin's fixative, and the number of macroscopic colonies was counted.

CFU-E and BFU-E determinations were made using a plasma clot culture system as described by Weinberg et al. [22]. Cells were plated at a final concentration of 2×10^5 to 1×10^6 cells/ml with 0.25 U/ml (CFU-E) or 3.0 U/ml (BFU-E) anemic sheep plasma, step III erythropoietin (lot no. 3092-2; Connaught Laboratories) as 0.4-ml plasma clots in four-well Nunclone culture dishes (Nunc). CFU-E and BFU-E cultures were placed into a humidified 37°C incubator with 5% CO_2 for 2.5 days and 8 days, respectively. Cultures were then harvested, fixed, stained, and evaluated as described by McLeod et al. [23].

GM-CFC (granulocyte–macrophage colony-forming cells) were assayed using the double layer agar technique basically as described by Hagan et al. [24]. The culture medium was double strength CMRL-1066 culture medium (Connaught Medical Research Laboratory) containing 10% (vol/vol) fetal calf serum, 5% (vol/vol) horse serum, 5% (wt/vol) trypticase soy broth, 20 g/ml L-asparagine, and penicillin–streptomycin. In the bottom layer of 35-mm plastic petri dishes was 1 ml of a 1:1 mixture of culture medium and 1.0% agar (Bactoagar; Difco) containing 50 μl PMUE (pregnant mouse uterine extract) as a source of colony-stimulating activity [25]. The top layer contained 1 ml of a 1:1 mixture of culture medium and 0.66% agar containing 5×10^4 to 5×10^6 cells for assay. Cultures were incubated at 37°C in 5% humidified CO_2 in air. After 10 days of culture, colonies >50 cells were scored as GM-CFC.

Table 2. Erythroid progenitor cells in bone marrow of mice 12 days after lethal irradiaton

Treatment[b]	% Normal values/femur[a]		
	Cells	CFU-E	BFU-E
9.5 Gy			
Saline	13 ± 6.1	21 ± 2.5	0 ± 0.0
rIL-1	50 ± 0.8[c]	44 ± 8.3[c]	77 ± 4.4[c]
10.5 Gy			
Saline	12 ± 1.6	21 ± 7.8	0 ± 0.0
rIL-1	17 ± 1.4[c]	35 ± 8.8	8 ± 0.7[c]

Female B6D2F1 mice 16 weeks old.
[a] Cells were pooled from both femurs of eight mice per group; values are mean ± SD of three studies.
[b] IP injection of saline or 150 ng rIL-1 20 h before exposure to cobalt-60 radiation at dose rate of 0.4 Gy/min.
[c] Significantly different from saline values ($p < 0.05$).

Statistics. Two-tailed Student's *t*-test was used to test for significant differences in colony-forming units and cells per tissue between groups of mice.

Results

Survival of irradiated mice pretreated with saline or rIL-1

The percentage of mice surviving beyond 30 days after irradiation was compared for rIL-1- and saline-injected mice (Table 1). The mean survival times of mice that died within 30 days were not significantly different for saline- or rIL-1-injected mice exposed to 9.5 or 10.5 Gy radiation. However, at lethal doses of radiation, more rIL-1-injected mice survived than saline-injected animals. For example, after 10.5 Gy irradiation, 93% of saline-injected mice died within 30 days, whereas only 15% of the rIL-1-injected animals died.

Effect of rIL-1 on early recovery of CFC after lethal irradiation

After lethal irradiation, there was evidence of an earlier recovery of CFC in bone marrow from rIL-1-injected mice than in saline-injected mice (Table 2). Twelve days after 9.5 or 10.5 Gy irradiation, cellularity was <15% of normal, CFU-E were 21% of normal, and BFU-E were not detectable in bone marrow from saline-injected mice. These values were at least twofold higher in bone marrow from rIL-1-injected mice 12 days after 9.5 Gy irradiation. A smaller, but still significant increase in bone marrow cellularity and BFU-E content was observed in rIL-1-injected mice 12 days after 10.5 Gy irradiation.

Table 3. Recovery of in vitro colony-forming cells from saline- or rIL-1-injected mice after 6.5 Gy irradiation

Assay[a]	Normal (n)[b]	Day 4		Day 8	
		Saline-injected	rIL-1-injected	Saline-injected	rIL-1-injected
Number/femur					
Cells ($\times 10^6$)	13.2 ± 2.63 (15)	1.8 ± 0.60	2.8 ± 1.14	7.8 ± 1.64	12.0 ± 3.53[c]
CFU-E ($\times 10^3$)	29.7 ± 5.64 (6)	0.8 ± 0.64	2.0 ± 1.63	15.4 ± 2.91	23.9 ± 6.36[c]
BFU-E ($\times 10^2$)	12.6 ± 5.83 (9)	0 ± 0	0 ± 0	0.9 ± 0.58	2.3 ± 0.50[c]
GM-CFC ($\times 10^3$)	21.3 ± 4.00 (10)	0.4 ± 0.12	0.7 ± 0.11[c]	1.3 ± 0.22	2.2 ± 0.02[c]
Number/spleen					
Cells ($\times 10^7$)	12.8 ± 1.86 (13)	1.1 ± 0.43	1.1 ± 0.27	1.6 ± 0.40	1.9 ± 0.26
CFU-E ($\times 10^3$)	39.6 ± 3.60 (5)	0 ± 0	0 ± 0	0.2 ± 0.38	1.0 ± 0.98
GM-CFC ($\times 10^2$)	7.0 ± 2.00 (8)	0.1 ± 0.14	0.2 ± 0.23	0.2 ± 0.07	0.4 ± 0.18

Female mice B6D2F1 12–16 weeks old exposed to cobalt-60 radiation (0.40 Gy/min) 20 h after injection of saline or 150 ng rIL-1.
[a] Cells were pooled from both femurs and the spleens of five mice per group in each study.
[b] Number of studies; values are the mean ± SD of mean values from three studies at day 4 and four studies at day 8.
[c] Values are significantly different from saline-injected mice at $p \leq 0.05$.

Table 4. Survival of day-8 and day-12 CFU-S 2 h after irradiation of saline- or rIL-1-injected mice

Radiation dose (Gy)	Day-8 CFU-S/femur ($\times 10^3$)[a]		Day-12 CFU-S/Femur ($\times 10^3$)[a]	
	Saline	rIL-1	Saline	rIL-1
1.0	1.5 ± 0.29	1.1 ± 0.12	3.7 ± 0.93	2.4 ± 0.81
1.0	1.5 ± 0.41	1.4 ± 0.59	2.5 ± 0.54	2.2 ± 0.82
3.0	0.2 ± 0.07	0.2 ± 0.04	0.3 ± 0.05	0.3 ± 0.09
5.0	0.02 ± 0.01	0.02 ± 0.01	0.05 ± 0.07	0.04 ± 0.01

Female B6D2F1 mice 12–16 weeks old were administered 150 ng rIL-1 20 h prior to their irradiation. Two hours after irradiation, cells from both femurs of three mice were pooled per group.
[a] CFU-S/femur were calculated from mean ± SD of the number of colonies from five spleens per group.

Effect of rIL-1 on early recovery of CFC after sublethal irradiation

After 6.5 Gy irradiation, 100% of both saline- and rIL-1-injected mice survived beyond 30 days. However, as early as 5 days after irradiation, the number of nucleated cells/mm^3 blood was more than twofold greater in rIL-1-injected mice (1330 ± 363 for $n = 3$) than in saline-injected mice (333 ± 115 for $n = 3$). In addition, 8 days after irradiation, bone marrow cellularity and the number of CFU-E, BFU-E, and GM-CFC per femur was approximately 1.5-fold higher in rIL-1-injected mice than in saline-injected mice (Table 3). No significant differences were observed in splenic cellularity and CFU-E and GM-CFC content from saline- and rIL-1-injected mice at these early time points after 6.5 Gy irradiation. Also, 5, 9, and 12 days after 6.5 Gy, the number of day-8 CFU-S (data not shown) and day-12 CFU-S (fig. 1) was twofold greater in bone marrow from rIL-1-injected mice than from saline-injected mice. These results demonstrate that rIL-1 injection prior to irradiation accelerated hematopoietic recovery in lethally (Table 2) and sublethally irradiated mice.

Effect of rIL-1 on survival of CFU-S after irradiation

The number of day-8 and day-12 CFU-S surviving "front-end" damage after irradiation was determined 2 h after irradiation of saline- and rIL-1-injected mice (Table 4). The number of CFU-S that survived decreased with increasing radiation dose from approximately 33% of normal after 1.0 Gy to 0.4% normal after 5.0 Gy. However, there was no significant difference in the number of CFU-S after irradiation of saline- or rIL-1-injected mice. In these studies rIL-1 injection did not increase the number of CFU-S that survived early after irradiation.

Effect of rIL-1 on late recovery of CFC in irradiated mice

Bone marrow cellularity and CFC content were determined for saline- and rIL-1-injected mice surviving 1.5 months after 9.5 or 10.5 Gy irradiation (Table 5). There was no significant difference ($p > 0.05$) in the number of cells, CFU-E, BFU-E, or GM-CFC per femur of saline- and rIL-1-injected mice. Bone marrow cellularity and CFC content were still <60% of normal values (Table 3) for both saline- and rIL-1-injected mice 1.5 months after lethal doses of radiation.

Seven months after lethal or sublethal doses of radiation, the number of day-8 CFU-S per femur of both the surviving saline- and rIL-1-injected mice was significantly lower than in age-matched nonirradiated animals (Table 6). For mice that received 6.5 Gy radiation, there was no significant difference in the number of CFU-S between saline- and rIL-1-injected mice. In these mice, the number of day-8 CFU-S per femur had recovered to approximately 40% of nonirradiated controls. These results demonstrate that a single injection of rIL-1 prior to irradiation did not promote a recovery of day-8 CFU-S to normal values.

Table 5. Effect of rIL-1 injection on recovery of colony-forming cells in mice surviving 1.5 months after irradiaton

Assay	9.5 Gy		10.5 Gy	
	Saline-injected	rIL-1-injected	Saline-injected	rIL-1-injected
Number/femur[a,b]				
Cells ($\times 10^6$)	5.6 ± 1.63	7.1 ± 0.99	8.4 ± 2.67	7.0 ± 0.70
CFU-E ($\times 10^3$)	14.9 ± 1.77	14.4 ± 1.41	11.1 ± 6.71	7.2 ± 2.18
BFU-E ($\times 10^2$)	ND[c]	ND	5.0 ± 3.00	3.7 ± 2.31
GM-CFC ($\times 10^3$)	ND	12.0 ± 0.99	4.1 ± 0.37	3.4 ± 0.25

Female B6D2F1 mice 12–16 weeks old were administered 150 ng rIL-1 20 h prior to irradiation.
[a] Cells were pooled from both femurs of three to five mice per group.
[b] Values represent mean ± SD of mean values from two groups for 9.5 Gy and four groups for 10.5 Gy.
[c] No data.

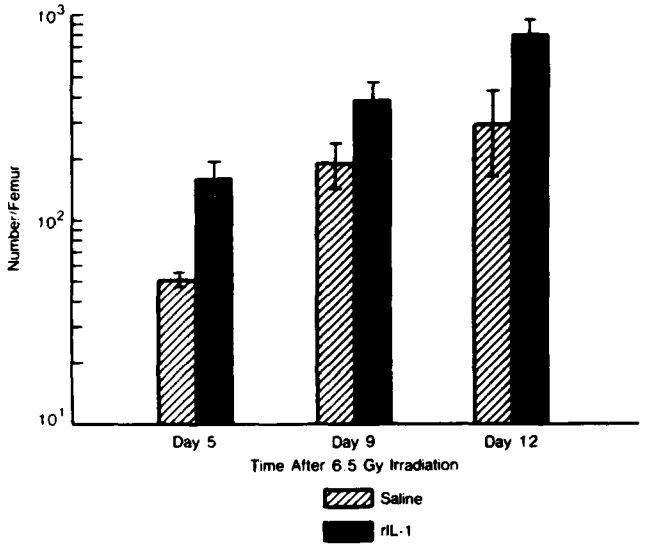

Fig. 1. Recovery of day-12 CFU-S in mice irradiated after saline or rIL-1 injection. Mice were administered 150 ng rIL-1 20 h prior to their exposure to 6.5 Gy gamma radiation. Cells were pooled from both femurs of five mice per group, and the number of CFU-S per femur was determined. Values represent the mean ± SD of colonies from five spleens per group. The number of day-12 CFU-S/femur of nonirradiated mice was 5.3 ± 1.1 ($\times 10^3$) for $n = 8$ groups.

Table 6. Recovery of day-8 CFU-S in bone marrow from saline- or rIL-1-injected mice surviving 7–8 months after irradiaton

Treatment	Number/femur ($\times 10^3$)[a]
Saline + 6.5 Gy	1.4 ± 0.39[c]
rIL-1 + 6.5 Gy	1.0 ± 0.37[c]
rIL-1 + 9.5 Gy	0.9 ± 0.11[c]
rIL-1 + 10.5 Gy	0.8 ± 0.29[c]
Normal[b]	3.2 ± 0.27

Female B6D2F1 mice 12–16 weeks old were administered 150 ng rIL-1 20 h prior to irradiation.
[a] Cells from both femurs of three to five mice were pooled per group; mean ± SD of mean values from five mice per group; two studies per group for 9.5 and 10.5 Gy and one study per group for 6.5 Gy.
[b] Normal mice were age-matched nontreated controls.
[c] Values are significantly different from normal mice at $p < 0.05$.

Discussion

Data presented in this report confirm that rIL-1 injection promoted an earlier recovery of CFU-E and BFU-E in lethally and sublethally irradiated B6D2F1 mice when administered 20 h prior to their irradiation. An earlier recovery was also observed for GM-CFC, day-8 CFU-S, and day-12 CFU-S. Results in this report further demonstrate that the earlier recovery of CFC observed in rIL-1-injected mice was not due to an increase in the number of day-8 or day-12 CFU-S that survived early damage after irradiation. Also, 7 months after irradiation, day-8 CFU-S had not returned to normal values in either saline- or rIL-1-injected mice.

Other studies have reported normal bone marrow and peripheral blood cellularity in mice within 3 to 4 weeks after irradiation [6, 26, 27]. However, those studies and others also demonstrated that the number of GM-CFC [28] and CFU-S [26–30] was still below normal as long as 1 year after irradiation. This inability to recover to normal levels is thought to be due to long-term damage to tissues of the hematopoietic microenvironment and/or damage to the hematopoietic stem cell compartments [27, 28]. A slower recovery of normal hematopoiesis in response to an additional stress such as irradiation, bleeding, or chemotherapy has been reported for animals in which complete recovery of the progenitor and stem cell compartments has not occurred [31, 32]. In the present report, rIL-1 injection accelerated early hematopoietic recovery in irradiated mice. However, 1.5 to 8 months after irradiation, CFC were still below normal values for both saline- and rIL-1-injected mice. The present studies demonstrate that rIL-1 injection did not prevent the expression of radiation-induced long-term damage to hematopoietic tissues. A similar lack of protection from long-term irradiation damage has been reported for endotoxin-injected mice [28].

In the present studies, within 5 days after 6.5 Gy there were twofold more CFU-S per femur from rIL-1-injected mice than from saline-injected mice. However, the number of CFU-S 2 h after irradiation was not significantly different for either group of mice. In preliminary studies ($n = 2$), there was no significant difference in seeding efficiency of day-8 CFU-S from nonirradiated mice 20 h after saline injection (2.3 ± 0.64) or rIL-1 injection (2.4 ± 0.57). These studies demonstrate that the earlier recovery of CFU-S in rIL-1-injected mice was not associated with an increase in the number of CFU-S surviving "front-end" damage by radiation. Similar results have been reported after sublethal irradiation of endotoxin injected mice [1, 11]. In those studies, the recovery of CFU-S in endotoxin injected mice was ap-

proximately 2 days earlier than for control mice and was not associated with an increase in the number of CFU-S that survived "front-end" damage by radiation.

In normal mice, CFU-S represent a population of slowly proliferating cells [33, 34], and only approximately 10% of CFU-S are in S-phase of the cell cycle. The proportion of proliferating CFU-S is significantly increased in regenerating bone marrow [35, 36]. However, CFU-S are recruited into cell cycle only after a delay of 14–16 h after irradiation [35]. Possible mechanisms for the earlier recovery of CFC after irradiation may be that IL-1 injection, or IL-1 induced by endotoxin injection, initiates DNA synthesis sooner or decreases the cell cycle time of CFU-S early after irradiation. Dinarello [15] proposed that many of the biological activities, including effects in cell proliferation assays, of IL-1 may be the result of IL-1 acting like a calcium ionophore. Others have demonstrated that CFU-S were rapidly stimulated into cell cycle in vitro by calcium ionophore A-23187 and other conditions that increased the intracellular influx of Ca^{2+} [37]. Thus, after IL-1 injection intracellular Ca^{2+} levels may be increased sufficiently to initiate DNA synthesis of noncycling populations of CFU-S early after irradiation.

An increased sensitivity of CFC to hematopoietic stimulatory factors may be another mechanism by which IL-1 injection enhances hematopoietic recovery in irradiated mice. Recent reports demonstrated that IL-1 is equivalent to hemopoietin 1 [38] and acts as a synergistic factor with CSF-1 or IL-3 to support the growth of colonies derived from more immature CFC [38–40]. One mechanism proposed for the synergistic activity of IL-1 with CSF-1 is that IL-1 directly or indirectly upregulates the receptors for CSF-1 on CFC, thus CFC become more responsive to lower levels of CSF-1 [38]. Recently, IL-6 was reported to act synergistically with IL-3 in supporting the growth of multipotential CFC from 5-FU-treated mice, and was found to be more effective than IL-1 [40]. In vivo and in vitro, rIL-1 induces the production of colony-stimulating activity for in vitro CFC [17, 41] and may also induce the production of IL-6 [40]. The production of a variety of hematopoietic stimulatory factors induced by IL-1 may be one mechanism for the earlier hematopoietic recovery observed after irradiation of rIL-1-injected mice. The results in the present report suggest that the effects of rIL-1 and other cytokines induced by rIL-1 injection on cell cycle kinetics of CFU-S are important in determining the radiation sensitivity and the recovery of irradiated stem cell populations.

Acknowledgments

We are grateful to Mr. Michael White, Ms. Rita Hardy, Ms. Susan Douches, and Mr. Richard Brandenburg for their excellent technical assistance and to Dr. Douglas Dooley and Dr. Charles L. Dorian for their editorial assistance.

References

1. Ainsworth EJ, Larsen RM (1969) Colony-forming units and survival of irradiated mice treated with AET or endotoxin. Radiat Res 40:149
2. Hanks GE, Ainsworth EJ (1967) Endotoxin protection and colony-forming units. Radiat Res 32:367
3. Patchen ML (1987) Use of Glucan-P and sixteen other immunopharmaceutical agents in prevention of acute radiation injury. Comments on Toxicology (in press)
4. Patchen ML, MacVittie TJ (1986) Comparative effects of soluble and particulate glucans on survival in irradiated mice. J Biol Response Mod 5:45
5. Smith WW, Brecker G, Budd RA, Fred S (1966) Effects of bacterial endotoxin on the occurrence of spleen colonies in irradiated mice. Radiat Res 27:369
6. Storer JB (1966) Acute responses to ionizing radiation. In: Green EM (ed) Biology of the laboratory mouse. New York: McGraw Hill, p 427
7. Smith WW, Maston RQ, Cornfield J (1959) Patterns of hemopoietic recovery in irradiated mice. Blood 14:737
8. Boggs SS, Boggs DR, Joyce RA (1980) Response to endotoxin of endotoxin-"resistant" C3H/HeJ mice: a model for study of hematopoietic control. Blood 55:444
9. Boggs SS, Boggs DR (1975) Earlier onset of hematopoietic differentiation after expansion of the endogenous stem cell pool. Radiat Res 63:165
10. Patchen ML, MacVittie TJ, Wathen LM (1984) Effects of pre- and post-irradiation glucan treatment on pluripotent stem cells, granulocyte, macrophage and erythroid progenitor cells and hemopoietic stromal cells. Experientia 40:1240
11. Smith WW, Brecker G, Fred S, Budd RA (1969) Effect of endotoxin on the kinetics of hemopoietic colony-forming cells in irradiated mice. Radiat Res 27:710
12. Fuhlbrigge RC, Chaplin DD, Kiely JM, Unanue ER (1987) Regulation of interleukin-1 gene expression by adherence and lipopolysaccharide. J Immunol 138:3799
13. Koide S, Steinman RM (1987) Induction of murine interleukin 1: stimuli and responsive primary cells. Proc Natl Acad Sci (USA) 84:3802
14. Mastro AM, Bortner DM, Pishak SA (1986) DNA synthesis and production of interleukin 1 by lymph node macrophages in culture. J Leukocyte Biol 39:63
15. Dinarello C (1984) Interleukin-1. Rev Infect Dis 6:51
16. Neta R, Douches S, Oppenheim JJ (1986) Interleukin-1 is a radioprotector. J Immunol 136:2483
17. Neta R, Vogel SN, Oppenheim JJ, Douches SD (1986) Cytokines in radioprotection: comparison of radioprotective effects of IL-1 to IL-2, GM-CSF, and INF. Lymphokine Res 5[Suppl]: S105
18. Schwartz GN, MacVittie TJ, Vigneulle RM, Patchen ML, Douches SD, Oppenheim JJ, Neta R (1987) Enhanced hematopoietic recovery in irradiated mice pretreated with interleukin-1 (IL-1). Immunopharm & Immunotox 9:371
19. Schwartz GN, MacVittie TJ, Hagan MP, Vigneulle RM, Douches SD, Neta R (1987) Early hematopoietic recovery in irradiated mice pretreated with interleukin-1 (IL-1). Proc Eighth Int Cong Radiat Res 1:282
20. Neta R, Oppenheim JJ, Douches SD, Giclas PC, Imbro RJ, Karin M (1986) Radioprotection with IL-1: comparison with other cytokines. Prog IMM VI:900
21. Till JE, McCulloch EA (1961) A direct measurement of the radiation sensitivity of normal bone marrow cells. Radiat Res 14:213
22. Weinberg SR, McCarthy EG, MacVittie TJ, Baum SJ (1981) Effect of low-dose irradiation on pregnant mouse haemopoiesis. Br J Haematol 48:127
23. McLeod DL, Shreeve MM, Axelrad AA (1974) Improved plasma system for production of erythrocytic colonies in vitro: quantitative assay method for CFU-E. Blood 44:517
24. Hagan MP, MacVittie TJ, Dodgen DP (1985) Cell kinetics of GM-CFC in steady state. Exp Hematol 13:532
25. Bradley TR, Stanley ER, Sumner MA (1971) Factors from mouse tissues stimulating colony growth of mouse bone marrow cells in vitro. Aust J Exp Biol Med Sci 49:595
26. Imai Y, Nakao I (1987) In vivo radiosensitivity and recovery pattern of the hematopoietic precursor cells and stem cells in mouse bone narrow. Exp Hematol 15:890
27. Zuze W, Xueying J, Shiren S, Shaozhi T, Huihua X (1981) The nature of radiation damage of haemopoietic stem cells under continuous irradiation at low dose rate. Sci Sin 25:1743

28. Shoefield R, Dexter TM (1982) CFU-S repopulation after low dose whole body radiation. Radiat Res 89:607
29. Peterson HP, Wangenhein KH von, Feihendegen LE (1986) Persisting radiation effect on murine 7-day and 12-day CFU-S. Exp Hematol 14:776
30. Von Wangenhein KH, Peterson HP, Hubner GE, Feihendegen LE (1985) Long term residual radiation effect in the murine hematopoietic stem cell compartment. Ann NY Acad Sci 459: 221
31. Baum SJ, Alpen EL (1959) Residual injury induced in the erythropoietic system of the rat by periodic exposures to x-radiation. Radiat Res 11:844
32. Braunschweiger PG, Schenken LL, Schiffer LM (1980) Adriamycin induced delayed erythropoietic injury expressed following anemia stress. Cancer Res 40:2257
33. Lajtha LG, Pozzi LV, Schofield R, Fox M (1969) Kinetic properties of haemopoietic stem cells. Cell Tissue Kinet 2:39
34. Hagan MP, MacVittie TJ (1981) CFU-S kinetics observed in vivo by bromodeoxyuridine and near-uv light treatment. Exp Hematol 9:123
35. Necas E (1982) Stem cell (CFU-S) proliferation in sublethally irradiated mice. Cell Tissue Kinet 15:667
36. Silini G, Elli G, Siracusa G, Pozzi LV (1968) Repopulation of the bone marrow stem-cell compartment after irradiation. Cell Tissue Kinet 1:111
37. Gallien-Lartigue O (1976) Calcium and ionophore A-23187 as initiators of DNA replication in the pluripotent haemopoiesis stem cell. Cell Tissue Kinet 9:533
38. Mochizuki DY, Eisenman JR, Conlon PJ, Larsen AS, Tushinski RJ (1987) Interleukin 1 regulates hematopoietic activity, a role previously ascribed to hemopoietin 1. Proc Natl Acad Sci USA 84:5267
39. Gallicchio VA, Watts TD, DellaPuca R (1987) Synergistic action of recombinant-derived murine interleukin-1 on the augmentation of colony stimulating activity on murine granulocyte–macrophage hematopoietic stem cells in vitro. Exp Cell Biol 55:83
40. Ikebuchi K, Wong GG, Clark SC, Ihle JN, Hirais Y, Ogawa M (1987) Interleukin-6 enhancement of interleukin-3-dependent proliferation of multipotential hemopoietic progenitors. Proc Natl Acad Sci 84:9035
41. Zucali JR, Broxmeyer HE, Dinarello CA, Gross MA, Weiner RS (1987) Regulation of early human hematopoietic (BFU-E and CFU-GEMM) progenitor cells in vitro by interleukin 1-induced fibroblast-conditioned medium. Blood 69:33

In: Cellular Antioxidant Defense Mechanisms, Volume II. C. K. Chow, ed. CRC Press, Inc., Boca Raton, Florida, 1988.

Chapter 24

ANTIOXIDANT MECHANISMS IN RADIATION INJURY AND RADIOPROTECTION

Joseph F. Weiss and K. Sree Kumar

TABLE OF CONTENTS

I. INTRODUCTION — ENDOGENOUS FACTORS AFFECTING RADIOSENSITIVITY

Organisms have evolved in an oxygen-rich environment as well as under the influence of radiation, and mechanisms exist to protect against oxidative damage due to many processes including radiation exposure. Some of the factors[1-3] that influence sensitivity to ionizing radiation are listed in Table 1. The role of antioxidant mechanisms in radiation injury may be somewhat similar to those involved in other deleterious processes, such as chemical carcinogenesis, oxygen toxicity, phagocytosis, inflammation, DNA degradation, photooxidation, aging processes, lipid peroxidation, and drug toxicity, insofar as similar reactive oxygen species are involved in damaging molecular or cellular targets. Exposure to ionizing radiation involves some unique aspects compared to other types of injury or disease involving oxidative damage. These include the initial radiochemical events, the variability of the insult ranging from low-dose background radiation to high exposures involved in localized radiotherapy and potential nuclear accidents, and the type of pharmacologic intervention required to prevent or treat radiation injury. The target and level of radiation determines whether long-term effects (carcinogenesis, stimulation of the aging process, etc.) or short-term effects (cell killing, loss of function) will occur.

Oxygen is a very important factor in determining radiosensitivity because it enhances the damage to cellular components caused by ionizing radiation. Intrinsic radiosensitivity is dependent on DNA repair enzymes.[4] DNA repair in some organisms is inducible by treatment with chemicals, UV radiation, or ionizing radiation,[5] but it is beyond the scope of this review to consider specific DNA repair systems. Although mechanisms involved in UV irradiation damage may overlap ionizing radiation effects, this paper will emphasize chemical protection against damage by ionizing radiation and predominantly against the effects of photons (X- and γ-radiation). It is possible that free radicals and their products induced by ionizing radiation can interact with reactive oxygen species formed during normal processes, such as superoxide and H_2O_2 produced by phagocytic cells or during enzymatic processes (xanthine oxidase activity; enzymes involved in eicosanoid metabolism). Metals such as iron can promote free radical damage,[6] whereas some bound metals have radioprotectant potential, e.g., metallothionein[7] and ceruloplasmin.[8] There is increasing evidence that maintenance of the proper oxidation-reduction state of cells by the interconversion of the peptide sulfhydryl, glutathione (GSH), and its disulfide form (GSSG) is a factor in the modulation of cellular radiosensitivity.[9,10] Other protein and nonprotein sulfhydryls may also play a role both as targets of radiation damage and as protectors.[10,11] The maintenance of glutathione function involves an array of enzymes, including glutathione peroxidase. Other physiological antioxidants (vitamin E) and antioxidant enzymes are interrelated in their function of controlling oxidative processes.[12] This review concentrates on the role of oxygen, glutathione, and antioxidant enzymes in radiosensitivity and how exogenous chemicals interact with these endogenous factors.

II. RADIATION CHEMISTRY

A. Direct and Indirect Action of Radiation

The generation of free radical species as a result of radiation exposure has been discussed in detail,[1,13-15] and only a summary of these reactions in the context of radiation injury and protection is given here. It is generally believed that the most important radiation target is DNA, although it is not clear how the precise lesions are related to ultimate effects. Because of the possibility of other radiation targets and interaction of damaged molecules with normal constituents, this paper presents a broader view of radiation damage with respect to protection. The energy transfer from radiation to molecules results in a variety of physicochemical

Table 1
ENDOGENOUS FACTORS AFFECTING RADIOSENSITIVITY

Oxygen concentration
Genetic components: DNA repair enzymes, cell cycle
Structural components: membrane proteins and lipids
Factors for maintaining redox states: thiols (glutathione) and disulfides, pyridine nucleotides
Regulatory factors: cyclic nucleotides, arachidonic acid metabolites, lymphokines
Normal processes involving reactive oxygen species: immunologic processes, enzyme reactions and interconversions
Antioxidant enzymes: glutathione peroxidase, superoxide dismutase, catalase, other enzymes involved in glutathione and glucose metabolism
Nutritional Factors: vitamins E, A, and C
Antioxidant and Prooxidant metals: iron, zinc, copper, selenium, metal-containing proteins (storage and acute-phase proteins)
Physical factors: temperature

reactions at $<10^{-12}$ sec. When the radiation causes excitation or ionization of critical biomolecules (such as DNA, enzymes, or membrane constituents [TH]), resulting in the ultimate change in the cell or organism, it is called direct action.

$$\text{radiation} + TH \rightarrow T^{\cdot} + H^{+} + e^{-} \quad (1)$$

In indirect action, radiation damage is caused by free radicals ($R^{\cdot}$) produced initially by the interaction of radiation with intermediate molecules, primarily with water.

$$TH + R^{\cdot} \rightarrow T^{\cdot} \quad (2)$$

The radiation effects of X and γ-rays, which are commonly used in radiotherapy, are predominantly due to indirect action. Irradiation with high linear energy transfer (LET, energy transferred per unit length of the track), such as heavy ions and neutrons, results in radiation damage predominantly by direct action.[16,17] In this case, endogenous or exogenous protectors would have to compete with the early events (very unlikely) or repair the radical damage to the target molecule.

B. Radiolysis of Water, Reactions of Oxygen, and Time Scale of Events for Radioprotection

Pulse radiolysis studies have been useful in elucidating radiochemical mechanisms in relation to radiation protection by providing data on free radical yields, pathways, and rates of reactions.[18-20] The time scale of events is very important in the context of development of free radical scavengers as radioprotectors.[1]

The initial reactions of ionizing radiation in cells involve mainly the radiolysis of water with the formation of reactive species (Equations 3 to 7).

$$\text{radiation} + H_2O \rightarrow H_2O^{+} + e^{-} \quad (3)$$

$$H_2O^{+} + H_2O \rightarrow H_3O^{+} + {}^{\cdot}OH \quad (4)$$

$$H_2O + e^{-} \rightarrow H^{\cdot} + {}^{\cdot}OH \quad (5)$$

$${}^{\cdot}OH + {}^{\cdot}OH \rightarrow H_2O_2 \quad (6)$$

$$e^{-} + H_2O \rightarrow e^{-}_{aq} \quad \text{(hydrated electron)} \quad (7)$$

These reactions occur within a period of 10^{-16} to 10^{-10} sec, and the approximate yields at 10^{-8} sec of $^{\cdot}OH$, e^-_{aq}, $H^{\cdot}$, H_2O_2 and H_2 per 100 eV (G values) formed on the radiolysis of water are 2.6, 2.6, 0.6, 0.75, and 0.45, respectively.[18] Since cellular water contains oxygen, $O_2^{\cdot-}$ and $HO_2^{\cdot}$ are also formed.

$$O_2 + e^-_{aq} \rightarrow O_2^{\cdot-} \quad (8)$$

$$H^{\cdot} + O_2 \rightarrow HO_2^{\cdot} \quad (9)$$

Strictly speaking, some of the radicals formed can have either a reducing or oxidizing effect,[21] as can some scavengers. It is generally believed that the most damaging effect resulting from the radiolysis of water in cells is the action of the oxidizing radical $^{\cdot}OH$.[22,23]

$$TH + {}^{\cdot}OH \rightarrow T^{\cdot} + H_2O \quad (10)$$

The most efficient radioprotectors are reducing agents or have antioxidant potential. The target free radical ($T^{\cdot}$) formed in Reaction 10 can be either repaired or protected by endogenous protectors (such as GSH, vitamin E, vitamin C) or exogenous protectors (such as aminothiols or other sulfhydryls). Efficacy of protection would include proximity of the protective agents to the site of damage.

$$T^{\cdot} + RSH \rightarrow TH + RS^{\cdot} \quad (11)$$

In a competitive reaction, biomolecules can be damaged (sensitized) by oxygen ("fixation of damage"),[24] e.g., by the following reaction:

$$T^{\cdot} + O_2 \rightarrow TOO^{\cdot} \quad (12)$$

In addition to Reaction 8, superoxide can also be formed as follows:[25]

$$T^{\cdot} + O_2 \rightarrow T^{+} + O_2^{\cdot-} \quad (13)$$

The generation of oxygen free radicals initially on the radiolysis of water, during further reactions, and their interconversions (see also Section II.C., below) suggest that antioxidant enzymes (superoxide dismutase, catalase, glutathione peroxidase) might act over a period of time.

The interaction of target products with reactive oxygen species formed at a later time or evolved during normal cellular processes suggests the possibility of protection or repair at later times.[25]

$$TOO^{\cdot} + O_2^{\cdot-} + H^{+} \rightarrow TOOH + O_2 \quad (14)$$

Alternatively, peroxyl radicals such as the long-lived peroxyl radicals of DNA and polynucleotides may react with thiols to form hydroperoxides.[26]

$$TOO^{\cdot} + RSH \rightarrow TOOH + RS^{\cdot} \quad (15)$$

Hydroperoxides (DNAOOH or Lipid-OOH) formed in Reaction 14 or 15 could be repaired by GSH and glutathione peroxidase to obtain the hydroxylated product, an altered target (T-OH), which may undergo further enzymatic transformation.

$$TOOH + GSH \rightarrow TOH + GSSG \quad (16)$$

Singlet oxygen can also be formed[27] as a secondary product from TOO·.

$$2TOO^{\cdot} \rightarrow TOOT + {}^1O_2 \quad (17)$$

In this case, protection by singlet oxygen scavengers, e.g., carotene, may be effective. The suggestion that peroxyl radical reactions are important in defining the oxygen effect (increased cell damage in the presence of oxygen) can provide insights into the development of agents that modify radiosensitivity.[28]

From consideration of the above reactions, it is expected that ·OH scavengers present or administered before radiation exposure would be effective protectors. Similarly, compounds that would donate hydrogen for repair immediately after radiation damage (Reaction 11) would be effective. Although the postirradiation administration of free radical scavengers would not be expected to have much effect, evidence exists that this may occur to some extent and is probably related to modulation of later reactions. There is some evidence for protection against lethality of mice administered the following protectors after irradiation: sulfhydryl compounds (mercaptopropionylglycine,[29] dithiothreitol[30]), superoxide dismutase,[31] and β-carotene.[32] In vitro studies have also indicated protection against mutagenic effects by the postirradiation addition of superoxide dismutase[33] or 2-(3-aminopropylamino)ethanethiol (WR-1065).[34]

C. Effect of Metal Ions

Iron enhances the formation of ·OH from $O_2^{-}\cdot$ and H_2O_2 (formed during the radiolysis of water or subsequently through SOD catalysis) by the metal-catalyzed Haber-Weiss reaction[23] (Reaction 18). Metal ions may also interact with lipid or other hydroperoxides and catalyze the formation of other free radicals[1] (Reaction 19).

$$H_2O_2 + O_2^{-} \xrightarrow{Fe} {}^{\cdot}OH + O_2 + OH^{-} \quad (18)$$

$$TOOH \xrightarrow{Fe,\ Cu} TO^{\cdot} + OH^{-} \quad (19)$$

Figure 1 represents results of a typical experiment indicating the promoting effect of Fe. Radiation-induced lipid peroxidation of erythrocyte membranes, measured as pentane formation, can be enhanced by the presence of Fe^{2+} (ferrous ammonium sulfate) during irradiation. Pentane evolution was inhibited by scavengers of $O_2^{-}\cdot$ (SOD), H_2O_2 (catalase), or ·OH (benzoate). This supports the interrelationship of radiation-induced reactive oxygen species through the iron-catalyzed Haber-Weiss reaction with the formation of ·OH species. There was inhibition with the radioprotector WR-2721 present during irradiation, but less with its free sulfhydryl form (WR-1065), suggesting oxidation of this compound during irradiation. The promoting effect of Fe on radiation-induced lipid peroxidation was also demonstrated in vivo (Figure 2). An increase in pentane in the expired air of irradiated rats was observed 1 day after irradiation, and pentane evolution was much higher in rats pretreated with iron-dextran before irradiation. These data indicate that chelation of metals is a valid concept in radioprotection.

III. CHEMICAL MODIFICATION OF RADIATION EFFECTS

A. Oxygen Effect and Chemical Sensitization

After briefly considering the radiochemical events occurring during radiation exposure and the overall endogenous factors in cells defining radiosensitivity, we can consider further

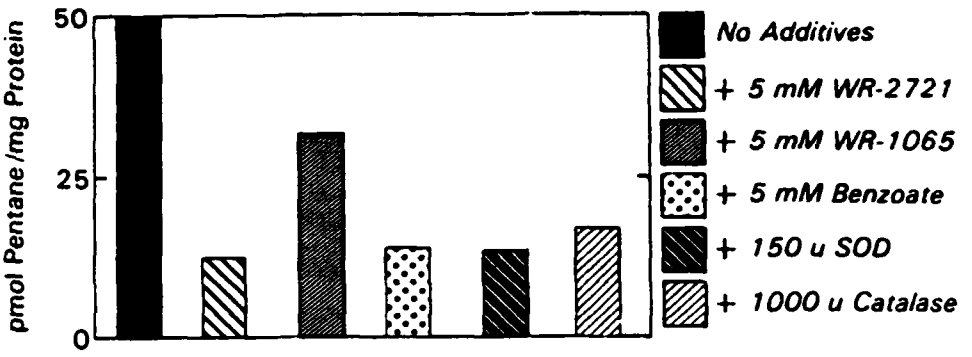

FIGURE 1. Effect of free radical scavengers on pentane evolution from irradiated erythrocyte membranes. Membranes were irradiated with 800 Gy cobalt-60 in presence of ferrous ammonium sulfate with and without scavengers. (Data obtained from References 35 and 36 and unpublished data.)

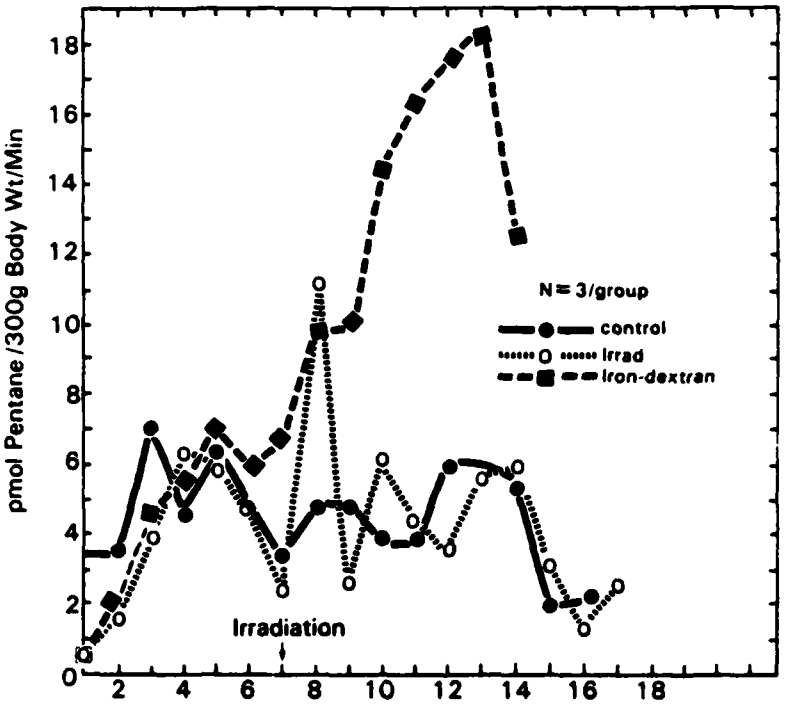

FIGURE 2. Effect of iron overload on pentane generation from irradiated rats. Rats were injected with iron dextran (300 mg/kg/day) for 7 days before irradiation with 10 Gy cobalt-60. Data obtained from Reference 36 and unpublished data.)

how specific chemicals modify radioprotective or sensitizing events. The major practical reason for studying radiosensitization by chemicals is to improve the efficacy of radiotherapy of tumors. Cell survival studies show the effect of oxygen in promoting cell kill during radiation exposure.[37,38] If the radiosensitivity of cells irradiated under anoxic conditions is assigned a value of 1, the radiosensitivity in oxygen for most cells varies between 2 and 3.5. The increase in radiosensitivity as the oxygen tension increases occurs from 0 to 30 mm of Hg, and further increases of oxygen content to that characteristic of air has little further effect. The oxygen enhancement ratio (OER) is defined as the ratio of absorbed doses

required to produce the same effect for irradiation in the absence and presence of oxygen. Much of the current research in radiobiology is based on the idea that human tumor cells in vivo are hypoxic. There are areas of necrosis and regions of hypoxia located away from the blood vessels as the source of oxygen supply. Tumor cells outgrow their blood supply, resulting in decreased availability of oxygen and become radioresistant. Increased radioresistance may also result from anaerobic metabolism, which increases the level of radioprotective-reducing equivalents. Selective sensitization of even a small fraction of hypoxic cells greatly improves treatment by increasing the therapeutic ratio of tumor cell killing to surrounding normal tissue damage. A number of ways have been proposed to overcome the hypoxia of tumor cells.[39] Intrinsically, the reoxygenation of tumor cells between fractionated radiation doses could have this effect. Extrinsic means that are potentially available in an attempt to reduce the total radiation dose to patients include the use of hyperbaric oxygen and oxygenated perfluorochemical emulsions. The use of high-LET radiation, as opposed to the more commonly used γ-irradiation, takes into account the fact that the oxygen effect is not reduced with high-LET radiation.[17] The most effort has been in the development and investigation of chemical radiosensitizers that mimic the oxygen effect. The prototype radiosensitizers, nitroimidazole derivatives, have been tested clinically with the main toxicity being peripheral and central nervous system neuropathies.

Proposed metabolic pathways of the most-studied sensitizer, misonidazole, 1-(2-nitro-1-imidazolyl)-3-methoxy-2-propanol, are shown below.[10] Misonidazole (RNO_2) is reduced by electron addition (RNO_2^-) and then is successively reduced under anoxic conditions (Reaction 20) or can react with oxygen (Reaction 21).

$$R\text{–}NO_2^- \xrightarrow[2H^+]{e^-} R\text{–}N{=}O \xrightarrow[H^+]{e^-} R\text{–}N^{\cdot}\text{–}OH \xrightarrow[H^+]{e^-} R\text{–}\underset{\displaystyle H}{\underset{|}{N}}\text{–}OH \qquad (20)$$

$$R\text{–}NO_2^- \xrightarrow{O_2} O_2^{\cdot-} \xrightarrow[2H^+]{e^-} H_2O_2 \qquad (21)$$

Studies on the complex interactions resulting from misonidazole metabolism have provided a basis for understanding the biochemistry of radiosensitization. In an anoxic situation (tumor cell), successive reduction steps by electron addition lead to intermediates which can conjugate with various molecules including DNA and GSH.[40,41] In hypoxic cells, misonidazole, in effect, substitutes for oxygen in fixing radiation damage by reacting with radicals of biomolecules, thereby sensitizing hypoxic cells.[42] Misonidazole itself is toxic to hypoxic cells, perhaps related to depletion of GSH and protein sulfhydryls.[10] In the presence of oxygen (Reaction 21), superoxide and hydrogen peroxide are by-products of oxygen reduction, which may be related to the toxicity of this compound.

B. Chemical Protectors

1. Drug Development

The study of radioprotectors in vitro and in vivo has also led to a better understanding of the fundamental mechanisms of radiosensitivity. The first in vivo report of protection by exogenous chemicals against ionizing radiation is generally credited to Patt et al.,[43] who found that cysteine could increase the survival of rats exposed to a lethal dose of X-rays. From that time, many classes of compounds have been studied as radioprotectors. The theories of radioprotection and the testing of different types of compounds have been examined in some excellent reviews[1,44-49] and will be discussed here only selectively. The most effective radioprotection has been by sulfhydryl derivatives administered shortly before

irradiation. It has been postulated that exogenous sulfhydryl compounds act by one or a combination of effects: scavenging radiation-induced free radicals directly before their reaction with biomolecules; interaction with cellular sulfhydryls (mixed disulfide hypothesis); metal scavenging, lowering oxygen tension; and hydrogen donation, which is currently the most prominent theory (Reaction 11). Some classes of nonsulfur compounds clearly act by inducing anoxia and therefore provide protection. Protection at the physiological or immunological level can also occur and may not be readily predicted by considering the radiochemical events. The early research programs in radioprotector synthesis and testing resulted in analogues of cysteine and mercaptoethanolamine (cysteamine) that proved to be too toxic. In the early 1950s, the Atomic Energy Commission initiated a program of radioprotector development, which led to the synthesis of AET (aminoethylisothiourea) and an increased understanding of the structural features of sulfur compounds which were important for protection. In 1959, the Antiradiation Drug Development Program was initiated by the U.S. Army Medical Research and Development Command, and approximately 4400 compounds were developed and tested from 1959 to 1973.[50] From this program, the prototype radioprotector was developed: WR-2721 or ethiofos, *S*-2-(3-aminopropylamino)ethylphosphorothioic acid. WR-2721 and related compounds are phosphorylated aminothiols, which were major improvements over earlier compounds in terms of potency, tolerance, and duration of action.[47] A new impetus for the study of radioprotective drugs came from the idea that tumor cells are less protected by WR-2721 than is normal tissue[51] (although a subject of controversy) and initial clinical studies on the use of WR-2721 as a radioprotector and chemoprotector.[52,53] Despite undesirable side effects observed in clinical[53] and animal studies,[54] WR-2721 remains the most effective chemical radioprotector. It is not yet clear whether other phosphorothioates with structural modifications will prove to be more useful than WR-2721 in terms of efficacy of preparations (oral vs. parenteral), preferential tissue protection, or effectiveness against different types of radiation (neutrons vs. gamma).[47,55-57]

2. End Points for Radioprotector Effects

In discussing chemical radioprotection, it is necessary to consider the various types of radiation injury.[58] The amount of radiation received by an experimental animal can be correlated with specific cell or tissue injury. The lowest amounts of whole-body radiation causing death (for mice approximately 6 to 9 Gy [600 to 900 rad]) results in hematopoietic death. Bone marrow cells are very sensitive targets, and their destruction leads to hematologic and immunologic impairment, with the death of mice not usually occurring before 1 week after exposure. In vivo radioprotection is most readily studied by determining the 30-day survival postirradiation (Figure 3), which indicates protection, for the most part, against hematopoietic injury, and to a lesser extent against gastrointestinal (GI) injury. Higher radiation doses result in GI death, which is more difficult to protect against, at times usually less than 1 week in mice. (One of the most effective nonsulfhydryl protectors against GI damage is 16,16-dimethyl prostaglandin E_2.)[59] Cellular end points also can be effectively used to evaluate radioprotective effects; these include protection against chromosomal aberrations[60] and survival of bone marrow and gut colony-forming units.[46] Little evidence exists for protection against CNS death, which occurs at high radiation doses, when chemicals are given systemically. Postirradiation decreases in cerebral blood flow (which may be related to behavioral effects caused by high radiation exposure to primates) can be partially alleviated by treatment with the mast-cell stabilizer disodium cromoglycate.[61] The possible free radical involvement in these events is suggested by the favorable effect of allopurinol, an inhibitor of xanthine oxidase-mediated superoxide formation, on the postirradiation decrease in regional cerebral blood flow in primates.[62]

The determination of 30-day survival at different radiation doses allows calculation of the dose reduction factor (DRF). The DRF is the ratio of (1) the dose of radiation needed to

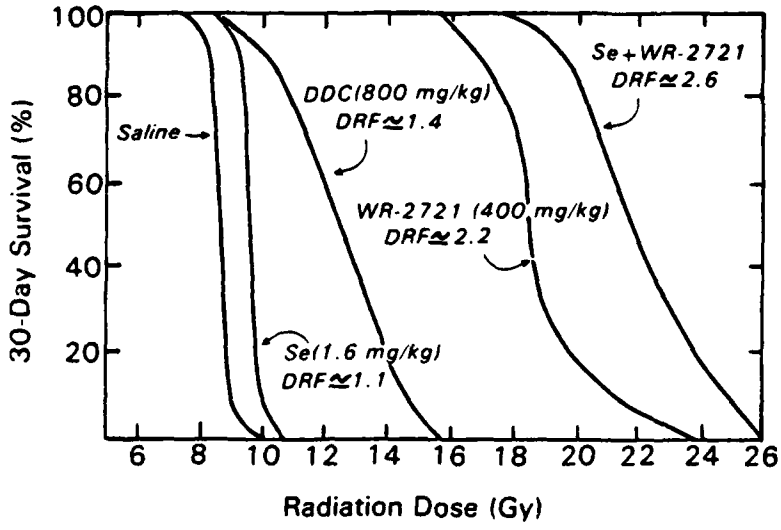

FIGURE 3. Survival curves of male CD2F1 mice treated with radioprotectors. WR-2721 or diethyldithiocarbamate (DDC) was given 30 min before irradiation, and sodium selenite (Se) was given 24 hr before irradiation. (Data obtained from References 63 and 64.)

have the same biological effect (usually 50% survival) with the drug to (2) the radiation dose without the drug. Calculation of the DRF allows comparison from laboratory to laboratory on the effects of potential radioprotectors, although it is not without difficulty, e.g., the use of different mouse strains can provide variable results. Survival studies are imperative since in vivo protection often differs from what would be expected from in vitro studies or radiochemical considerations. Figure 3 compares survival curves for WR-2721 with diethyldithiocarbamate (DDC) administered at equitoxic doses. Injection of selenium as sodium selenite (1.6 mg/kg) provides a small radioprotective effect, but when injected 24 hr before WR-2721, the combination increases the radioprotective effect of WR-2721 (pretreatment with Se also decreases the toxicity of WR-2721). This synergistic effect of Se and WR-2721, providing one of the highest DRFs reported in mice,[64] points out the possibility of combined radioprotector regimens. Increased radioprotection by combining agents has been shown previously using compounds with different major mechanisms of action.[65] Treatment with WR-2721 consistently gives a DRF of 2 or greater in mice in many different laboratories. Most other compounds, including sulfhydryl compounds such as DDC that are not structurally related to WR-2721, provide moderate protection, whereas a large number of treatments have been reported to provide a small amount of protection (DRF in the range of 1.2). One of the problems in comparing DRFs is that further evaluation of substances having small DRFs may not be attempted, although these compounds may have value in specific circumstances or may have low toxicity.

The effects of chemical modifiers may be complex. This is exemplified by the properties of DDC which are emphasized in this report. Even though DDC inhibits superoxide dismutase[66] and in some instances can act as a radiosensitizer,[67] it does provide overall protection against whole-body irradiation.

3. Immunological and Systemic Effects

Stimulation, as well as protection of the immunohematopoietic system, is an important aspect of radioprotection. The most attempted postirradiation treatment of whole-body irradiated patients and accident victims involves bone marrow transplantation, and in addition, other procedures for maintaining a supply of functional hematopoietic and lymphoid cells

are desirable. The use of biologic response modifiers to stimulate hematopoietic proliferation and differentiation and modulate immune responses is under intensive investigation in relation to treatment of various diseases and for use in conjunction with cytotoxic therapies. With respect to radioprotection, a modest increase in survival has been obtained with various "immunostimulants". Among these compounds, the most defined effects have been obtained for endotoxin,[68] the polysaccharide glucan[69] (probably the most radioprotective of the nonsulfhydryl immunomodulator class), and the lymphokine interleukin-1.[70] Typically, these compounds are most effective when injected into mice approximately 1 day before irradiation, suggesting that adequate time is needed for pluripotent hematopoietic stem cells to proliferate and differentiate into progenitor cells of the immune system. Injection of these substances also gives rise to a large variety of mediators and other immunomodifiers such as acute-phase proteins, arachidonic acid metabolites, and histamine. One aspect of radioprotection by interleukin-1 has been proposed[70] to be the induction of increased levels of metallothionein and the acute-phase protein ceruloplasmin, both of which have antioxidant and radioprotective potential.[7,8] Much remains to be determined about the radioprotective mechanisms of immunomodulators. For instance, recent experiments that appear to conflict with other studies have shown that glucan provides a DRF similar to sulfhydryl compounds when administered 15 min before irradiation.[71] Increasing evidence shows that the action of some immunomodulators involves the mediation or modulation of free radical processes, e.g., interferon, which also may have radioprotective effects,[72] induces xanthine oxidase.[73] The role of GSH in modulating immune responses is becoming established, as is the possibility that exogenous sulfhydryl immunomodulators, as well as nonsulfhydryl antioxidants, interact with GSH in immune cells.[74] The modest radioprotective effects of some nutritional factors (such as vitamins E, A, and C, zinc, and selenium) may involve to some extent the enhancement of immune responses, leading to an increased ability to control postirradiation pathogenic effects.[32,75,76] (The greatest DRFs reported for nutritional substances were provided by increased β-carotene or vitamin A in the diet, even when first administered after irradiation.)[32]

The systemic effects of radiation, which may be related to some long-term effects, are somewhat similar to those occurring in other types of traumatic injury or inflammatory processes. These include induction of acute-phase proteins, altered eicosanoid metabolism, increased histamine, altered trace metal metabolism, increased iron levels, and nutritional derangements. In a situation of prolonged low-level radiation exposure or other oxidative stress postirradiation, these changes would result in further modulation of deleterious effects, especially on the immune system.[77] Some sulfhydryl compounds have immunomodulatory effects, but is is not clear how this activity is related to their radioprotective activity. The main clinical and experimental studies of DDC involve stimulation of predominantly T cell-mediated responses.[78] Most of these effects are obtained at much lower concentrations than those required for protection against whole-body irradiation (Figure 3). The overall protection of immune status by potential radioprotectors has been estimated by measuring the effect on delayed-type hypersensitivity to oxazolone in mice irradiated with a sublethal dose of radiation[79] (Figure 4). Comparison of immunoprotection by WR-2721 and DDC given at equitoxic doses again shows a greater protective effect of WR-2721. The delayed-type hypersensitivity response represents a complex interaction of macrophages, lymphocytes, and lymphokines, but for the most part the protection obtained probably reflects protection of progenitor cells.[79] Comparison of immunoprotection against a sublethal dose of radiation and protection against a lethal dose by various sulfhydryl compounds is shown in Table 2. The drugs were administered in equitoxic doses, and a comparison is also given of their behavioral toxicities. It is seen that the most effective compound for one parameter is not always the preferred compound for another. In relation to toxicity, WR-2721 appears to be the most effective protector against lethal and sublethal irradiation.

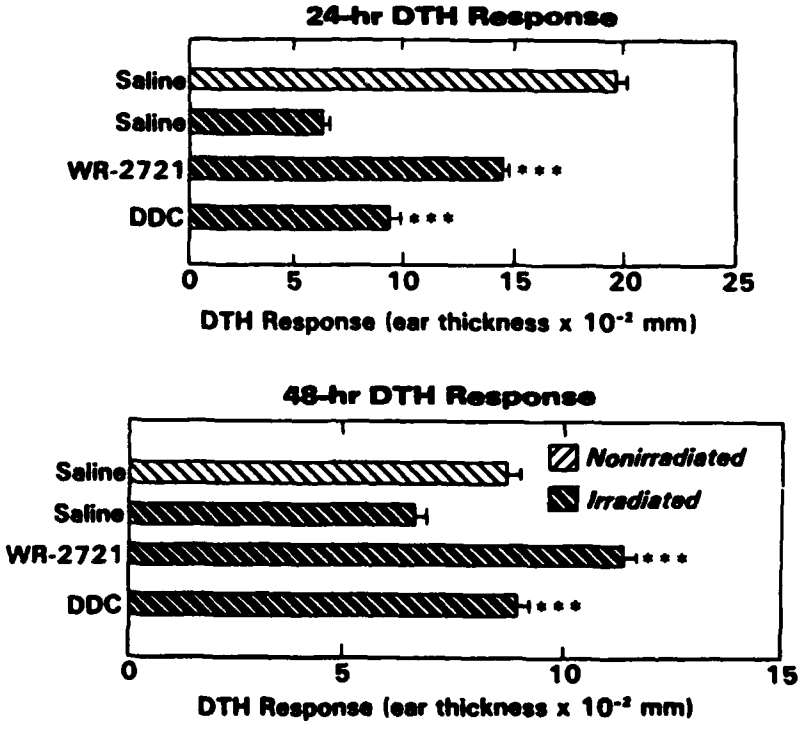

FIGURE 4. Effect of WR-2721 and DDC on delayed-type hypersensitivity in irradiated mice. Mice were sensitized to oxazolone 3 days before irradiation and challenged with oxazolone 2 days after irradiation (7 Gy cobalt-60). Drug treatment as in Figure 3. (Data obtained from Reference 63 and unpublished data.)

Table 2
TOXICITY AND RELATIVE RADIOPROTECTIVE EFFECTS OF SOME SULFHYDRYL COMPOUNDS IN MICE[80-82]

Survival after a Lethal Dose of Radiation[a]

Most effective — Least effective

WR-2721 ≥ DDC ≥ MEA > NAC > GSH

Immunoprotection to a Sublethal Dose of Radiation[b]

Most effective — Least effective

WR-2721 > MEA > NAC ≥ GSH > DDC

Behavioral Toxicity[c]

Least toxic — Most toxic

GSH ≥ NAC > WR-2721 ≥ MEA ≥ DDC

[a] 30-day survival of male CD2F1 mice exposed to 13 Gy cobalt-60 after i.p. injection of one half the LD_{10} dose of WR-2721 (400 mg/kg); DDC, diethyldithiocarbamate (800 mg/kg); MEA, cysteamine (200 mg/kg); NAC, *N*-acetylcysteine (1000 mg/kg); and GSH (1000 mg/kg).

[b] Delayed-type hypersensitivity to oxazolone determined in mice treated with one half the LD_{10} dose of the drugs injected before 7 Gy cobalt-60.

[c] Locomotor activity evaluated using an automated activity monitor after one quarter the LD_{10} dose of the drugs.

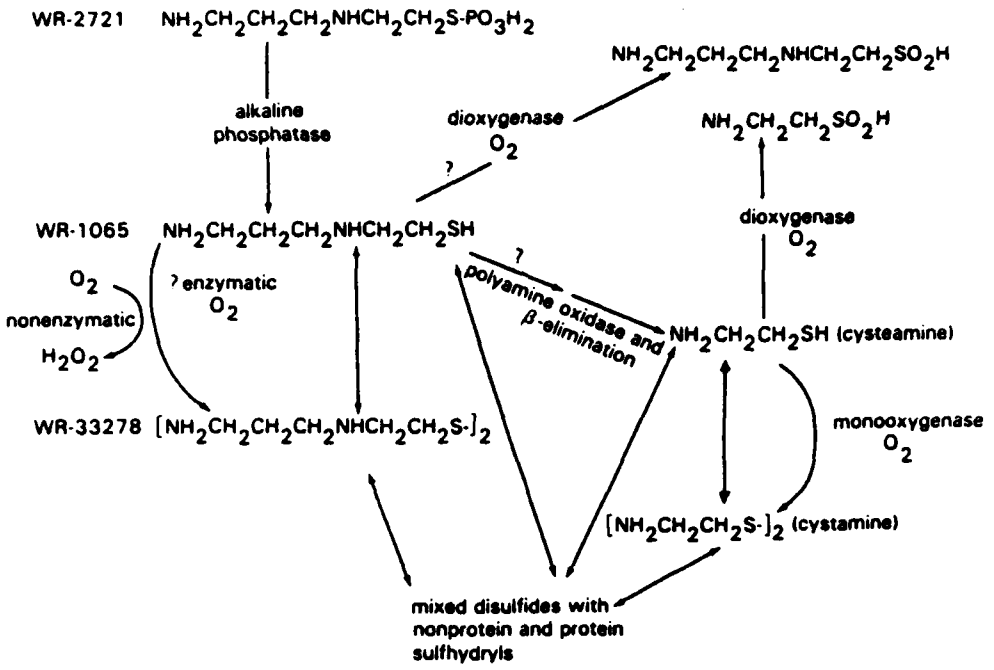

FIGURE 5. Proposed metabolic transformations of WR-2721.

Levamisole is a radioprotector of minimal efficacy which has been extensively studied as an immunostimulant.[83,84] We found that its main metabolite, a sulfhydryl derivative, OMPI, promoted microsomal lipid peroxidation induced by ADP-Fe or NADPH/ascorbate when present in low concentrations, but inhibited lipid peroxidation at higher concentrations.[85] Many immunomodulators have bimodal effects, and OMPI was also found to have a biphasic effect in its interaction with cellular microtubules.[86] The anomalous behavior of sulfhydryl compounds is suggested by in vitro studies or studies with cell-free systems, indicating H_2O_2 formation due to oxidation of the compounds or other prooxidant effects.[87] One might expect different pharmacologic effects of sulfhydryl compounds at different concentrations. At low concentrations, the overall effect might be determined by interaction with endogenous sulfhydryl groups; at higher concentrations, the cells would be flooded or overwhelmed with antioxidant sulfhydryl groups. The relation of pharmacologic effect to cellular concentration might be especially true for DDC, which has an immunostimulatory effect at very low levels[78] and either sensitizing or protecting effects at higher levels, dependeing on the endogenous milieu[67,88] (this is further discussed in Section V). The pharmacokinetics and activity of WR-2721 and related compounds can differ markedly from other sulfhydryl radioprotectors due to the fact that it is inactive until dephosphorylated at the cell membrane level or in the cell, which probably is a major factor in its relatively lower toxicity and increased radioprotective effect.[47]

4. Metabolism of WR-2721 and Effect of Oxygen on Sulfhydryl Radioprotection

Proposed metabolic pathways of WR-2721 based on various studies on the metabolism of thiol-containing radioprotectors[89-92] are shown in Figure 5. The pathways indicate the interaction of oxygen in the metabolism of this compound. After the sulfhydryl derivative WR-1065 is formed by the action of alkaline phosphatase, it can oxidize to the disulfide with H_2O_2 as a byproduct (a toxic side effect [?]). The WR-1065 or disulfide may interact with protein and nonprotein sulfhydryls to form mixed disulfides, and these interactions can

go back and forth until the drug is eventually eliminated. It is not clear whether WR-1065 can be metabolized in a similar fashion as cysteamine,[89] i.e., to a disulfide utilizing a monoxygenase or to a sulfinic acid compound utilizing a dioxygenase. The latter would not revert back to an active sulfhydryl compound. Evidence exists that WR-1065 is metabolized to cysteamine, a naturally-occurring aminothiol, through the action of a polyamine oxidase.[90,91] It is ironic that WR-2721, which was developed partly to replace toxic protectors such as cysteamine, may be metabolized to cysteamine as one of its active metabolites.

Whether the mechanism of radioprotection by WR-2721 is partially related to oxygen effects is under investigation and being debated. Purdie,[93] e.g., has concluded that oxygen consumption during the formation of the disulfide can induce local tissue hypoxia, which may be responsible for the early protection by WR-2721 or protection by lower concentrations of the drug. Only later would protection due to hydrogen transfer predominate. Also, selective tissue hypoxia probably occurs at the physiological level, since early work by Yuhas[94] indicated that splenomegaly was caused by WR-2721 in mice due to sequestration of red blood cells. In splenectomized mice, little protective effect was seen. In any case, the protective effect of WR-2721 in vivo has been shown to be influenced by oxygen tension. According to Denekamp et al.,[95] if oxygen and the sulfhydryl compounds are competing for repair and fixation of the initial radiation lesions, the most effective competition would occur in the region where the oxygen concentration was barely adequate for providing radiosensitization. In one of their studies,[96] epidermal cell survival was determined in irradiated mice treated with WR-2721 and irradiated in various concentrations of oxygen. No protection was seen in nitrogen, a large effect was seen in air, and a reduced effect in 100% oxygen. The maximum skin protection was observed in air-breathing animals, but it fell dramatically when the surrounding oxygen concentration was increased or decreased. Sensitization by misonidazole in the same type of experiment essentially showed a mirror image of protection by WR-2721, clearly demonstrating that both sensitization and protection are oxygen dependent.[95]

IV. ENDOGENOUS GLUTATHIONE, SENSITIZATION, AND PROTECTION

Glutathione (GSH) represents 90 to 95% of the total nonprotein sulfhydryls in cells, and as such it is believed to play an important role in the termination of the free radical reactions and oxidative processes that occur in radiation exposure.[9,10,97] Other nonprotein sulfhydryl compounds with potential radioprotective effects are cysteine, CoASH dipeptides, cysteamine, and their disulfide forms. GSH may have a unique role as a mobile and transient reservoir of sulfhydryl groups in organs such as liver, kidney, and blood, acting in detoxification mechanisms in relation to oxidative damage and xenobiotic metabolism.[98] GSH has the potential for scavenging radicals formed by ionizing radiation, e.g., $^{\cdot}OH$ and other free radicals, or by hydrogen transfer to altered (damaged) biomolecules (Equation 11 or 15). It has the ability to detoxify H_2O_2 nonenzymatically and H_2O_2 and other peroxides through the action of glutathione peroxidase[99] (see Section V). The sulfur-centered radicals formed due to the action of ionizing radiation have been extensively studied by pulse radiolysis.[48] One potential radical, $GSOO^{\cdot}$, may have importance in defining the interrelationship of GSH and the oxygen effect.[100] The alteration of GSH levels in cells is an effective method for determining the effects of potential treatment modalities involving GSH depletion. The GSH levels in tumor cell lines appear to have a large variation, and there is therapeutic potential for reducing GSH levels in radiation- and drug-resistant tumors as well as in relation to metabolism of some chemotherapeutic agents.[101] Figure 6 shows some possible means of altering GSH levels. Some reagents have been used for many years to accomplish this, such as diethylmaleate (DEM) and *N*-ethyl maleimide (NEM).[102] NEM acts rapidly with cellular thiols, including protein thiols, to form covalent adducts. However,

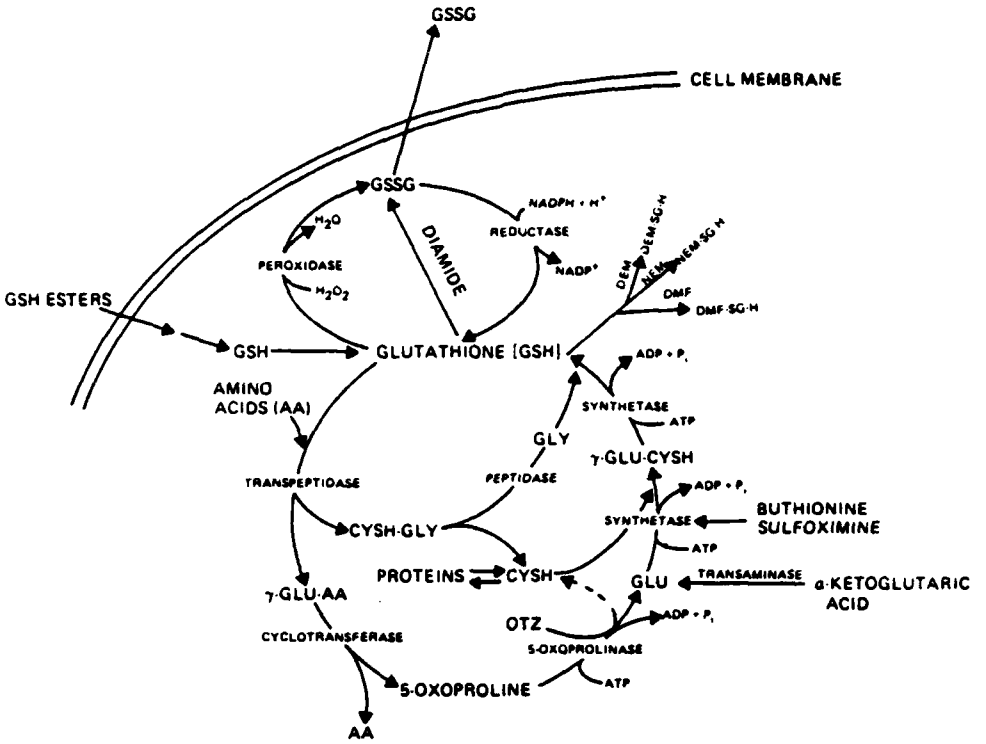

FIGURE 6. Chemical manipulation of glutathione levels in cells. DEM = diethylmaleate; NEM = *N*-ethylmaleimide; DMF = dimethylformamide; and OTZ = oxathiazolidine.

the high reactivity of NEM affords little specificity and results in considerable toxicity. DEM reacts similarly, but it is less reactive; again, it is not specific for GSH, and its effects are of short duration because the rate of GSH synthesis may increase sharply after depletion of GSH. Diamide is an oxidant resulting in the formation of GSSG. Although useful information has been obtained using this drug, the effects are generally short lived, being normally reversed within a few seconds unless the reductive capacity of the cell is suppressed. In general, the depletion of GSH, e.g., by DEM, results in greater sensitization of hypoxic cells.[103] Meister and co-workers[104] have developed reagents for the inhbition of GSH that are more specific for GSH depression. Buthionine sulfoximine (BSO) inhibits γ-glutamylcysteine synthetase so that glutathione synthesis cannot proceed and can lead to radiosensitivity,[104] especially in combination with nitroimidazole radiosensitizers.[105] The beneficial effects of combined BSO and radiosensitizer treatment are yet to be clearly shown in vivo, and the results may depend on the type of tumor and percentage of hypoxic cells.[106]

Another approach to the study of the role of GSH in radiosensitivity is the use of GSH-deficient cells such as human fibroblasts with a deficiency in GSH synthetase. Revesz and Edgren[107,108] have concluded from their studies that GSH participates in the oxygen effect. In deficient cells, GSH levels are about 6% of normal, although other nonprotein sulfhydryls, not clearly identified, are 50% of normal. For GSH-deficient cells, the hypoxic radiosensitivity (single-strand breaks and cell survival) is almost the same as the oxic radiosensitivity. The explanation for depressed oxygen effects in the absence of GSH is based on the competition hypothesis, wherein oxygen and aminothiols compete for radiation-induced radicals in key target molecules (see Equations 11 and 12). Somewhat similar conclusions were obtained when cells were irradiated hypoxically in the presence of misonidazole; only slight

sensitization of GSH-deficient cells was seen. Further studies with BSO-depleted normal cells led to the conclusion that GSH is rather specific in defining the enhancing effect of oxygen in cellular radiosensitivity, although not absolute, since other thiols could substitute.[109] The specificity might be due to some particular chemical properties or location of GSH at specific sites in the cell. Some practical aspects to glutathione depletion exist in relation to radiation exposure and combinations of injuries, since it is rather easy to depress GSH in some, but not all, cell types by fasting, aspirin, acetominophen, organophosphates, and other drugs.[110]

While evidence exists that GSH depletion potentiates radiosensitization, it is less clear whether increasing cellular levels of GSH result in radioprotection. For example, treatment with oxathiazolidine (OTZ) leads to increased GSH level in cells[111] (see scheme in Figure 6). When cultured cells were pretreated for 2 hr with OTZ, a dramatic increase in GSH was seen (230% of controls), but no radioprotective effects.[112] This implies that there may be a minimal level of GSH needed for radioprotection, e.g., in conjunction with GSH peroxidase.

GSH esters have been developed as a means of getting GSH into cells (Figure 6), and the monoethyl ester of GSH provided radioprotection to cultured human lymphoid cells that had been depleted of GSH with BSO.[113] Some protection also has been observed in HeLa cells irradiated under air by treatment with GSH monomethyl ester.[114] In BSO-treated cells, GSH ester, which increased the cellular GSH level by 40%, provided radioprotection under nitrogen.[114] Although some studies have indicated that cysteamine causes an increase in GSH levels in cells,[115] perhaps by displacement from mixed disulfides, no increase in GSH levels were observed in BSO-treated cells after cysteamine treatment. However, cysteamine protected cells irrespective of whether they were depleted of GSH or not, and protection was greater than for normal cells irradiated under nitrogen. This suggests that endogenous protective systems might be overwhelmed by efficient exogenous sulfhydryl protectors.[114]

V. ANTIOXIDANT ENZYMES

A. Peroxide Metabolism

Antioxidant enzymes are among the endogenous systems that are available for the removal/detoxification of reactive oxygen species and their products formed by the action of ionizing radiation. These are catalase, superoxide dismutase, glutathione peroxidase, other related enzymes involved in glutathione metabolism such as glutathione transferase and glutathione reductase, and enzymes involved in glucose metabolism that maintain NADPH levels. The interrelationship of hydrogen peroxide, catalase, and glutathione peroxidase with endogenous and exogenous redox systems in irradiated cells has been reviewed previously.[116] An integrated scheme of the reactions of antioxidant enzymes is shown in Figure 7. The levels of peroxides depend on the concerted action of these enzymes as well as the availability of reduced glutathione (GSH), which is a substrate for glutathione peroxidase and glutathione transferase. With transferase, GSH reacts with hydroperoxy fatty acids to form leukotrienes which play a major role in inflammatory and immunologic responses.[117] The reactions catalyzed by the antioxidant enzymes mentioned above are the following:

Catalase (EC 1.11.1.6)

$$2H_2O_2 \rightarrow 2H_2O + O_2 \qquad (22)$$

Superoxide dismutase (EC 1.15.1.1)

(Cu-Zn and Mn)

$$2O_2^{\cdot -} + 2H^+ \rightarrow H_2O_2 + O_2 \qquad (23)$$

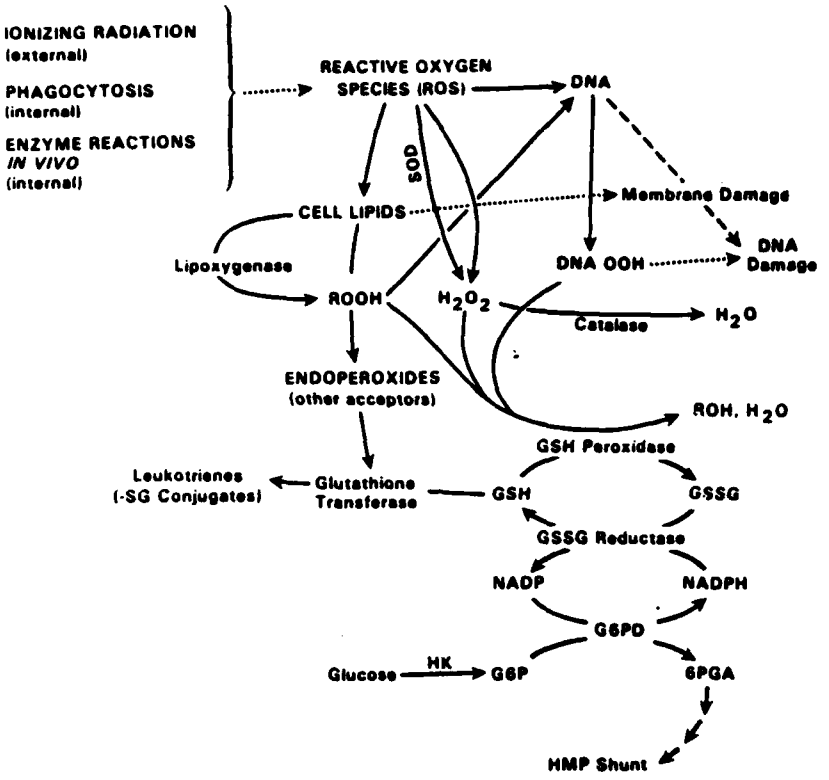

FIGURE 7. Peroxide metabolism. G6PD = glucose-6-phosphate dehydrogenase; 6PGA = 6-phosphogluconic acid; HMP = hexose monophosphate; and HK = hexokinase.

Glutathione peroxidase (EC 1.11.1.9)

Se-independent

$$ROOH + GSH \rightarrow ROH + H_2O + GSSG \quad (24)$$

Se-dependent

$$HOOH + GSH \rightarrow HOH + H_2O + GSSG \quad (25)$$

Glutathione transferase (EC 2.5.1.18)

$$ROOH + GSH \rightarrow \underset{\displaystyle SG}{\overset{\displaystyle |}{RO\text{–}H}} + H_2O \quad (26)$$

The order in which antioxidant enzymes detoxify reactive oxygen species and their products may depend on enzyme affinity for the respective substrates. Although the rate of H_2O_2 removal by catalase is high ($\sim 10^6$ molecules/sec), at low concentrations of H_2O_2, glutathione peroxidase detoxifies H_2O_2 more readily.[118] An important factor to be considered in the concerted action of antioxidant enzymes is their subcellular localization and their availability at critical points of radiation damage, e.g., the content and relative distribution of these

enzymes in cell nuclei is not well characterized. Enzyme activity during different stages of the cell cycle may also influence cellular radiosensitivity. In human kidney T1 cells, catalase and SOD activity increased markedly in G_1 phase, one of the stages in the cell cycle resistant to radiation.[119]

B. Catalase

On the time scale of radiation-induced events, H_2O_2 is one of the first reactive oxygen species that can be scavenged by an endogenous enzyme. Therefore, catalase activity can be considered an early enzymatic defense mechanism involved in radiation protection. In a review of early studies on catalase effects on radiation, Thomson[120] concluded that the role of catalase on the effect of radiation in the mammalian organism was negligible. Addition of catalase to a catalase-negative *E. coli* strain prevented postirradiation inactivation. Experiments using the three catalase-positive *E. coli* strains showed no positive correlation between catalase activity and radiation resistance.[121]

Catalase (5000 units) complexed to polyethylene glycol was found to provide a dose reduction factor of 1.2 when given to female B6CBF1 mice before irradiation, but no protective effect was seen in male C57BL/6 mice.[122] In vitro studies have shown that catalase can protect macrophages[123] from radiation damage. The radiosensitization of *Bacillus megaterium* spores by misonidazole was diminished by catalase.[124] We have observed that catalase can inhibit radiation-induced lipid peroxidation in rat erythrocyte membranes in vitro (Figure 1). There are conflicting reports on the effects of radiation on catalase in mammalian tissues.[120] An increase in catalase activity in cultured cells was found after the addition of selenium (Se), which may play a role in the inhibition of radiation-induced mutagenesis by Se.[125] We found an increase in catalase activity in mouse bone marrow cells 24 hr after the administration of selenium or 1 hr after irradiation (Table 3).

C. Superoxide Dismutase

Superoxide is formed on irradiation by secondary reactions of free radicals (e.g., see Equations 8 and 13), and the endogenous level of superoxide dismutase may contribute to cellular radiosensitivity. Studies, mostly done by Petkau, have demonstrated radioprotection by SOD in model systems (DNA, bacteria, cells, cell membranes) and in rodents.[31,128,129] The best reported DRF (1.56) was obtained when SOD was injected i.v. before and after irradiation of mice,[31] although in other studies little or no protective effect was observed,[122,130] probably due to different modes of administration. The protective ability of SOD was also suggested by (1) the inhibition of the enzyme in cultured cells by diethyldithiocarbamate[131] and (2) the radioresistance of *Drosophila* larvae with a highly active SOD allele.[132] Studies with seven human cell lines did not indicate any correlation between radiation sensitivity parameters and SOD content, with the exception of a comparatively radioresistant mesothelioma cell line with high MnSOD activity.[133] A link between the SOD content of human tumors and their radiosensitivity has been proposed,[134,135] but few clinical data support this view. However, the exploration of the differences in SOD content of tumor cells (in general a decrease in MnSOD) for cancer therapy is a valid concept for further study.[136]

We have found that mouse bone marrow SOD activity (expressed as total SOD activity in units/mg protein) increased significantly (50%) within 1 hr after exposure to 10 Gy (1 Gy/min) ^{60}Co irradiation and remained almost at the same level even after 24 hr (Table 3). A similar observation was made by other workers who showed a seven- to eightfold increase in bone marrow SOD activity 3 days after irradiation (earliest time period studied) when expresed on the basis of number of cells.[137] We have also observed increases in SOD in other mouse tissue after irradiation (data not shown), indicating that there may be a general inductive effect of irradiation on SOD similar to induction by agents such as paraquat.[138] Radioprotectors like cystamine,[137] DDC,[66] and WR-2721 inhibit SOD activity, although the inhibition by WR-2721 was limited to the newly increased activity (Table 3).

Table 3
ANTIOXIDANT ENZYMES IN BONE MARROW CELLS FROM MICE TREATED WITH SELENIUM, WR-2721, AND IRRADIATED

Enzyme / Treatment	Enzyme activity (units/mg protein)			
	Control		Irradiated	
	1 hr	24 hr	1 hr	24 hr
Catalase				
Saline	38.6 ± 2.8	34.5 ± 1.8	44.1 ± 5.4	32.7 ± 1.6
Selenium	47.2 ± 4.0	36.7 ± 2.5	43.6 ± 3.8	30.0 ± 1.6
WR-2721	33.5 ± 2.2	33.5 ± 2.0	33.8 ± 2.0	26.6 ± 0.6
Se + WR-2721	39.6 ± 4.4	35.8 ± 5.0	32.6 ± 2.7	26.8 ± 1.8
Superoxide dismutase				
Saline	15.3 ± 1.5	14.9 ± 2.2	22.8 ± 0.9	20.2 ± 4.0
Se	18.9 ± 1.1	19.6 ± 1.4	14.7 ± 1.1	19.2 ± 2.4
WR-2721	15.7 ± 1.1	17.3 ± 0.5	13.7 ± 0.5	14.7 ± 0.8
Se + WR-2721	14.0 ± 0.7	14.2 ± 0.7	14.2 ± 0.4	14.3 ± 0.4
Se-dependent glutathione peroxidase				
Saline	141.0 ± 6.0	152.0 ± 7.0	161.0 ± 14.0	155.0 ± 14.0
Se	204.0 ± 14.0	147.0 ± 8.0	209.0 ± 20.0	158.0 ± 9.3
WR-2721	141.0 ± 8.0	156.0 ± 2.0	126.0 ± 16.0	152.0 ± 7.8
Se + WR-2721	162.0 ± 12.0	149.0 ± 14.0	117.0 ± 12.0	109.0 ± 26.0
Total glutathione peroxidase				
Saline	190.0 ± 11.2	185.0 ± 14.0	198.0 ± 12.0	247.0 ± 19.0
Se	264.0 ± 13.8	200.0 ± 13.0	234.0 ± 14.0	274.0 ± 15.0
WR-2721	214.0 ± 10.0	227.0 ± 11.0	198.0 ± 11.0	229.0 ± 14.0
Se + WR-2721	235.0 ± 12.0	189.0 ± 10.0	207.0 ± 11.0	213.0 ± 24.0

Note: Physiological saline, selenium (1.6 mg/kg body weight), and WR-2721 (400 mg/kg body weight) were administered i.p. at 24 or 0.5, 24, and 0.5 hr, respectively, before irradiation (10 Gy at 1 Gy/min). Bone marrow was removed 1 and 24 hr after irradiation for enzyme assays on bone marrow cells. SOD and glutathione peroxidase were assayed by published methods.[126,127] Catalase was assayed by the disappearance of H_2O_2 at 240 μm at pH 7.0.

The activity of SOD in erythrocytes determined 5 hr after blood was drawn from persons working in radiation hazard areas was found to be 11 to 27%, compared to 63% in control workers.[139] Both groups had almost the same activity immediately after the blood was drawn. These studies suggest the decreased stability or increased turnover of the enzyme in people exposed to radiation. However, Petkau[129] has provided evidence for increased SOD activity in leukocytes of atomic radiation workers with a trend toward higher levels as a function of occupational dose.

Addition of SOD either before or 24 hr after irradiation inhibited neoplastic transformation by X-rays.[33] However, another study indicated that SOD promotes radiation-induced transformation in cells.[140] Major differences between these two experiments include the use of short-term primary cultures vs. an established cell line and the addition of different units of SOD. SOD mimetics, such as the copper complexes of 3-mercapto-2-hydroxypropyl ether of dextran[141] and of diisopropylsalicylic acid (Cu-DIPS),[142] can also affect radiosensitivity. These compounds have very low SOD-like activity, although they have mild radioprotective activity which may be due to their ability to reach cellular locations of radiation injury.

D. Glutathione Peroxidase

Very little information is available on the role of glutathione peroxidase (GSH-Px) in radiation sensitivity. GSH-Px can convert the hydroperoxides formed from lipids[143] or DNA[144] as a result of the action of reactive oxygen species generated by radiation to a nontoxic hydroxy product. It has been suggested that such a reduction of the hydroperoxide of nucleic

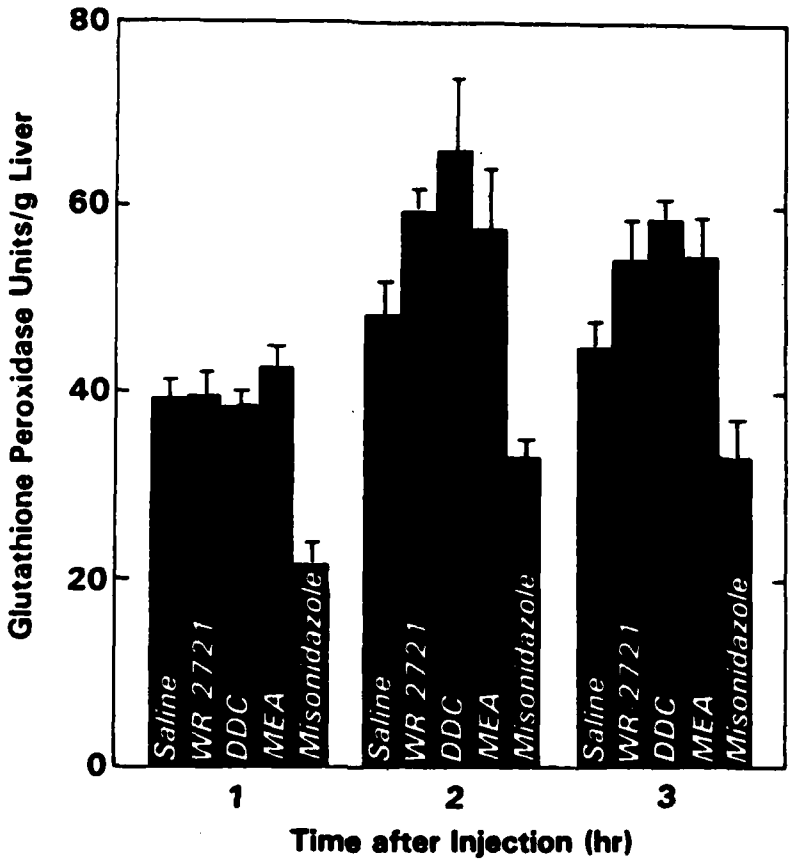

FIGURE 8. Effect of radioprotectors and a radiosensitizer on mouse liver cytosol glutathione peroxidase. (Data obtained from Reference 148 and unpublished data.) Glutathione peroxidase was assayed using cumene hydroperoxide as substrate.[127]

acid is a prerequisite for repair.[145] The stability of GSH-Px to peroxides[146] also enables the enzyme to detoxify peroxides without becoming inactivated itself. The widespread presence of the enzyme in the cytosol, in mitochondria, and plasma membranes makes it an efficient tool to handle radiation-induced hydroperoxides at these locations of the cell. GSH-Px detoxifies both H_2O_2 and lipid hydroperoxide[127] with reduced glutathione (GSH) as the second substrate. The former reaction is catalyzed by selenium-dependent GSH-Px, which can also use organic hydroperoxides as its substrate instead of H_2O_2. The residual enzyme activity observed in Se deficiency is the non-Se-dependent GSH-Px, which was later shown to be glutathione transferase.[99] The activity obtained with cumene hydroperoxide and H_2O_2 are referred to as total GSH-Px and selenium-dependent GSH-Px, respectively.

Among the three antioxidant enzymes, only GSH-Px showed any relationship to radiation sensitivity in seven human cell lines.[133] This was also suggested by Biaglow[10] in his studies with Chinese hamster cells. We have observed a 35% increase in the activity of the enzyme in mouse bone marrow cells 24 hr after ^{60}Co irradiation. However, the increase was limited to the total GSH-Px (Table 3). This may be a phenomenon similar to the observed increase in GSH-Px in mouse liver and intestine after lipid hydroperoxide administration.[147]

Data from our laboratory indicate a relationship between the radiosensitizing and radioprotective effects of drugs and their influence on GSH-Px activity. The radiosensitizer misonidazole was found to inhibit total GSH-Px activity in liver homogenate, cytosol (Figure 8), and microsomes shortly after injection into mice. The inhibition was more pronounced

Table 4
GLUTATHIONE-PEROXIDASE (GSH-Px) ACTIVITY OF RADIOPROTECTORS[88]

Addition to GSH-Px assay system	340 nm/min
None, blank	0.013
0.01 Unit GSH-Px	0.055
Diethyldithiocarbamate, 1.00 m*M*	0.195
WR-1065, 1.0 m*M* 2-(3-Aminopropylamino)ethanethiol dihydrochloride	0.055
Dithiothreitol, 1.00 m*M*	0.033
2-Mercaptoethane sulfonic acid, 1.00 m*M*	0.013
Cysteamine, 1.0 m*M*	0.013
S-(2-aminoethyl)isothiouronium-Br-HBr, 1.0 m*M*	0.013
N-(2-mercaptopropriony1)glycine, 1.00 m*M*	0.013

From Kumar, K. S., Sancho, A. M., and Weiss, J. F., *Int. J. Radiat. Oncol. Biol. Phys.*, 12, 1463, 1986. With permission.

in microsomes. Se-dependent GSH-Px and glutathione transferase were also inhibited, but to a lesser extent than total GSH-Px.[148] Treatment with the radioprotectors WR-2721, DDC, and cysteamine (MEA) resulted in an increase in GSH-Px activity in mouse liver at 2 and 3 hr after administration (Figure 8). Se administered in the drinking water[149] or injected is mildly radioprotective (Figure 3), and Se treatment increases GSH-Px activity. Vitamin E is also mildly radioprotective and protects against the radiation-induced decline in mouse liver cytosol GSH-Px.[75] These studies indicate that one of the possible modes of action of sensitizers or protectors is by inhibiting or promoting GSH-Px activity, thereby affecting peroxide levels in tissues.

In addition to SeGSH-Px, other types of small-molecular-weight, Se-containing compounds (such as selenodiglutathione, selenocysteine, dimethylselenide, and other minor forms of selenium) are also identified in rats injected with selenite.[146,150] In fact, two thirds of the Se in rats is in the form of selenocysteine-containing proteins,[146] with no demonstrable GSH-Px activity. The role of these selenocysteine-containing proteins (non-GSH-Px) in radiation sensitivity is not clear.[151-153] It is known that synthetic selenium compounds, such as selenomethionine, have radioprotective activity. It is possible that a part of the radioprotective effect of Se injection is due to formation of low-molecular-weight Se compounds similar to selenomethione. Studies with cultured cells indicate that Se treatment results in increased catalase as well as GSH-Px activity. We have found marginal increases in catalase and SOD activity in bone marrow cells, concurrent with larger increases in GSH-Px activity 24 hr after the administration of Se (as sodium selenite) in mice. The "new increased" levels of these enzymes in irradiated and/or Se-administered (24 hr prior) mice were counteracted by the administration of WR-2721 1/2 hr before irradiation (Table 3). Despite this effect, it is of interest that the radioprotection observed with WR-2721 alone is potentiated by the administration of Se at 24 hr before irradiation (Figure 3). The lethal toxicity of WR-2721 is also decreased by pretreatment with Se.

Some selenoorganic compounds may have potential as modulators of radiation sensitivity since they have GSH-Px-like activity[154,155] and low toxicity. DDC also possesses GSH-Px-like activity.[88] Among several sulfhydryl compounds known to possess some radioprotective ability, DDC exhibited the greatest GSH-Px-like activity (Table 4). As noted previously, DDC is a radioprotector although it inhibits SOD. DDC has been reported to sensitize tumor tissue and protect normal tissue at radiation doses in the clinical range in the same animal.[67] These findings indicate the complex nature of the mechanism of action of DDC, but also point out the potential for chemical modification when tumors and normal tissue have different biochemical characteristics. Since MnSOD is usually low in tumors,[136] further inhibition of

Cu-Zn SOD by DDC could lead to sensitization, whereas normal tissue, in general, would be protected. Other aspects of the cell milieu are also important in determining the activity of DDC.[88] Alterations in other enzymes that are important in the scheme of protection against oxidative damage are also possible by drug and dietary treatment. Glutathione reductase could be inhibited by BCNU (1,3-bis(2-chloroethyl)-1-nitrosourea),[156] and glutathione transferase activity can be induced by a variety of antioxidants.[157,158]

Research in the area of radiation sensitivity and antioxidant enzymes is far from the stage of deriving any definitive conclusions about the role of these enzymes in radiation protection and damage. Further investigations are needed in this important field.

ACKNOWLEDGMENTS

The research from our laboratory reported here was supported by the Armed Forces Radiobiology Research Institute, Defense Nuclear Agency, under Work Unit B1162. The views presented in this paper are those of the authors; no endorsement by the Defense Nuclear Agency has been given or should be inferred. Research was conducted according to the principles enunciated in the Guide for the Care and Use of Laboratory Animals prepared by the Institute of Laboratory Animal Resources, National Research Council. The authors thank Dr. L. S. Myers, Jr. and Dr. W. F. Blakely for their critical reviews of the manuscript, and Mrs. M. Waldbillig for typing the manuscript. Editorial and graphics support by the AFRRI Information Services Department is gratefully acknowledged.

REFERENCES

1. **Singh, A. and Singh, H.**, Time-scale and nature of radiation-biological damage: approaches to radiation protection and postirradiation therapy, *Prog. Biophys. Mol. Biol.*, 39, 69, 1982.
2. **Szumiel, I.**, Intrinsic radiosensitivity of proliferating mammalian cells, *Adv. Radiat. Biol.*, 9, 281, 1981.
3. **Russo, A., Mitchell, J., Kinsella, T., Morstyn, G., and Glatstein, E.**, Determinants of radiosensitivity, *Semin. Oncol.*, 12, 332, 1985.
4. **Walker, G. C.**, Inducible DNA repair systems, *Annu. Rev. Biochem.*, 54, 425, 1985.
5. **Painter, R. B.**, The role of DNA damage and repair in cell killing induced by ionizing radiation, in *Radiation Biology in Cancer Research*, Meyn, R. E. and Withers, H. R., Eds., Academic Press, New York, 1980, 59.
6. **Aust, S. D. and Swingen, B. A.**, The role of iron in enzymatic lipid peroxidation, in *Free Radicals in Biology*, Vol. 5, Pryor, W. A., Ed., Academic Press, New York, 1982, 1.
7. **Karin, M.**, Metallothioneins: proteins in search of function, *Cell*, 41, 9, 1985.
8. **Goldstein, I. M. and Charo, I. F.**, Ceruloplasmin: an acute phase reactant and antioxidant, in *Lymphokines*, Vol. 8, Pick, E., Ed., Academic Press, New York, 1983, 373.
9. **Meister, A. and Anderson, M. E.**, Glutathione, *Annu. Rev. Biochem.*, 52, 711, 1983.
10. **Biaglow, J. E., Varnes, M. E., Astor, M., Mitchell, J., and Russo, A.**, Intracellular thiols: involvement in drug metabolism and radiation response, in *Radioprotectors and Anticarcinogens*, Nygaard, O. F., and Simic, M. G., Eds., Academic Press, New York, 1983, 203.
11. **Leyko, W., and Bartosz, G.**, Membrane effects of ionizing radiation and hyperthermia, *Int. J. Radiat. Biol.*, 49, 743, 1986.
12. **Chow, C. K.**, Nutritional influence on cellular antioxidant defense systems, *Am. J. Clin. Nutr.*, 32, 1066, 1979.
13. **Ward, J. F.**, Molecular mechanisms of radiation-induced damage to nucleic acids, *Adv. Radiat. Biol.*, 5, 181, 1975.
14. **Chapman, J. D. and Gillespie, C. J.**, Radiation-induced events and their time scale in mammalian cells, *Adv. Radiat. Biol.*, 9, 143, 1981.
15. **Alper, T.**, *Cellular Radiobiology*, Cambridge University Press, London, 1979.
16. **Hall, E. J.**, *Radiobiology for the Radiologist*, 2nd ed., Harper & Row, Hagerstown, Md., 1978.
17. **Blakely, E. A., Ngo, F. Q. H., Curtis, S. B., and Tobias, C. A.**, Heavy-ion radiobiology: cellular studies, *Adv. Radiat. Biol.*, 11, 295, 1984.

18. **Thomas, J. K.**, The hydrated electron and the H atom in the radiolysis of water, in *Radiation Research*, Silini, G., Ed., North-Holland, Amsterdam, 1967, 179.
19. **Willson, R. L., Greenstock, C. L., Adams, G. E., Wageman, R., and Dorfman, L. M.**, The standardization of hydroxyl radical rate data from radiation chemistry, *Int. J. Radiat. Phys. Chem.*, 3, 211, 1971.
20. **Simic, M. G.**, Radiation chemistry of water-soluble food components, in *Preservation of Food by Ionizing Radiation*, Vol. 2, Josephson, E. S. and Peterson, M. S., Eds., CRC Press, Boca Raton, Fla., 1983, 1.
21. **Myers, L. S., Jr.**, Free-radical damage of nucleic acids and their components: the direct absorption of energy, in *Free Radicals in Biology*, Vol. 4, Pryor, W. A., Ed., Academic Press, New York, 1980, 95.
22. **Roots, R. and Okada, S.**, Protection of DNA molecules of cultured mammalian cells from radiation-induced single-strand scissions by various alcohols and SH compounds, *Int. J. Radiat. Biol.*, 21, 329, 1979.
23. **Greenstock, C. L.**, Oxygen radicals and ions and their control in biology, in *Advances on Oxygen Radicals and Radioprotectors*, Breccia, A., Greenstock, C. L., and Tamba, M., Eds., Lo Scarabeo, Bologna, 1984, 29.
24. **Howard-Flanders, P.**, Effect of oxygen on the radiosensitivity of bacteriophage in the presence of sulphydryl compounds, *Nature (London)*, 186, 485, 1960.
25. **Greenstock, C. L.**, Oxy-radicals and the radiobiological oxygen effect, *Isr. J. Chem.*, 24, 1, 1984.
26. **Schulte-Frohlinde, D., Behrens, G., and Onal, A.**, Lifetime of peroxyl radicals of poly(U), poly(A) and single- and double-stranded DNA and the rate of their reaction with thiols, *Int. J. Radiat. Biol.*, 50, 103, 1986.
27. **Sies, H. and Cadenas, E.**, Biological basis of detoxication of oxygen free radicals, in *Biological Basis of Detoxication*, Caldwell, J. and Jakoby, W. B., Eds., Academic Press, New York, 1983, 181.
28. **Quintiliani, M.**, Introductory remarks on oxygen and oxy-radicals in model systems, in *Advances in Oxygen Radicals and Radioprotectors*, Breccia, A., Greenstock, C. L., and Tamba, M., Eds., Lo Scarabeo, Bologna, 1984, 11.
29. **Sztanyik, L. B. and Santha, A.**, Synergistic effect of radioprotective substances having different mechanisms of action, in *Modification of Radiosensitivity of Biological Systems*, International Atomic Energy Agency, Vienna, 1976, 47.
30. **Falconi, C., Scotto, P., and De Franciscis, P.**, Radioprotection and recovery by dithiothreitol, *Experientia*, 26, 172, 1970.
31. **Petkau, A.**, Radiation protection by superoxide dismutase, *Photochem. Photobiol.*, 28, 765, 1978.
32. **Seifter, E., Rettura, G., Padawer, J., Stratford, F., Weinzweig, J., Demetriou, A. A., and Levenson, S. M.**, Morbidity and mortality reduction by supplemental vitamin A or β-carotene in CBA mice given total-body γ-radiation, *J. Natl. Cancer Inst.*, 73, 1167, 1984.
33. **Borek, C. and Troll, W.**, Modifiers of free radicals inhibit *in vitro* the oncogenic actions of x-rays, bleomycin, and the tumor promoter 12-*O*-tetradecanoylphorbol 13-acetate, *Proc. Natl. Acad. Sci. U.S.A.*, 80, 1304, 1983.
34. **Grdina, D. J., Nagy, B., Hill, C. K., Wells, R. L., and Peraino, C.**, The radioprotector WR1065 reduces radiation-induced mutations at the hypoxanthine-guanine phosphoribosyl transferase locus in V79 cells, *Carcinogenesis*, 6, 929, 1985.
35. **Sancho, A. M., Kumar, K. S., Vaishnav, Y. N., and Weiss, J. F.**, Inhibition of erythrocyte lipid peroxidation and hemolysis by the radioprotectant WR-2721, S-2-(3-aminopropylamino)ethylphosphorothioic acid, *Fed. Proc. Fed. Am. Soc. Exp. Biol.*, 45, 1930, 1986.
36. **Vaishnav, Y. N., Kumar, K. S., and Weiss, J. F.**, Measurement of volatile hydrocarbon evolution *in vitro* and *in vivo* for study of radiation damage and its chemical modification, *Fed. Proc. Fed. Am. Soc. Exp. Biol.*, 45, 1723, 1986.
37. **Gray, L. H., Conger, A. D., Ebert, M., Hornsey, S., and Scott, O. C. A.**, The concentration of oxygen dissolved in tissues at the time of irradiation as a factor in radiotherapy, *Br. J. Radiol.*, 26, 638, 1953.
38. **Elkind, M. M., Swain, R. W., Alescio, T., Sutton, H., and Moses, W. B.**, Oxygen, nitrogen, recovery and radiation therapy, in *Cellular Radiation Biology*, Williams & Wilkins, Baltimore, 1965, 442.
39. **Coleman, C. N.**, Hypoxic cell radiosensitizers: expectations and progress in drug development, *Int. J. Radiat. Oncol. Biol. Phys.*, 11, 323, 1985.
40. **Varghese, A. J. and Whitmore, G. F.**, Misonidazole-glutathione conjugates in CHO cells, *Int. J. Radiat. Oncol. Biol. Phys.*, 10, 1341, 1984.
41. **Varghese, A. J.**, Glutathione conjugates of misonidazole, *Biochem. Biophys. Res. Commun.*, 112, 1013, 1983.
42. **Bingiow, J. E.**, The effects of ionizing radiation on mammalian cells, *J. Chem. Educ.*, 58, 144, 1981.
43. **Patt, H. M., Tyree, E. B., Straube, R. L., and Smith, D. E.**, Cysteine protection against X irradiation, *Science*, 110, 213, 1949.
44. **Foye, W. O.**, Radiation-protective agents in mammals, *J. Pharm. Sci.*, 58, 283, 1969.

45. **Klayman, D. E. and Copeland, E. S.**, Radioprotective agents, in *Kirk-Othmer: Encyclopedia of Chemical Technology*, Vol. 19, John Wiley & Sons, New York, 1982, 801.
46. **Giambarresi, L. and Jacobs, A. J.**, Radioprotectants, in *Military Radiobiology*, Conklin, J. J. and Walker, R. I., Eds., Academic Press, Orlando, Fla., 1987, 265.
47. **Davidson, D. E., Grenan, M. M., and Sweeney, T. R.**, Biological characteristics of some improved radioprotectors, in *Radiation Sensitizers: Their Use in the Clinical Management of Cancer*, Brady, L. W., Ed., Masson Publishing, New York, 1980, 309.
48. **Livesey, J. C., Reed, D. J., and Adamson, L. F.**, *Radiation-Protective Drugs and Their Reaction Mechanisms*, Noyes Publications, Park Ridge, N.J., 1984.
49. **Prasad, K. N.**, Modification of cellular radiation damage, in *CRC Handbook of Radiobiology*, CRC Press, Boca Raton, Fla., 1984, 49.
50. **Sweeney, T. R.**, A Survey of Compounds from the Antiradiation Drug Development Program of the U.S. Army Medical Research and Development Command, Walter Reed Army Institute of Research, Washington, D.C., 1979.
51. **Yuhas, J. M., Spellman, J. M., and Culo, F.**, The role of WR-2721 in radiotherapy and/or chemotherapy, in *Radiation Sensitizers: Their Use in the Clinical Management of Cancer*, Brady, L. W., Ed., Masson Publishing, New York, 1980, 303.
52. **Blumberg, A. L., Nelson, D. F., Gramkowski, M., Glover, D., Glick, J. H., Yuhas, J. M., and Kligerman, M. M.**, Clinical trials of WR-2721 with radiation therapy, *Int. J. Radiat. Oncol. Biol. Phys.*, 8, 561, 1982.
53. **Glick, J. H., Glover, D. J., Turrisi, A., Weiler, C., Yuhas, J. M., and Kligerman, M.**, Clinical trials of WR-2721 with chemotherapy, in *Radioprotectors and Anticarcinogens*, Nygaard, O. F. and Simic, M. G., Eds., Academic Press, New York, 1983, 719.
54. **Bogo, V., Jacobs, A. J., and Weiss, J. F.**, Behavioral toxicity and efficacy of WR-2721 as a radioprotectant, *Radiat. Res.*, 104, 182, 1985.
55. **Rasey, J. S., Nelson, N. J., Mahler, P., Anderson, K., Krohn, K. A., and Menard, T.**, Radioprotection of normal tissue against gamma rays and cyclotron neutrons with WR-2721: LD_m studies and ^{35}S-WR2721 biodistribution, *Radiat. Res.*, 97, 598, 1984.
56. **Weiss, J. F., Jacobs, A. J., Rankin, W. A., Hoover, R. L., and Kumar, K. S.**, Comparison of radioprotective effects of WR-2721 and WR-3689, in *Abstr. of Papers for the 33rd Annu. Meet. of the Radiation Research Society*, Radiation Research Society, Philadelphia, 1985, 43, Eh-7.
57. **Brown, D. Q., Yuhas, J. M., MacKenzie, L. J., Graham, W. J., III, and Pittock, J. W., III**, Differential radioprotection of normal tissues by hydrophilic chemical protectors, *Int. J. Radiat. Oncol. Biol. Phys.*, 10, 1581, 1984.
58. **Yuhas, J. M. and Storer, J. B.**, Chemoprotection against three modes of radiation death in the mouse, *Int. J. Radiat. Biol.*, 15, 233, 1969.
59. **Hanson, W. R. and Ainsworth, E. J.**, 16-16 Dimethyl prostaglandin E2 induces radioprotection in murine intestinal and hematopoietic stem cells, *Radiat. Res.*, 103, 196, 1985.
60. **Gupta, R. and Devi, P. U.**, Protection against radiation induced chromosome injury by sulfhydryl compounds, *Acta Radiobiol. Oncol.*, 24, 419, 1985.
61. **Cockerham, L. G., Doyle, T. F., Pautler, E. L., and Hampton, J. D.**, Disodium cromoglycate, a mast-cell stabilizer, alters postirradiation regional blood flow in primates, *J. Toxicol. Environ. Health*, 18, 91, 1986.
62. **Cockerham, L. G., Arroyo, C. M., and Hampton, J. D.**, Effects of 4-hydroxypyrazolo (3,4-d) pyrimidine (Allopurinol) on postirradiation cerebral blood flow: implications of free radical involvement, *Free Rad. Biol. Med.*, 1988, in press.
63. **Weiss, J. F., Jacobs, A. J., and Rankin, W. A.**, Effects of diethyldithiocarbamate and WR-2721 on delayed-type hypersensitivity and survival of irradiated mice, in *Proc. 7th Int. Congr. Radiation Research*, Broerse, J. J., Barendsen, G. W., Kal, H. B., and van der Kogel, A. J., Eds., Martinus Nijhoff, Amsterdam, 1983.
64. **Weiss, J. F., Hoover, R. L., and Kumar, K. S.**, Selenium pretreatment enhances the radioprotective effect and reduces the lethal toxicity of WR-2721, *Free Rad. Res. Commun.*, 3, 33, 1987.
65. **Maisin, J. R., Gerber, G. B., Lambiet-Collier, M., and Mattelin, G.**, Chemical protection against long-term effects of whole-body exposure of mice to ionizing radiation. III. The effects of fractionated exposure to C57B1 mice, *Radiat. Res.*, 82, 487, 1980.
66. **Heikkila, R. E., Cabbat, F. S., and Cohen, G.**, *In vivo* inhibition of superoxide dismutase in mice by diethyldithiocarbamate, *J. Biol. Chem.*, 251, 2182, 1976.
67. **Evans, R. G.**, Tumor radiosensitization with concomitant bone marrow radioprotection: a study in mice using diethyldithiocarbamate (DDC) under oxygenated and hypoxic conditions, *Int. J. Radiat. Oncol. Biol. Phys.*, 11, 1163, 1985.
68. **Nowotny, A., Behling, U. H., and Chang, H.**, Relationship of structure to function in bacterial endotoxins. VIII. Biological activities in a polysaccharide-rich fraction, *J. Immunol.*, 115, 199, 1975.

69. **Patchen, M. L. and MacVittie, T. J.**, Stimulated hemopoiesis and enhanced survival following glucan treatment in sublethally and lethally irradiated mice, *Int. J. Immunopharmacol.*, 7, 923, 1985.
70. **Neta, R., Oppenheim, J. J., Douches, S. D., Giclus, P. C., Imbra, R. J., and Karin, M.**, Radioprotection with IL-1. Comparison with other cytokines, *Prog. Immunol.*, 6, 900, 1987.
71. **Maisin, J. R., Kondi-Tamba, A., and Mattelin, G.**, Polysaccharides induce radioprotection of murine hemopoietic stem cells and increase the LD_{30}/30 days, *Radiat. Res.*, 105, 276, 1986.
72. **Lvovsky, E., Baze, W. B., Hilmas, D. E., and Levy, H. B.**, Radiation damage and the interferon system, *Tex. Rep. Biol. Med.*, 35, 388, 1977.
73. **Ghezzi, P., Bianchi, M., Mantovani, A., Spreafico, F., and Salmona, M.**, Enhanced xanthine oxidase activity in mice treated with interferon inducers, *Biochem. Biophys. Res. Commun.*, 119, 144, 1984.
74. **Hoffeld, J. T., Metzger, Z., and Oppenheim, J. J.**, Oxygen-derived metabolites as suppressors of immune responses *in vitro*, in *Lymphokines*, Vol. 2, Pick, E., Ed., Academic Press, New York, 1981, 63.
75. **Srinivasan, V., Jacobs, A. J., Simpson, S. A., and Weiss, J. F.**, Radioprotection by Vitamin E: effects on hepatic enzymes, delayed type hypersensitivity, and postirradiation survival of mice, in *Modulation and Mediation of Cancer by Vitamins*, Meyskens, F. L. and Prasad, K. N., Eds., S. Karger, Basel, 1983, 119.
76. **Tengerdy, R. P., Mathias, M. M., and Nockels, C. F.**, Vitamin E, immunity and disease resistance, *Adv. Exp. Med. Biol.*, 135, 27, 1981.
77. **Weiss, J. F. and Chretien, P. B.**, Acute-phase proteins and systemic immunity, in *The Pathophysiology of Combined Injury and Trauma*, Walker, R. I., Gruber, D. F., MacVittie, T. J., and Conklin, J. J., Eds., University Park Press, Baltimore, 1985, 137.
78. **Renoux, G., Renoux, M.**, DTC. A summary of the current status, in *Current Concepts in Human Immunology and Cancer Immunomodulation*, Serrou, B., Rosenfeld, C., Daniels, J. C., and Saunders, J. P., Eds., Elsevier, Amsterdam, 1982, 575.
79. **Srinivasan, V. and Weiss, J. F.**, Suppression of delayed-type hypersensitivity to oxazolone in whole-body-irradiated mice and protection by WR-2721, *Radiat. Res.*, 98, 438, 1984.
80. **Weiss, J. F., Srinivasan, V., Jacobs, A. J., and Rankin, W. A.**, Effect of sulfur comounds on radiation-induced suppression of delayed-type hypersensitivity to oxazolone in mice, *Proc. Am. Assoc. Cancer Res.*, 25, 235, 1984.
81. **Landauer, M. R., Davis, H. D., Dominitz, J. A., and Weiss, J. F.**, Dose and time relationships of the radioprotector WR-2721 on locomotor activity in mice, *Pharmacol. Biochem. Behav.*, 27, 573, 1987.
82. **Landauer, M. R., Davis, H. D., Dominitz, J. A., and Weiss, J.F.**, Comparative behavioral toxicity of four sulfhydryl radioprotective compounds in mice: WR-2721, cysteamine, diethyldithiocarbamate and *N*-acetylcysteine, *Pharm. Ther.*, in press.
83. **Dobbs, C. R., Weiss, J. F., Kumar, K. S., and Chirigos, M. A.**, Antioxidant and radioprotective properties of levamisole, in *Oxygen and Oxy-Radicals in Chemistry and Biology*, Rogers, M. A. J. and Powers, E. L., Eds., Academic Press, New York, 1981, 622.
84. **Kumar, K. S., Chirigos, M. A., and Weiss, J. F.**, Protection of rat liver microsomes from NADPH-, ascorbate-, and X-irradiation-induced lipid peroxidation by levamisole, *Int. J. Immunopharmacol.*, 1, 85, 1979.
85. **Kumar, K. S., Dobbs, C. R., Weiss, J. F., and Chirigos, M. A.**, Levamisole inhibition of microsomal lipid peroxidation as related to its sulfhydryl metabolite DL-2-oxo-3-(2-mercaptoethyl)-5-phenyl imidazolidine, *J. Immunopharmacol.*, 2, 73, 1980.
86. **De Brabander, M., Aerts, F., Geuens, G., Van Glinckel, R., Van De Veire, R., and Van Belle, H.**, DL-2-oxo-3-(2-mercaptoethyl)-5-phenylimidazolidine. A sulfhydryl metabolite of levamisole that interacts with microtubules, *Chem. Biol. Interact.*, 23, 45, 1978.
87. **Vina, J., Saez, G. T., Wiggins, D., Roberts, A. F. C., Hems, R., and Krebs, H. A.**, The effect of cysteine oxidation on isolated hepatocytes, *Biochem. J.*, 212, 39, 1983.
88. **Kumar, K. S., Sancho, A. M., and Weiss, J. F.**, A novel interaction of diethyldithiocarbamate with the glutathione/glutathione peroxidase system, *Int. J. Radiat. Oncol. Biol. Phys.*, 12, 1463, 1986.
89. **Ziegler, D. M., Poulsen, L. L., and Richerson, R. B.**, Oxidative metabolism of sulfur-containing radioprotective agents, in *Radioprotectors and Anticarcinogens*, Nygaard, O. F. and Simic, M. G., Eds., Academic Press, New York, 1983, 191.
90. **Butler, J. D., Gahl, W. A., and Tietze, F.**, Cystine depletion by WR-1065 in cystinotic cells. Mechanism of action, *Biochem. Pharmacol.*, 34, 2179, 1985.
91. **Gaugas, J. M.**, Mechanisms of *in vitro* cytotoxicity of *S*-2-(3-aminopropylamino)ethylphosphorothioic acid, in *Advances in Polyamine Research*, Vol. 3, Caldarera, C. M., Zappila, V., and Bachrach, U., Eds., Raven Press, New York, 1981, 441.
92. **Fischmeister, L., Swynnerton, N. F., Ludden, T. M., and Mangold, D. J.**, Bioavailability and newer methods of delivery of phosphorothioate radioprotectors, *Pharm. Ther.*, 1988, in press.
93. **Purdie, J. W., Inhaber, E. R., Schneider, H., and Labelle, J. L.**, Interaction of cultured mammalian cells with WR-2721 and its thiol WR-1065: implications for mechanisms of radioprotection, *Int. J. Radiat. Biol.*, 43, 517, 1983.

94. **Yuhas, J. M., Proctor, J. O., and Smith, L. H.**, Some pharmacologic effects of WR-2721: their role in toxicity and radioprotection, *Radiat. Res.*, 54, 222, 1973.
95. **Denekamp, J., Rojas, A., and Stewart, F. A.**, Is radioprotection by WR-2721 restricted to normal tissues?, in *Radioprotectors and Anticarcinogens*, Nygaard, O. F. and Simic, M. G., Eds., Academic Press, New York, 1983, 655.
96. **Denekamp, J., Michael, B. D., Rojas, A., and Stewart, F. A.**, Radioprotection of mouse skin by WR-2721: the critical influence of oxygen tension, *Int. J. Radiat. Oncol. Biol. Phys.*, 8, 531, 1982.
97. **Okada, S.**, Current status of thiol studies in radiobiology, *Radiosensitiz. Newsl.*, 5, 5, 1986.
98. **Reed, D. J. and Meredith, M. J.**, Glutathione conjugation systems and drug disposition, in *Drug and Nutrients*, Roe, D. A. and Campbell, T. C., Eds., Marcel Dekker, New York, 1984, 179.
99. **Flohe, L.**, Glutathione peroxidase brought into focus, in *Free Radicals in Biology*, Vol. 5, Pryor, W. A., Ed., Academic Press, New York, 1982, 223.
100. **Quintiliani, M., Badiello, R., Tamba, M., and Gorin, G.**, Radiation chemical basis for the role of glutathione in cellular radiation sensitivity, in *Modification of Radiosensitivity of Biological Systems*, International Atomic Energy Agency, Vienna, 1976, 29.
101. **Arrick, B. A., and Nathan, C. F.**, Glutathione metabolism as determinant of therapeutic efficiency: a review, *Cancer Res.*, 44, 4224, 1984.
102. **Bump, E. A., Yu, N. Y., and Brown, J. M.**, The use of drugs which deplete intracellular glutathione in hypoxic cell radiosensitization, *Int. J. Radiat. Oncol. Biol. Phys.*, 8, 439, 1982.
103. **Bump, E. A., Yu, N. Y., and Brown, J. M.**, Radiosensitization of hypoxic tumor cells by depletion of intracellular glutathione, *Science*, 217, 544, 1982.
104. **Dethmers, J. K. and Meister, A.**, Glutathione export by human lymphoid cells: depletion of glutathione by inhibition of its synthesis decreases export and increases sensitivity to irradiation, *Proc. Natl. Acad. Sci. U.S.A.*, 78, 7492, 1981.
105. **Yu, N. Y. and Brown, J. M.**, Depletion of glutathione *in vivo* as a method of improving therapeutic ratio of misonidazole and SR 2508, *Int. J. Radiat. Oncol. Biol. Phys.*, 10, 1265, 1984.
106. **Guichard, M., Lespinasse, F., and Malaise, E. P.**, Influence of buthionine sulfoximine and misonidazole on glutathione level and radiosensitivity of human tumor xenografts, *Radiat. Res.*, 105, 115, 1986.
107. **Revesz, L.**, The role of endogenous thiols in intrinsic radioprotection, *Int. J. Radiat. Biol.*, 47, 361, 1985.
108. **Revesz, L. and Edgren, M.**, Glutathione dependent yield and repair of single-strand DNA breaks in irradiated cells, *Br. J. Cancer*, 49(Suppl. 6), 55, 1984.
109. **Revesz, L. and Edgren, M.**, Mechanisms of radiosensitization and protection studied with glutathione deficient human cell lines, in *Progress in Radio-Oncology*, Vol. 2, Karcher, K. H., Kogelnik, H. D., and Reinartz, G., Eds., Raven Press, New York, 1982, 235.
110. **Harris, J. W.**, Cellular thiols in radiation and drug response: use of specific reagents, in *Radioprotectors and Anticarcinogens*, Nygaard, O. F. and Simic, M. G., Eds., Academic Press, New York, 1983, 255.
111. **Williamson, J. M. and Meister, A.**, Stimulation of hepatic glutathione formation by administration of L-2-oxo thiazolidine-4-carboxylate, a 5-oxo-L-prolinase substrate, *Proc. Natl. Acad. Sci. U.S.A.*, 78, 936, 1981.
112. **Russo, A. and Mitchell, J. B.**, Radiation response of Chinese hamster cells after elevation of intracellular glutathione levels, *Int. J. Radiat. Oncol. Biol. Phys.*, 10, 1243, 1984.
113. **Wellner, V. P., Anderson, M. E., Puri, R. N., Jensen, G. L., and Meister, A.**, Radioprotection by glutathione ester: transport of glutathione ester into human lymphoid cells and fibroblasts, *Proc. Natl. Acad. Sci. U.S.A.*, 81, 4732, 1984.
114. **Vos, O. and Roos-Verhey, W. S. D.**, Endogenous versus exogenous thiols in radioprotection, *Pharm. Ther.*, 1988, in press.
115. **Stoklasova, A., Krizala, J., and Ledvina, M.**, The concentrations of SH-groups in some radiosensitive tissues after the administration of radioprotectors in rats, *Strahlentherapie*, 156, 205, 1980.
116. **Burk, D. and Woods, M.**, Hydrogen peroxide, catalase, glutathione peroxidase, quinones, nordihydroguaiaretic acid, and phosphopyridine nucleotides in relation to X-ray action on cancer cells, *Radiat. Res. Suppl.*, 3, 212, 1963.
117. **Samuelsson, B.**, Leukotrienes: mediators of immediate hypersensitivity reactions and inflammation, *Science*, 220, 568, 1983.
118. **Halliwell, B.**, Free radicals, oxygen toxicity and aging, in *Age Pigments*, Sohal, R. S., Ed., Elsevier/North-Holland, Amsterdam, 1981, 1.
119. **Blakely, W. F., Kumar, K. S., Chang, P. S., Blakely, E. A., and Weiss, J. F.**, unpublished data, 1986.
120. **Thomson, J. F.**, Possible role of catalase in radiation effects on mammals, *Radiat. Res. Suppl.*, 3, 93, 1963.
121. **Adler, H. I.**, Catalase, hydrogen peroxide, and ionizing radiation, *Radiat. Res. Suppl.*, 3, 110, 1963.
122. **Gray, B. H. and Stull, R. W.**, Radioprotection by polyethylene glycol-protein complexes in mice, *Radiat. Res.*, 93, 581, 1983.

123. **McLennan, G., Oberley, L. W., and Autor, A. P.,** The role of oxygen-derived free radicals in radiation-induced damage and death on nondividing eucaryotic cells, *Radiat. Res.*, 84, 122, 1980.
124. **Gazgo, G. L. and Dam, A.,** Influence of catalase on the radiation sensitizing effect of misonidazole, *Acta Radiobiol. Oncol.*, 24, 189, 1985.
125. **Borek, C.,** The role of nutritional factors in cellular protection against DNA damage, altered gene expression and malignant transformation, in *Mechanisms of DNA Damage and Repair: Implications for Carcinogenesis and Risk Assessment*, Simic, M. G., Grossman, L., and Upton, A. C., Eds., Plenum Press, New York, 1986, 557.
126. **McCord, J. M. and Fridovich, I.,** Superoxide dismutase — an enzymatic function of erythrocuprein (hemocuprein), *J. Biol. Chem.*, 244, 6049, 1969.
127. **Lawrence, R. A. and Burk, R. F.,** Glutathione peroxidase activity in selenium-deficient rat liver, *Biochem. Biophys. Res. Commun.*, 71, 952, 1976.
128. **Michelson, A. M. and Buckingham, M.E.,** Effects of superoxide radicals on myoblast growth and differentiation, *Biochem. Biophys. Res. Commun.*, 58, 1079, 1974.
129. **Petkau, A.,** Role of superoxide dismutase in modification of radiation injury, *Br. J. Cancer*, 55(Suppl. 8), 87, 1987.
130. **Abe, M., Nishidai, T., Yukawa, Y., Takahashi, M., Ono, K., Hiraoka, M., and Ri, N.,** Studies on the radioprotective effects of superoxide dismutase in mice, *Int. J. Radiat. Oncol. Biol. Phys.*, 7, 205, 1981.
131. **Lin, P. S., Kwock, L., and Butterfield, C. E.,** Diethyldithiocarbamate enhancement of radiation and hyperthermic effects on chinese hamster cells *in vitro*, *Radiat. Res.*, 77, 501, 1979.
132. **xuPeng, T., Moya, A., and Ayala, F. J.,** Irradiation-resistance conferred by superoxide dismutase: possible adaptive role of a natural polymorphism in *Drosophila melanogaster*, *Proc. Natl. Acad. Sci. U.S.A.*, 83, 684, 1986.
133. **Marklund, S. L., Westman, N. G., Roos, G., and Carlsson, J.,** Radiation resistance and the CuZn superoxide dismutase, Mn superoxide dismutase, catalase, and glutathione peroxidase activities of seven human cell lines, *Radiat. Res.*, 100, 115, 1984.
134. **Petkau, A., Chelak, W. S., Kelly, K., and Friesen, H. G.,** Superoxide dismutase and radiosensitivity: implications for mammary carcinomas, in *Pathology of Oxygen*, Autor, A. P., Ed., Academic Press, New York, 1982, 223.
135. **Issels, R. D., Schalhorn, A., and Thiel, E.,** Superoxide dismutase activity in T and B lymphoma and its possible relationship to radiation sensitivity, in *Oxygen and Oxy Radicals in Chemistry and Biology*, Rogers, M. A. J. and Powers, E. L., Eds., Academic Press, New York, 1981, 667.
136. **Oberley, L. W., and Buettner, G. R.,** Role of superoxide dismutase in cancer: a review, *Cancer Res.*, 39, 1141, 1979.
137. **Krizsan, J., Stoklasova, A., Kovarova, H., and Ledvina, M.,** The effect of γ-irradiation and cystamine on superoxide dismutase activity in the bone marrow and erythrocytes of rats, *Radiat. Res.*, 91, 507, 1982.
138. **Hassan, H. M. and Fridovich, I.,** Superoxide radical and the oxygen enhancement of the toxicity of paraquat in *Escherichia coli*, *J. Biol. Chem.*, 253, 8143, 1978.
139. **Schweitzer, K., Benko, Gy., and Bekes, P.,** Investigation into the superoxide dismutase (SOD) activity of human erythrocytes at work places exposed to radiation hazard, *Radiobiol. Radiother.*, 26, 629, 1985.
140. **Kennedy, A. R., Troll, W., and Little, J. B.,** Role of free radicals in the initiation and promotion of radiation transformation *in vitro*, *Carcinogenesis*, 5, 1213, 1984.
141. **Wieczorek, Z., Gieldanowski, J., Zimecki, M., Mioduszewski, J. Z., Szymanice, S., and Daczynska, R.,** Radioprotective activity of the complex of bivalent copper with 3-mercapto-2-hydroxypropyl ether of dextran (C-79), *Arch. Immunol. Ther. Exp.*, 31, 715, 1983.
142. **Sorenson, J. R. J.,** Bis(3,5 diisopropyl salicylato)copper (II), a potent radioprotectant with superoxide dismutase mimetic activity, *J. Med. Chem.*, 27, 1747, 1984.
143. **Smith, C. V., Hughes, H., Lauterburg, B. H., and Mitchell, J. R.,** Chemical nature of reactive metabolites determines their biological interactions with glutathione, in *Functions of Glutathione: Biochemical Physiological, Toxicological and Clinical Aspects*, Larsson, A., Orrenius, S., Holmgren, A., and Mannervik, B., Eds., Raven Press, New York, 1983, 125.
144. **Christophersen, B. O.,** Reduction of X-ray-induced DNA and thymine hydroperoxides by rat liver glutathione peroxidase, *Biochim. Biophys. Acta*, 186, 387, 1969.
145. **Flohé, L., Gunzler, W. A., and Ladenstein, R.,** Gluthathione peroxidase, in *Gluthathione: Metabolism and Function*, Arias, I. M. and Jakoby, W. B., Eds., Raven Press, New York, 1976, 115.
146. **Tappel, A. L.,** Selenium-glutathione peroxidase: Properties and synthesis, *Curr. Topics in Cell Regul.*, 24, 87, 1984.
147. **Batist, G., Raymond, A., Katki, A. G., Travis, E. L., Shoemaker, M. C., Greene, R. F., and Myers, C. E.,** Enzymatic defense against radiation damage in mice. Effect of selenium and vitamin E depletion, *Biochem. Pharmacol.*, 35, 601, 1986.

148. **Kumar, K. S. and Weiss, J. F.**, Inhibition of glutathione peroxidase and glutathione transferase in mouse liver by misonidazole, *Biochem. Parmacol.* 35, 3143, 1986.
149. **Jacobs, A. J., Rankin, W. A., Srinivasan, V., and Weiss, J. F.**, Effects of vitamin E and selenium on glutathione peroxidase activity and survival of irradiated mice, in *Proc. 7th Int. Congr. Radiation Research*, Broerse, J.J., Barendsen, G. W., Kal, H. B., and van der Kogel, A. J., *Eds.*, Martinus Nijhoff, Amsterdam, 1983, D5-15.
150. **Ganther, H. E.**, Enzymatic synthesis of dimethyl selenide from sodium selenite in mouse liver extracts, *Biochemistry*, 5, 1089, 1966.
151. **Hawkes, W. C., Wilhelmsen, E. C., and Tappel, A. L.**, Abundance and tissue distribution of selenocysteine-containing proteins in the rat, *J. Inorg. Biochem.*, 23, 77, 1985.
152. **Cekan, E., Slanina, P., Bergman, K., and Tribukait, B.**, Effects of dietery supplementation with selenomethionine on the teratogenic effect of ionizing radiation in mice, *Acta Radiobiol. Oncol.*, 24, 459, 1985.
153. **Breccia, A., Badiello, R., Trenta, A., and Mattii, M.**, On the chemical radioprotection by organic compounds in vivo, *Radiat. Res.*, 38, 483, 1969.
154. **Wendel, A., Fausel, M., Safayhi, H., Tiegs, G., and Otter, R.**, A novel biologically active seleno-organic compound. II. Activity of PZ51 in relation to glutathione peroxidase, *Biochem. Pharmacol.*, 33, 3241, 1984.
155. **Oberley, L. W. and Sierra, E.**, Radiation sensitivity testing of cultured eukaryotic cells, in *Handbook of Methods for Oxygen Radical Research*, Greenwald, R. A., Ed., CRC Press, Boca Raton, Fla., 1985, 417.
156. **Ahmad, T. and Fricker, H.**, Active site-specific inhibition by 1,3-bis(2-chloroethyl)-1-nitrosourea of two genetically homologus flavoenzymes: glutathione reductase and lipoamide dehydrogenase, *J. Lab. Clin. Med.*, 105, 464, 1985.
157. **Pearson, W. R., Windle, J. J., Morrow, J. F., Benson, A. M., and Talalay, P.**, Increased synthesis of glutathione-*S*-transferase in response to anticarcinogenic antioxidants. Cloning and measurement of messenger RNA, *J. Biol. Chem.*, 258, 2052, 1983.
158. **Stohs, S. J., Lawson, T. A., Anderson, L., and Bueding, E.**, Effects of oltipraz, BHA, ADT and cabbage on glutathione metabolism, DNA damage and lipid peroxidation in old mice, *Mech. Ageing Dev.*, 37, 137, 1986.

Biochem. J. (1988) 255, 1037–1043 (Printed in Great Britain)

Inositol 1,4,5-trisphosphate concentrations increase after adherence in the macrophage-like cell line J774.1

Vivian ZABRENETZKY and Elaine K. GALLIN*
Department of Physiology, Armed Forces Radiobiology Research Institute, Bethesda, MD 20814-5145, U.S.A.

Several properties of macrophages change when suspended cells become adherent. To determine the intracellular signals involved in these changes, concentrations of the second messenger inositol 1,4,5-trisphosphate [Ins(1,4,5)P_3] were monitored during adherence of J774.1 cells, a macrophage-like cell line. When cells grown in suspension were allowed to adhere to a glass surface, there was a transient increase in InsP_3 that reached a peak between 100 and 120 s after plating. Inositol mono- and bis-phosphate concentrations were also elevated 100 and 120 s after plating. Analysis of isomer distribution showed significant 3-fold increases in Ins(1,4,5)P_3 and inositol 1,3,4,5-tetrakisphosphate [Ins(1,3,4,5)P_4] at 100 s after plating. These values were maintained at 120 s, with the additional appearance of a 4-fold increase in inositol 1,3,4-trisphosphate. The adherence-induced generation of Ins(1,4,5)P_3 was decreased, and Ins(1,3,4,5)P_4 formation was blocked, in Ca^{2+}-free medium. However, doubling intracellular [Ca^{2+}] by addition of the Ca^{2+} ionophore ionomycin (1 μM) did not increase Ins(1,4,5)P_3 in suspended cells. Adherence of J774.1 cells to fibronectin-coated glass also induced an increase in InsP_3.

INTRODUCTION

The migration of macrophages to areas of chronic inflammation and infection involves adherence to a variety of surfaces. Studies *in vitro* have shown that the process of adherence triggers a number of functional changes in macrophages. These changes include an increase in peroxidase staining in the rough endoplasmic reticulum in rabbit blood monocytes 2 h after adherence (Bodel *et al.*, 1977), an increased expression of the FMC 17 antigen in human monocytes 12 h after plating of cells that were suspended for 16 h (Triglia *et al.*, 1985), and increases in the transport of lysine and adenosine 30 min after monolayer formation in rabbit lung macrophages (Pofit & Strauss, 1977). In the murine-derived macrophage-like cell line J774.1, membrane-potential measurements using a lipophilic radiolabelled cation indicate that adherence is associated with a hyperpolarization from −15 mV to −80 mV (Sung *et al.*, 1985). Patch-clamp studies in J774.1 cells have demonstrated the differential expression of two voltage-dependent K^+ conductances with time after adherence (Gallin & Sheehy, 1985). One of these conductances is responsible for maintaining the −80 mV membrane potential in adherent cells (Gallin & Sheehy, 1985). In all of these studies, the nature of the signal(s) that mediates the adherence-induced changes in macrophages is unknown.

Signal transduction in many cells, including white blood cells, occurs via receptor-mediated stimulation of phospholipase C that cleaves the plasma-membrane phospholipid phosphatidylinositol 4,5-bisphosphate. Two products which possess second-messenger function are formed: inositol 1,4,5-trisphosphate [Ins(1,4,5)P_3], which releases Ca^{2+} from intracellular stores, and *sn*-1,2-diacylglycerol, which activates protein kinase C (Berridge & Irvine, 1984; Nishizuka, 1984; Downes & Michell, 1985). In macrophages, platelet-activating factor, *N*-formylmethionyl-leucylphenylalanine (fMet-Leu-Phe) (Downes & Michell, 1985; Whetton *et al.*, 1986) and bacterial lipopolysaccharide activate this pathway (Prpic *et al.*, 1987). The present paper addresses the question of whether the process of adherence of J774.1 cells is associated with the generation of the second messenger Ins(1,4,5)P_3.

MATERIALS AND METHODS

Culture of J774.1 cells

J774.1 cells were obtained from American Type Culture Collection (Rockville, MD, U.S.A.) and were stored at −70 °C until needed. Cells were maintained in tissue-culture medium containing RPMI 1640 supplemented with penicillin (10 units/ml), streptomycin (10 μg/ml), 0.03% (w/v) glutamine and 10% (v/v) heat-inactivated fetal bovine serum. Stock cultures were maintained as a non-adherent population in spinner flasks treated with Sigmacote. Cultures were kept at 37 °C in a 5%-CO_2 incubator and fed every 2 days. Only early-passage cells (< 20) were used in these studies. In all cases freshly thawed cells were able to generate the InsP_3 signal when measured at 100 s after plating.

Labelling of cells with *myo*-[2-^{3}H]inositol

Approx. 7×10^5 cells/ml in a final volume of 45 ml of supplemented RPMI 1640 medium were incubated with 100 μCi of *myo*-[^{3}H]inositol (13 Ci/mmol) for 18 h. Each portion of [^{3}H]inositol was purified by centrifugation through Dowex AG 1-X8 resin before use. Longer periods of labelling cells, from 20 to 42 h, did not yield a substantially higher specific radioactivity of radioisotope incorporation.

Abbreviations used: Ins(1,4,5)P_3, inositol 1,4,5-trisphosphate; Ins(1,3,4)P_3, inositol 1,3,4-trisphosphate; Ins(1,3,4,5)P_4, inositol 1,3,4,5-tetrakisphosphate; InsP_1, inositol 1-phosphate; InsP_2, inositol 1,4-bisphosphate; $Ca^{2+}{}_o$, extracellular Ca^{2+}; $Ca^{2+}{}_i$, intracellular Ca^{2+}.

* To whom reprint requests should be sent.

Adherence protocol

Labelled cells were pelleted (850 *g* for 5 min) and then resuspended in serum-free RPMI 1640 for 10 min at room temperature. The cells were pelleted again and resuspended in 15 ml of NaCl Hanks (145 mM-NaCl, 4.6 mM-KCl, 1.3 mM-$MgCl_2$, 1.6 mM-$CaCl_2$ and 10 mM-Hepes, pH 7.3). This suspension was immediately pelleted and the cells were resuspended in NaCl Hanks at approx. 14×10^6 cells/ml. After equilibration for 10 min, 1.5 ml of cell suspension was applied to a 50 mm-diameter glass dish and allowed to adhere for various times. At the end of the adherence period, the non-adherent cells were removed by flooding the surface with 5 ml of NaCl Hanks and immediately aspirating the supernatant. The reaction was stopped by addition of 4.5 ml of cold 4.5% $HClO_4$/NaCl Hanks (2:1, v/v) to the glass dish. The dishes were chilled and then scraped. Suspended cells served as the control group; 3 ml of 4.5% $HClO_4$ was added to 1.5 ml of the suspended cell sample. Portions (100 μl) of suspended and adherent samples were set aside for protein determination.

In preliminary experiments incubation with 10 mM-LiCl for 10 min did not affect InsP_3 generation. Therefore LiCl was not used in subsequent studies.

Separation of [^{3}H]inositol metabolites

The $HClO_4$ extracts from suspended and adherent cells were chilled at 0 °C and then centrifuged to pellet the acid-extractable material. Lipid-soluble material was extracted from these pellets. The lipids from the acid-extracted pellet were solubilized by addition of chloroform/methanol (1:1, v/v) (containing 1 M-KCl and 10 mM-inositol) and centrifuged (6000 *g*, 3 min). Portions (100 μl) of the chloroform extract were evaporated before radioactivity counting in 10 ml of Aquasol (New England Nuclear) to determine d.p.m. in the lipid extract for the normalization procedure (see below).

The supernatants were prepared for separation of the [^{3}H]inositol metabolites by adjusting the pH to 8.0 with a solution of 0.5 M-KOH/9.0 mM-$Na_2(BO_4)_2$/1.9 mM-EDTA (Burgess *et al.*, 1985). This separation procedure was compared with one using trichloroacetic acid precipitation followed by diethyl ether extraction (Berridge *et al.*, 1983), and similar recoveries were obtained. The samples were stored at −20 °C. After thawing, the $KClO_4$ salts had precipitated and were pelleted (850 *g*, 5 min). The supernatant was applied to 1 ml of a 50% (w/v) suspension of Dowex AG 1-X8 resin (formate form; 100–200 mesh). The [^{3}H]inositol phosphates were eluted by the method of Berridge *et al.* (1983). Inositol, glycerophosphoinositol, inositol 1-phosphate (InsP_1), inositol 1,4-bisphosphate (InsP_2) and inositol trisphosphates (InsP_3) were sequentially eluted with water (24 ml), 5 mM-disodium tetraborate/60 mM-sodium formate (24 ml), 100 mM-formic acid/200 mM-ammonium formate (36 ml), 100 mM-formic acid/400 mM-ammonium formate (24 ml), and 100 mM-formic acid/1.0 M-ammonium formate (38 ml). Each eluate was collected in at least two fractions, and 1 ml of each fraction was counted for radioactivity in 10 ml of Aquasol. *myo*-[^{3}H]Inositol, [^{14}C]inositol 1-phosphate and [^{3}H]-Ins(1,4,5)P_3 were run as standards with and without the water extract from unlabelled cells to verify the elution sequence. There was a 96% recovery of standards.

Protein determination

Protein was determined in the acid extracts of suspended and adherent cells. Portions (100 μl) from each sample were frozen and thawed, and the acid-extracted protein was then pelleted (6000 *g*, 3 min). NaOH (50 μl; 1 M) was added to dissolve the protein, and 10 μl samples were used in the Bradford micro-assay (Bio-Rad, Richmond, CA, U.S.A.).

Normalization procedure

The adherent cell population represented only a fraction of the suspended cell population at each of the time points surveyed. Therefore, to determine if concentrations of inositol phosphates changed after adherence, it was necessary to normalize the adherent-cell data to the suspended-cell data. Because it was not clear which normalization procedure was best, data were normalized in two different ways: normalizing to cell protein and normalizing to d.p.m. in the lipid-soluble extract.

Normalized InsP_3 was calculated by the following equation: $[(I_a \times N)/I_s] \times 100$ = adherent InsP_3 (expressed as % of suspended cells), where $L_s/L_a = N$ (normalization factor), L_s = d.p.m. in the suspended-cell lipid-soluble extract, L_a = d.p.m. in the adherent-cell lipid-soluble extract, I_s = d.p.m. in the suspended-cell InsP_3 fraction, and I_a = d.p.m. in the adherent-cell InsP_3 fraction. For normalization to protein, the term 'lipid-soluble extract' can be replaced by 'cell protein' in these expressions.

Separation of InsP_3 isomers by h.p.l.c.

The InsP_3 fractions from the Dowex columns were acidified and salt-extracted by passing them over Dowex 50 resin (H^+ form); they were frozen, freeze-dried, and stored at −70 °C until further analysis. The freeze-dried [^{3}H]InsP_3 fractions were solubilized in 2 ml of water and filtered through 0.22 μm-pore-size filter before manual injection on to a Whatman Partisil 10 SAX column ($H_2PO_4^-$ form) and chromatographed in accordance with modifications of the procedure of Batty *et al.* (1985). The sample was eluted at 1.2 ml/min by a non-linear gradient, consisting first of water for 4.9 min, followed by a linear gradient of 0.8 M-ammonium formate (adjusted to pH 3.7 with H_3PO_4) to 1.7 M-ammonium formate (adjusted to pH 3.7 with H_3PO_4) at 5–30 min. The 1.7 M-ammonium formate buffer (100%) was run for a further 5 min, and then the gradient was returned linearly to water over 5 min. Throughout, 1 min fractions were collected, and 0.5 ml of each fraction was counted for radioactivity in 1.0 ml of water and 10 ml of Aquasol. Standard retention times were determined by running a mixture of 0.025 μCi of D-[4,5-^{32}P]Ins(1,4,5)P_3, 0.025 μCi of D-[*inositol*]-2-^{3}H(n)]inositol 1,3,4,5-tetrakisphosphate-{[^{3}H]Ins(1,3,4,5)P_4} and 150 μM-ATP in water and monitoring each fraction for both radioactivity and ATP (by the A_{245}). Another run, consisting of the ^{3}H-labelled cell fraction eluted from the Dowex column with 1.0 M-ammonium formate (InsP_3 fraction) mixed with 0.025 μCi of [^{32}P]Ins(1,4,5)P_3 fraction, was done. This run gave the same retention time for Ins(1,4,5)P_3 as the standard run. Approx. 96% of each standard was recovered in both standard runs, and approx. 90% of each cell-derived sample was recovered in the experimental runs.

Statistical analysis

The significance of the differences between means was assessed by Student's two-tailed *t* test for paired samples.

Materials

myo-[2-^{3}H(n)]Inositol, D-[*inositol*-2-^{3}H(n)]Ins(1,4,5)P_3, D-[4,5-^{32}P]Ins(1,4,5)P_3 and D-[*inositol*-2-^{3}H(n)]Ins-(1,3,4,5)P_4 were obtained from New England Nuclear (Boston, MA, U.S.A.). L-*myo*-[U-^{14}C]Inositol-1-phosphate was purchased from Amersham (Arlington Heights, IL, U.S.A.). Ammonium formate and sodium formate were obtained from Sigma (St. Louis, MO, U.S.A.). Whatman Partisil 10 SAX columns were obtained from American Scientific Products (Columbia, MD, U.S.A.). AG 1-X8 resin (formate form) and Dowex 50 W-X8 resin were obtained from Bio-Rad.

RESULTS

Time-dependence of adherence

Fig. 1(*a*) shows data from three different experiments in which the adherent-cell protein was measured at various times after plating on a glass surface. There was a time-dependent increase in adherence, with approx. 40% of all cells adhering 100 s after plating, and 50% of the cells adhering 160 s after plating. Experiments carried out for longer time periods (190 and 310 s) did not result in a significant increase in the number of adherent cells, indicating that by 160 s cell adherence had plateaued. A visual examination of the dishes indicated that the cells were approaching confluence. A study was performed to determine whether the cells that did not adhere after the first plating were able to adhere if plated a second time. Non-adherent cells from a dish plated for 300 s were harvested and replated for another 300 s; 83% of these cells adhered during the second plating, indicating that approx. 90% of the total population of J774.1 cells was adherent. Results (not shown) from one batch of J774.1 cells (probably plated at a lower density) showed 90% adherence 160 s after the first plating. These cells did not differ in their ability to generate InsP_3 after adherence.

InsP_3 generation as a consequence of adherence

Fig. 1(*b*) shows the time-dependent increase in InsP_3 produced after adherence in J774.1 cells. The [^{3}H]inositol phosphate content of adherent cells was normalized to the radioactivity (d.p.m.) in the lipid extracts of suspended cells and was expressed as a percentage of the [^{3}H]inositol content of the suspended cells. A peak value of approx. 145% of control was reached at 100 s after plating and remained significantly elevated at 120 s. InsP_3 contents decreased to control values by 190 s and remained at 100% of control until 310 s. Though the number of cells adhering between 100 and 160 s was increasing (from ~40% to ~50%), the observed InsP_3 signal had reached a peak and was decreasing. If the process of adherence simply selected cells with higher basal contents of InsP_3, a time-dependent increase followed by a decrease in InsP_3 would not have been expected. Therefore these data indicate that adherence can generate an InsP_3 signal in J774.1 cells.

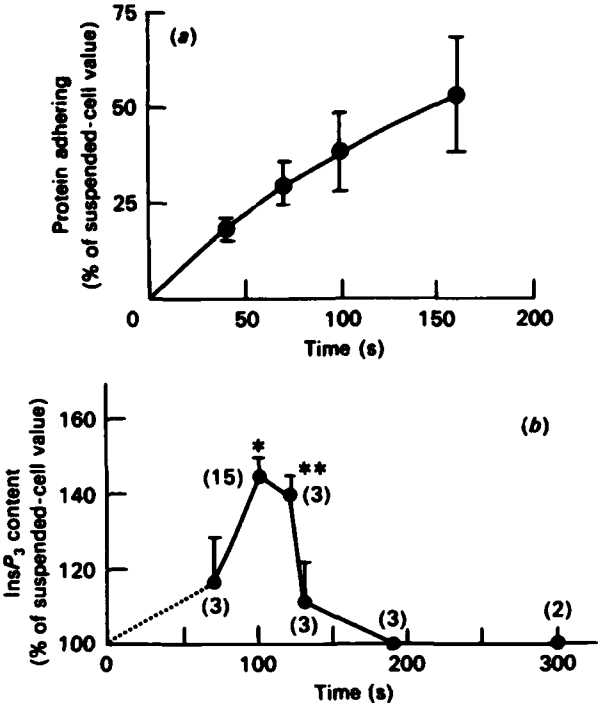

Fig. 1. (*a*) Percentage of cell protein adhering to glass, and (*b*) time course of adherence-induced InsP_3 generation

(*a*) Cells were allowed to adhere for the indicated times, and the adherent protein was measured. Each time point represents the mean ± S.E.M. for three experiments (done in duplicate), from different passages of J774.1 cells. The data are presented as percentages of total protein for suspended cells. (*b*) InsP_3 content was analysed by Dowex chromatography of cells plated for the indicated times. Data, normalized to lipid, are expressed as percentages of suspended-cell values. Each point represents the mean ± S.E.M.: $^*P < 0.001$, $^{**}P < 0.05$.

Table 1. Time course of formation of inositol phosphates

Data (means ± S.E.M.), expressed as percentages of suspended-cell inositol phosphate contents, were normalized either to d.p.m. in the lipid-soluble extract of suspended cells or to suspended cell protein: $^aP < 0.001$, $^bP < 0.01$, $^cP < 0.02$, $^dP < 0.05$.

Time of adherence (s)	No. of expts.	InsP_1		InsP_2		InsP_3	
		Lipid	Protein	Lipid	Protein	Lipid	Protein
100	8	170 ± 11^a	189 ± 12^a	113 ± 3.2^b	122 ± 3.5^a	145 ± 8.1^a	160 ± 14^b
120	3	133 ± 6.5^d	150 ± 7^c	126 ± 6.9^d	153 ± 9.2^d	140 ± 6.4^c	180 ± 14^c
190	3	97 ± 16	106 ± 5.2	93 ± 16	118 ± 9.8	101 ± 2.0	115 ± 12

Comparison of normalization procedures

Table 1 compares data from the same studies that were normalized to either protein or lipid. The average value of InsP_3 at 100 s after plating was slightly higher when normalized to protein than when normalized to lipid. At 120 s the InsP_3 signal was still significantly elevated when either normalization procedure was used. At 190 s after plating, both normalization procedures indicated that the InsP_3 signal had returned to control.

There were also adherence-associated changes in the contents of InsP_1 and InsP_2, when either normalization procedure was used (Table 1). At 100 s there was a significant increase in InsP_1 and a smaller but significant increase in InsP_2. At 120 s InsP_1 and InsP_2 were still significantly increased. By 190 s InsP_1, InsP_2 and InsP_3 had returned to basal values. These data show that normalizing to lipid or protein gave equivalent results; therefore data presented below have been normalized to d.p.m. in the lipid-soluble fraction.

Distribution of InsP_3 isomers

At 100 and 120 s after plating, InsP_3 contents were elevated to ~ 145% of control. To identify the isomers that were increased at these times, the InsP_3 fractions were separated into their component isomers by h.p.l.c. In five separate studies, at 100 s after plating the Ins(1,4,5)P_3 and Ins(1,3,4,5)P_4 contents were 3.11 ± 0.22 ($P < 0.01$) and 3.14 ± 0.35 ($P < 0.01$) times suspended-cell values respectively. A representative experiment is shown in Fig. 2(*a*). An additional peak was eluted at a later retention time than Ins(1,3,4,5)P_4 (which was eluted at 32 min), suggesting that another inositol phosphate, possibly Ins(1,3,4,5,6)P_5, was present (Stephens *et al.*, 1988). Further studies will have to be done to determine its identity.

At 120 s after plating (Fig. 2*b*) the increases in both Ins(1,4,5)P_3 and Ins(1,3,4,5)P_4 were sustained. In addition, there was a 4-fold increase in Ins(1,3,4)P_3, which is consistent with other studies indicating that Ins(1,3,4)P_3 is a metabolic product of the action of 5′-phosphomonoesterase on Ins(1,3,4,5)P_4 (Hawkins *et al.*, 1986). The control (suspended-cell) inositol phosphate profiles were somewhat variable, as depicted by the difference between the control runs in Figs. 2(*a*) and 2(*b*).

Role of Ca^{2+} in the generation of the InsP_3 signal

In other cells the stimulation of InsP_3 production sometimes requires extracellular Ca^{2+} (Ca^{2+}_o) (Lew *et al.*, 1986; Beaven *et al.*, 1984). In order to examine the role of Ca^{2+}_o in adherence-induced InsP_3 formation, cells that had equilibrated for 5 min in Ca^{2+}-free Hanks medium containing 1 mM-EGTA were compared with cells from the same batch plated in Ca^{2+}-containing media. The percentage of cells adhering in Ca^{2+}-free medium + 1 mM-EGTA at 100 s after plating was equivalent to the percentage of cells adhering in normal Hanks medium (Fig. 3*a*). In contrast, the increase in InsP_3, InsP_1 and InsP_2 was inhibited by 77%, 60% and 58% respectively (Table 2). In these studies the cells were incubated for 5 min in Ca^{2+}-free media; therefore it was possible that intracellular Ca^{2+} concentration ($[Ca^{2+}]_i$) was lowered at the time of adherence, and the decrease in the contents of the inositol phosphates was due to this decrease rather than to the removal of Ca^{2+}_o. To obviate this possibility, experiments were performed in which a bolus of 5 mM-EGTA was added to cells in normal Hanks medium (containing 1.6 mM-$CaCl_2$) immediately before plating. The generation of InsP_3 in these cells was compared with

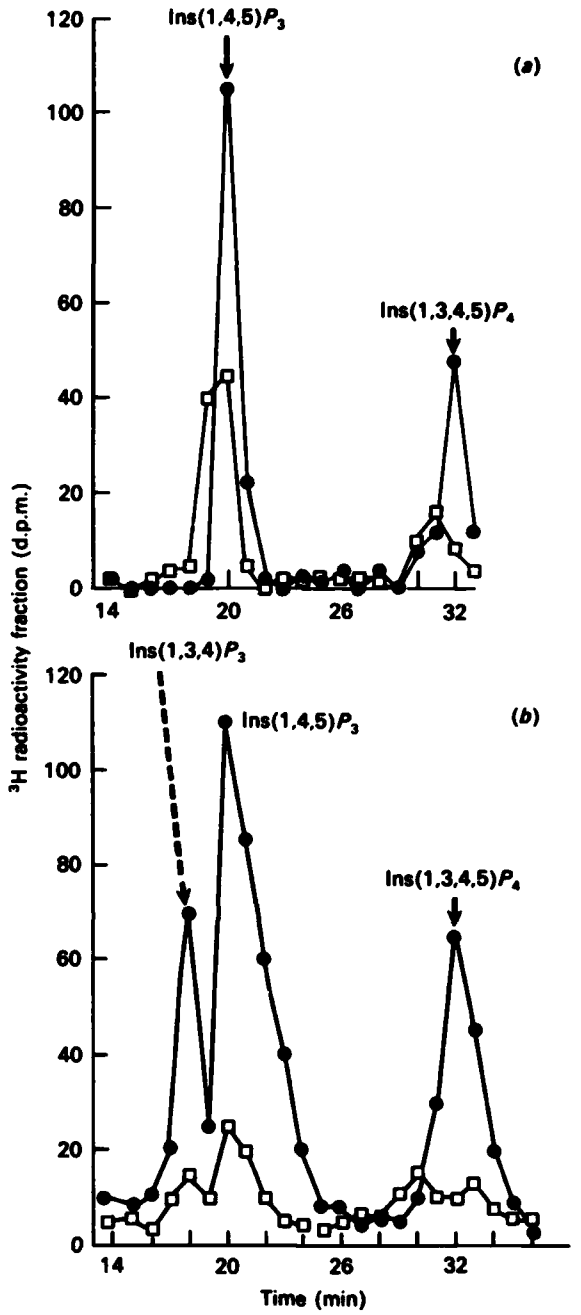

Fig. 2. H.p.l.c. profiles of InsP_3 fractions from Dowex columns

(*a*) Fractions from adherent cells 100 s after plating (●) and from suspended cells (□). Data are from a single experiment, with each point derived from duplicates. Adherent-cell data were normalized to the d.p.m. in the lipid-soluble fraction. The means ± S.E.M. for Ins(1,4,5)P_3 and Ins(1,3,4,5)P_4 peaks for the suspended cells in five experiments were 53 ± 27 and 45 ± 23 d.p.m. respectively. (*b*) Fractions from adherent cells 120 s after plating (●) and from suspended cells (□). Derivation of data is as presented in Fig. 2(*a*). The mean values for Ins(1,4,5)P_3, Ins(1,3,4)P_3 and Ins(1,3,4,5)P_4 peaks for the suspended cells in two experiments were 20, 15 and 13 d.p.m. respectively.

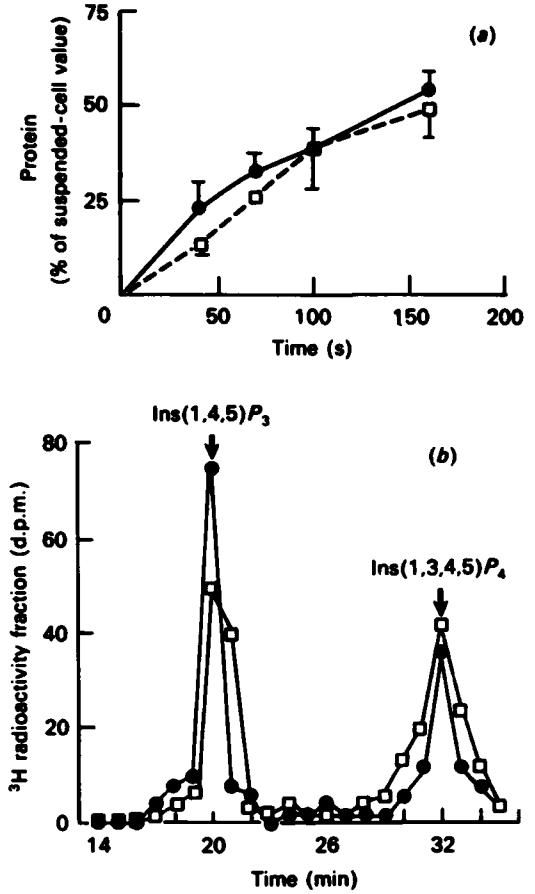

Fig. 3. Effect of Ca^{2+}-free media on (*a*) time course adherence and (*b*) h.p.l.c. profile of InsP_3 fraction

Each point represents the mean ± S.E.M. for three experiments, each done in duplicate. The data are expressed as percentages of suspended-cell protein in either normal Hanks medium (●) or Ca^{2+}-free Hanks medium + 1 mM-EGTA (□) as appropriate. (*b*) H.p.l.c. profile of InsP_3 fraction from cells plated for 100 s in Ca^{2+}-free medium + 1 mM-EGTA (●) and from cells suspended in Ca^{2+}-free medium + 1 mM-EGTA (□). Data are from a representative experiment, with each point derived from duplicates. The adherent-cell data were normalized to the d.p.m. in the lipid-soluble fraction. The means ± S.E.M. for the Ins(1,4,5)P_3 and Ins(1,3,4,5)P_4 peaks for suspended cells from three separate studies were 52 ± 12 and 62 ± 19 d.p.m. respectively.

Table 2. Distribution of inositol phosphates at 100 s after plating

Cells were plated in normal Hanks (+Ca_o) or Ca^{2+}-free Hanks + 1 mM-EGTA (−Ca_o). The data (means ± S.E.M. of three experiments in duplicate), expressed as percentages of total suspended-cell inositol phosphate content, were normalized to d.p.m. in the lipid-soluble extract of suspended cells. $^aP < 0.05$.

	InsP_1	InsP_2	InsP_3
+Ca_o	200 ± 20^a	137.5 ± 3.4	162 ± 7^a
−Ca_o	135 ± 20	115 ± 26	113 ± 15

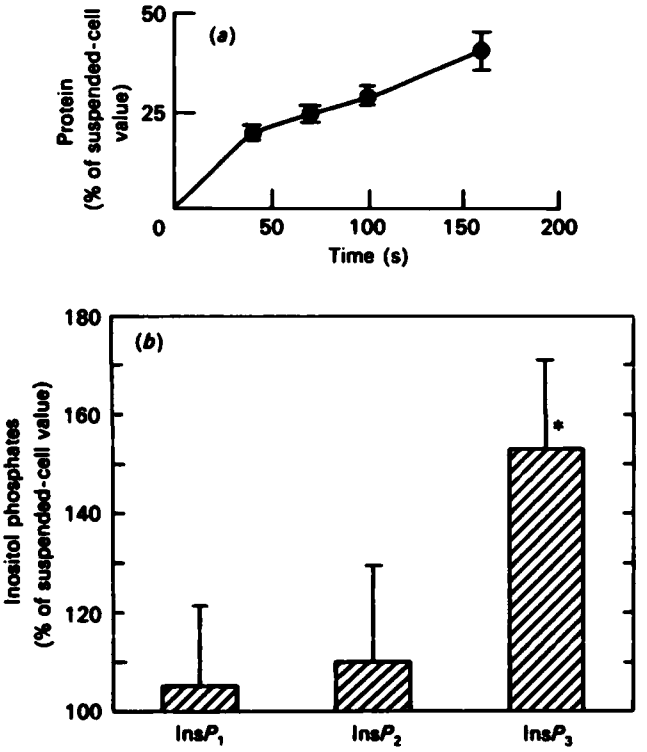

Fig. 4. Effect of fibronectin-coated glass on (*a*) time course of adherence and (*b*) amounts of inositol phosphates

(*a*) The data, presented as percentages of suspended-cell protein, represent means ± S.E.M. of three separate experiments done in duplicate. Protein corresponding to fibronectin was subtracted from the total protein to determine cell protein. (*b*) Distribution of inositol phosphates 120 s after adherence to fibronectin. Data, presented as percentages of suspended-cell values, normalized to d.p.m. in lipid-soluble fraction, represent means ± S.E.M. of three experiments done in duplicate: $^*P < 0.05$.

that in cells plated in Ca^{2+}-containing media. These conditions (results not shown) also inhibited adherence-induced InsP_3 formation at 100 s, suggesting that generation of the signal requires $Ca^{2+}{}_o$.

Analysis of the isomer distribution of the InsP_3 fraction was examined for cells suspended in Ca^{2+}-free medium + 1 mM-EGTA for 5 min before adherence (two experiments), and for cells in which a bolus of 5 mM-EGTA was added to Ca^{2+}-containing medium immediately before plating (one experiment). All three experiments showed that there was no change in the Ins(1,3,4,5)P_4 peak. Summing fractions 19–21, the Ins(1,4,5)P_3 fraction, showed an average increase of 42 ± 31%, compared with an average increase of 251 ± 91% observed in the presence of Ca^{2+}. Fig. 3(*b*) shows one of these studies. Suspended cells in Ca^{2+}-free medium had Ins(1,4,5)P_3 or Ins(1,3,4,5)P_4 contents that did not differ from values obtained for suspended cells in Ca^{2+}-containing medium. These data show that the generation of InsP_3 and its isomers during adherence is inhibited in Ca^{2+}-free media.

Since the preceding studies demonstrated that $Ca^{2+}{}_o$ is

required for the generation of the InsP_3 signal, experiments were done to determine whether raising $[Ca^{2+}]_i$ with the Ca^{2+} ionophore ionomycin could induce formation of InsP_3 in suspended cells. Studies in these cells using the Ca^{2+} indicator fura-2 indicated that ionomycin (1 μM), in the presence of 1.6 mM-Ca^{2+}_o, doubled $[Ca^{2+}]_i$ within 30 s after its addition and that this increase was maintained for the 2 min assay period (results not shown). However, incubation in 1 μM-ionomycin for 30 s, 1 min or 3 min did not affect the contents of InsP_3, InsP_2 or InsP_1 in suspended cells, indicating that doubling $[Ca^{2+}]_i$ is not a sufficient stimulus to increase InsP_3.

Adherence to fibronection-coated surfaces and InsP_3 generation

J774.1 cells were placed on fibronectin-coated dishes to determine whether adherence to other surfaces resulted in similar increases in InsP_3. As shown in Fig. 4(*a*), there was a slight decrease (10%) in the number of cells adhering to fibronectin-coated dishes compared with adherence to glass. We chose the 120 s time point to measure InsP_3 contents, since more cells were adherent at this time than at 100 s. Fig. 4(*b*) shows that InsP_3 was significantly increased above control, which is similar to the results obtained after adherence to glass. However, InsP_1 and InsP_2 were not significantly elevated.

DISCUSSION

This report demonstrates that there is a transient increase in the second messenger Ins(1,4,5)P_3 in J774.1 cells 100–120 s after adherence to glass and that this increase is dependent on Ca^{2+}_o. An increase in InsP_3 was also noted 120 s after adherence to fibronectin-coated glass.

In these studies adherence was not synchronized, since cells settle at different rates. The peak of an adherence-induced transient signal (measured in a population of cells) will be diminished by differences in adherence times. Plating the cells in a volume sufficient just to cover the surface of the dish minimized this problem. Despite an unavoidable (but small) variation in adherence times, the total InsP_3 values 100 s after plating were significantly higher than suspended-cell values, and the isomers Ins(1,4,5)P_3 and Ins(1,3,4,5)P_4 were increased 3-fold above values for suspended cells.

The increases in InsP_3 contents described in this paper could result from the selection of a subpopulation of adherent cells that have endogenously higher contents of InsP_3. Three findings argue strongly against this possibility. First, whereas only 50% of the J774.1 cells plated adhered to the glass surfaces (presumably because of physical constraints caused by the high cell density), ~ 90% of the cells were capable of adhering. Second, there is a time-dependence for the increase in InsP_3, with the contents returning to suspended-cell values 3 min after plating. Third, the InsP_3 signal was decreased in cells plated in Ca^{2+}-free medium, even though there was no decrease in the percentage of cells adhering or any change in the time course of adherence.

The generation of the InsP_3 signal has been shown to be dependent on $[Ca^{2+}]_o$ in some studies on different cells. For example, the peak and rate of rise of the substance-P-induced InsP_3 and InsP_4 signals in parotid cells is dependent on $[Ca^{2+}]_o$ (Merritt & Rink, 1987), and Beaven *et al.* (1984) have shown that antigen-stimulated production of inositol phosphates is dependent on $[Ca^{2+}]_o$, with a concentration-dependence similar to that of histamine release. Pribluda & Metzger (1987) have shown that antigen-stimulated production of inositol phosphates is decreased to 25% of control in the 2H3-HR$^+$ subline of rat basophilic leukaemia cells in Ca^{2+}-free media. These reports are consistent with our data that demonstrate a decrease in InsP_3 (77%), InsP_2 (58%), and InsP_1 (60%) in cells plated in Ca^{2+}-free media compared with cells in Ca^{2+}-containing media. Isomer determination of the InsP_3 fraction revealed an inhibition of Ins(1,4,5)P_3 and Ins(1,3,4,5)P_4 production in Ca^{2+}-free media. These findings indicate that Ca^{2+}-free medium may inhibit phospholipase C, which is consistent with previous reports of a Ca^{2+} requirement for the activity of purified phospholipase C (Ryu *et al.*, 1987). Since the adhesion process is not impaired by the removal of extracellular Ca^{2+}, the data suggest that the production of inositol phosphates is not required for adherence, but plays a role in the functional changes that follow adherence. Attenuation of the inositol phosphate signal consequent to adherence in Ca^{2+}-free media may effect these changes.

Lew *et al.* (1986) have reported that dimethyl sulphoxide-differentiated HL-60 cells (neutrophil-like cells) respond to fMet-Leu-Phe with an increase in Ins(1,4,5)P_3 that is followed by a slower and more sustained increase in Ins(1,3,4)P_3. Increasing $[Ca^{2+}]_i$ to micromolar with ionomycin enhanced the contents of inositol phosphates and the Ins(1,3,4)P_3 isomer in the absence of fMet-Leu-Phe. These findings are in contrast with our data indicating a lack of effect of a 30 s, 1 min or 3 min incubation with ionomycin on InsP_3 contents in suspended J774.1 cells. The reason for this difference is not clear. Our measurements of $[Ca^{2+}]_i$ after ionomycin treatment indicated that $[Ca^{2+}]_i$ doubled. It is possible that greater increases in $[Ca^{2+}]_i$ are necessary to generate inositol phosphates, or, conversely, that changes in $[Ca^{2+}]_i$ in the absence of other changes have no effect on the generation of inositol phosphates in J774.1 cells.

In HL-60 cells Ins(1,3,4)P_3 generation was not directly linked to receptor activation, but resulted from an increased $[Ca^{2+}]_i$ and Ins(1,4,5)P_3 (Lew *et al.*, 1986). A comparison of the h.p.l.c. data in the present paper obtained 100 s after plating (Fig. 2*a*) and 120 s after plating (Fig. 2*b*) indicates that Ins(1,3,4)P_3 increases after the increase in Ins(1,4,5)P_3, which is similar to the sequence found in HL-60 cells.

It will be of interest, in future studies, to determine whether $[Ca^{2+}]_i$ in J774.1 cells is increased after adherence, and whether this is related to the increases in Ins-(1,4,5)P_3 described in this paper. A paper by Kruskal & Maxfield (1987) demonstrated that adherence of mouse thioglycollate-induced peritoneal macrophages to either opsonized or unopsonized tissue-culture plates induces transient increases in $[Ca^{2+}]_i$. In a large percentage of the cells studied, $[Ca^{2+}]_i$ oscillated after adherence. In addition to changes in $[Ca^{2+}]_i$, the adherence and spreading of macrophages are associated with a re-distribution of actin (Amato *et al.*, 1983). Interestingly, Janmey *et al.* (1987) have shown that gelsolin, the Ca^{2+}-activated actin-binding protein, binds to phosphatidylinositol bisphosphate. This binding inhibits the filament-severing activity of gelsolin and dissociates gelsolin–actin complexes. The changes in actin that occur

after adherence may be mediated by both a rise in $[Ca^{2+}]_i$ and hydrolysis of phosphatidylinositol bisphosphate, resulting in a subsequent increase in $InsP_3$.

Adherence may be acting via a non-receptor-mediated pathway to generate $Ins(1,4,5)P_3$. Conversely, the membrane perturbations occurring during adherence may cause the rearrangement and thereby the activation of receptors linked to phospholipase C, or adherence may be acting to induce the activation of phospholipase A_2. In macrophages the generation of arachidonic acid through activation of phospholipase A_2 requires Ca^{2+}_o (Wightman *et al.*, 1981), an thromboxane, an arachidonic acid metabolite, has been shown to generate $Ins(1,4,5)P_3$ via receptor-mediated activation of phospholipase C (Rittenhouse, 1985).

The relationship of the adherence-induced changes in inositol metabolism to macrophage function is unknown. A variety of changes occur in macrophages after adherence. Rabbit and human blood monocytes with no cytochemically observable peroxidase activity in rough endoplasmic reticulum will develop such activity within 2 h post-adherence (Bodel *et al.*, 1977). Adherent rabbit lung macrophages transport lysine and adenosine at faster rates than do suspended cells (Pofit & Strauss, 1977). Human blood monocytes lose FMC-17-antigen expression after 4 h in suspension and regain expression after adherence (Triglia *et al.*, 1985). In J774.1 macrophages, both the resting membrane potential (Sung *et al.*, 1985) and the K^+ conductances (Gallin & Sheehy, 1985) change after adherence. Future studies are needed to determine if the adherence-induced alterations in secretory capacity, antigen expression, enzyme appearance, nutrient uptake and membrane electrophysiology that have been described in macrophages are mediated by an increase in $InsP_3$ contents.

We thank Dr. Leslie McKinney and Dr. Kevin Foskett for critically reading the manuscript, and Mr. Tom Dalton for his technical assistance setting up the h.p.l.c. This work was supported by the Armed Forces Radiobiology Research Institute, Defense Nuclear Agency, under work unit 00020. V.Z. was supported by a National Research Council Fellowship. Views presented in this paper are those of the authors; no endorsement by the Defense Nuclear Agency has been given or should be inferred.

REFERENCES

Amato, P. A., Unanue, E. R. & Taylor, D. L. (1983) J. Cell Biol. **96**, 750–761

Batty, I. R., Nahorski, S. R. & Irvine, R. F. (1985) Biochem. J. **232**, 211–215

Beaven, M. A., Moore, J. P., Smith, G. A., Hesketh, T. & Metcalfe, J. C. (1984) J. Biol. Chem. **259**, 7137–7142

Berridge, M. J. & Irvine, R. F. (1984) Nature (London) **312**, 315–321

Berridge, M. J., Dawson, R. M. C., Downes, C. P., Heslop, J. P. & Irvine, R. F. (1983) Biochem. J. **212**, 473–482

Bodel, P. T., Nichols, B. A. & Bainton, D. F. (1977) J. Exp. Med. **145**, 264–274

Burgess, G. M., McKinney, J. S., Irvine, R. F. & Putney, J. W. (1985) Biochem. J. **232**, 237–243

Downes, C. P. & Michell, R. H. (1985) in Molecular Aspects of Cell Regulation, Vol. 4: Molecular Mechanisms of Transmembrane Signalling (Cohen, P. & Houslay, M. D., eds.), pp. 3–56, Elsevier, Amsterdam

Gallin, E. K. & Sheehy, P. A. (1985) J. Physiol. (London) **369**, 475–499

Hawkins, P. T., Stephens, L. & Downes, C. P. (1986) Biochem. J. **238**, 507–516

Janmey, P. A., Iida, K., Yin, H. & Stossel, T. P. (1987) J. Biol. Chem. **262**, 12228–12236

Kruskal, B. & Maxfield, F. (1987) J. Cell Biol. **105**, 2685–2691

Lew, P. D., Monod, A., Krause, K.-H., Waldvogel, F. A., Biden, T. J. & Schlegel, W. (1986) J. Biol. Chem. **261**, 13121–13127

Merritt, J. E. & Rink, T. J. (1987) J. Biol. Chem. **262**, 14912–14916

Nishizuka, Y. (1984) Nature (London) **308**, 693–698

Pofit, J. F. & Strauss, P. R. (1977) J. Cell. Physiol. **92**, 49–256

Pribluda, V. S. & Metzger, H. (1987) J. Biol. Chem. **262**, 11449–11454

Prpic, V., Weiel, J. E., Somers, S. D., DiGuiseppi, J., Gonias, S. L., Pizzo, S. V., Hamilton, T. A., Herman B. & Adams, D. O. (1987) J. Immunol. **139**, 526–533

Rittenhouse, S. E. (1985) in Inositol and Phosphoinositides (Bleasdale, J. E., Eichberg, J. & Hauser, G., eds.), pp. 459–473, Humana Press, Clifton, NJ

Ryu, S. H., Suh, P. G., Cho, K. S., Lee, K. Y. & Rhee, S. G. (1987) Proc. Natl. Acad. Sci. U.S.A. **84**, 6649–6653

Stephens, L. R., Hawkins, P. T., Carter, N., Chawala, S. B., Morris, A. J., Whetton, A. D. & Downes, P. C. (1988) Biochem. J. **249**, 271–282

Sung, S. S., Young, J. D., Origlio, A. M., Heiple, J., Kaback, H. R. & Silverstein, S. C. (1985) J. Biol. Chem. **260**, 13442–13449

Triglia, T., Burns, G. F. & Werkmeister, J. A. (1985) Blood **65**, 921–928

Whetton, A. D., Monk, R. N., Consalvey, S. D. & Downes, C. P. (1986) EMBO J. **5**, 3281–3286

Wightman, P. D., Humes, J. L., Davis, P. & Bonney, R. J. (1981) Biochem. J. **195**, 427–433

Received 22 March 1988/2 June 1988; accepted 6 July 1988

Radiation Protection Dosimetry
Vol. 23 No. 1-4 pp. 317-320 (1988)
Nuclear Technology Publishing

INTERCOMPARISON OF NEUTRON DOSIMETRY TECHNIQUES AT THE AFRRI TRIGA REACTOR

G. H. Zeman†, M. Dooley†, D. M. Eagleson†, L. J. Goodman‡, R. B. Schwartz‡, C. M. Eisenhauer‡ and J. C. McDonald§
†Armed Forces Radiobiology Research Institute, Bethesda, MD 20814, USA
‡US National Bureau of Standards, Gaithersburg, MD 20899, USA
§Battelle Pacific Northwest Laboratory, Richland, WA 99352, USA

Abstract — In 1983 a programme of neutron dosimetry validation was undertaken at the TRIGA Mark F nuclear reactor at the Armed Forces Radiobiology Research Institute (AFRRI). Since the International Neutron Dosimetry Intercomparison (INDI) of 1973, the development of neutron dosimetry protocols in both the USA and Europe as well as improved knowledge of the physical factors (W, K) involved in neutron dosimetry necessitated a re-evaluation of earlier techniques. The purpose of the present programme was to validate the accuracy of AFRRI ionisation chamber neutron dosimetry by intercomparison with independently calibrated neutron measurement techniques. Two reference configurations of the AFRRI TRIGA nuclear reactor have been used for the intercomparisons, namely unshielded and shielded by a 15 cm lead shield. Calculated neutron and gamma ray energy spectra were available for these reference fields. Neutron dosimetry techniques used in the intercomparisons include (1) paired ionisation chambers, consisting of tissue-equivalent (TE) ionisation chambers with either a magnesium or graphite ionisation chamber or a GM counter, (2) activation foils, (3) fission chambers, (4) a calorimeter, and (5) tissue-equivalent proportional counter (TEPC). The results of this ongoing programme at the AFRRI TRIGA reactor support the general conclusion that fission neutron spectrum kerma values determined by the separate independent techniques agree within the uncertainties of the experimental measurements.

INTRODUCTION

There exists no national standard instrument or radiation field for calibration of absorbed dose of neutron radiations used in radiobiology or radiotherapy. Standardisation is largely achieved by:

(i) Adherence to specific protocols, such as those of the American Association of Physicists in Medicine (AAPM)[1] or European Clinical Neutron Dosimetry Group (ECNEU)[2] for neutron beam dosimetry.

(ii) Intercomparisons between different centres using similar measurement techniques, notably International Neutron Dosimetry Intercomparison (INDI)[3] and European Neutron Dosimetry Intercomparison Project (ENDIP)[4].

(iii) Intercomparisons between fundamentally different dosemeters[5], e.g. ionisation chambers, calorimeters, activation foils, and proportional counters.

The objective of the present work is to measure accurately tissue kerma due to neutrons in the mixed neutron gamma ray radiation fields used for radiobiology research at the Armed Forces Radiobiology Research Institute (AFRRI) TRIGA reactor. Specifically, the aim is to validate the accuracy of neutron dosimetry by intercomparing results from fundamentally different detection technologies which have independent calibrations. Ionisation chamber measurements of absorbed doses of neutron radiation are limited in absolute accuracy to ± 5-10% due to uncertainties in the physical constants used to calculate dose from the measured ionisation. Calorimetry is similarly limited to an overall accuracy of the order of ± 3%. Neutron activation provides information only on the neutron portion of total dose, with accuracy dependent on knowledge of the neutron energy spectrum, kerma factors and cross sections.

An earlier intercomparison of ionisation chamber measurements with activation techniques at AFRRI was reported by Eisenhauer *et al*[6]. This paper describes the present status of the intercomparison programme, including results from a tissue-equivalent (TE) calorimeter and a TE proportional counter.

RADIATION FIELDS

The reactor is a General Atomics TRIGA Mark F water-pool type thermal research reactor, capable of pulsed or steady state operation at various locations within its pool. A semicylindrical portion of the reactor pool projects into the exposure room (Figure 1), which is lined with a gadolinium-cadmium shield to minimise scattered thermal neutron fluence. A lead shield can be rolled into

place in front of the reactor core (Figure 1) to increase the neutron to gamma ratio for radiobiology research. The dosimetry measurement point was 70 cm from the centre of the reactor tank wall, and 120 cm above the wood floor (centre height of the reactor core). Measurements are reported for both the unshielded and 15 cm Pb shielded configurations.

STATUS OF THE INTERCOMPARISON PROGRAMME

Ionisation chambers

The paired ionisation chamber method is the primary technique used at AFRRI for neutron dosimetry[7]. We use Exradin 0.5 cm^3 chambers, an A-150 plastic chamber with TE gas and an Mg chamber with Ar (Table 1). AFRRI and NBS staff have completed concurrent absorbed dose measurements with ionisation chambers at the AFRRI TRIGA reactor[8], with excellent overall agreement (1-2%) between the two groups. To ensure the constancy of neutron dosimetry results, a ^{252}Cf irradiator has been built for periodic neutron sensitivity checks of the ionisation chambers, in addition to ^{60}Co calibration of the chambers.

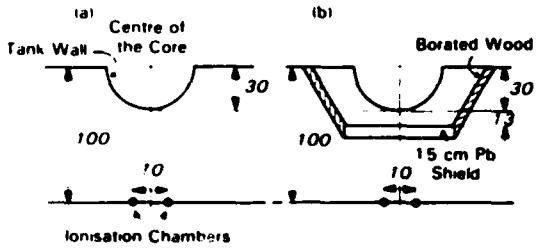

Figure 1. Diagram of the experimental arrangement at the AFRRI TRIGA reactor. All lengths are in cm. (a) With the reactor core brought into place in the pool behind the semicylindrical projection, only a ~2.5 cm thick water layer and the 0.64 cm thick aluminium tank wall separate the edge of the 30 cm radius core from the air in the exposure room. In this bare unshielded array, gamma rays comprise 67% of the total (fission neutron plus gamma ray) tissue kerma in free-air at the measurement point. (b) The 15 cm Pb shield travels laterally on a track for reproducible alignment directly in front of the core, and the borated wood is positioned to reduce scattered radiation. In this 15 cm Pb shielded array, gamma rays comprise 9% of the total kerma in free-air at the measurement point.

Table 1. Physical constants for ionisation chamber measurements.

Reactor Field	Bare	15 cm Pb
Tissue kerma weighted mean neutron energy (MeV)	2.63	1.67
W_n/W_{Co-60}	1.092	1.099
$K_{n\,RU\,muscle}(10^{-11}Gy.cm^2)$	2.06	1.73
$K_{A-150}(10^{-11}Gy.cm^2)$	2.12	1.76
$K_{Mg,Ar}(10^{-11}Gy.cm^2)$	2.10	1.75
k_t	0.939	0.922
k_u(Mg-Ar)	0.02	0.01
$h_t \cdot h_u \cdot r_{mg}$	1.00	1.00

Transport calculations

Neutron and gamma ray energy spectra (Figure 2) and fluences were calculated for AFRRI for selected geometries by two independent investigators [9,10]. Neutron energy spectra calculated by the two independent investigators showed good agreement in spectral shape, especially in the high energy region of the spectra. The calculations are utilised as *a priori* energy spectra to estimate the response of energy dependent detectors, such as activation foils, and to calculate other spectrum dependent quantities, such as lineal energy spectra, for comparison with measurements.

Activation and fission foils

Fission and non-fission foils have been irradiated in the bare and 15 cm Pb shielded reactor fields. Initial neutron kerma rates were derived from the detector measurements using the *a priori* neutron energy spectra (Table 2). Coarse group adjustments to the *a priori* spectra were performed by minimising disagreements between observed and predicted reaction rates. The adjusted spectra were used to form final estimates of the neutron kerma from the foil responses [6,11].

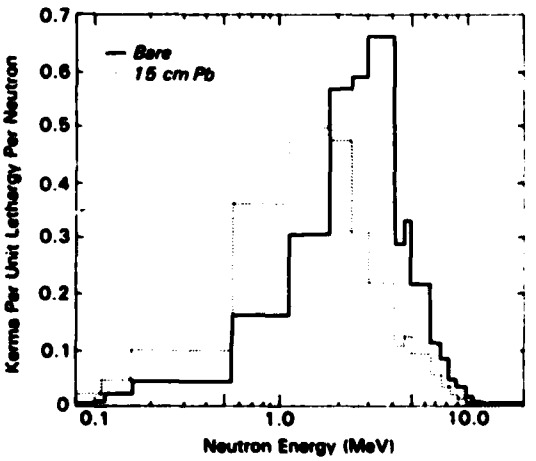

Figure 2. Calculated neutron energy spectra at the dosimetry measurement point[9,10].

Table 2. Dosimetry results in the bare and 15 cm Pb shielded reactor fields.

	Kerma (mGy.kW^{-1}.s^{-1})	
	Neutron	Total
Bare		
Activation/Fission: *a priori*	1.74	
Adjusted	1.88±0.11*	-
Ionisation chamber	2.05±0.10	6.16±0.31
TE calorimeter	-	6.03±0.18
TE proportional counter	-	-
15 cm Pb		
Activation/Fission: *a priori*	0.98	
Adjusted	1.07±0.05	-
Ionisation chamber	1.19±0.06	1.31±0.07
TE calorimeter	-	1.32±0.04
TE proportional counter	1.06±0.16	-

Measurement uncertainties are the estimated standard deviations.

Calorimetry

Intercomparison of TE calorimeter and paired ionisation chambers has been completed in steady state and in single pulse (10 ms FWHM) reactor fields. Total neutron plus gamma ray dose agreement was within ± 5% for both steady state (Table 2) and for pulse (data not shown) irradiations. Due to technical challenges in making the calorimeter measurements, we do not plan to use this instrument in routine reactor dosimetry.

Tissue-equivalent proportional counters

Data have been obtained from TEPC measurements in the 15 cm Pb shielded reactor. The neutron kerma rate measured by a TEPC agrees with other methods (Table 2). Comparison of the shapes of measured and calculated[13] y-spectra show good agreement above 15 keV.μm^{-1} (Figure 3). Above 15 keV.μm^{-1}, y-spectra measured at midline 15 and 18 cm diameter phantoms were identical in shape to the spectrum in air (Figure 4). Below 15 keV.μm^{-1}, the measured y-spectra show the expected increase in the gamma ray fraction of dose with increasing phantom size (Figure 4).

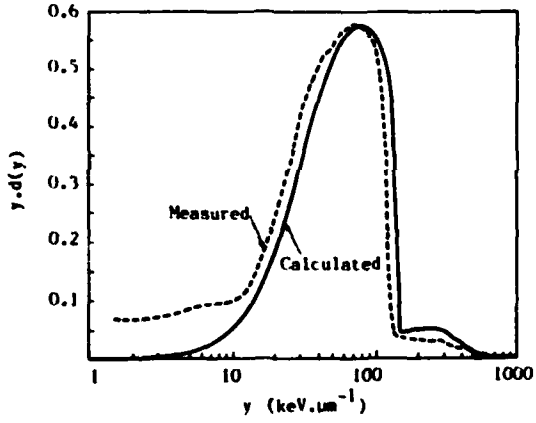

Figure 3. Measured and calculated y-spectra for the 15 cm Pb radiation field in free air. The calculated spectrum was normalised to measurements at the peak.

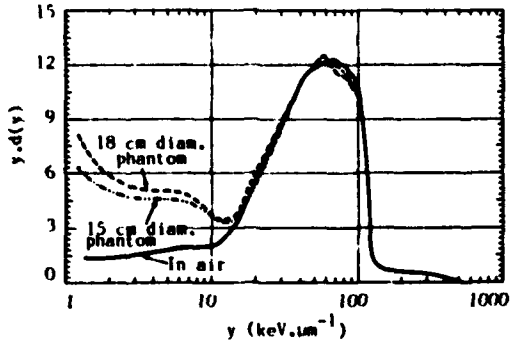

Figure 4. Measured y-spectra for the 15 cm Pb radiation field, normalised to the peak of the in-air spectrum.

CONCLUSIONS

Intercomparison of neutron dosimetry results from separate independent measurement techniques can provide confirmation of the accuracy of measured doses. Measurements of total dose by ionisation chambers and by a calorimeter agreed within 5% in the bare and 15 cm Pb fields.

Measurements of the neutron component of dose by the different techniques agreed within 9% (bare) and 12% (15 cm Pb).

Further efforts in this intercomparison programme will emphasise repeating and extending the present measurements with an improved in-room monitor system to reduce the uncertainty involved in comparing data taken at dose rates (reactor power levels) differing by up to four orders of magnitude.

We interpret the present results as confirming the accuracy of neutron dosimetry measurements at the AFRRI TRIGA reactor within the uncertainties of the experimental measurements.

The opinions and assertions contained herein are those of the authors and should not be construed as reflecting the views of the Department of Defense or the Defense Nuclear Agency.

REFERENCES

1. AAPM. *Protocol for Neutron Beam Dosimetry*. Report No. 7, (New York:AAPM) (1980).
2. Broerse, J. J., Mijnheer, B. J. and Williams, J. R. *European Protocol for Neutron Dosimetry for external Beam Therapy*. Br. J. Radiol. **54**, 882 (1981).
3. ICRU. *An International Neutron Dosimetry intercomparison*. Report 27 (Bethesda, MD:ICRU Publications) (1980).
4. Zoetelief, J. and Schraube, H. *Experimental Procedures for the On-site Neutron Dosimetry Intercomparison ENDIP-2*. IN Proc. 5th Symp. on Neutron Dosimetry, eds H. Schraube, G. Burger and J. Booz (Luxembourg:Commission of the European Communities) EUR 9762 Vol. II, pp. 1179-1190 (1985).
5. McDonald, J. C., Ma, L., Liang, J., Eenmaa, J., Awschalom, M., Smathers, J. B., Graves, R., August, L. and Shapiro, P. *Calorimetric and Ionometric Dosimetry Intercomparisons I:U.S. Neutron Radiotherapy Centers*. Med. Phys. **8**, 39-43 (1981).
6. Eisenhauer, C., Grundl, J., Cassapakis, C. and Verbinski, V. *Use of Threshold Activation Detectors to obtain Neutron Kerma for Biological Irradiations*. IN Proc. 5th Symp. on Neutron Dosimetry, eds H. Schraube, G. Burger and J. Booz (Luxembourg:Commission of the European Communities) EUR 9762 Vol. II, pp. 939-947 (1985).
7. Goodman, L. *A Practical Guide to Ionization Chamber Dosimetry at the AFRRI TRIGA Reactor*. Armed Forces Radiobiology Research Institute Technical Report AFRRI TR85-1, Bethesda, Maryland (1985).
8. Dooley, M., Goodman, L. J., Zeman, G. H., Schwartz, R. B., Eisenhauer, C. M. and Blake, P. K. *Ionization Chamber Intercomparison in Mixed Neutron and Gamma-ray Radiation Fields by NBS and AFRRI*. Armed Forces Radiobiology Research Institute Technical Report AFRRI TR86-3, Bethesda, Maryland, (1986).
9. Verbinski, V. V. and Cassapakis, C. G. *Calculation of the Neutron and Gamma-ray Environment in and around the AFRRI TRIGA Reactor*, Vol. II. Defense Nuclear Agency report DNA 5893F-2, Washington, DC (1981).
10. Johnson, J. O., Emmett, M. B. and Pace, J. V. *Calculations of Radiation Field and Mid-head and Mid-thorax Responses in AFRRI TRIGA Reactor Facility Experiments*. Oak Ridge National Laboratory ORNL/TM-8807, Oak Ridge, Tennessee (1983).
11. Grundl, J. *Derivation of Neutron Exposure Parameters from Threshold Detector Measurements*. IN Proceedings of the 6th Astm-Euratom Symposium of Reactor Dosimetry, Jackson Hole, Wyoming ASTM STP 1001 (Philadelphia PA: ASTM) (in press, 1988).
12. Zeman, G. H., Dooley, M. and McDonald, J. *Calorimeter and Ion Chamber Comparison in Reactor Radiation Fields*. 27th Ann. Mtg. of the AAPM, Seattle, Washington (August 1985).
13. Gerstenberg, H. M. and Coyne, J. J. *Calculated Microdosimetric Energy Distribution Spectra and their Use to indicate Neutron Source Quality*. IN 8th Int. Cong. on Radiation Research, Edinburgh, Scotland (July 1987).